INFORMATION TO USERS

This manuscript has been reproduced from the microfilm master. UMI films the text directly from the original or copy submitted. Thus, some thesis and dissertation copies are in typewriter face, while others may be from any type of computer printer.

The quality of this reproduction is dependent upon the quality of the copy submitted. Broken or indistinct print, colored or poor quality illustrations and photographs, print bleedthrough, substandard margins, and improper alignment can adversely affect reproduction.

In the unlikely event that the author did not send UMI a complete manuscript and there are missing pages, these will be noted. Also, if unauthorized copyright material had to be removed, a note will indicate the deletion.

Oversize materials (e.g., maps, drawings, charts) are reproduced by sectioning the original, beginning at the upper left-hand corner and continuing from left to right in equal sections with small overlaps. Each original is also photographed in one exposure and is included in reduced form at the back of the book.

Photographs included in the original manuscript have been reproduced xerographically in this copy. Higher quality 6" x 9" black and white photographic prints are available for any photographs or illustrations appearing in this copy for an additional charge. Contact UMI directly to order.

UMI

A Bell & Howell Information Company
300 North Zeeb Road, Ann Arbor MI 48106-1346 USA
313/761-4700 800/521-0600

Studies in Generalized Hydrodynamics for Chemical Reactions and Shock Waves

by

Mazen Al-Ghoul

Department of Chemistry, McGill University

Montréal, Québec

Canada

February 1997

A Thesis submitted to the

Faculty of Graduate Studies and Research

in partial fulfillment of the requirements for the degree of

Doctor of Philosophy

This Thesis is dedicated to my parents Hassan and Fatimah and my sister Rola

"To admit not knowing is half the knowledge" *Arabic saying*

Abstract

This thesis is made of two parts. In the first part, we study pattern formations and dissipation of energy and matter by using hyperbolic reaction-diffusion equations for reacting systems. Two-dimensional hyperbolic reaction-diffusion equations are numerically solved for the Selkov model and the Brusselator. It is shown that the evolution equations used can give rise to various kinds of patterns such as hexagonal structures, stripes, maze structures, chaotic structures, etc., depending on the values of the reaction-diffusion number and the initial and boundary conditions. The values of the entropy production computed indicate that the system maintains the particular organized local structures at the expense of energy and matter. However, when the system produces a chaotic pattern, the entropy production is lower than the locally organized structures. The phase speed of travelling oscillating chemical waves can be obtained from the linearized hyperbolic reaction-diffusion equations. The Luther-type speed formula is obtained in the lowest order approximation in the case of the Brusselator. The two-dimensional power spectra computed for chaotic patterns still preserve some kind of symmetry.

In the second part of this thesis, the generalized hydrodynamics is applied to calculate the shock profiles, shock widths, and calortropy production for a Maxwell gas. Shock solutions are shown to exist for all Mach numbers. This is in contrast to the Grad moment equation method which does not admit shock solution for $N_M \geq 1.65$ and to the method of Anile and Majorana which breaks down for $N_M \geq 2.09$. The energy dissipation in the shock is shown to increase with the Mach number as a power law of the form $(N_M - a)^\alpha$ where a and α are real constants.

Résumé

Cette thèse est divisée en deux parties. La première traite la formation des modèles et la dissipation d'énergie et de matiere en utilisant les équations hyperboliques de reaction-diffusion pour les systèmes réactifs. Celles ci sont résolues numériquement en deux dimensions pour le modèle de Selkov et celui de Brusselator. Il a été demontré que les équations d'évolution utilisées fournissent différents modèles comme des formes hexagonales, des raies, des structures labyrinthés et chaotiques etc., dépendement du nombre de réaction-diffusion ainsi que des conditions initiales et celles aux limites. Les valeurs de production d'entropie montrent que le système maintient les structures locales organisées sur la dépense d'énergie et de matière. Cependant, lorsque le système produit un modèle chaotique, la production d'entropie dans celui-ci est plus petite que celle d'un système produisant des structures locales organisées. La vitesse de phase de l'onde propagée peut être obtenue à partir du système des équations hyperboliques de réaction-diffusion linéairisées. Une formule de type Luther est obtenue pour le moidre ordre d'approximation. Les spectres de puissance bidimensionels calculés pour des modèles chaotiques gardent un certain genre de symétrie.

La deuxième partie traite l'application de équations hydrodynamiques géneralisées pour étudier les profiles de l'onde du choc, la largeur du choc et la production de calortropie pour un gaz de Maxwell. La solution du choc existe pour tous les nombres de Mach, contrairement au traitement de Grad où il n'y a pas de solution du choc pour $N_M \geq 1.65$ et celui de Anile et Majorana pour $N_M \geq 2.09$. La dissipation d'énergie dans le choc augmente avec le nombre de Mach comme une loi de puissance de la forme $(N_M - a)^\alpha$ où a et α sont des nombres constants réels.

Acknowledgments

First and foremost, I would sincerely like to thank my research supervisor Professor B. C. Eu for his constant support throughout my graduate work. His deep insights into the field of irreversible phenomena provided me with many answers. I am indebted to him for the help he provided not only on the scientific aspects but also on the personal aspects. He created a wonderful and pleasant atmosphere and I enjoyed every moment of research with him. He made me set high standards and always pushed me to work hard in order to meet them.

I would like to thank Professor Davis Ronis for very interesting discussions, comments and explanations which helped me very much in building myself as a scientist. I am grateful for the long time he spent answering my questions.

I would like to thank Dr. Hin Hark Gan for his patience, encouragement and help specially in the beginning of my graduate work. I always enjoyed the scientific and philosophical issues he constantly brought to our laboratory.

Also I would like to thank Hikmat, Kyun-Il, Imad, Mohamed, Alvin, Nikolai, Sergei, James, Tim and Kuo-Bin for their friendship and support.

Last but not least, I want to thank my fiancée Rana for her encouragement. She always made things easier and her presence took away all the stress and pressure.

Contents

List of Figures

Part I

Chemical Waves

Chapter 1

Introduction

1.1 History

The phenomena treated in this thesis involve chemical oscillations, patterns and turbulence. These have become of great interest in the chemistry and physics community. However, there is a long history that has unfolded in this area paving the way for the explosion of activity in the last two decades. In what follows, we shall present some important history of the theoretical and experimental aspects of the aforementioned phenomena. In the seventeenth century, Robert Boyle[1] noted a periodic flaring-up of phosphorus in a loosely stoppered container, which is currently understood to arise from the interaction of chemical kinetics and diffusion. The reaction between phosphorus and oxygen is a branched chain process that leads to an ignition. The ignition consumes the oxygen available in the flask and so the reaction ceases. As more oxygen diffuses into the flask, the reaction does not immediately recommence. Instead, the oxygen concentration must reach a critical value before the chain branching leads to another ignition process. Published observations of chemical oscillations date back at least to the early nineteenth century when Fechner[69] discovered an oscillatory dissolution and Davy[70] the cool

flames[1]. In the eighteen thirties, Munck performed the oscillatory P ignition. In those early days, oscillating chemical reactions did not attract attention. By the beginning of the twentieth century, two excellent examples of heterogeneous oscillating reactions had been discovered: the so called "iron nerve"– the periodic dissolution of an iron wire in nitric acid by Heathcote[3], and the "mercury heart"–the oscillatory decomposition of hydrogen peroxide on the surface of metallic mercury by Bredig[2]. Soon after that, attempts to understand mechanisms of chemical oscillations were made. However, the study of heterogeneous reactions was difficult at that time since they involve phase transitions and transport processes. Homogeneous reactions are much simpler; so it was natural to begin a theoretical study of such systems. In 1910, Hirniak[5] proposed some cyclic reactions that can oscillate and tried to link those oscillations to thermodynamics. About the same time, Lotka[6] proposed his famous models of oscillating chemical reactions based on irreversible autocatalytic steps. These models attracted the attention of biologists who made the link between Lotka's chemical oscillations and the multiplications and oscillations in the population densities. Chemists did not accept the Lotka models for the reason that his mechanisms were oversimplified. Also in 1910, Luther[15] was the first to observe a single trigger wave in the permanganate-oxalate reaction and stated without proof that the wave speed is a simple consequence of the differential equations that describe the reaction kinetics. In 1921, Bray[7] published the recipe of the first oscillating chemical reaction in the liquid phase: the catalytic decomposition of hydrogen peroxide under the influence of iodate ion. Again, the chemistry community did not accept the oscillations and attributed instead these oscillations to impurities. In 1937, Fisher[8] suggested a nonlinear reaction-diffusion equation as a deterministic version of a stochastic model for the spatial spread of a favored gene in a population. This equation admits travelling wave solutions and was studied first by Kolmogorov et al.[9]. In the late 1930s and begining1940s, Newitt and Thornes obtained cool flames in propane oxidation[37]. Denbigh theoretically

[1]Cool flame is an oscillatory mode that occurs in closed systems during the oxidation of hydrocarbons.

studied autocatalytic reactions and Sal'nikov proposed a model for thermokinetic oscillations[38]. In early 1950s, Ashmore and Norrish[71] discovered the CO oscillations and Alan Turing[32] published his influential paper on pattern formation and morphogenesis in chemical systems. In 1955, Prigogine[10] showed that oscillations can exist far from equilibrium systems. This was still not enough to convince the chemistry community, and for half a century, chemists believed that the oscillations of homogeneous chemical reactions are impossible even though there was no logical basis for their assumption! In 1951, B. Belousov discovered his famous reaction. He tried several times to publish his results, but his paper was repeatedly rejected by chemical journals. Only in 1959 he was able to publish it in an obscure journal entitled "A collection of Short Papers on Radiation Medicine"[11]. In the Belousov reaction, color oscillates during the cerium-catalyzed oxidation of citric acid by bromate. Among other things Belousov showed that the period of oscillations decrease with temperature. The real mechanism of Belousov reaction was unknown. Around this time, Aris and Amundson performed the stability analysis[39]. In early 1960s, Zhabotinsky took over the Belousov reaction and studied it extensively to clearly establish the evidence of the existence of a genuine, homogeneous, oscillating chemical reaction[12, 13]. At about the same time, a series of papers by B. Chance et al.[14] appeared on glycolytic oscillations in yeast. Selkov[67] proposed a model to describe glycolytic oscillations. During this period, an extensive theoretical work was carried out by Prigogine and Nicolis[19] who proposed the famous Brusselator model for the Belousov-Zhabotinsky reaction. Linnett, Reuben and Wheatley studied the CO-O_2 oxidation[48] and then Gray and Young performed the local stability analysis for hydrocarbons and presented a unified theory of explosions, cool flames and two-stage ignitions[49]. On the other hand, Lorenz[33] proposed his famous set of equations that exhibit chaos. From 1972 to 1974, Field, Körös and Noyes[23] elucidated the B-Z mechanism and the Oregonator[25] was proposed as a skeletal model for the B-Z reaction. Winfree[19] began the study of spiral waves in the B-Z reaction. In 1973, the Briggs-Rauscher[30] oscillating reaction was discovered. In late 1970s, Epstein, De Kepper, Orban and Kustin[47] began the design of chemical oscillators. Boisson-

ade and de Kepper[50] proposed the cross-shaped diagrams in the CSTRs. Chaos and mixed mode oscillations in the B-Z reaction were discovered experimentally[43]. Olsen and Degn[21] discovered chaos in enzyme systems. Moreover, Rössler[42] proposed his model that exhibits chaos. In early 1980s, the Texas chaos[73] in the B-Z systems was discovered. Showalter and Ganapathisubamarian[72] experimentally discovered the existence of isolas and mushrooms. The Brandeis group[77] proposed a systematic approach to designing oscillating reactions which led to the development of literally dozens of new oscillators. Digital imaging techniques introduced by Müller, Plesser, and Hess allowed precision measurements of the spiral wave dynamics[20]. Hudson began the study of electrodissoultion reactions[74]. Tyson and Keener[40] began an extensive theoretical study of spiral waves and scrolls in the B-Z reaction. In late 1980's till now, De Kepper, Boissonade[81], Ouyang and Swinney[44, 81] and Epstein and Lengyel[81] experimentally studied pattern formation in unstirred flow reactors. New techniques for manipulating dynamical systems, originating with the Ott-Grebogi-Yorke[75] method for controlling chaos, have stimulated a flurry of experimental applications[76].

1.2 Phenomenology

Nonlinearities and feedback are the key features of the chemical kinetics underlying the exotic phenomena to be described in this part of the present thesis. Feedback arises when the products of later steps in the mechanism influence the rate of some of the earlier reactions. Very interesting behaviors arise from this feedback, and they are described in the following subsections:

1.2.1 Clocks

Clock-type behavior is observed not only in solution phase reactions, but also in a wider context like gas phase reactions. The classic clock reaction, discovered by Landolt[16] in 1886, involves autocatalytic iodate-bisulfite system. The reactants are

colorless in water in the presence of starch as an indicator. There is a long induction period during which the iodide ion concentration increases slowly, followed by a rapid acceleration in the rate which leads to a sharp color change. If the reductant is in stoichiometric excess, the color fades again. The induction period depends on the initial concentrations of the reactants iodate and reductant:

$$t_{ind} = k/[IO_3^-]_0[HSO_3^-]_0,$$

with $k = 4 \times 10^{-3} M^2 s$. By varying the initial concentrations, the clock time can be adjusted over a wide range. A reaction that is initially $0.01M$ in each of the reactants has a $40s$ induction time. In gas phase reactions involving the oxidation of simple hydrocarbons such as n-butane, long induction periods of the order of days is observed. Clock reaction behavior has also been observed in the polymerization of a mutant form of haemoglobin, associated with the sickle cell anemia, to form a highly viscous gel[51]. The apparent rate law here indicates a dependence of rate on somewhere between the 20th and 30th power of the initial haemoglobin concentration. In some cases, the clock induction time appears not to be repeatable from experiment to experiment. Instead, the observed clock times are distributed statistically about a mean value which is reproducible from one experiment to the other. The origin of this phenomena is not clear and it is termed *supercatalysis*[29] to indicate a high degree of chemical feedback through the autocatalytic species.

1.2.2 Fronts

Instead of a well-mixed solution to capture a clock behavior, the reaction can be performed in a petri dish in which we can initiate the reaction using a thin Pt electrode negatively biased with respect to the counter electrode in the case of the Landolt system. This causes a local increase in the concentation of I^- via electrochemical reduction of IO_3^-. In this case, the clock reaction spreads away from the initiation site, giving rise to a spatially resolved clock or chemical wavefront. The reactants ahead of any wavefront. are thus effectively frozen kinetically in their initial state

and rely on the diffusion of iodide from the wave to initiate the conversion to products locally. Once the reaction begins, locally, much more iodide is produced and this can then diffuse into neighboring regions, initiating the clock reaction there. Thus the wave is a combined reaction-diffusion process that converts the system from its initial state to its final equilibrium composition. This is what we call a front. The fronts travel at a constant velocity through the reaction mixture. Typical wave speeds for the iodate-arsenite reaction are of the order of 1 $mm\ min^{-1}$. This is to be compared with the time taken for diffusion to cause spreading over 1 cm which is approximately 400 min! Reaction-diffusion processes are believed to underlie the signal mechanisms in many biological systems which exploit this potential for enhanced propagation velocity[34]. For the B-Z reaction, the wave velocity was found to be strongly dependent on the initial concentrations of sulfuric acid and sodium bromate but independent of malonic acid concentration[24]. In addition, a slight dependence on ferroin concentration was found[26]. This velocity dependence on initial concentrations was expressed in the following formula [26] as

$$c = (a[NaBrO_3][H_2SO_4])^{1/2} + b.$$

where a and b are constants. It is also believed that the speed of the wave goes as the square root of the diffusion coefficient[34]. Systems which exhibit waves following quadratic autocatalysis include the bromate-and nitrate-ferroin reactions. It also occurs in population models, Fisher-Kolmogorov equation and in models for the spread of infectious diseases such as AIDS or rabies[34]. Also flames are reaction diffusion fronts travelling at a constant speed. The role of the autocatalyst is played by temperature rise resulting from the chemical heat release with the feedback acting through the Arrhenius temperature dependence of the rate constant. The flame speed can be expressed[27]:

$$c = [(2\kappa/c_p\sigma)k(T)/B^2]^{1/2},$$

where $2\kappa/c_p\sigma$ is the thermal diffusivity and B is a numerical factor. Typical flame speeds are of the order of 0.1 to 1 ms^{-1}. For circular waves[45], the initial wave-speed is usually slower than that predicted earlier because of the curvature effect. A curved wave front allows the autocatalyst diffusing ahead to become diluted, thus reducing the chemical reaction rate, leading to a lower speed of the front. However, as the radius of the circle increases, the wave front appears locally planar and the aforementioned formula applies. Oscillatory wave speeds are observed experimentally in solid pyrotechnic mixtures, for example.

1.2.3 Pulses

An excitable system is characterized by having a stable steady state and hence is not spontaneously oscillatory. Small perturbation, e.g., by small reduction in bromide concentration in the case of the B-Z reaction, disturbs the system from this state transiently, but the system returns quickly without any changes in color. With slightly larger perturbations, the system is stimulated into a single excursion, with a color change back and a single large peak in the intermediate concentrations, similar to a large oscillation, before returning to the original steady state. The system responds in a qualitatively different way to perturbations that are below and above some critical or threshold value. The perturbations get amplified above this value. An excitable system subjected to a single, sufficiently large perturbation will support a single wave pulse. Usually, the front of the pulse is little different from the front discussed earlier. To illustrate more of this kind of waves we use again the B-Z system as explained by the Field-Körös-Noyes(FKN) mechanism[23]. This can be summarized by the following two processes:

$$\text{Process A} \quad : \quad BrO_3^- + 2Br^- + 3H^+ \longrightarrow 3HOBr$$

$$\text{Process B} \quad : \quad BrO_3^- + HBrO_2 + 2M_{red} + 3H^+ \longrightarrow 2HBrO_2 + 2M_{ox} + H_2O$$

Ahead of the front, the mixture is in the reduced state (red). The front is a wave of oxidation which causes an increase in $HBrO_2$ and M_{ox}, with a consequent decrease in Br^-. Immediately after the wave, there is a period during which $[HBrO_2]$ falls only slowly. Just some distance behind a "wave back" follows. This is a reduction wave through which $HBrO_2$ and M_{ox} are consumed and Br^- is recovered. The wave propagates at constant speed of the order of 1 $mm\ min^{-1}$. In two dimensions this is nothing but a circle wave or target pattern of blue circles nested in a blue background. The spontaneous initiation of these target patterns seems to rely on heterogeneities like dust or defects on the surface of the petri dish. Each target reflects the frequency of the initiation at its centre. When targets collide they create cusp-shaped regions and then annihilate each other. The highest frequency source will entrain the whole dish after some time[17]. .

1.2.4 Spirals

If targets are broken, for example, by gently tilting the dish, the circular waves may break up and give rise to a pair of counter-rotating spirals. In the B-Z reaction, all spirals rotate with the same period and wavelength, reflecting the bulk kinetics rather than local heterogeneities. The propagation speed of the spiral must be constant or the spiral will deform as it evolves. Spirals with multiple arms rotating around a common core have also been created experimentally. At the centre of a given spiral is a region of the order of 350 μm in which the concentration variations are distinctly less than in the development front. At the centre of this region is a core with a diameter of the order of 30 μm. The tip of the spiral, where the oxidation front and the reduction back meet, rotates around the core with the same frequency as the bulk spiral. As the conditions are varied, the tip of the spiral begins to meander. This means that the tip begins to follow a quasi-periodic motion. The motion may become very complicated and its trajectory may close, indicating a 'phase locked' quasi-periodic motion[53, 54]. Spirals are also observed in the growth cycle of the slime mould *Dictyostelium discoideum*[52].

1.2.5 Scrolls

In three dimensional systems, spirals are generalized to scrolls. The axis or filament of the scroll is straight in the simplest case. In other situations, the filament may bend or twist. In some cases, the inner sheets of the spirals may collide with outer turns, leading to annihilations. Some very complex three dimensional structures are created with the filament forming a loop or becoming knotted, giving rise to very complicated structures[78]. On the other hand, scroll waves have been linked reasonably firmly to *cardiac arrhythmias*[46]..

1.2.6 Phase Waves

If the period of the spontaneous oscillations varies in space, this can give rise to an apparent travelling wave[22]. This happens when there is a temperature or pH gradient established along a tube which contains the B-Z reagents, for example. When reactants are left unstirred in a vertical cylindrical tube, horizontal bands of blue and red form. These bands usually start to appear at the bottom of the tube and move slowly upwards.. Eventually, the cylinder is filled by these bands with nonuniform density, the closer to the bottom, the denser the wave packing. This phase wave has little to do with diffusion since there is no spatial gradient.

1.2.7 Turing Patterns

In 1952, Alan Turing[32] predicted theoretically that chemical systems showing feedback in situations where not all species diffuse with the same mobility might give rise to *spontaneous pattern formation.* An initially well-mixed, homogeneous solution would then evolve of its own volition to produce spatial gradients in the participating species. Turing suggested that this reaction-diffusion process might underlie the spontaneous development of spatial form in morphogenesis like a developing embryo. The mechanism has also been implicated in the spots and stripes marking animal coats and how these change with the size of the animal[34]. The main condition on the diffusion coefficients, as derived by Turing, is that the autocatalytic species

must be sufficiently less than that for the reactant. Since ions have very comparable diffusion constants in solution, Turing structures have not been widely observed in chemical systems. However, only recently, Turing patterns were discovered in chemical systems by the Bordeaux and Texas groups independently[55, 56].

1.3 Irreversible Thermodynamics

According to the second law of thermodynamics, an isolated system reaches in time the state of thermodynamic equilibrium which is the state of maximum entropy. This law applies to both equilibrium and nonequilibrium systems. In the 19th century, classical thermodynamics was developed but it dealt mainly with equilibrium situations. Based on the work of Onsager[79], classical thermodynamics was extended to what is called "linear irreversible thermodynamics" which covers the range of situations in which the fluxes in irreversible processes are linear functions of "thermodynamic forces" like temperature or concentration gradients. Linear irreversible thermodynamics can be applied to study is the coupling between heat and diffusion, namely, thermal diffusion. If we apply a thermal gradient to a mixture of two different gases, we observe an enrichment of one of the components at the hot wall while the other concentrates at the cold wall. Clearly, the entropy of such a process is lower than that of the uniform mixture. From this, one can conclude that *nonequilibrium may be a source of order.* Prigogine and Nicolis termed "dissipative structures"[19] the ordered structures which occur far from equilibrium and contrast the equilibrium structures like crystals and liquids, and can be maintained far-from-equilibrium through a sufficient flow of energy and matter into the system.

The aim of this part of the thesis is the study of self-organization in nonequilibrium systems, characterized by the appearance of dissipative structures through the amplification of appropriate fluctuations, and of a quantification of this order with relation to the second law of irreversible thermodynamics. Assuming that a dissipative structure has been formed, we would like to find a set of thermodynamic properties characterizing this structure as uniquely as possible or try to seek a state

function whose properties are indicative of the properties of the dissipative structure itself. This is a very difficult task because there exists in general no potential whose value would characterize the state of the system[80]. Instead, we consider how a state function like *calortropy*[2] or *calortropy production*[59] behaves on a dissipative structure. Then, we may come up with a criterion for evolution and dissipation during the formation and development of a pattern, thus a thermodynamic theory of pattern formation. In addition, bifurcation theory is a natural approach to the problem and is used to study the possible branching of solutions that arises under certain conditions.

1.4 Kinetic Theory and Generalized Hydrodynamics

In this thesis, we use kinetic theory to derive a set of evolution equations for the macroscopic variables that describe the system. In what follows, we shall introduce the kinetic theory approach. In fact, if the thermodynamic gradients are small enough, the fluid is in a near equilibrium state and may be adequately described by linearized constitutive relations such as Newton's law of viscosity, Fourier's law of heat conduction, Fick's law of diffusion, etc. On the other hand, when a fluid is subject to a large thermodynamic force, such as a steep temperature or concentration gradient, the system is said to lie far-from-equilibrium, and the linear or time independent constitutive equations are inadequate for proper description of the process. A kinetic equation for reacting liquids is assumed to be the equation describing the dynamics of the particles on the microscopic level[60]. To link this description to something we can measure, i.e., to thermodynamics, we project the description onto the thermodynamic space by always respecting the second law of

[2]Calortropy, Ψ, is a nonequilibrium generalization of Clausius entropy. It is a differentiable function such that $d\Psi = \frac{dQ}{T} + dN$, where dN is the infinitesimal uncompensated heat and dQ is the infinitesimal heat transfer. T is the temperature. Ψ is exact in the extended thermodynamic space.

thermodynamics which should be at the heart of any macroscopic theory. In this description, the physical macroscopic variables of interest are defined as statistical averages of corresponding microscopic quantities or moments with respect to a distribution function. This function is a probability density distribution function over the phase space of position and velocity coordinates. Once the distribution function is known, various macroscopic variables can in principle be determined from their statistical definitions. A generalized Boltzmann equation[60] is assumed to govern the distribution function. So the goal is to solve this equation subject to appropriate initial and boundary conditions. The solution of such an equation in phase space involves solving an N-body problem which makes the task impossible. Instead, we use the modified moment method initially developed by Eu[57, 58] to solve the Boltzmann equation for gases and extended later to liquids. The method assumes a canonical form of the distribution function which would ensure that the *calortropy production*[59] remains positive semidefinite to any order of approximation. The method yields a set of generalized hydrodynamic equations for the evolution of the various macroscopic variables. The resulting constitutive equations include nonlinear terms absent in other theories. The dissipation terms arising from different irreversible processes are determined by means of a cumulant expansion which provides an effective method of series resummation. The calortropy production is closely related to the collisional processes imbedded in those dissipative terms and it is a highly nonlinear function of the fluxes as opposed to the case of linear irreversible thermodynamics. However, the calortropy production reduces to the Rayleigh-Onsager quadratic form when the thermodynamic forces are small. When the constitutive equations are derived, we couple them to the conservation equations. Now we have the complete tools to describe any macroscopic process.

We have studied chemical waves and patterns far-from-equilibrium. The generalized hydrodynamic equations are simplified a great deal to mimic the experimental conditions of the system in hand, i.e., the conditions of homogeneous temperature and no flow inside the system. Since we are interested in reaction-diffusion processes, all other nonequilibrium fluxes are neglected except for the diffusion fluxes. The

constitutive equations of these fluxes are assumed to be linear but time dependent contrary to Fick's law which assumes that the diffusion fluxes reach equilibrium faster than the corresponding concentration. When these linear time-dependent constitutive equations are used together with the highly nonlinear evolution equations for species concentration, a set of hyperbolic reaction-diffusion equations are derived and they are believed to be more adequate to describe wave phenomena and patterns. Our hyperbolic reaction-diffusion equations can be reduced to the conventional parabolic reaction-diffusion equations[61, 34] as a limiting or special case. The resulting equations subject to appropriate initial and boundary conditions are numerically solved for different chemical systems by using suitable techniques. We showed that indeed these equations can explain a great deal of the phenomenology cited earlier in this introduction. To gain more insight into the problem described by hyperbolic reaction-diffusion equations, we develop a multiple scale perturbation theory to the equations from the Brusselator that describes heuristically the B-Z system[66]. The resulting amplitude equations are much more complicated than the ones obtained from their parabolic counterparts. An explicit expression for the speed of the chemical pulse is also obtained from the hyperbolic reaction-diffusion equations[64, 65]. It has the same form of the expression suggested by Luther[15]. With these hyperbolic reaction-diffusion equations, we also study glycolysis using the modified Selkov model[68]. We explored a wide region of the stability phase diagram and obtained a wide collection of chemical patterns and turbulence[62, 63]. The calortropy production of these patterns is calculated and a criterion was formulated regarding organization of patterns and waves and the rate of dissipation of matter and energy. It turns out that the system, in order to maintain its structures, needs to dissipate larger amount of energy and matter as opposed to the state of the system when it is chaotic or homogeneous.

Bibliography

[1] E. N. Harvey, *A History of Luminescence. from the Earliest Times until 1900* (Am. Philos. Soc., Philadelphia, 1957).

[2] G. Bredig and J. Weinmayr, Z. Phys. Chem. **42**, 601(1903).

[3] H. L. Heathcote, Z. Phys. Chem. **37**, 368 (1901).

[4] E. S. Hedges, Nature (London) **128**, 398 (1931).

[5] J. Hirniak, Z. Phys. Chem. **76**, 675 (1910).

[6] A. J. Lotka, J. Phys. Chem. **14**, 271 (1910).

[7] W. C. Bray, J. Am. Chem. Soc. **43**,1262 (1921).

[8] R. A. Fisher, Ann. Eugenics **7**, 353 (1937).

[9] A. Kolmogorov, I. Petrovsky, and N. Piccounov, Moscow Univ. Bull. Math. **1**. 1 (1937).

[10] I. Prigogine and R. Balescu, Bull. Acad. R. Belg. **41**, 917 (1955); **42**,256 (1956).

[11] B. P. Belousov, *Collection of Short Papers on radiation Medicine* (Med. Publ., Moscow, 1959); In: R. J. Field and M. Burger (eds.), *Oscillations and Travelling waves in Chemical Systems* (Wiley, New York, 1985, pp. 605).

[12] A. M. Zhabotinsky, Biofizika **9**, 306 (1964).

[13] A. M. Zhabotinsky, *Concentrational Self-Oscillations* (Science Publ., Moscow, 1974).

[14] B. Chance et al., Proc. Matl. Acad. Sci. U.S.A. **51**, 1244; **52**, 377 (1964).

[15] R. Luther, Z. Electrochem. **12**, 596 (1906).

[16] A. T. Winfree, J. Chem. Edu. **61**, 661 (1984).

[17] J. J. Tyson and J. P. Keener, Physica D **32**, 327 (1988).

[18] J. P. Keener and J. J. Tyson, Physica D **21**, 307 (1986).

[19] A. T. Winfree, Science **175**, 634 (1972); Sci. Amer. **240**, 82 (1974).

[20] S. C. Müller, T. Plesser and B. Hess, Science **230**, 661 (1985); A. Pagola and C. Vidal, J. Phys. Chem. **91**, 501 (1987).

[21] L. F. Olsen and H. Degn, Nature **267**, 177 (1977).

[22] J. Ross, S.C. Müller, and C. Vidal, Science **240**, 460 (1988).

[23] R. J. Field, E. Körös, and R. M. Noyes, J. Am. Chem. Soc. **94**, 8649 (1972).

[24] R. J. Field and R. M. Noyes, J. Am. Chem. Soc. **96**, 2001 (1974).

[25] R. J. Field and R. M. Noyes, J. Chem. Phys. **60**, 1877 (1974).

[26] P. M. wood and J. Ross, J. Chem. Phys. **82**, 1924 (1985).

[27] P. Gray and S. K. Scott, *Chemical Oscillations and Instabilities: Nonlinear Chemical Kinetics* (Oxford University Press, 1990).

[28] G. Nicolis and I. Prigogine, *Self-organization In Nonequilibrium Systems* (Wiley, New York, 1977).

[29] I. Nagypal and I. R. Epstein, J. Chem. Phys. **89**, 6925 (1988).

[30] T. S. Briggs and W. C. Rauscher, J. Chem. Educ. **50**, 496 (1973).

[31] P. De Kepper, J. Boissonade, and I. R. Epstein, J. Phys. Chem. **94**, 4404, (1990).

[32] A. M. Turing, Phil. Trans. R. Soc. Lond. **B237**, 37 (1952).

[33] E. N. Lorenz, J. Atmos. Sci. **20**, 131 (1963).

[34] J. D. Murray, *Mathematical Biology,* (Springer-Verlag, Berlin, 1990).

[35] P. De Kepper and J. Boissonade, in *Oscillations and travelling waves in chemical systems*, (ed. R. J. Field and M. J. Burger), Chap. 7, Wiley, New York (1985).

[36] J. F. Griffiths, Adv. Chem. Phys. **64**, 203 (1986); J. F. griffith and S. K. Scott, Prog. Energy Combust. Sci. **13**, 161.

[37] D. M. Newitt and L. S. Thornes, J. Chem. Soc., **57**, 1657 (1937).

[38] L. Salnikov, Dokl. Akad. Nauk SSSR, **60**, 405 (1948); Zh. Fiz. Khim., **23**, 258 (1949).

[39] To review the early analysis see: R. Aris, *Introduction To the Analysis of Chemical Reactors* (Prentice-Hall, Englewood Cliffs, N. J.)

[40] J. J. Tyson and J. P. Keener, Physica D **32**, 327 (1988).

[41] J. P. Keener and J. J. Tyson, Physica D **21**, 307 (1986); Physica D **44**, 191 (1990); physica D **53**, 151 (1991).

[42] O. E. Rössler, Z. Naturforsh Teil A **31**, 1664 (1976); **31**, 259 (1979); O. E. Rossler and K. Wegman, Nature (London) **271**, 89 (1978).

[43] R. A. Schmitz, K. R. Craziani, and J. L. hudson, J. Chem. Phys. **71**, 1601 (1977); J. L. Hudson, M. Hart, and D. Marinko, J. Chem. Phys. **71**, 1601 (1979).

[44] Q. Ouyang and H. L. Swinney, Chaos **1**, 411 (1991).

[45] A. Hanna, A. Saul, and K. Showalter, J. Am. Chem. Soc. **104**, 3838 (1982).

[46] L. Glass and M. C. Mackey, *From Clocks to Chaos; the Rhythms of Life*. (Princeton University Press, New Jersey, 1988).

[47] I. R. Epstein, K. Kustin, P. De Kepper, and M. Orban. Sci. Am. **248**, 96 (1983).

[48] J. W. Linett, B. G. reuben and T. F. Wheatley, Combust. Flame, **12**. 325 (1968).

[49] B. F. Gray and C. H. Yang, J. Phys. Chem., **69**, 1965; Trans. Faraday Soc.. **65**, 1614 (1969).

[50] J. Boissonade and P. de Kepper, J. Phys. Chem. **84**, 501 (1980).

[51] S. K. Scott, *Oscillations, Waves, and Chaos in Chemical Kinetics* (Oxford University Press, New York, 1994).

[52] A. J. Durston. J. Theor. Biol. **42**, 483 (1973).

[53] A. T. Winfree, Chaos **1**, 303 (1991).

[54] W. Jahnke and A. T. Winfree, Int. J. Bifurcation and Chaos **1**, 445 (1991).

[55] V. Castets, E. Dulos, J. Boissonade, and P. De Kepper, Phys. Rev. Lett. **64**, 2953 (1990).

[56] Q. Ouyang and H. L. Swinney, Nature **352**, 610 (1991); Chaos **1**, 411 (1991).

[57] B. C . Eu, J. Chem. Phys. **73**, 2958 (1980); **74**, 2998 (1981); **74**, 3006 (1981); **80**, 2123 (1984); **87**, 1220 (1987).

[58] B. C. Eu, Ann. Phys. (NY) **140**, 341 (1982).

[59] B. C. Eu, J. Chem. Phys. **102**, 7169 (1995).

[60] B. C. Eu, Kinetic *Theory and Irreversible Thermodynamics* (Wiley, new York, 1992).

[61] P. Gray and S. K. Scott, *Chemical waves and Instabilities* (Clarendon, Oxford, 1990); P. J. Ortoleva, *Nonlinear Chemical Waves* (Wiley, New York, 1992).

[62] M. Al-Ghoul and B. C. Eu, Physica D **90**, 119 (1996).

[63] M. Al-Ghoul and B. C. Eu, Physica D **97**, 531 (1996)..

[64] M. Al-Ghoul and B. C. Eu, J. Phys. Chem. **100**, 18900 (1996).

[65] M. Al-Ghoul and B. C. Eu, Proc. 50th Anniversary conf. Korean Chem. Soc., May 24, 483 (1996).

[66] M. Al-Ghoul and B. C. Eu (In preperation).

[67] E. E. Selkov, Eur. J. Biochem. **4**, 79 (1968).

[68] P. Richter, P. Rehmus, and J. Ross, Prog. Theoret. Phys. Japan **66**, 385 (1981).

[69] G. Th. Fechner, J. Chem. phys. **53**, 129 (1828).

[70] J. F. Griffiths, Adv. Chem. Phys. **64**, 203 (1986); J. F. Griffiths and S. K. Scott, Prog. Energy Combust. Sci.**13**, 161 (1987).

[71] P. G. Ashmore and R. G. W. Norrish, Nature **167**, 390 (1951).

[72] N. Ganapathisubramanian and K. J. Showalter, J. Chem. Phys. **87**, 1098, 4014 (1983).

[73] J. Turner, J. C. Roux, W. D. McCormick and H. L. Swinney, Phys. Lett. A **85**, 9 (1981).

[74] For an extensive review see: J. L. Hudson and T. T. Tsotsis, Chem Eng. Sci. **49**, 1493 (1994).

[75] E. Ott, C. Grebogi, and J. A. Yorke, Phys. Rev. Lett. **64**, 1196 (1990).

[76] For recent reviews, see: T. Shinbrot; C. Grebogi, E. Ott; J. A. Yorke, Nature **363**, 411 (1993); W. L. Ditto, L. Pecora, Sci. Am. **269**(2), 78 (1993); E. Ott, M. Spano, Phys. Today **48**(5), 34, 1995; K. Showalter, Chem. Br. **31**, 202 (1995).

[77] I. R. Epstein, K. Kustin., P. De Kepper, M. Orbán, Sci. Am. **248**(3), 112, 1983; M. Orbán and I. R. Epstein, J. Am. Chem. Soc. **107**, 2302 (1985).

[78] B. J. Welsh and J. Gomatam, Physica D **43**, 304 (1990).

[79] L. Onsager, Phys. Rev. **37**, 405 (1931); **38**, 2265 (1931).

[80] M. C. Cross and P. C. Hohenberg, Rev. Mod. Phys. **65**, 851 (1993).

[81] For a recent review of experimental and theoretical aspects see: R. Kapral and K. Showalter (eds.), *Chemical Waves and Patterns* (Kluer Academic Publishers, the Netherlands, 1995).

Chapter 2

Model for Glycolysis in One Dimension

2.1 Introduction

Systems undergoing chemical reactions show many different pattern-forming phenomena which combine hydrodynamics with the molecular reactions taking place in chemistry. Many of the traditional spatial patterns occurring in hydrodynamics and in thermodynamics, like Liesegang patterns[1], diffusive instabilities in photochemical reactions[2], and various types of catalytic reactions[3] are strongly influenced by chemical processes[5]. Chemical oscillations and waves have been extensively studied experimentally and theoretically in recent years[5]. More complicated phenomena are biological oscillators, switches and patterns, morphogenesis, etc. In fact, the immensely complex biological systems behave in a highly and compactly efficient manner. Such systems concisely store the information and means of generating the mechanisms required for repetitive cellular reproduction, organization and control. Important examples are the periodic pacemaker in the heart[6], nerve action potentials which are the electrical impulses propagating along a nerve fibre[7], and glycolysis which is treated in this thesis using a very simplified mechanism but captures some qualitative aspects of this very important phenomena. Glycolysis is the process

that breaks down glucose to provide the energy for cellular metabolism: oscillations periods of several minutes are observed in the concentrations of certain chemicals in the process[4]. To study those macroscopic phenomena, continuum theory is used to supply the evolution equations of the macroscopic fields that act on and inside the system. In the field of chemical oscillations and waves, parabolic reaction-diffusion equations have been used to study them theoretically. Since macroscopic processes and phenomena are believed to be subject to the thermodynamic laws, efforts have been made by Prigogine and his school[6, 7] to frame a thermodynamic theory of such phenomena associated with dissipative structures. Their theory has been formulated under the local equilibrium hypothesis and linear thermodynamic force-flux relations for diffusion, heat conduction, and stress with the exception of chemical reactions. In the case of chemical reactions, the constitutive relations are generally nonlinear because of the mass action law. The linear thermodynamic force-flux relations necessarily give rise to a set of parabolic hydrodynamic equations, and the reaction-diffusion equations commonly used for studying chemical waves are typical examples. As a thermodynamic theory, the theory of dissipative structures under the local equilibrium hypothesis requires a generalization since there is no physically inevitable reason that the diffusion fluxes, heat fluxes, or stresses should be constant in time, especially, when the system is in the early stage of evolution, and should obey linear constitutive relations if the system is removed far from equilibrium or subjected to steep thermodynamic gradients. It is indeed possible to formulate a more general thermodynamic theory[8] by removing the local equilibrium hypothesis and generalize the linear thermodynamic force-flux relations to nonlinear relations. In such a generalized theory the evolution equations for macroscopic variables, such as the fluid velocity, concentrations, temperature, etc., can be hyperbolic but not parabolic[1]. In fact, the hyperbolicity of the evolution equations is a more desirable

[1]Second-order partial differential equations are classified into three different types according to the eigenvalues of the characteristic equation. Hyperbolic and parabolic types are two of them. To give simple examples, the well-known diffusion equation is a parabolic differential equation whereas the classical wave equation is a hyperbolic differential equation. The parabolic partial differential equations have only a first-order time derivative and thus the disturbance in the system instan-

feature than the parabolicity since disturbances characterizing waves in macroscopic systems cannot propagate in infinite speed which parabolic partial differential equations for the evolution equations predict them to have[54]. This feature was already noticed by Nicolis and Prigogine in ref. [6], but no attempt has since been made, except in a couple of papers[11, 12], to remedy the weakness of parabolic differential equations as mathematical representations for chemical waves in excitable media. It is true that as far as the mathematical structure of the differential equations in long time is concerned, this aspect is not a great problem for many situations in practice, since if the steady state is stable the fluxes decay to their steady-state values in a sufficiently long time which is often the regime of time where experiments are done, and in that limit the aforementioned distinction between the types of evolution equations disappears because the time dependence is no longer a matter of interest. In fact, both parabolic and hyperbolic differential equations give rise to the same partial differential equation in space. In other words, if the phenomenon of interest reduces to or requires a time-independent description, then the distinction of hyperbolic and parabolic systems disappears. However, if the system is nonlinear and evolves through transient states, despite the mathematical convergence of their structures in the longtime limit one can expect some subtle effects of the hyperbolicity that would not vanish and make the longtime behavior of the system different from the behavior of the system described by a set of parabolic differential equations from the beginning. The reason is that the transient effects survive in time and affect the behavior of the solutions at later times because of the nonlinearity and the well-recognized sensitivity of nonlinear systems to their history.

We assume that the system is free from convection, the temperature is uniform so that there is no heat flow, and there is no stress applied to the system. Furthermore, the fluid is incompressible. Especially, the first set of assumptions is liable

taneously propagates to infinity (*i.e.*, the speed of disturbance propagation is infinite), whereas the hyperbolic partial differential equations have a second-order time derivative and a finite speed of disturbance propagation. For discussions on the classification of second-order partial differential equations, see S. G. Mikhlin, *Mathematical Physics, An Advanced Course* (North-Holland, Amsterdam, 1970).

to be broken in real systems, but they are made to reduce the number of evolution equations so that they become numerically more tractable. These assumptions are also implicit in almost all the works that deal with reaction-diffusion equations in the literature. They will have to be removed in more complete studies in the future. We consider the case of linear diffusion flux evolution equations since it is desired to make comparison with the results by the conventional parabolic reaction-diffusion equations. One must bear in mind that the diffusion flux evolution equations are not generally linear if there is a steep concentration gradient or diffusion is coupled with the stress in the system.

2.2 Generalized Hydrodynamics

Irreversible kinetic equations are not derivable from reversible equations of motion unless approximations are made to break their time reversal invariance symmetry. That is why it is more convenient to postulate a kinetic equation which contains two distinctive features offered by the Boltzmann equation and the Liouville equation. If we add to Liouville equation an irreversible collision term we can obtain such a kinetic equation[15]. It is not necessary to have an explicit form of this collision term to formulate the theory. This collision term is split into two contributions. the elastic collision term denoted by $C[F^{(N)}]$ and the reactive collision term denoted by $\mathcal{R}[F^{(N)}]$. $F^{(N)}$ denotes the N-particle distribution function which obeys the following kinetic equation:

$$\left[\frac{\partial}{\partial t} + L^{(N)}\right] F^{(N)}(x^{(N)};t) = C\left[F^{(N)}\right] + \mathcal{R}\left[F^{(N)}\right], \tag{2.1}$$

where

$$L^{(N)} = \sum_{i=1}^{N} \frac{\mathbf{p}_i}{m_i} \cdot \frac{\partial}{\partial \mathbf{r}_i} - \sum\sum_{i>j} \frac{\partial V_{ij}}{\partial \mathbf{r}_i} \cdot \frac{\partial}{\partial \mathbf{p}_i}. \tag{2.2}$$

It is proven[15] that the collision operator $C[F^{(N)}]$, in the context of a mixture without chemical reactions, has to obey the following general properties: First it

has collision invariants; second, it should be postulated so that the H theorem is satisfied; and third, it should be invariant to canonical transformations for Liouville equation is invariant under such transformations. As a consequence, at equilibrium, the system is described by a Liouville equation:

$$\left[\frac{\partial}{\partial t} + L^{(N)}\right] F_e^{(N)}(x^{(N)}; t) = 0. \tag{2.3}$$

where the collision terms cancel. From equation (2.1) we can derive the evolution of any macroscopic variable which is given as an average of certain microscopic quantities. Note that the development of this theory completely parallels that of gases except for the complications arising from molecular interactions. The statistical average of any molecular quantities $A(x^{(N)}) = \sum_{a=1}^{r} \sum_{j=1}^{N_a} \alpha_{ja}(x^{(N)})\delta(\mathbf{R}_{ja} - \mathbf{r})$ of a species, assuming only pairwise additivity for the two-particle contributions, is given by

$$\bar{A}\left(x^{(N)}, t\right) = \left\langle \sum_{a=1}^{r} \sum_{ja=1}^{N_a} \alpha_{ja}(x^{(N)})\delta(\mathbf{R}_{ja} - \mathbf{r}) F^{(N)} \right\rangle. \tag{2.4}$$

where the angular brackets denotes integration made over phase space variables $x^{(N)}$.

The local form of the evolution of α is given by[15]

$$\rho \frac{d}{dt}\alpha(\mathbf{r}, t) = -\boldsymbol{\nabla} \cdot \boldsymbol{\psi}^{(A)} + \frac{d}{dt}\mathbf{u} \cdot \bar{\mathbf{B}}_1^{(A)} + \bar{\mathbf{B}}_2^{(A)} : (\boldsymbol{\nabla}\mathbf{u})^t - \mathbf{T}_2^{(A)} - \mathbf{T}_3^{(A)} + \Lambda^{(A)}. \tag{2.5}$$

where $\frac{d}{dt} = \frac{\partial}{\partial t} + \mathbf{u} \cdot \boldsymbol{\nabla}$ is the substantial time derivative and

$$\boldsymbol{\psi}^{(A)} = \left\langle \sum_{a=1}^{r} \sum_{ja=1}^{N_a} \mathbf{C}_{ja}\alpha_{ja}(x^{(N)})\delta(\mathbf{R}_{ja} - \mathbf{r}) F^{(N)} \right\rangle, \tag{2.6}$$

$$\bar{\mathbf{B}}_1^{(A)} = \left\langle \sum_{a=1}^{r} \sum_{ja=1}^{N_a} \delta(\mathbf{R}_{ja} - \mathbf{r}) \left[\frac{\partial}{\partial \mathbf{u}}\alpha_{ja}(x^{(N)})\right] F^{(N)} \right\rangle, \tag{2.7}$$

$$\bar{\mathbf{B}}_2^{(A)} = \left\langle \sum_{a=1}^{r} \sum_{ja=1}^{N_a} \mathbf{C}_{ja}\delta(\mathbf{R}_{ja} - \mathbf{r}) \left[\frac{\partial}{\partial \mathbf{u}}\alpha_{ja}(x^{(N)})\right] F^{(N)} \right\rangle, \tag{2.8}$$

$$\mathbf{T}_2^{(A)} = \left\langle \sum_{a=1}^{r} \sum_{ja=1}^{N_a} \delta(\mathbf{R}_{ja} - \mathbf{r}) \frac{\mathbf{p}_{ja}}{m_a} \cdot \left[\nabla_{\mathbf{R}_{ja}} \alpha_{ja}(x^{(N)}) \right] F^{(N)} \right\rangle, \tag{2.9}$$

$$\mathbf{T}_3^{(A)} = \left\langle \sum_{a=1}^{r} \sum_{ja=1}^{N_a} \delta(\mathbf{R}_{ja} - \mathbf{r}) \left(\nabla_{\mathbf{R}_{ja}} V \right) \cdot \left(\nabla_{\mathbf{R}_{ja}} \alpha_{ja}(x^{(N)}) \right) F^{(N)} \right\rangle, \tag{2.10}$$

$$\begin{aligned} \Lambda^{(A)} &= \left\langle \sum_{a=1}^{r} \sum_{ja=1}^{N_a} \alpha_{ja} \delta(\mathbf{R}_{ja} - \mathbf{r}) \left\{ \mathcal{C}[F^{(N)}] + \mathcal{R}[F^{(N)}] \right\} \right\rangle, \\ &= \left\langle \sum_{a=1}^{r} \sum_{ja=1}^{N_a} \alpha_{ja} \delta(\mathbf{R}_{ja} - \mathbf{r}) \mathcal{C}[F^{(N)}] \right\rangle + \left\langle \sum_{a=1}^{r} \sum_{ja=1}^{N_a} \alpha_{ja} \delta(\mathbf{R}_{ja} - \mathbf{r}) \mathcal{R}[F^{(N)}] \right\rangle \\ &= \Lambda_e^{(A)} + \Lambda_R^{(A)}, \end{aligned} \tag{2.11}$$

where $\mathbf{C}_{ja}$ is the peculiar velocity of particle ja of species r. In equation (2.11) $\Lambda^{(A)}$ is the dissipation term due to elastic and reactive collisions. This term is separated into $\Lambda_e^{(A)}$ and $\Lambda_R^{(A)}$ which describe elastic and reactive collisions, respectively. From equation (2.5) we can identify various statistical expressions for the nonconserved variables or fluxes. For example, the mass density is given by

$$\rho = \sum_{a=1}^{r} \rho_r = \left\langle \sum_{a=1}^{r} \sum_{ja=1}^{N_a} m_j \delta(\mathbf{R}_{ja} - \mathbf{r}) F^{(N)} \right\rangle, \tag{2.12}$$

then for $c_a = \rho_a / \rho$,

$$\rho \frac{d}{dt} c_a = -\nabla \cdot \mathbf{J}_a + \Lambda_a^r(c), \tag{2.13}$$

and

$$\mathbf{J}_a = \left\langle h_a^{(\mathbf{J})} \right\rangle = \left\langle \sum_{ja=1}^{Na} m_a \mathbf{C}_{ja} \delta(\mathbf{R}_{ja} - \mathbf{r}) \right\rangle \tag{2.14}$$

is the expression for the diffusion flux. The statistical definitions of other fluxes can be written as: .

$$\mathbf{Q} = \sum_{a=1}^{r} \mathbf{Q}_a = \sum_{a=1}^{r} \left(\left\langle h_a^{(\mathbf{Q})} \right\rangle + \hat{h}_a \mathbf{J}_a \right), \tag{2.15}$$

$$\mathbf{P} = \sum_{a=1}^{r} \mathbf{P}_a = \sum_{a=1}^{r} \left(\left\langle h_a^{(\mathbf{\Pi})} \right\rangle + \left\langle h_a^{(\mathbf{\Delta})} \right\rangle \mathbf{U} + p_a \mathbf{U} \right), \tag{2.16}$$

$$\mathbf{F} = \sum_{a=1}^{r} c_a \mathbf{F}_a, \tag{2.17}$$

with the following definitions of the moments:

$$\begin{aligned} h_a^{(\Pi)} &= \sum_{ja=1}^{N_a} [m_a \mathbf{C}_{ja} \mathbf{C}_{ja}]^{(2)} \, \delta(\mathbf{R}_{ja} - \mathbf{r}) \\ &\quad + \int_0^1 d\lambda \frac{1}{2} \sum_{b=1}^{r} \sum_{ja=1}^{N_a} \sum_{kb=1}^{N_b} F_{jakb} \, [\mathbf{R}_{ja} \mathbf{R}_{ja}]^{(2)} \exp(-\lambda \mathbf{R}_{ja} \cdot \boldsymbol{\nabla}) \, \delta(\mathbf{R}_{jb} - \mathbf{r}). \end{aligned} \tag{2.18}$$

$$\begin{aligned} h_a^{(\Delta)} &= \sum_{ja=1}^{N_a} \frac{1}{3} m_a \mathbf{C}_{ja} \delta(\mathbf{R}_{ja} - \mathbf{r}) - \sum_{ja=1}^{N_a} (m_a p_a / \rho_a) \, \delta(\mathbf{R}_{ja} - \mathbf{r}) \\ &\quad + \int_0^1 d\lambda \frac{1}{6} \sum_{b=1}^{r} \sum_{ja=1}^{N_a} \sum_{kb=1}^{N_b} F_{jakb} \mathbf{R}_{ja} \cdot \mathbf{R}_{ja} \exp(-\lambda \mathbf{R}_{ja} \cdot \boldsymbol{\nabla}) \, \delta(\mathbf{R}_{jb} - \mathbf{r}), \end{aligned} \tag{2.19}$$

$$\begin{aligned} h_a^{(\mathbf{Q})} &= \sum_{ja=1}^{N_a} \left[\frac{1}{2} m_a \mathbf{C}_{ja} + m_a \Psi_a(\mathbf{R}_{ja}) + \frac{1}{2} \sum_{b=1}^{r} \sum_{kb=1}^{N_b} V_{jakb} - m_a \hat{h}_a \right] \mathbf{C}_{ja} \delta(\mathbf{R}_{ja} - \mathbf{r}) \\ &\quad + \int_0^1 d\lambda \frac{1}{2} \sum_{b=1}^{r} \sum_{ja=1}^{N_a} \sum_{kb=1}^{N_b} F_{jakb} \mathbf{R}_{ja} \mathbf{R}_{ja} \exp(-\lambda \mathbf{R}_{ja} \cdot \boldsymbol{\nabla}) \, \delta(\mathbf{R}_{jb} - \mathbf{r}). \end{aligned} \tag{2.20}$$

$$F_{jakb} = -(\partial V_{jakb} / \partial R_{jakb}). \tag{2.21}$$

$$R_{jakb} = | \mathbf{R}_{ja} - \mathbf{R}_{kb} |. \tag{2.22}$$

V_{jakb} in equation (2.21) is the potential between particles ja and kb. In general, fluxes of species a obey the following general evolution equation:

$$\rho \frac{d}{dt} \hat{\Phi}_a^{(A)} = Z_a^{(A)} + \Lambda_a^{(A)}, \tag{2.23}$$

where $Z_a^{(A)}$ is called the kinematic term and is given by

$$Z_a^{(A)} = \left\langle \sum_{ja=1}^{N_a} \left[\left(d_t + \bar{L}^{(N)} \right) h_{ja}^{(\alpha)} \right] \delta(\mathbf{R}_{ja} - \mathbf{r})] F^{(N)} \right\rangle + \left\langle \sum_{ja=1}^{N_a} h_{ja}^{(\alpha)} \left[\bar{L}^{(N)} \delta(\mathbf{R}_{ja} - \mathbf{r}) \right] F^{(N)} \right\rangle, \tag{2.24}$$

$$\bar{L} = = \sum_{a=1}^{r} \sum_{ja=1}^{N_a} \mathbf{C}_{ja} \cdot \frac{\partial}{\partial \mathbf{R}_{ja}} - \frac{\partial V}{\partial \mathbf{R}_{ja}} \cdot \frac{\partial}{\partial \mathbf{P}_{ja}} + \mathbf{F}_a \cdot \frac{\partial}{\partial \mathbf{P}_{ja}}. \tag{2.25}$$

Suppose the fluid consists of an r-component reacting mixture. The generalized hydrodynamic equations for the system, consistent with the thermodynamic laws, are the partial differential equations governing the fluid density ρ, mass fractions c_a of species a, velocity $\mathbf{u}$, internal energy density $\mathcal{E}$, diffusion flux $\mathbf{J}_a$, net heat flux $\mathbf{Q}'_a = \mathbf{Q}_a - \hat{h}_a \mathbf{J}_a$ given in terms of the heat flux $\mathbf{Q}_a$ and the enthalpy $\hat{h}_a$ per mass of species a, shear stress $\mathbf{\Pi}_a = \mathbf{P}_a - \frac{1}{3} Tr \mathbf{P}_a$, excess normal stress $\mathbf{\Delta}_a = \mathbf{P}_a - p_a \mathbf{U}$, etc., where $\mathbf{P}_a$ is the stress (pressure) tensor of species a and p_a is the hydrostatic pressure. The constitutive equations for the mentioned fluxes are then obtained by using equations (2.18), (2.20) and (2.19) into (2.5):

$$\frac{\partial \rho}{\partial t} = -\nabla \cdot \rho \mathbf{u}, \tag{2.26}$$

$$\rho d_t c_a = -\nabla \cdot \mathbf{J}_a + \Lambda_a^r(c), \tag{2.27}$$

$$\rho d_t \mathbf{u} = -\nabla \cdot \mathbf{P} + \rho \mathbf{F}, \tag{2.28}$$

$$\rho d_t \mathcal{E} = -\nabla \cdot \mathbf{Q} - \mathbf{P} : \nabla \mathbf{u} + \sum_{a=1}^{r} \mathbf{F}_a \cdot \mathbf{J}_a, \tag{2.29}$$

$$\rho d_t \hat{\mathbf{J}}_a = -\nabla \cdot \mathbf{P}_a - \rho_a (d_t \mathbf{u} - \mathbf{F}_a) - \mathbf{J}_a \cdot \nabla \mathbf{u} + \mathbf{V}_a^{(\mathbf{J})} + \Lambda_a^{(\mathbf{J})}, \tag{2.30}$$

$$\begin{aligned}\rho d_t \hat{\mathbf{Q}}'_a &= -\boldsymbol{\nabla}\cdot\boldsymbol{\psi}_a^{(\mathbf{Q})} - (d_t\mathbf{u}-\mathbf{F}_a)\cdot(\mathbf{P}_a - p_a\boldsymbol{\delta}) - \left(\mathbf{Q}'_a - \boldsymbol{\varphi}_a^{(\mathbf{Q})}\right)\cdot\boldsymbol{\nabla}\mathbf{u} \\ &\quad -\mathbf{J}_a d_t\hat{h}_a - \mathbf{P}_a\cdot\boldsymbol{\nabla}\hat{h}_a + \mathbf{V}_a^{(\mathbf{Q})} + \Lambda_a^{(\mathbf{Q})}, \end{aligned} \tag{2.31}$$

$$\begin{aligned}\rho d_t \hat{\boldsymbol{\Pi}}_a &= -\boldsymbol{\nabla}\cdot\boldsymbol{\psi}_a^{(\boldsymbol{\Pi})} - 2\left[(d_t\mathbf{u}-\mathbf{F}_a)\,\mathbf{J}_a\right]^{(2)} - 2\left[(\boldsymbol{\Pi}_a + \boldsymbol{\Delta}_a\boldsymbol{\delta})\cdot\boldsymbol{\nabla}\mathbf{u}\right]^{(2)} \\ &\quad -2p_a\left[\boldsymbol{\nabla}\mathbf{u}\right]^{(2)} + \left[\mathbf{V}_a^{(\mathbf{P})}\right]^{(2)} + \Lambda_a^{(\boldsymbol{\Pi})}. \end{aligned} \tag{2.32}$$

$$\begin{aligned}\rho d_t \hat{\boldsymbol{\Delta}}_a &= -\boldsymbol{\nabla}\cdot\boldsymbol{\psi}_a^{(\boldsymbol{\Delta})} - \frac{2}{3}(d_t\mathbf{u}-\mathbf{F}_a)\cdot\mathbf{J}_a - \frac{2}{3}(\boldsymbol{\Pi}_a + \boldsymbol{\Delta}_a\boldsymbol{\delta})\cdot\boldsymbol{\nabla}\mathbf{u} \\ &\quad -p_a d_t ln(p_a v^{5/3}) - \boldsymbol{\nabla}\cdot(\mathbf{J}_a p_a/\rho_a) + \frac{1}{3}\mathbf{V}_a^{(\mathbf{P})} : \mathbf{U} + \Lambda_a^{(\boldsymbol{\Delta})}. \end{aligned} \tag{2.33}$$

In these equations, the various symbols are defined by

$\hat{\mathbf{J}}_a = \mathbf{J}_a/\rho$, $\hat{\mathbf{Q}}'_a = \mathbf{Q}'_a/\rho$, $\hat{\boldsymbol{\Pi}}_a = \boldsymbol{\Pi}_a/\rho$, $\hat{\boldsymbol{\Delta}}_a = \boldsymbol{\Delta}_a/\rho$, $\mathbf{P} = \sum_{a=1}^{r}\mathbf{P}_a$, $\mathbf{Q} = \sum_{a=1}^{r}\mathbf{Q}_a$, $\Lambda_a^r(c)$ is the reaction rate for species a; $\Lambda_a^{(\mathbf{J})}$, $\Lambda_a^{(\mathbf{Q})}$, $\Lambda_a^{(\boldsymbol{\Pi})}$, and $\Lambda_a^{(\boldsymbol{\Delta})}$ are the dissipation terms which are generally nonlinear functions of the macroscopic variables (Gibbs variables) T, ρ, c_a, $\mathbf{J}_a$, $\mathbf{Q}'_a$, $\boldsymbol{\Pi}_a$, $\boldsymbol{\Delta}_a$, etc.; $\boldsymbol{\psi}_a^{(\mathbf{Q})}$, $\boldsymbol{\psi}_a^{(\boldsymbol{\Pi})}$, and $\boldsymbol{\psi}_a^{(\boldsymbol{\Delta})}$ are fluxes of $\mathbf{Q}'_a$, $\boldsymbol{\Pi}_a$, and $\boldsymbol{\Delta}_a$, respectively. They are given by

$$\begin{aligned}\boldsymbol{\psi}_a^{(\boldsymbol{\Delta})} &= \sum_{ja=1}^{N_a}\Big\langle \mathbf{C}_{ja}\left[m_a\mathbf{C}_{ja}\mathbf{C}_{ja}\right]^{(2)}\delta(\mathbf{R}_{ja}-\mathbf{r}) \\ &\quad +\frac{1}{2}\sum_{b=1}^{r}\sum_{kb\neq ja}^{N_b}\mathbf{F}_{jakb}\mathbf{C}_{ja}\left[\mathbf{R}_{jakb}\mathbf{R}_{jakb}\right]^{(2)}\delta(\mathbf{R}_{ja}-\mathbf{r})\Big\rangle, \end{aligned} \tag{2.34}$$

$$\boldsymbol{\psi}_a^{(\boldsymbol{\Pi})} = \frac{1}{3}\sum_{ja=1}^{N_a}\left\langle \delta(\mathbf{R}_{ja}-\mathbf{r})\left[m_a C_{ja}^2 + \frac{1}{2}\sum_{b=1}^{r}\sum_{kb\neq ja}^{N_b}\mathbf{F}_{jakb}\mathbf{R}_{jakb}\cdot\mathbf{R}_{jakb} - \frac{m_a p_a}{\rho_a}\right]\mathbf{C}_{ja}\right\rangle, \tag{2.35}$$

$$\begin{aligned}\boldsymbol{\psi}_a^{(\mathbf{Q})} &= \sum_{ja=1}^{N_a}\left\langle \delta(\mathbf{R}_{ja}-\mathbf{r})\left[\frac{1}{2}m_a C_{ja}^2 + \frac{1}{2}\sum_{b=1}^{r}\sum_{kb\neq ja}^{N_b}V_{jakb}\right]\mathbf{C}_{ja}\mathbf{C}_{ja}\right\rangle \\ &\quad +\Big\langle\frac{1}{2}\delta(\mathbf{R}_{ja}-\mathbf{r})\sum_{b=1}^{r}\sum_{kh\neq ja}^{N_b}\mathbf{F}_{jakb}\left(\mathbf{R}_{jakb}\mathbf{C}_{ja}\cdot\mathbf{C}_{ja}\mathbf{R}_{jakb} + \mathbf{R}_{jakb}\mathbf{R}_{jakb}\cdot\mathbf{C}_{ja}\mathbf{C}_{ja}\right. \\ &\quad \left.+\mathbf{R}_{jakb}\mathbf{C}_{ja}\mathbf{R}_{jakb}\cdot\mathbf{C}_{ja} + \mathbf{C}_{ja}\mathbf{R}_{jakb}\mathbf{R}_{jakb}\cdot\mathbf{C}_{ja}\right)\Big\rangle - \hat{h}_a\mathbf{P}_a. \end{aligned} \tag{2.36}$$

The higher order flux $\varphi_a^{(\mathbf{Q})}$ is a function of T, ρ, c_a, $\mathbf{J}_a$, $\mathbf{Q}'_a$, $\mathbf{\Pi}_a$, $\mathbf{\Delta}_a$, etc.

$$\varphi_a^{(\mathbf{Q})} = \sum_{ja=1}^{N_a} \left\langle \delta(\mathbf{R}_{ja} - \mathbf{r}) \left[m_a \mathbf{C}_{ja}\mathbf{C}_{ja}\mathbf{C}_{ja} + \frac{1}{2} \sum_{b=1}^{r} \sum_{kb \neq ja}^{N_b} \mathbf{F}_{jakb} \left[\mathbf{R}_{jakb}\mathbf{R}_{jakb}\mathbf{C}_{ja} \right] \right] \right\rangle . \tag{2.37}$$

The $\mathbf{F}$ is the external force per mass and $\mathbf{F}_a$ is the species component of $\mathbf{F}$ such that $\mathbf{F} = \sum_a c_a \mathbf{F}_a$. The $\boldsymbol{\delta}$ is the unit second-rank tensor and $[\mathbf{A}]^{(2)}$ denotes the traceless symmetric part of the second-rank tensor $\mathbf{A}$. The terms $\mathbf{V}_a^{(\mathbf{P})}$, $\mathbf{V}_a^{(\mathbf{Q})}$, and $\mathbf{V}_a^{(\mathbf{J})}$ are higher order moments which contain some molecular information:

$$\begin{aligned} \mathbf{V}_a^{(\mathbf{P})} &= \sum_{b=1}^{r} \sum_{\substack{ja=1 \\ (ja \neq kb)}}^{N_a} \sum_{kb=1}^{N_b} \langle \delta(\mathbf{R}_{ja} - \mathbf{r}) \mathbf{F}_{jakb} \left\{ (\mathbf{C}_{ja} - \mathbf{C}_{kb}) \mathbf{R}_{jakb} \right\} \rangle \\ &\quad + \left\langle \frac{1}{2} \delta(\mathbf{R}_{ja} - \mathbf{r}) \mathbf{F}^{(2)}_{jakb} (\mathbf{C}_{ja} - \mathbf{C}_{kb}) \cdot \mathbf{R}_{jakb}\mathbf{R}_{jakb}\mathbf{R}_{jakb} \right\rangle , \end{aligned} \tag{2.38}$$

$$\begin{aligned} \mathbf{V}_a^{(\mathbf{Q})} &= \sum_{b=1}^{r} \sum_{\substack{ja=1 \\ (ja \neq kb)}}^{N_a} \sum_{kb=1}^{N_b} \langle \delta(\mathbf{R}_{kb} - \mathbf{r}) \mathbf{F}_{jakb} \left(\mathbf{C}_{ja} \cdot \mathbf{C}_{ja}\mathbf{R}_{jakb} + 2\mathbf{C}_{ja}\mathbf{R}_{jakb} \cdot \mathbf{C}_{ja} \right) \rangle \\ &\quad + \langle \delta(\mathbf{R}_{ja} - \mathbf{r}) \mathbf{F}_{jakb} \left[(\mathbf{C}_{ja}\mathbf{C}_{kb} - \mathbf{C}_{kb}\mathbf{C}_{ja}) \cdot \mathbf{R}_{jakb} + \mathbf{C}_{ja} \cdot (\mathbf{C}_{ja} - \mathbf{C}_{kb}) \mathbf{R}_{jakb} \right] \rangle \\ &\quad + \left\langle \delta(\mathbf{R}_{ja} - \mathbf{r}) \mathbf{F}^{(2)}_{jakb} (\mathbf{C}_{ja} - \mathbf{C}_{kb}) \cdot \mathbf{R}_{jakb}\mathbf{R}_{jakb} \cdot \mathbf{C}_{ja}\mathbf{R}_{jakb} \right\rangle \\ &\quad + \langle \delta(\mathbf{R}_{ja} - \mathbf{r}) \mathbf{F}_{jakb}\mathbf{R}_{jakb}\mathbf{R}_{jakb} (V_{jakb} + \mathbf{F}_{jakb}\mathbf{R}_{jakb} \cdot \mathbf{R}_{jakb}) \rangle , \end{aligned} \tag{2.39}$$

$$\mathbf{V}_a^{(\mathbf{J})} = -\frac{1}{2} \sum_{\substack{ja=1 \\ (ja \neq kb)}}^{N_a} \sum_{kb=1}^{N_b} \left\langle \left(\frac{\partial V_{jakb}}{\partial R_{jakb}} \right) \left[\delta(\mathbf{R}_{ja} - \mathbf{r}) + \delta(\mathbf{R}_{kb} - \mathbf{r}) \right] \right\rangle . \tag{2.40}$$

2.3 Hyperbolic Reaction-Diffusion Equations and Irreversible Thermodynamics

Chemical oscillations and waves are macroscopic phenomena and, as such, their description is made by means of the evolution equations of macroscopic variables which must be subjected to the thermodynamic laws. The generalized hydrodynamic

theory[8] on which the present work is based is consistent with the thermodynamic laws. The collection of evolution equations for macroscopic variables required to describe flow phenomena in a general context is presented in the previous section. In what follows we will derive thermodynamic quantities which we will use in connection with the dissipative structures computed later in this chapter. The dissipation terms, together with the kinematic terms (*i.e.*, the rest of the terms on the right-hand side of the flux evolution equations), obey an inequality related to the second law of thermodynamics, and when the dissipation terms are chosen under such condition, the system of evolution equations (2.26)-(2.33) is made consistent[16] with the thermodynamic laws. If the stoichiometric coefficient times the mass of species a involved in reaction k is denoted by ν_{ak} under the convention that it is counted as positive if it is associated with a product and negative if it is associated with a reactant, then for a system of m reactions the reactive dissipation term is given by the reaction rate formula

$$\Lambda_a^r(c) = \sum_{k=1}^{m} \nu_{ak} R_k \tag{2.41}$$

where R_k is the rate of reaction k obeying the mass action law. It is convenient to write the evolution equations (2.30)-(2.33) for nonconserved variables ($\mathbf{J}_a$, $\mathbf{Q}'_a$, $\mathbf{\Pi}_a$, $\mathbf{\Delta}_a$) in a general form

$$\rho d_t \hat{\Phi}_a^{(q)} = -\nabla \cdot \psi_a^{(q)} + \mathcal{Z}_a^{(q)} + \Lambda_a^{(q)} \qquad (q \geq 1) \tag{2.42}$$

by suitably ordering the nonconserved variables. Here $\Lambda_a^{(q)}$ represents the dissipative terms $\Lambda_a^{(\mathbf{J})}$, $\Lambda_a^{(\mathbf{Q})}$, etc. appearing in (2.30)-(2.33) and $\mathcal{Z}_a^{(q)}$ the remainder of the right-hand side of the evolution equation. These evolution equations (2.42), which are constitutive equations, and the conservation laws (2.26)-(2.29) must be subjected to the second law of thermodynamics if their description of macroscopic processes is to be thermodynamically legitimate. According to the theory developed in Refs. [8, 16, 18], the second law of thermodynamics demands that there exists an exact

differential $d_t\hat{\Psi}$ in the form

$$d_t\hat{\Psi} = T^{-1}(d_t\mathcal{E} + pd_tv - \sum_{a=1}^{r}\hat{\mu}_a d_t c_a + \sum_{a=1}^{r}\sum_{q\geq 1} X_a^{(q)} d_t\hat{\Phi}_a^{(q)}) \tag{2.43}$$

where $X_a^{(q)}$ are constitutive parameters depending on the variables $G = (\mathcal{E}, v, c_a, \mathbf{J}_a, \mathbf{Q}'_a, \mathbf{\Pi}_a, \mathbf{\Delta}_a, ...)$. In the phenomenological theory these constitutive parameters should be suitably assumed to be functions of the variables in G. The quantity $\hat{\Psi}$ is called the calortropy[18]. This is a nonequilibrium generalization of the equilibrium entropy introduced by Clausius for reversible processes or equilibrium. The second law also demands that the following inequality is satisfied by the evolution equations (2.26)-(2.33):

$$\Xi_c \equiv -T^{-1}\sum_{a=1}^{r}[(\mathbf{\Pi}_a + \Delta_a\delta) : \nabla\mathbf{u} + \mathbf{Q}_a^c \cdot \nabla lnT + \mathbf{J}_a \cdot (\nabla\hat{\mu}_i - \mathbf{F}_a) -$$
$$\sum_{q\geq 1}\psi_a^{(q)} \cdot \nabla X_a^{(q)} + \sum_{k=1}^{m}\hat{\mu}_a\nu_{ak}R_k] + T^{-1}\sum_{a=1}^{r}\sum_{q\geq 1} X_a^{(q)}\left(\mathcal{Z}_a^{(q)} + \Lambda_a^{(q)}\right) \geq 0. \tag{2.44}$$

Here

$$\mathbf{Q}_a^c = \mathbf{Q}_a - \hat{\mu}_a\mathbf{J}_a + \psi_a^{(q)}X_a^{(q)}. \tag{2.45}$$

The Ξ_c is called the calortropy production. This condition (2.44) is a generalized form of the calortropy production obtained in Refs. [16, 18]. The present generalized form includes a reactive contribution absent in the previous form. If we adopt the assumptions stated earlier, then there remain the evolution equations (2.27) and (2.30). Furthermore, we linearize the kinematic terms $\mathcal{Z}_a^{(\mathbf{J})}$ and retain only the thermodynamic force term depending on the concentration gradient:

$$\mathcal{Z}_a^{(\mathbf{J})} = -\left(\frac{k_bT}{m_a}\right)\nabla\rho_a. \tag{2.46}$$

We also linearize the dissipation terms to the linear form:

$$\Lambda_a^{(\mathbf{J})} = -\sum_{b=1}^{r} L_{ab}\mathbf{J}_b \tag{2.47}$$

where L_{ab} are phenomenological coefficients obeying the Onsager reciprocal relations:

$$L_{ab} = L_{ba} \tag{2.48}$$

The diffusion coefficients are defined in terms of $\mathbf{L} = (L_{ab})$

$$D_{ab} = \left(\frac{k_b T}{m_a}\right)\left(L^{-1}\right)_{ab}. \tag{2.49}$$

In addition to the aforementioned assumptions, the constitutive parameters $X_a^{(\mathbf{J})}$ are approximated by the linear form[8]

$$X_a^{(\mathbf{J})} = -\mathbf{J}_a/\rho_a = -\hat{\mathbf{J}}_a/c_a. \tag{2.50}$$

In these approximations, the calortropy production (2.44) takes the form

$$\Xi_c = -T^{-1}\sum_{a=1}^{r}\left[\mathbf{J}_a\cdot\boldsymbol{\nabla}\hat{\mu}_a - \psi_a^{(\mathbf{J})}\cdot\boldsymbol{\nabla}X_a^{(\mathbf{J})} + \sum_{k=1}^{m}\hat{\mu}_a\nu_{ak}R_k\right] + T^{-1}\sum_{a=1}^{r}X_a^{(\mathbf{J})}(\mathcal{Z}_a^{(\mathbf{J})}+\Lambda_a^{(\mathbf{J})}) \geq 0. \tag{2.51}$$

The term $\sum_a \psi_a^{(\mathbf{J})}\boldsymbol{\nabla}X_a^{(\mathbf{J})}$ does not appear in the approximation neglecting higher-order fluxes other than $\mathbf{J}_a$. Furthermore, if the solution is assumed to be ideal, then the chemical potentials are given by $\mu_a = \mu_a^0(T,P) + k_b T ln\rho_a$. Consequently, by using this form of chemical potential μ_a and approximations (2.46) and (2.50), we find

$$-\mathbf{J}_a\cdot\boldsymbol{\nabla}\hat{\mu}_a + \sum_{i=1}^{r}X_a^{(\mathbf{J})}\mathcal{Z}_a^{(\mathbf{J})} = 0. \tag{2.52}$$

Moreover, the chemical reaction part of the calortropy production may be written in the form

$$\Xi_{chem} = -T^{-1}\sum_{a=1}^{r}\sum_{k=1}^{m}\hat{\mu}_a\nu_{ak}R_k, \tag{2.53}$$

where $R_k^{(+)}$ and $R_k^{(-)}$ are the forward and reverse reaction rates of the kth reaction, respectively, for which we have used the mass action law. On use of (2.47) for $\Lambda_a^{(\mathbf{J})}$ in (2.51), we find the diffusion part of Ξ_c to be in the form

$$\sum_{a=1}^{r} X_a^{(\mathbf{J})} \Lambda_a^{(\mathbf{J})} = \sum_{a=1}^{r} \sum_{b=1}^{r} \rho_a^{-1} L_{ab} \mathbf{J}_a \cdot \mathbf{J}_b. \tag{2.54}$$

Therefore, the total calortropy production is given by the formula

$$\Xi_c = k_b \sum_{k=1}^{m} \left(R_k^{(+)} - R_k^{(-)} \right) \ln \left(\frac{R_k^{(+)}}{R_k^{(-)}} \right) + T^{-1} \sum_{a=1}^{r} \sum_{b=1}^{r} \rho_a^{-1} L_{ab} \mathbf{J}_a \cdot \mathbf{J}_b \geq 0. \tag{2.55}$$

In the approximations enumerated earlier, this form of calortropy production Ξ_c completely coincides with the entropy production in the theory of linear irreversible processes[6]. Therefore, we will henceforth use the more familiar but less general term, entropy production, for it in deference to the traditional terminology. (This does not mean that the calortropy production is the same as the entropy production in general.) This form of entropy production clearly consists of two parts: one is chemical and the other is diffusion. It will be examined numerically when various patterns emerge for the solutions of the hyperbolic partial differential equation system under consideration. Under the assumptions enumerated earlier, the hyperbolic differential equations are

$$\frac{\partial}{\partial t} \rho_a = -\nabla \cdot \mathbf{J}_a + \sum_{k=1}^{m} \nu_{ak} R_k \ (a = 1, ..., r), \tag{2.56}$$

$$\frac{\partial}{\partial t} \mathbf{J}_a = -(k_b T / m_a) \nabla \rho_a - \sum_{b=1}^{r} L_{ab} \mathbf{J}_b \ (a = 1, ..., r). \tag{2.57}$$

This set of evolution equations will be used for a cubic reversible chemical reaction model.

2.4 Cubic Reversible Chemical Reaction Model

In this thesis, we compare hyperbolic and parabolic reaction-diffusion equations, this time, by using a model mimicking the nonlinearity of the modified form[55] of the Selkov model[14] for glycolysis and therefore reversible in chemical kinetics. We note that the Selkov model has been studied in the literature[15] by means of a lattice Boltzmann equation devised to yield parabolic reaction-diffusion equations. However, the Boltzmann equation generally gives rise to hyperbolic partial differential equations presented below, if the Maxwell-Grad moment method is used[8]. In addition to assessing the utility of hyperbolic reaction-diffusion equations, we examine the modes of energy-matter dissipation by the system and its possible connection with, or implications for, pattern formations when a particular pattern emerges from another as the system evolves under a given set of initial and boundary conditions. As will be shown later, a rather interesting picture emerges as to how the system utilizes energy or matter to organize itself into a pattern in space-time and maintain it. We hope to better understand eventually the role of thermodynamic principles, if they play a role at all, in pattern formation through this type of study. In the study of control and dissipation in chemical engines, Richter et al.[55] modified the Selkov model[14] which consists of three steps of chemical reactions

$$A \underset{k_{-1}}{\overset{k_1}{\rightleftharpoons}} S$$

$$S + 2P \underset{k_{-2}}{\overset{k_2}{\rightleftharpoons}} 3P$$

$$P \underset{k_{-3}}{\overset{k_3}{\rightleftharpoons}} B$$

In these reactions A and B are kept at fixed concentrations and the intermediates S and P change in time. In this work, we take this chemical reaction system as a model and construct the evolution equations under the assumption that these species also depend on position. The reaction rates for the two intermediate species S and

P are given by

$$R_s = k_1\rho_a - k_{-1}\rho_s - k_2\rho_s\rho_p^2 + k_{-2}\rho_p^3 \tag{2.58}$$

$$R_p = k_2\rho_s\rho_p^2 - k_{-2}\rho_p^3 - k_3\rho_p + k_{-3}\rho_b \tag{2.59}$$

where k_i and k_{-i} represent the reaction rate constants for the forward and reverse reactions in the ith step, respectively. To make our equations simpler we assume that the phenomenological coefficients $L_{sp} = L_{ps}$ are equal to zero. We remark that this assumption is generally not valid for real systems, but it is taken here to make the equations simpler to study. This assumption is also taken in virtually all works on chemical waves in the literature. The evolution equations then are:

$$\partial_t\rho_p = -\nabla\cdot\mathbf{J}_p + k_2\rho_s\rho_p^2 - k_{-2}\rho_p^3 - k_3\rho_p + k_{-3}\rho_b, \tag{2.60}$$

$$\partial_t\rho_s = -\nabla\cdot\mathbf{J}_s + k_1\rho_a - k_{-1}\rho_s - k_2\rho_s\rho_p^2 + k_{-2}\rho_p^3, \tag{2.61}$$

$$\partial_t\mathbf{J}_p = -(k_bT/m_p)\nabla\rho_p - L_{pp}\mathbf{J}_p, \tag{2.62}$$

$$\partial_t\mathbf{J}_s = -(k_bT/m_s)\nabla\rho_s - L_{ss}\mathbf{J}_s. \tag{2.63}$$

Here $\partial_t = \partial/\partial t$. Since it is convenient to work with dimensionless equations, the following reduced variables are introduced:

$$\tau = k_3t,\ \xi = r/L,$$

$$X = \rho_p/(k_3/k_2)^{1/2},\ Y = \rho_s/(k_3/k_2)^{1/2},$$

$$\mathbf{u} = \mathbf{J}_p/Lk_3(k_3/k_2)^{1/2},\ \mathbf{v} = \mathbf{J}_s/Lk_3(k_3/k_2)^{1/2},$$

$$A = (k_1/k_3)(k_2/k_3)^{1/2}\rho_a,\ B = (k_{-3}/k_3)(k_2/k_3)^{1/2}\rho_b,$$

$$K = k_{-2}/k_2,\ R = k_{-1}/k_3.$$

With these reduced variables, the evolution equations take the forms

$$\partial_\tau X = -\boldsymbol{\nabla}_\xi \cdot \mathbf{u} + B - X + X^2Y - KX^3, \tag{2.64}$$

$$\partial_\tau Y = -\boldsymbol{\nabla}_\xi \cdot \mathbf{v} + A - RY - X^2Y + KX^3, \tag{2.65}$$

$$\partial_\tau \mathbf{u} = -N_{rd} f(\hat{D}_x \boldsymbol{\nabla}_\xi X + \mathbf{u}), \tag{2.66}$$

$$\partial_\tau \mathbf{v} = -N_{rd} f^{-1}(\hat{D}_y \boldsymbol{\nabla}_\xi Y + \mathbf{v}), \tag{2.67}$$

where the reaction-diffusion number N_{rd} is defined by

$$N_{rd} = [k_b T/(m_p m_s)^{1/2}]k_3^{-1}(D_s D_p)^{-1/2} \tag{2.68}$$

and other dimensionless parameters are:

$$f = (m_s D_s/m_p D_p)^{1/2}, \tag{2.69}$$

$$\hat{D}_x \equiv \hat{D}_p = D_p/(k_3 L^2), \tag{2.70}$$

$$\hat{D}_y \equiv \hat{D}_s = D_s/(k_3 L^2). \tag{2.71}$$

The diffusion coefficients D_p and D_s are defined by the diagonal components of $\mathbf{D}_{ab}$ in (2.49). They are essentially the self-diffusion coefficients. The reaction-diffusion number gives a measure of relative time scales of the diffusion flux evolution to the chemical evolution of material species X and Y when the reduced time is reckoned in the relative scale of the rate constant k_3 and the mean diffusion constant to the sound speed; see (2.68). The characteristic determinant of this system of differential equations (2.64), (2.65) and (2.66), (2.67) is

$$\det \begin{pmatrix} -\lambda & 0 & 1 & 0 \\ 0 & -\lambda & 0 & 1 \\ N_{rd} D_x f & 0 & -\lambda & 0 \\ 0 & N_{rd} D_y / f & 0 & \lambda \end{pmatrix} = 0$$

which gives the eigenvalues

$$\lambda_1, \lambda_2, \lambda_3, \lambda_4 = \pm\sqrt{(N_{rd}\hat{D}_x f)}, \pm\sqrt{(N_{rd}\hat{D}_y/f)} \tag{2.72}$$

Since these eigenvalues are all real, the system is seen to be hyperbolic. If the mean diffusion coefficient is of the order of $10^{-9} m^2 s^{-1}$ and the rate constant is of the order of $10^{12} s^{-1}$, then the reaction-diffusion number N_{rd} is of the order of 10^2 at the room temperature. In this case, the transient time regime must be described by the hyperbolic wave equations, but in the longtime regime the system behaves as if it is parabolic. It is helpful to put the equations in the form of wave equations to have better insight to them in relation to the classical theory of waves. To this end, if the first two equations (2.64) and (2.65) in the aforementioned set of evolution equations are differentiated with τ and the flux evolution equations (2.66) and (2.67)

are used, the following second-order partial differential equations in time and space are obtained:

$$\partial_\tau^2 \mathbf{Z} + \bar{N}_{rd}\mathbf{H}\partial_\tau \mathbf{Z} - \bar{N}_{rd}\mathbf{D}\nabla_\xi^2 \mathbf{Z} = \bar{N}_{rd}\mathbf{R}(X,Y) \tag{2.73}$$

where $\bar{N}_{rd} = N_{rd}f$,

$$\mathbf{Z} = \begin{pmatrix} X \\ \\ Y \end{pmatrix}. \tag{2.74}$$

$$\mathbf{R} = \begin{pmatrix} B - X + X^2Y - KX^3 \\ \\ (A - RY - X^2Y + KX^3)f^{-2} \end{pmatrix} =$$

$$\begin{pmatrix} 1 & 0 \\ \\ 0 & f^{-2} \end{pmatrix} \begin{pmatrix} B - X + X^2Y - KX^3 \\ \\ A - RY - X^2Y + KX^3 \end{pmatrix} \equiv f_2\mathbf{R}', \tag{2.75}$$

$$\mathbf{D} = \begin{pmatrix} \hat{D}_x & 0 \\ \\ 0 & \hat{D}_y f^{-2} \end{pmatrix} = \begin{pmatrix} 1 & 0 \\ \\ 0 & f^{-2} \end{pmatrix} \begin{pmatrix} \hat{D}_x & 0 \\ \\ 0 & \hat{D}_y \end{pmatrix}, \tag{2.76}$$

$$\mathbf{H} = \begin{pmatrix} H_{xx} & H_{xy} \\ \\ H_{yx} & H_{yy} \end{pmatrix}. \tag{2.77}$$

with the definitions

$$H_{xx} = 1 + (1 - 2XY + 3KX^2)/\bar{N}_{rd}, \tag{2.78}$$

$$H_{xy} = -X^2/\bar{N}_{rd}, \tag{2.79}$$

$$H_{yx} = (2XY - 3KX^2)/\bar{N}_{rd}, \tag{2.80}$$

$$H_{yy} = f^{-2} + (R + X^2)/\bar{N}_{rd}. \tag{2.81}$$

Eq. (2.73) is a set of coupled nonlinear telegraphist equations. This kind of wave equations also appears in the context of shear flows in a non-Newtonian fluid[8]. Since the eigenvalues in (2.72)–roughly speaking, of the inverse coefficient matrix to the spatial second derivative term in (2.73)–are the wave velocities (group velocity, more precisely) which are proportional to $\sqrt{\bar{N}_{rd}}^2$, we see that as $\sqrt{\bar{N}_{rd}}$ or the wave speed increases to infinity, the coupled wave equations reduce to the parabolic reaction-diffusion equations

$$\partial_\tau \mathbf{Z} - \hat{\mathbf{D}}\nabla_\xi^2 \mathbf{Z} = \mathbf{R}'(X, Y), \tag{2.82}$$

for which use is made of $\mathbf{H}_\infty = \mathbf{H}(\bar{N}_{rd} = \infty) = f_2$ and

$$f_2 = \begin{pmatrix} 1 & 0 \\ 0 & f^{-2} \end{pmatrix}, \tag{2.83}$$

$$\hat{\mathbf{D}} = \begin{pmatrix} \hat{D}_x & 0 \\ 0 & \hat{D}_y \end{pmatrix}, \tag{2.84}$$

$$\mathbf{R}' = \begin{pmatrix} B - X + X^2 Y - KX^3 \\ A - RY - X^2 Y + KX^3 \end{pmatrix}. \tag{2.85}$$

Eq. (2.82) clearly shows that the parabolic differential equation system is the infinite wave speed limit of the corresponding hyperbolic differential equation system. Since the disturbance cannot propagate at infinite speed, the hyperbolic system is physi-

[2]The mean wave velocity c may be defined by $2/c^2 = 1/c_x^2 + 1/c_y^2$. If $\hat{D}_x = \hat{D}_y f^2$, then $c = (\bar{N}_{rd}\hat{D}_x)^{1/2}$.

cally more appropriate than the parabolic system, which can give rise to physically unrealistic situations. For example, if the medium is inflammable, our everyday experience indicates that the flame set off at a point (say, a boundary) cannot propagate instantly through the medium to infinity. But the parabolic reaction-diffusion equations would predict otherwise.

For further study on the difference between the hyperbolic and parabolic systems with respect to the wave speed, one can look at the appendix at the end of the chapter.

2.5 Steady States

The steady states can be homogeneous or inhomogeneous. Since the properties of homogeneous and inhomogeneous steady states are significantly different, they will be studied separately.

2.5.1 Homogeneous Steady States

If the system is homogeneous in space, then

$$\nabla_\xi^2 \mathbf{Z}_h = 0 \tag{2.86}$$

and the wave equation becomes

$$\partial_\tau^2 \mathbf{Z}_h + \bar{N}_{rd} \mathbf{H}_h \partial_\tau \mathbf{Z}_h = \bar{N}_{rd} \mathbf{R}(X_h, Y_h) \tag{2.87}$$

where $\mathbf{Z}_h$, X_h, and Y_h denote the spatially homogeneous solutions and $\mathbf{H}_h$ stands for $\mathbf{H}$ evaluated with such solutions. The homogeneous steady state solution is then defined by

$$\partial_\tau \mathbf{Z}_0 = 0, \tag{2.88}$$

or

$$\mathbf{R}(X_0, Y_0) = 0. \tag{2.89}$$

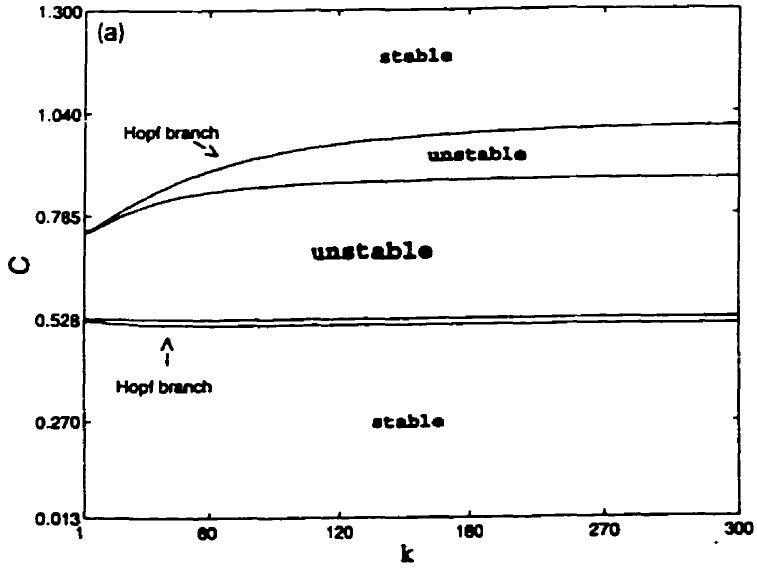

Figure 2-1: *Stability phase diagram for the hyperbolic system. This diagram is constructed by using the Hurwitz conditions in the case of* $R = 0.1$. $K = 1$, $f = 1$, *and* $B = 0.09$. *It must be noted that all modes of* k *can give rise to an unstable steady state. They are therefore potential candidates for a Turing instability mode. This feature is distinctive from the parabolic case shown in Fig. 2-3.*

Written out explicitly, this equation yields a pair of the algebraic equations

$$B - X_0 + X_0^2 Y_0 - K X_0^3 = 0, \tag{2.90}$$

$$A - R Y_0 - X_0^2 Y_0 + K X_0^3 = 0. \tag{2.91}$$

This set may be rearranged to the equations

$$Y_0 = (A + B - X_0)/R, \tag{2.92}$$

$$K X_0^3 + a_2 X_0^2 + a_1 X_0 + a_0 = 0, \tag{2.93}$$

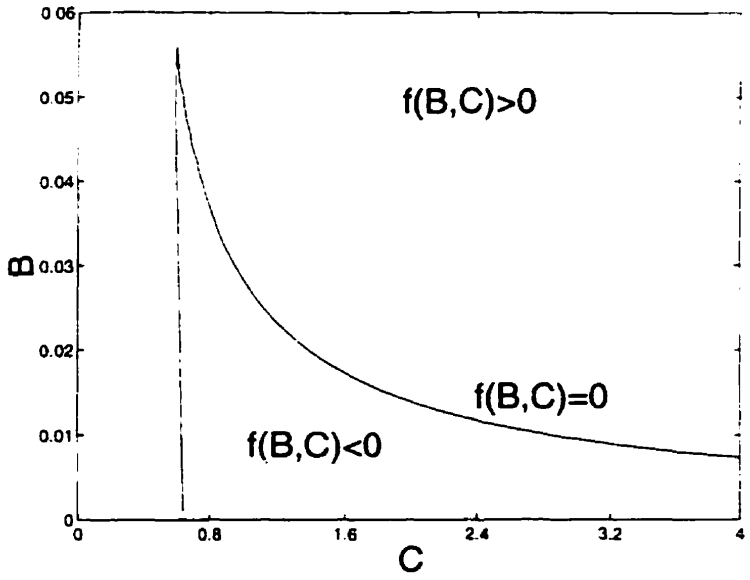

Figure 2-2: *Stability phase diagram for homogeneous steady states. In the domain where $f(B,C) > 0$, there are one real root and two complex conjugate roots. In the domain where $f(B,C) < 0$, there are three distinct real roots. One root is unstable and the other two are stable; thus the system is bistable. On the curve $f(B,C) = 0$, there are one single and a pair of double roots all of which are real.*

where

$$a_2 = -(A+B)/(1-KR), \tag{2.94}$$

$$a_1 = R/(1-KR), \tag{2.95}$$

$$a_0 = -RB/(1-KR) = -Ba_1. \tag{2.96}$$

There can be one or three real roots of the algebraic equation, depending on the values of the parameters. There are two parameters which are experimentally variable: A and B. Therefore, it is useful to investigate the domains of the variables A and B where the root structure changes. For this purpose it is convenient to use a new parameter set (B,C), where $C = A + B$, instead of the set (A,B). The

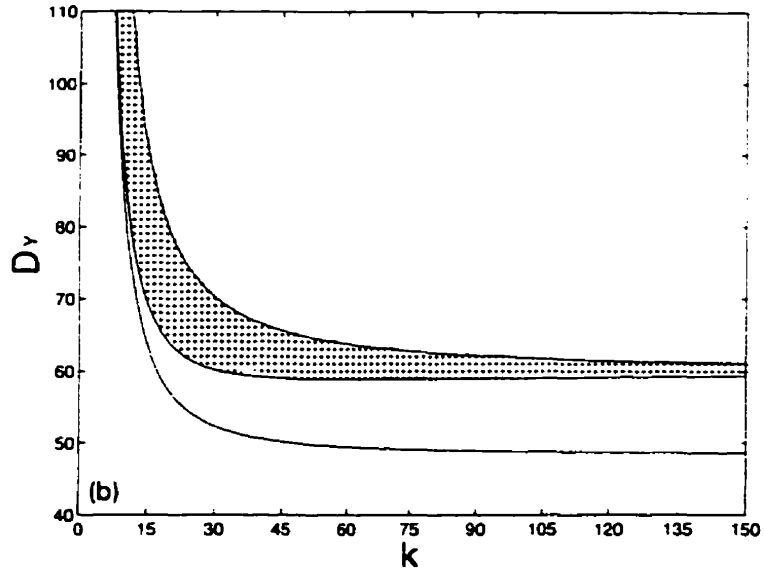

Figure 2-3: *Stability phase diagram for the hyperbolic system plotted in another way in the* $(k, \hat{D}_y)$ *plane. The shaded region is for the stable phase. For this diagram* $\hat{D}_x$ *is fixed at* $\hat{D}_x = 0.006$ *together with* $f = 1$. *The ordinate is in the units of* 10^{-4}.

discriminant of (2.93) takes the following form

$$f(B, C) = 4\alpha^{-2}\left[B^2 + 4\lambda B/\alpha + 4(\lambda^2 - q^3)/\alpha^2\right]. \tag{2.97}$$

where

$$\alpha = a_1, \tag{2.98}$$

$$\lambda(C) = -\alpha^2 C/6R + \alpha^3 C^3/27R^3, \tag{2.99}$$

$$q(C) = (\alpha/3)\left(\alpha C^2/3R^2 - 1\right). \tag{2.100}$$

Therefore, there is one real and two complex conjugate roots if $f(B,C) > 0$ which yields the conditions

$$B + 2\left[\lambda(C) \pm q^{3/2}(C)\right]/\alpha > 0, \tag{2.101}$$

or

$$B + 2\left[\lambda(C) \pm q^{3/2}(C)\right]/\alpha < 0. \tag{2.102}$$

There are three real roots if $f(B,C) < 0$ for which there holds the condition

$$-2\left[\lambda(C) + q^{3/2}(C)\right]/\alpha < B < -2\left[\lambda(C) - q^{3/2}(C)\right]/\alpha. \tag{2.103}$$

There are three real roots with two of them being equal if $f(B,C) = 0$ which is satisfied by

$$B = -2\left[\lambda(C) \pm q^{3/2}(C)\right]/\alpha. \tag{2.104}$$

In Fig. 2-2, the curve $f(B,C) = 0$ is plotted in the (B,C) plane where the domains of positive and negative $f(B,C)$ are indicated: one real root for $f(B,C) > 0$; three real roots, of which two are double roots, for $f(B,C) = 0$, that is, on the curve; three distinct real roots for $f(B,C) < 0$.

To analyze the stability of the homogeneous steady states in the time domain, we define the fluctuations of the solution from the steady state (X_0, Y_0) and linearize the wave equations. Thus, with the definitions

$$x = X - X_0, y = Y - Y_0, \tag{2.105}$$

we obtain

$$\partial_\tau^2 \mathbf{Z}_l + \bar{N}_{rd}\mathbf{H}_0\partial_\tau \mathbf{Z}_l = \bar{N}_{rd}\mathbf{R}_0\mathbf{Z}_l. \tag{2.106}$$

Here various symbols are defined as follows:

$$\mathbf{Z}_l = \begin{pmatrix} X \\ \\ Y \end{pmatrix}, \tag{2.107}$$

$$\mathbf{R}_0 = \begin{pmatrix} -1 + 2X_0Y_0 - 3KX_0^2 & X_0^2 \\ (-2X_0Y_0 + 3KX_0^2)f^{-2} & -(R - X_0^2)f^{-2} \end{pmatrix}. \quad (2.108)$$

$$\mathbf{H}_0 = \begin{pmatrix} H_{xx}^0 & H_{xy}^0 \\ H_{yx}^0 & H_{yy}^0 \end{pmatrix}, \quad (2.109)$$

with the definitions

$$H_{xx}^0 = 1 + (1 - 2X_0Y_0 + 3KX_0^2)/\bar{N}_{rd}, \quad (2.110)$$

$$H_{xy}^0 = -X_0^2/\bar{N}_{rd}, \quad (2.111)$$

$$H_{yx}^0 = (2X_0Y_0 - 3KX_0^2)/\bar{N}_{rd}, \quad (2.112)$$

$$H_{yy}^0 = f^{-2} + (R + X_0^2)/\bar{N}_{rd}, \quad (2.113)$$

Eq. (2.106) will be analyzed together with the inhomogeneous steady state.

2.5.2 Inhomogeneous Steady States

If the system is inhomogeneous in space, the steady state is defined by the condition

$$\partial_\tau \mathbf{Z}_t = 0 \quad (2.114)$$

which yields the equation

$$-\mathbf{D}\nabla_\xi^2 \mathbf{Z}_t = \mathbf{R}(X_t, Y_t) \quad (2.115)$$

where

$$\mathbf{Z}_t = \begin{pmatrix} X_t \\ \\ Y_t \end{pmatrix}, \tag{2.116}$$

$$\mathbf{R}_t = \mathbf{R}(X = X_t, Y = Y_t). \tag{2.117}$$

At this steady state, the hyperbolic and parabolic systems of differential equations coincide. However, the temporal evolutions of the two systems (2.73) and (2.82) differ significantly since the manner in which the inhomogeneous steady state is asymptotically reached by the two systems can be qualitatively different. The evidence for this difference will be shown numerically in a later section.

Eq. (2.115) describes steady-state Turing structures for the system of interest. Since it is useful to examine the linear stability of such structures, the evolution equation (2.115) is linearized with respect to the state of vanishing reaction rates, namely, (X_0, Y_0) defined earlier. Then, with the definition

$$x = X_t - X_0, y = Y_t - Y_0. \tag{2.118}$$

Eq. (2.115) may be written in terms of new variables x and y as

$$-\nabla_\xi^2 \mathbf{Z}_l = \mathbf{M}\mathbf{Z}_l + \Lambda(x, y) \tag{2.119}$$

where

$$\mathbf{M} = -\mathbf{D}^{-1}\mathbf{R}_0, \tag{2.120}$$

$$\Lambda(x, y) = \mathbf{D}^{-1} \begin{pmatrix} Kx^3 + (3KX_0 - Y_0)x^2 - x^2 y - 2X_0 xy \\ \\ -[Kx^3 + (3KX_0 - Y_0)x^2 + x^2 y + 2X_0 xy]f^{-2} \end{pmatrix} \tag{2.121}$$

Dropping the Λ term yields the linearized evolution equation

$$\nabla_\xi^2 \mathbf{Z}_l = \mathbf{M}\mathbf{Z}_l. \tag{2.122}$$

Combining this equation with the temporal equation (2.106), we obtain the linearized wave equation

$$\partial_\tau^2 \mathbf{Z}_l + \bar{N}_{rd}\mathbf{H}_0 \partial_\tau \mathbf{Z}_l - \bar{N}_{rd}\mathbf{D}\nabla_\xi^2 \mathbf{Z}_l = -\bar{N}_{rd}\mathbf{D}\mathbf{M}\mathbf{Z}_l \tag{2.123}$$

which may be used to calculate the linearized waves and their dispersion relations. Solving this equation by Fourier transform

$$\mathbf{Z}_l = \sum_\omega \sum_k \Phi(k,\omega) \exp[i(k\cdot\xi - \omega\tau)], \tag{2.124}$$

we obtain the linear algebraic set

$$(-\omega^2\mathbf{I} - i\omega\bar{N}_{rd}\mathbf{H}_0 + k^2\bar{N}_{rd}\mathbf{D} + \bar{N}_{rd}\mathbf{D}M)\Phi(k,\omega) = 0. \tag{2.125}$$

The dispersion relation is given by the secular determinant

$$\det|(-i\omega)^2\mathbf{I} - i\omega\bar{N}_{rd}\mathbf{H}_0 + k^2\bar{N}_{rd}\mathbf{D} + \bar{N}_{rd}\mathbf{D}\mathbf{M}| = 0. \tag{2.126}$$

This is a fourth order polynomial of $z = -i\omega$ and k :

$$P_4(z,k) = z^4 + Pz^3 + Qz^2 + Tz + S = 0 \tag{2.127}$$

with the definitions

$$K_{xx} = k^2\mathbf{D}_{xx} + (\mathbf{D}\mathbf{M})_{xx} \tag{2.128}$$

$$K_{yy} = k^2\mathbf{D}_{yy} + (\mathbf{D}\mathbf{M})_{yy}, \tag{2.129}$$

$$P = \bar{N}_{rd}(H^0_{xx} + H^0_{yy}), \tag{2.130}$$

$$Q = \bar{N}_{rd}(K_{xx} + K_{yy}) + \bar{N}^2_{rd}(H^0_{xx}H^0_{yy} - H^0_{xy}H^0_{yx}), \tag{2.131}$$

$$T = \bar{N}^2_{rd}[K_{xx}H^0_{yy} + K_{yy}H^0_{xx} - H^0_{xy}(\mathbf{DM})_{yx} - H^0_{yx}(\mathbf{DM})_{xy}], \tag{2.132}$$

$$S = \bar{N}^2_{rd}[K_{xx}K_{yy} - (\mathbf{DM})_{xy}(\mathbf{DM})_{yx}]. \tag{2.133}$$

To write these terms out in less formal forms, we define

$$l_x = \bar{N}_{rd}, \tag{2.134}$$

$$l_y = \bar{N}_{rd}/f^2, \tag{2.135}$$

$$\epsilon_x = \bar{N}_{rd}\hat{D}_x, \tag{2.136}$$

$$\epsilon_y = \bar{N}_{rd}\hat{D}_y/f^2. \tag{2.137}$$

and with the abbreviations

$$a_1 = 1 - 2X_0Y_0 + 3KX_0^2, \tag{2.138}$$

$$a_2 = -X_0^2, \tag{2.139}$$

$$b_1 = -3KX_0^2 + 2X_0Y_0, \tag{2.140}$$

$$b_2 = R + X_0^2. \tag{2.141}$$

The following quantities

$$\alpha_1 = \epsilon_x + \epsilon_y, \tag{2.142}$$

$$\alpha_2 = \epsilon_x(l_y + b_2) + \epsilon_y(l_x + a_1), \tag{2.143}$$

$$\alpha_3 = b_2\epsilon_x l_y + a_1\epsilon_y l_x, \tag{2.144}$$

$$\beta_1 = (b_2 + a_1)(l_x + l_y) + l_x l_y + a_1 b_2 - a_2 b_1, \tag{2.145}$$

$$\beta_2 = (a_1 b_2 - a_2 b_1)(l_x + l_y) + l_x l_y (b_2 + a_1), \tag{2.146}$$

$$\beta_3 = (a_1 b_2 - a_2 b_1) l_x l_y, \tag{2.147}$$

$$\epsilon = \epsilon_x \epsilon_y. \tag{2.148}$$

Then, P, Q, etc. can be written as

$$P = b_2 + a_1 + l_x + l_y, \tag{2.149}$$

$$Q = \alpha_1 k^2 + \beta_1, \tag{2.150}$$

$$T = \alpha_2 k^2 + \beta_2, \tag{2.151}$$

$$S = \epsilon k^4 + \alpha_3 k^2 + \beta_3. \tag{2.152}$$

For the polynomials to have all the roots with the negative imaginary part the

following Hurwitz conditions[23] must be fulfilled:

$$P > 0, \tag{2.153}$$

$$PQ - T > 0, \tag{2.154}$$

$$PQT - T^2 - P^2S > 0. \tag{2.155}$$

The first condition (2.153) is independent of k and a function of B and C. The second condition $f_2(k, C, B) \equiv PQ - T$ and the third condition $f_3(k, C, B) \equiv PQT - T^2 - P^2S$ are even functions of k. Since the polynomial $P_4(z, k)$ is real, it has two pairs of complex conjugate roots. The level curves of the Hurwitz conditions $f_2(k, C, B) = 0$ and $f_3(k, C, B) = 0$ for a given value of B are plotted in Figs. 2-2 and 2-3. Note that the first condition gives a point on the C axis. On the level curves the real parts of the roots vanish and the solution of the wave equation (2.123) becomes oscillatory in time.

In the case of the parabolic system the linearized evolution equation takes the form

$$\partial_\tau \mathbf{Z}_l - \hat{\mathbf{D}}\nabla_\xi^2 \mathbf{Z}_l = -\hat{\mathbf{D}}\mathbf{M}\mathbf{Z}_l \tag{2.156}$$

which gives rise to the secular equation

$$z^2 + P'z + Q' = 0 \tag{2.157}$$

where

$$P' = a_1 + b_2 + (\hat{D}_x + \hat{D}_y)k^2 = a_1 + b_2 + (l_x l_y)^{-1}(\epsilon_x l_y + \epsilon_y l_x)k^2, \tag{2.158}$$

$$Q' = \hat{D}_x\hat{D}_y k^4 + (a_1\hat{D}_y + b_2\hat{D}_x)k^2 + a_1 b_2 - b_1 a_2 = f^2 S. \tag{2.159}$$

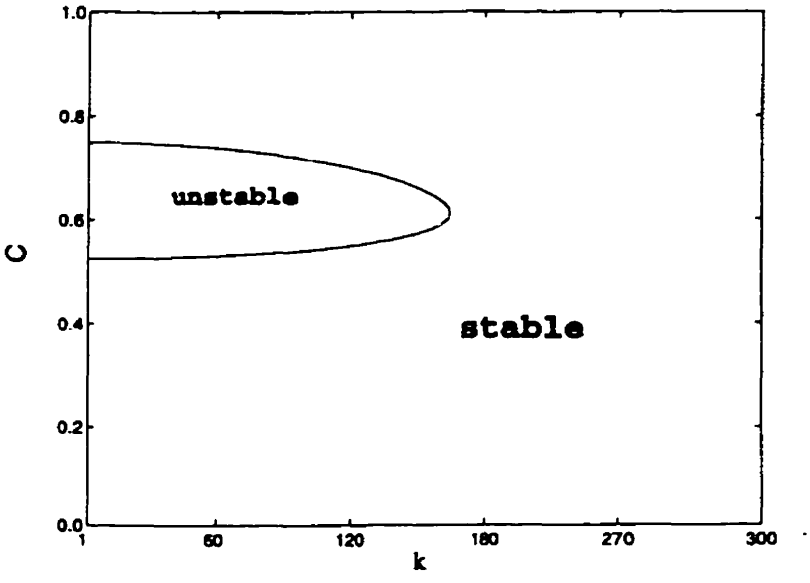

Figure 2-4: *Stability phase diagram for the parabolic system. This diagram is constructed by using the Hurwitz conditions in the case of* $R = 0.1$, $K = 1$, $f = 1$, *and* $B = 0.09$. *The unstable domains are closed. Therefore, the Turing instability modes can occur within the closed domain. This is in contrast to the hyperbolic system presented in Fig. 2-1.*

The Hurwitz conditions for negative real roots are

$$\tilde{P}' \equiv l_x l_y P' = (a_1 + b_2) l_x l_y + (\epsilon_x l_y + \epsilon_y l_x) k^2 > 0, \tag{2.160}$$

$$P'Q' \equiv P' S f^2 > 0. \tag{2.161}$$

The level curves are plotted in Fig. 2-4 which are qualitatively different from the level curves for the hyperbolic system presented in Fig. 2-1. There is only one level curve since the second condition $Q'(k, C, B)$ or $S(k, B, C)$ is always positive for the parameter set chosen for C and B and hence does not appear in the figures. Comparison of the two figures indicates that the domain of instability is much larger for the hyperbolic system than the parabolic system which has a maximum

k value beyond which instability does not occur whereas there is no such maximum value for the wave number in the case of the hyperbolic system. This difference in stability diagrams indicates that the dynamics of the two system can be considerably different. Othmer[11] also observed that the stability diagram of a hyperbolic system is qualitatively different from that of the corresponding parabolic system. The present result confirms his observation.

According to the Turing theory[24] the diffusion coefficients $\hat{D}_x$ and $\hat{D}_y$ must be different for the Turing instability to occur. This conclusion was drawn based on the parabolic reaction-diffusion equations (2.156). However, the wave equations–namely, the hyperbolic reaction-diffusion equations–do not require the diffusion coefficients to be different for the homogeneous stable steady states to be destabilized by diffusion. We discuss this aspect here before presenting numerical solutions of the hyperbolic wave equations.

We examine the homogeneous steady states of the reacting system for which all the eigenvalues of the matrix $-\hat{\mathbf{D}}\mathbf{M}$ in (2.156) to have negative real parts. namely, the steady states are stable. As shown originally by Turing[24] and later by others[21, 20], they are destabilized by diffusion, provided that the diffusion coefficients $\hat{D}_x$ and $\hat{D}_y$ are different. This can be readily seen from the secular determinant of (2.156):

$$\det | - \hat{\mathbf{D}}\mathbf{M} - \hat{\mathbf{D}}k^2 + z\mathbf{I}| = 0. \tag{2.162}$$

Let us assume that $\hat{\mathbf{D}} = D\mathbf{I}$, $\mathbf{I}$ being the unit matrix, and denote the eigenvalues $of\ -M$ by λ_i $(i = 1, 2)$. Then it is easy to see that

$$z_i = -Dk^2 + \lambda_i \ (i = 1, 2), \tag{2.163}$$

and $\mathrm{Re}\, z_i < 0$ since $\mathrm{Re}\, \lambda_i < 0$ and $k^2 \geq 0$. Therefore, if $\hat{\mathbf{D}} = D\mathbf{I}$, then the stable steady states for which $\mathrm{Re}\, \lambda_i < 0$ cannot be destabilized by diffusion. This conclusion cannot be drawn if $\hat{\mathbf{D}} \neq D\mathbf{I}$, namely, if $\hat{D}_x \neq \hat{D}_y$ as is well known[21, 24, 20].

In the case of the hyperbolic system under the assumption that $\hat{D}_x = \hat{D}_y$ and $\mathrm{Re}\,\lambda_i < 0$, the secular determinant for (2.123) is

$$\det|-D\mathbf{M} - z\sqrt{\bar{N}_{rd}}\mathbf{H}^0 - (Dk^2 + z^2)\mathbf{I}| = 0. \tag{2.164}$$

where $z = -i\omega/\sqrt{\bar{N}_{rd}}$. The presence of the term $z\sqrt{\bar{N}_{rd}}\mathbf{H}^0$ prevents us from drawing a conclusion regarding the sign of $\mathrm{Re}\,z_i$ similarly to the one drawn earlier for the parabolic system. To make this point more definite, let us assume that $\sqrt{\bar{N}_{rd}}\mathbf{H}^0 = hI$ where h is positive or negative. Then, since $\mathrm{Re}\,\lambda_i < 0$ by assumption and $k^2 \geq 0$, (2.164) implies that

$$Re(z_i^2 - z_i h) < 0. \tag{2.165}$$

Setting $z_i = \alpha_i + i\beta_i$, we can express this condition in the form

$$\frac{1}{2}[h - (h^2 + 4\beta_i^2)^{1/2}] < \alpha_i < \frac{1}{2}[h + (h^2 + 4\beta_i^2)^{1/2}]. \tag{2.166}$$

If this condition is not satisfied, $\mathrm{Re}\,z_i$ is not guaranteed a negative real part and the homogeneous steady states can be destabilized, namely, the Turing instability can occur even if $\hat{D}_x = \hat{D}_y$. This feature is also one of the properties of the hyperbolic system distinctive from the parabolic system. Numerical evidence of this difference will be shown later.

2.6 Numerical Solution in One Dimension

In this section, we examine numerical solutions for one dimension by using the hyperbolic and parabolic equations. The main aim is to compare the behaviors predicted by the hyperbolic and parabolic systems of partial differential equations and see if there are any characteristic differences which may be discernible in the laboratory or numerical data on chemical waves.

The boundary and initial conditions are chosen as follows:

$$\begin{aligned} X(0,t) &= X(1,t) = C_x \\ Y(0,t) &= Y(1,t) = C_y, \\ X(\xi,0) &= C_x, Y(\xi,0) = C_y, \\ u(\xi,0) &= v(\xi,0) = 0. \end{aligned} \tag{2.167}$$

where C_x and C_y are constants which have been chosen to be 0.2 in reduced units for most of calculations performed in this work unless stated otherwise. The reason for choosing this set of boundary and initial conditions is that in many experiments the reacting system is initially well stirred and made spatially uniform before the system is let evolve. This experimental condition is consistent with the initial conditions chosen here. In order to ascertain the reliability of the numerical results obtained, typical numerical solutions have been obtained by the IMSL subroutine MOLCH and also by the Fourier spectral method[21] combined with Gear's method for stiff ordinary differential equations. The number of collocation points taken for the spectral method was 128 for all the cases studied. The two methods have produced tolerable agreements for the cases compared.

2.7 Effects of Diffusion via Hyperbolic or Parabolic Systems

We first consider the case of no chemical reactions which yields linear wave equations, both parabolic or hyperbolic. In both cases, the steady state is stable and the waves get damped in amplitude owing to the effect of diffusion. To show the effect of diffusion on the evolution of chemical reactions and pattern formation, we have set

u and v equal to zero (*i.e.*, no diffusion) and solved the resulting ordinary differential equations in time for the parameters chosen to yield a limit cycle.

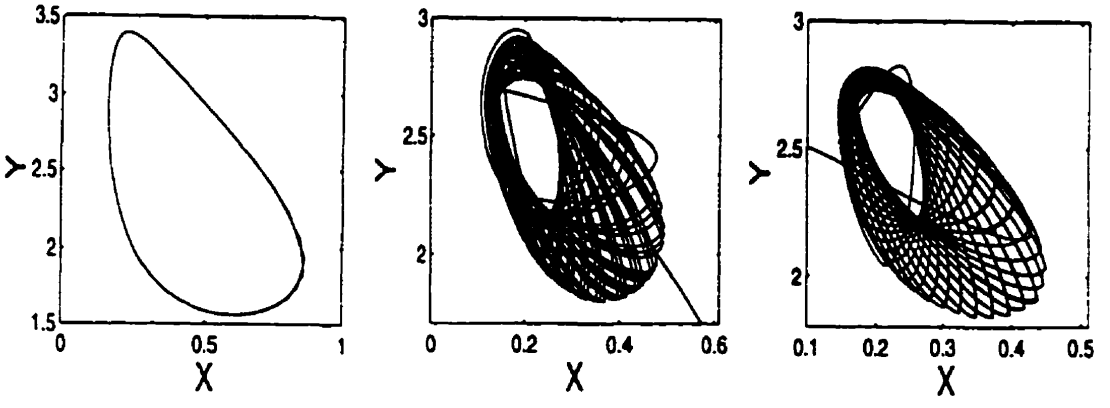

Figure 2-5: *(a)A limit cycle in the case of no diffusion. Two different initial conditions tend to the same limit cycle. (b)A quasiperiodic motion shown by the hyperbolic system at* $N_{rd} = 0.1$. *(c)A quasiperiodic motion shown by the parabolic system. If the diffusion is turned on, the trajectory winds a torus.*

The result is shown in Fig. 2-5a. When diffusion is turned on, the temporal oscillation gets affected. In the case of $N_{rd} = 0.1$, the oscillation becomes quasi-periodic in the XY plane, winding a torus as is shown in Fig. 2-5b. The power spectrum shows that there are three fundamental frequencies and their subharmonics. This is shown in Fig. 2-6a. This result should be compared with the case of the parabolic system which may be regarded as the hyperbolic system in the limit of $N_{rd} \rightarrow \infty$. We have ascertained that the hyperbolic system becomes practically parabolic and gives the same results as the latter if N_{rd} is increased to at least about 20 and beyond. (The maximum value studied was 50). In this regime of large N_{rd}, although the maximum amplitudes are a little reduced, the trajectories are similarly quasiperiodic in the XY plane (Fig. 2-5c) as is the hyperbolic system, but the power spectrum in Fig. 2-6b shows that there are only two fundamental frequencies. Since this seems to suggest that the reaction-diffusion number plays a role in changing the number of fundamental frequencies, the value of N_{rd} is further decreased to $N_{rd} = 0.01$ so that the hyperbolicity is amplified. It must be remarked

here that for this case the initial conditions for fluxes were taken $u(\xi, 0) = 0.1$ and $v(\xi, 0) = 0$ to get physical solutions to the hyperbolic differential equations. Below this particular value of $N_{rd} = 0.01$ the present set of boundary and initial conditions failed to produce physical solutions. In any case, at $N_{rd} = 0.01$ the motion now begins to show a chaotic behavior and its power spectrum (Fig. 2-6c) shows a broad and diffuse structure. This trend probably will continue as the reaction-diffusion number gets smaller and the initial and boundary conditions are varied suitably. From this investigation the following picture seems to emerge for the particular case of parameters of the system: *If there is no diffusion, there is a single frequency limit cycle. As diffusion is turned on at a very large value of N_{rd} so that the disturbance propagates at infinite speed and thus the system is parabolic, there appears a two-fundamental frequency quasiperiodic motion–period doubling. As the reaction-diffusion number is reduced so that the disturbance propagates at a finite speed and the system thus becomes hyperbolic, the number of frequencies is increased to three or more and eventually to infinity, and the motion becomes chaotic.*

Unlike the parabolic system the hyperbolic system enables us to examine the evolution of diffusion fluxes in time. Intuitively, we know that the parabolic system of hydrodynamic equations emerges when the diffusion fluxes change rapidly compared with the concentrations. This picture is borne out when the reaction-diffusion number is sufficiently large. When the value of the reaction-diffusion number is in the range where the trajectories are not chaotic in the XY plane (*e.g.*, $N_{rd} \geq 0.1$), the diffusion fluxes fluctuate rapidly and their spatial mean values, namely, their spatial integrals, become very small in magnitude, indicating that they do not change over a significant span of time. This is shown in Fig. 2-7a and the power spectrum is shown in Fig. 2-7b. As evident from the figures in this regime of the reaction-diffusion number the diffusion fluxes may be regarded as stochastic variables. However, as the reaction-diffusion number is lowered well below $N_{rd} = 0.1$, say, to $N_{rd} = 0.01$ and the trajectories of X and Y become chaotic, the trajectories of $\mathbf{u}$ and $\mathbf{v}$ become regular as is shown in Fig. 2-7c which shows the trajectory of $(\mathbf{u}, \mathbf{v})$ integrated over space, namely, the spatial means of $\mathbf{u}$ and $\mathbf{v}$. We thus see that *the stochasticity*

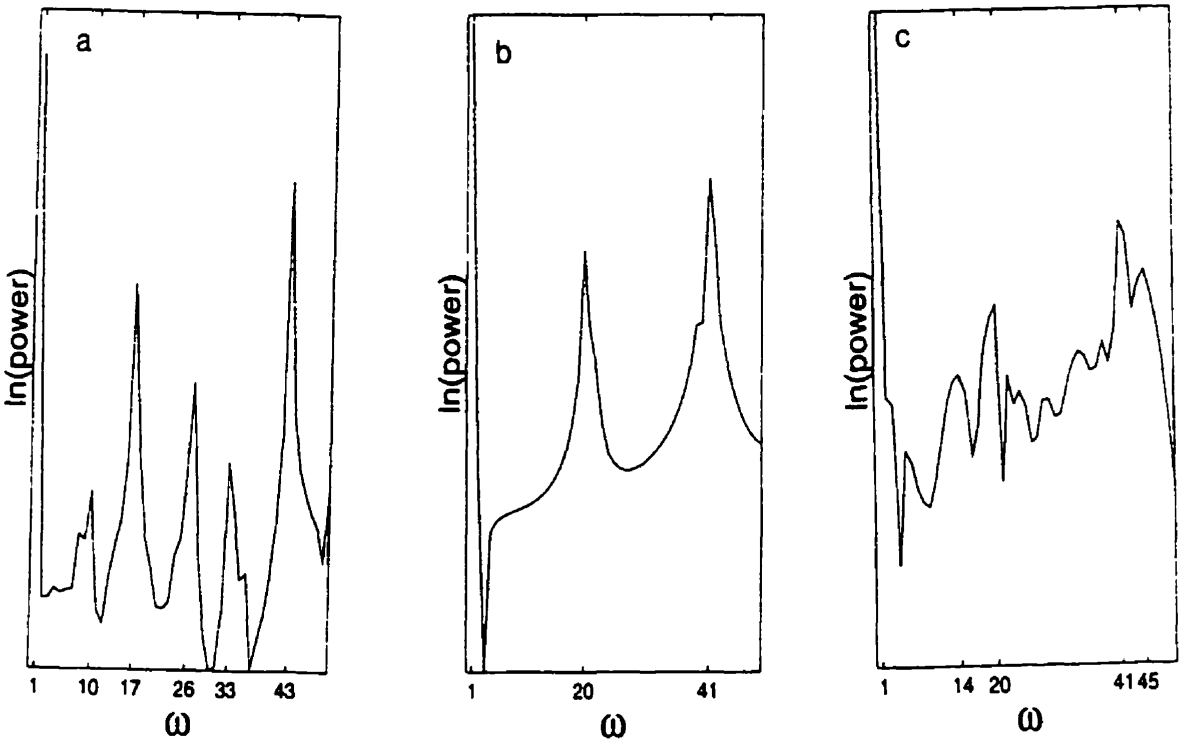

Figure 2-6: *(a)The power spectrum of the hyperbolic system at* $N_{rd} = 0.1$. *It indicates that there are three fundamental frequencies in the case of b at* $\nu_1 = 1$, $\nu_2 = 17$, *and* $\nu_3 = 43$, *and subharmonics at* $\nu_1 - 2\nu_2 + \nu_3 = 10$, $\nu_3 - \nu_2 = 26$, $2\nu_2 - \nu_1 = 33$, *etc.* *(b)The power spectrum for the case of the parabolic system (the limit of* $N_{rd} \rightarrow \infty$*). It shows that there are two fundamental frequencies at* $\nu_1 = 1$ *and* $\nu_2 = 20$. *The other is a subharmonic:* $\nu_1 + 2\nu_2 = 41$. *(c)The power spectrum of the hyperbolic system at* $N_{rd} = 0.01$. *The fundamentals are still discernable at* $\nu_1 = 1$, $\nu_2 = 20$, *and* $\nu_3 = 41$. *However, the spectrum has become broader and diffuse, indicating a chaotic motion.*

is exchanged between the two sets of variables (X, Y) *and* $(\mathbf{u}, \mathbf{v})$*, that is, the slow variables have become fast variables and the previously fast variables have become slow variables.* This indicates that the hyperbolicity will become significant as

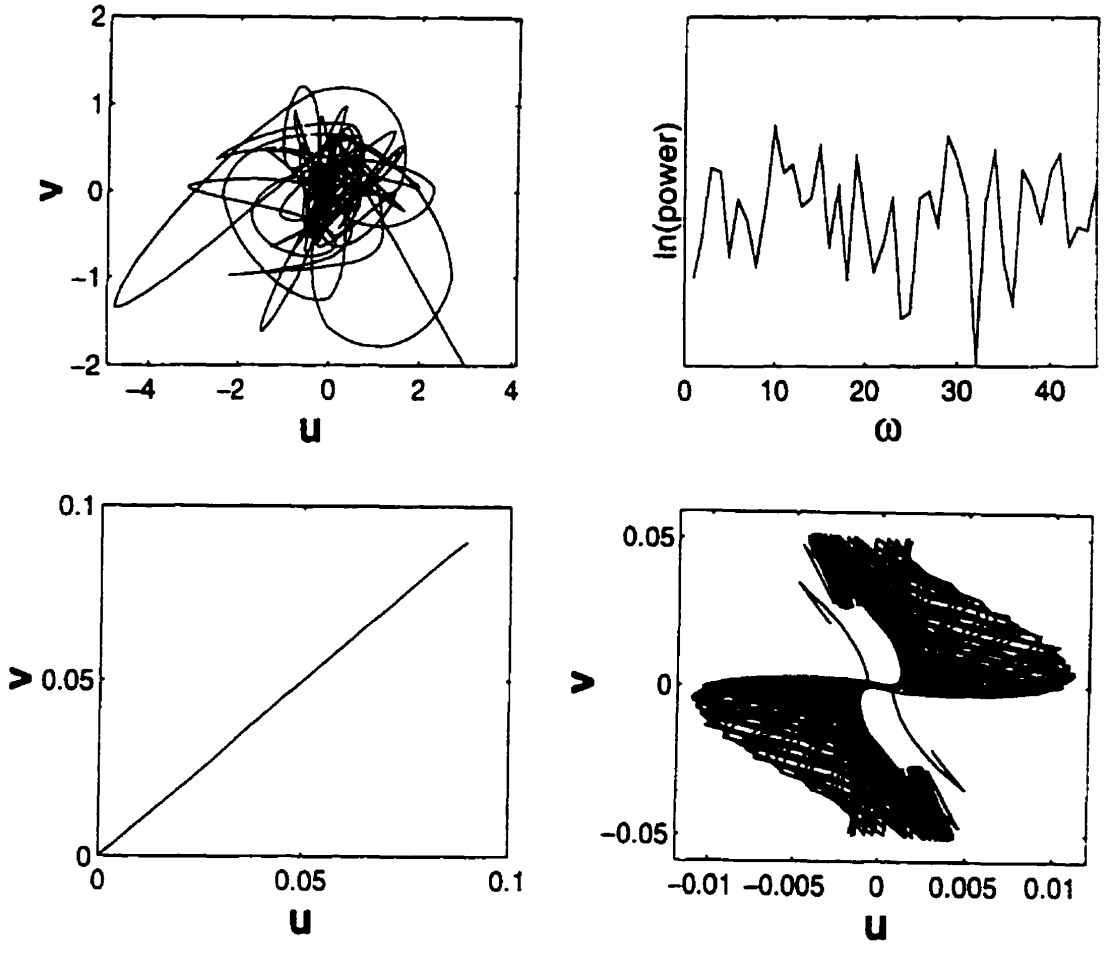

Figure 2-7: *(a) Trajectory of space-integrated (mean) fluxes* $\mathbf{u}$ *and* $\mathbf{v}$ *in the* $\mathbf{uv}$ *plane. This figure is in the units of* 10^{-19} *for the abscissa and* 10^{-18} *for the ordinate. Notice that their magnitudes are rather small.* $N_{rd} = 0.1$*. (b) The corresponding power spectrum of* $\mathbf{u}$ *indicating a chaotic motion. (c) Trajectory of space-integrated (mean) fluxes* $\mathbf{u}$ *and* $\mathbf{v}$ *in the* $\mathbf{uv}$ *plane in the case of* $N_{rd} = 0.01$*. The fluxes do not oscillate and their motions are regular, whereas the concentrations* X *and* Y *fluctuate chaotically in this case.*

the matter begins to diffuse on the time scale of change comparable to the concentration variations in the reacting species. This aspect of course is absent in the parabolic system since the fluxes are necessarily steady, namely, $\mathbf{u} = -\hat{D}_x \nabla X$ and

$\mathbf{v} = -\hat{D}_y \nabla Y$. Fig. 2-7d shows the trajectories in the $(\mathbf{u}, \mathbf{v})$ plane which are not integrated over space unlike those in Figs. 2-7$a - c$. If the parameters are chosen in the stable steady-state region of Fig. 2-2, then the trajectory in the XY plane tends to a fixed point as shown in Fig. 2-8.

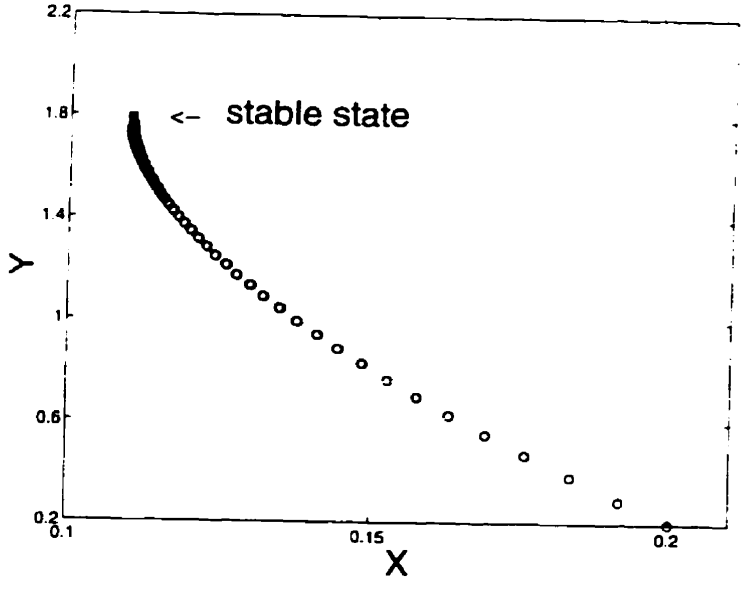

Figure 2-8: *Trajectory of X and Y in the XY plane in the case of the parameters in the stable steady state domain in Fig. 2-2. The trajectory tends to the stable steady state.* $A = 0.2$, $B = 0.09$, $N_{rd} = 0.1$, $\hat{D}_x = 0.006$, $\hat{D}_y = 0.0016$, *and* $f = 1.0$.

There is a characteristic difference between the behaviors of the travelling waves predicted by the hyperbolic and parabolic systems. In the case of the former, the wave maintains a sharp front whereas the wave is rather diffuse and nonzero in amplitude throughout the space in the case of the latter, reflecting an instantaneous propagation of matter. This probably is the most noticeable from the experimental viewpoint when a travelling wave is involved. This characteristic difference is demonstrated in Fig. 2-98a where waves travelling from the boundaries to the center are shown. The solid curve denotes the prediction by the hyperbolic system at $N_{rd} = 0.1$ and the curve of open circles the prediction by the parabolic system. This kind of difference will be later exhibited in space-time for other values of the

reaction diffusion number and for different boundary conditions in this work. The mid portions of these curves are not equal to zero because the concentrations are built up locally owing to the initial conditions chosen for the numerical study made here; see (2.167).

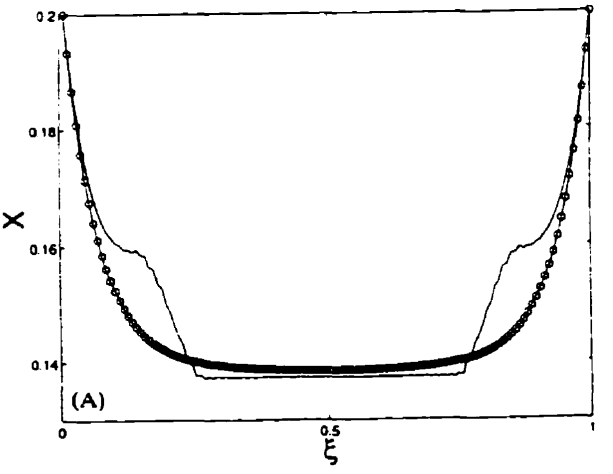

Figure 2-9: *Comparison of travelling wave patterns predicted by the hyperbolic and parabolic systems. The solid curve is for the hyperbolic system whereas the curve of open circles is for the parabolic system.* $N_{rd} = 0.1$. *Notice the sharp fronts in the case of the hyperbolic system.*

It is also noticed that after the waves travel toward the middle and merge, they split and travel back toward the boundaries, and then get reflected and travel back toward the middle. This process is repeated. An example of this behavior is presented in Fig. 2-10 where a sequence of wave merging and splitting is shown. This behavior appears for all values of N_{rd} studied: from $N_{rd} = 0.01$ on to $N_{rd} = 20$ which is the maximum value of the reaction-diffusion number studied in this work under the initial and boundary conditions. It probably happens for higher values of the reaction-diffusion number since Petrov et al.[22] have observed the phenomenon with a system of one-dimensional parabolic reaction-diffusion equations for a cubic reaction model. The wave splitting behaviors are shown in space-time in Figs. 2-11a and 2-11b for the case of $N_{rd} = 50$. At this value of N_{rd} the hyperbolic system

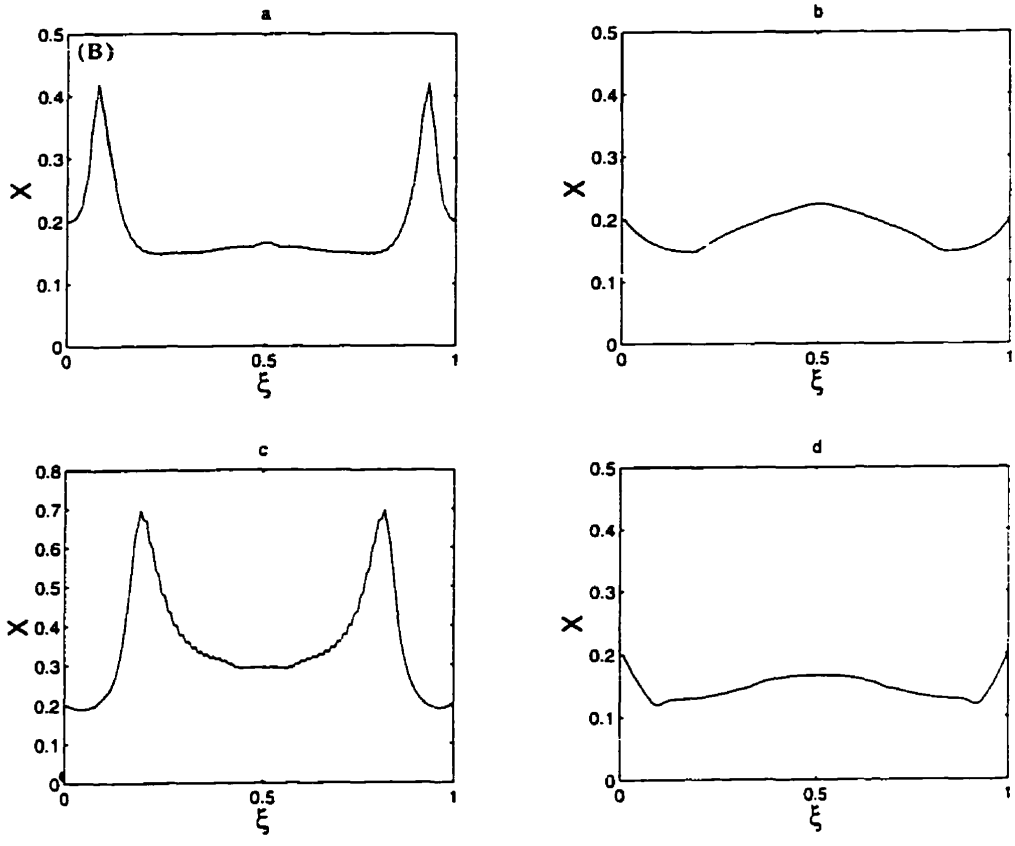

Figure 2-10: *Sequence of wave merging and splitting: $a \rightarrow b \rightarrow c \rightarrow d$. This process is repeated over a long time span.*

practically behaves as if it is parabolic and gives the results virtually coinciding with the latter in all qualitative aspects. In the figures in color, the amplitude of the wave increases in the following order of colors: **dark orange, yellow, green, light blue, dark blue, pink, and red**[3] as shown in the color code strip in Fig. 2-11. In these figures the waves are plotted in space-time over 1000 units of τ (reduced time); the abscissa is for time (τ) whereas the ordinate is for space (ξ). Notice that there are more than one wave length discernible and the waves merge and split in the middle of $\xi = [0, 1]$. The hyperbolic system at $N_{rd} = 0.1$ predicts more complicated patterns of waves in space-time which are generally shorter in

[3]The original figures were published in color, and these colors follows these original figures.

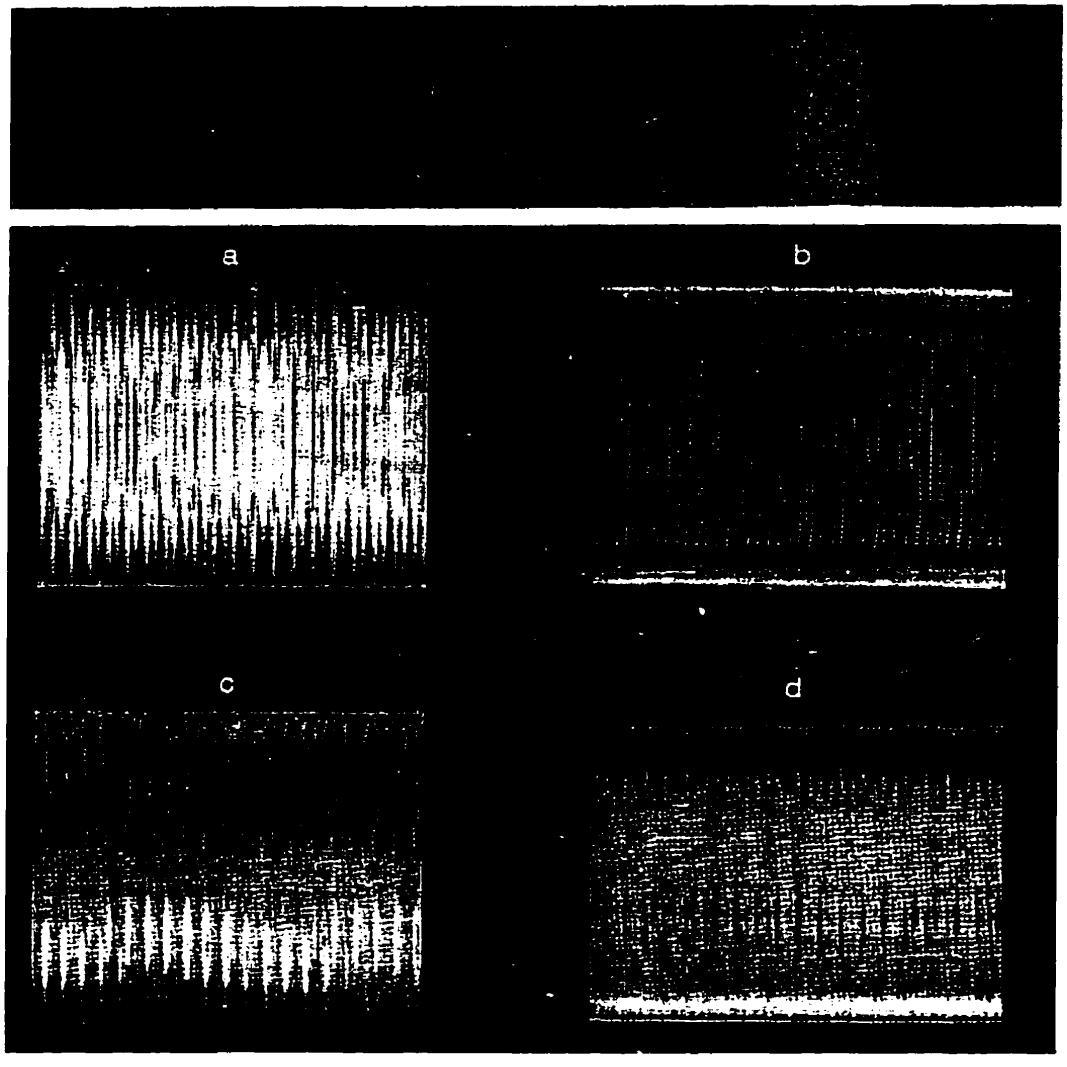

Figure 2-11: *Space-time plot of concentration waves for X in the case of the parabolic system for $X = Y = 0.2$ at the boundaries. $(a)X$, $(b)Y$, $(c)u$, and $(d)v$. These result coincide with those of the hyperbolic system at $N_{rd} = 50$. In the accompanying color code the intensity increases from left to right in the order of* **dark orange, yellow, green, light blue, dark blue, pink, and red**. *All the figures in color in this work conform to this color code.*

wavelength. These waves and the corresponding fluxes are shown in Figs. 2-12$a-d$. The wave merging and splitting phenomenon is still discernible at this value of

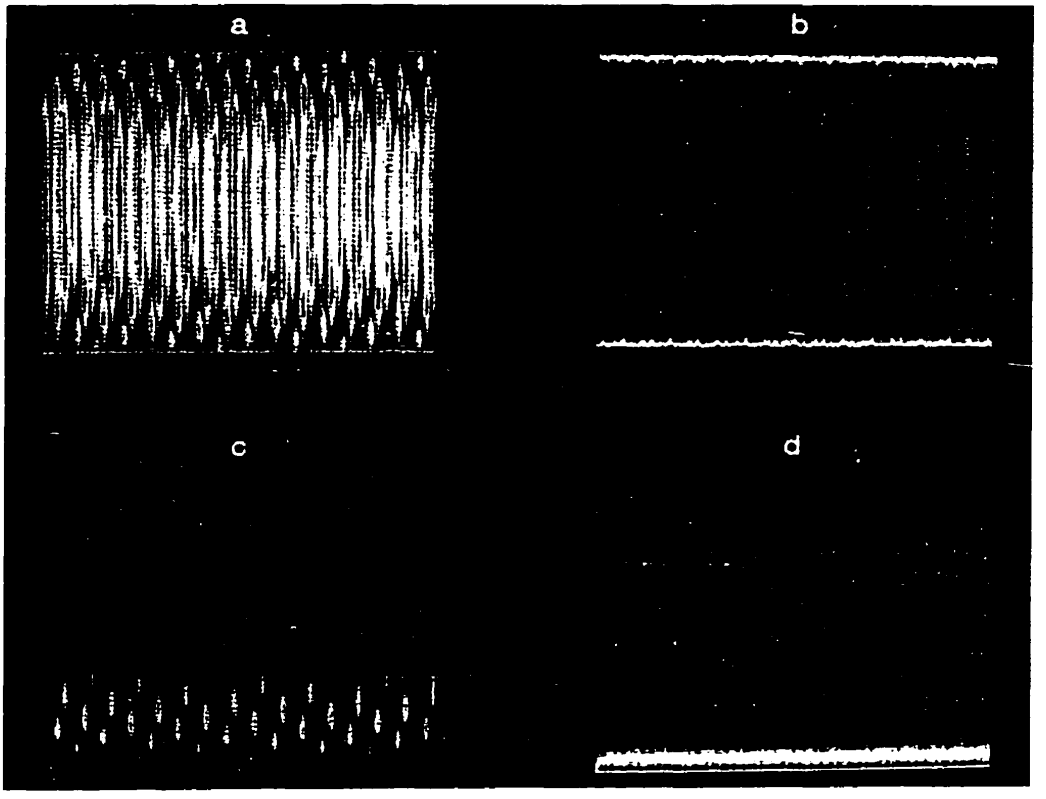

Figure 2-12: *Space-time plot of concentration waves for X in the case of the hyperbolic system for $X = Y = 0.2$ at the boundaries and $N_{rd} = 0.1$. $(a)X$, $(b)Y$, $(c)u$, and $(d)v$.*

N_{rd}. These patterns may be regarded as an example of one-dimensional patterns where the spots appear and disappear as time progresses. This behavior reminds us of the recent experimental results by Lee et al.[23] on birth and demise of spots in a reacting system. In Figs. 2-13a and 2-13b the waves are plotted in space-time in the case of $N_{rd} = 0.01$. The wave merging and splitting phenomenon is still noticeable in them.

To study the effect of the boundary conditions, the hyperbolic system was solved for different boundary conditions $X = 1.5$ and $Y = 2.5$ which are quite different from those for the results in the previous figures. As shown in Figs. 2-14, the pat-

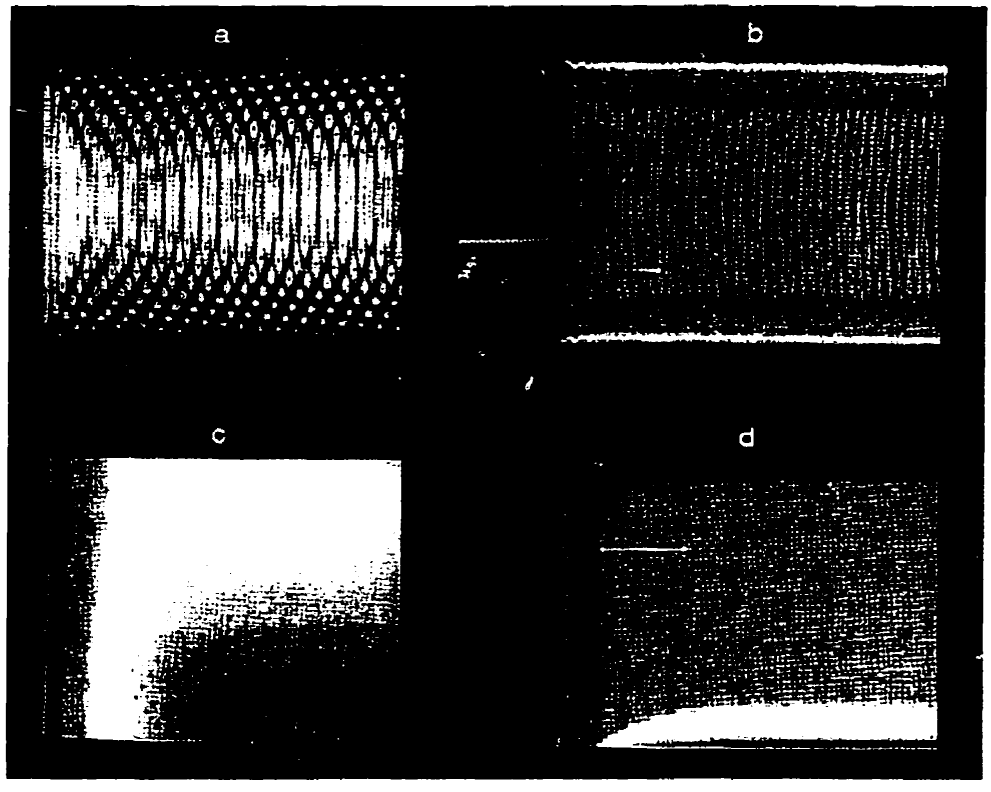

Figure 2-13: *Space-time plot of concentration waves for X in the case of the hyperbolic system for $X = Y = 0.2$ at the boundaries and $N_{rd} = 0.01$. $(a)X$, $(b)Y$, $(c)u$, and $(d)v$.*

terns have changed significantly. We observe that the nonstationary waves in the early stages (on the left edge in the figures) evolve to a steady peak in the center flanked by steady waves of long fixed wave lengths. These may be regarded as a pattern in space-time. They appear to satisfy the necessary requirements of Turing patterns that the pattern is stationary, symmetry is spontaneously broken, and the wavelength is intrinsic[24]. In particular, the central peak may be regarded as what

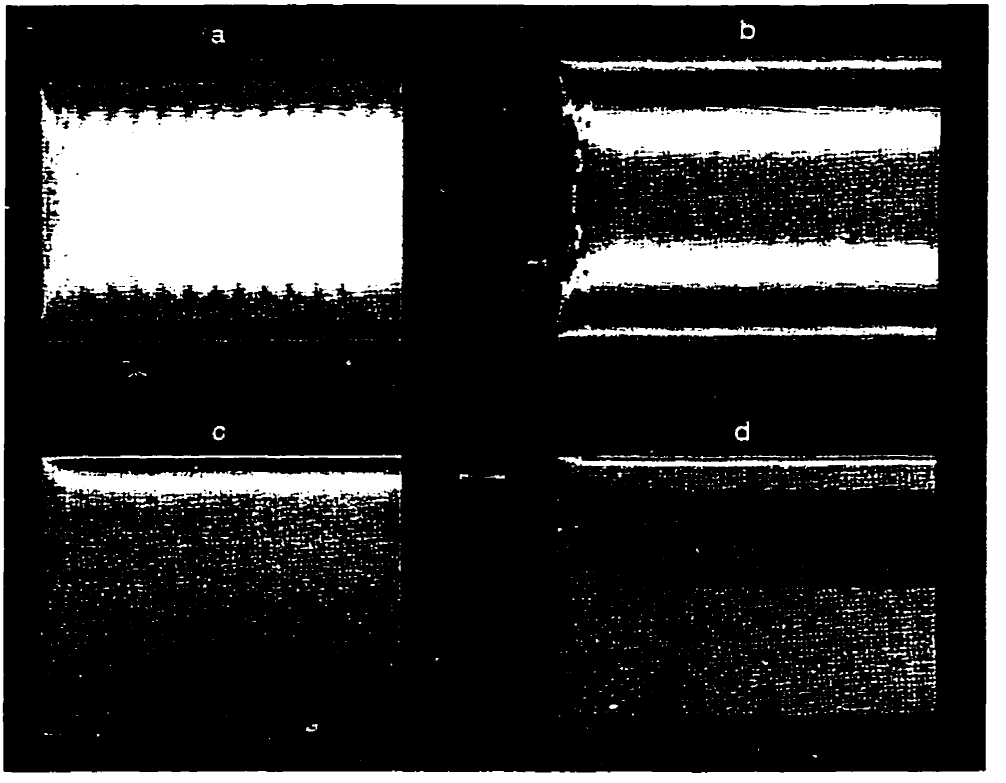

Figure 2-14: *Space-time plot of the hyperbolic system at* $X = 1.5$ *and* $Y = 2.5$ *and* $N_{rd} = 0.02$. $(a)X$, $(b)Y$, $(c)u$, *and* $(d)v$.

is termed as the Turing hole in the literature[26]. For the same initial and boundary conditions chosen, the parabolic reaction-diffusion equations did not produce this kind of patterns where the Turing hole is flanked by waves; they produced only diffusive waves in space. In order to see the effect of the difference in the diffusion coefficients we have set them equal and solved the hyperbolic equations. The results are shown in 2-15A. As is shown, there still appears a space-time pattern although

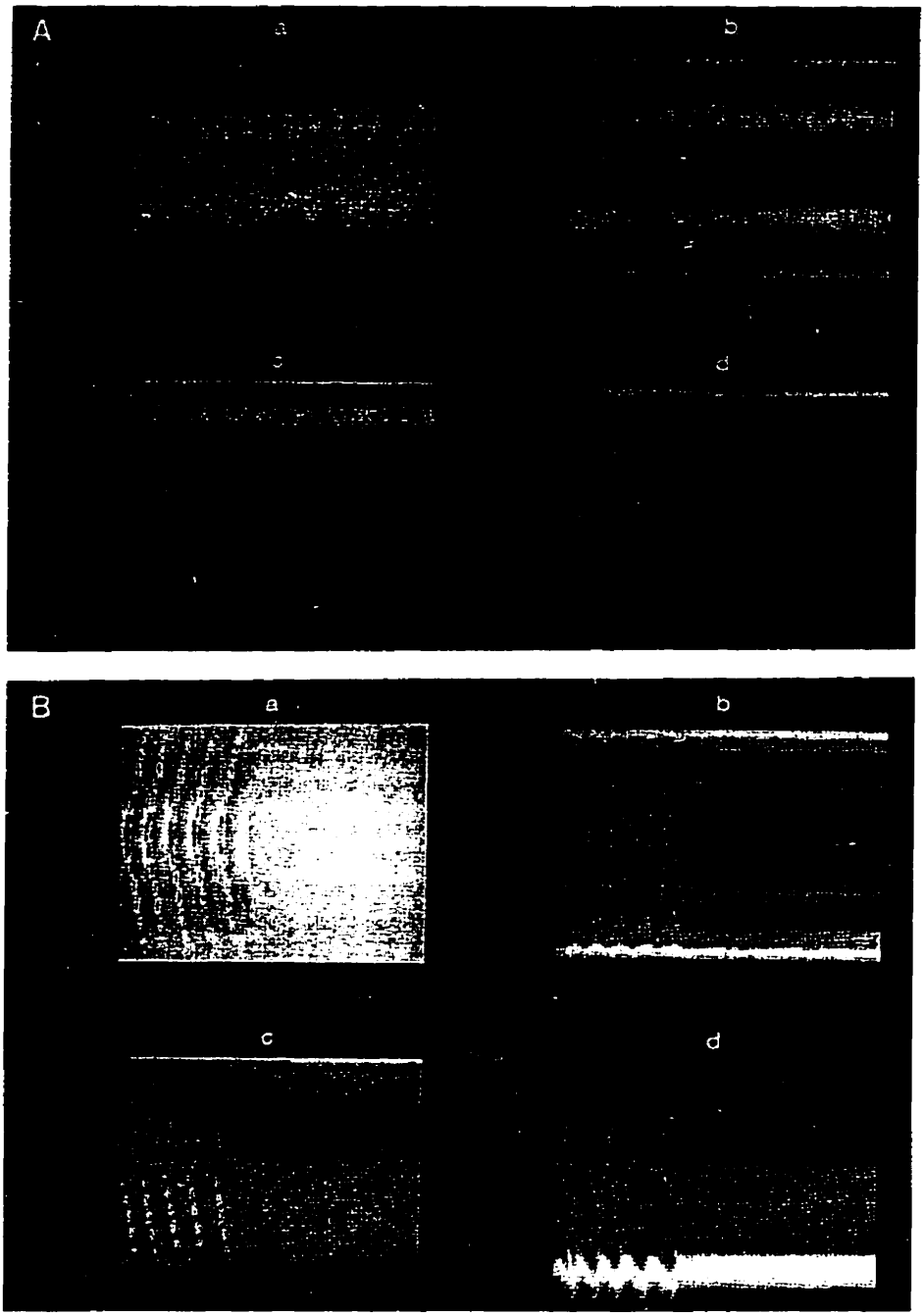

Figure 2-15: *Space-time plot of concentration waves for X in the case of the hyperbolic system at $X = 1.5$ and $Y = 2.5$ and $N_{rd} = 0.1$, $f = 0.1$, and $\hat{D}_x = \hat{D}_y = 0.006$. $(a)X$, $(b)Y$, $(c)u$, and $(d)v$. (B) Same as in (A) except for f=1.*

they are quite different and less striking than those in Figs. 2-14$a-d$ which are for different diffusion coefficients. The Turing theory[24] predicts that the diffusion coefficients must be different in order for spatial patterns to appear, but the hyperbolic system indicates otherwise as we have discussed earlier. Numerical evidence for this can be seen in 2-15A for which $\hat{D}_x = \hat{D}_y = 0.006$ and $f = 0.1$ were taken. We show how the patterns change as the parameter f is changed in 2-15B where $\hat{D}_x = \hat{D}_y = 0.006$ and $f = 1$ are taken. In this case, a more structured pattern appears in the early time, but it is transformed to another stationary form of a different symmetry for the rest of time. These patterns are rather sensitive to the parameters taken.

2.8 Energy and Matter Dissipation in the Case of a Single Steady State

Macroscopic systems evolve to a dissipative structure at the expense of energy and matter on the part of the surroundings. The mode of energy and matter dissipation to create a structure therefore is of considerable interest. The theory of irreversible processes on which the present theory is based shows that the calortropy production must be positive semidefinite for the irreversible process involved. In the case of the present chemical system described by the hyperbolic reaction-diffusion equations under the assumptions stated earlier, this calortropy production coincides with the entropy production in the theory of linear irreversible processes as we have shown earlier. We now investigate how the entropy production (2.53) depends on the frequency and wave number of a pattern evolved from a given set of initial and boundary conditions. Since we have noticed that the patterns change as the reaction-diffusion number changes, we study the N_{rd} dependence of the entropy production. First, we have examined the global entropy production integrated over a period, namely, the integral of the entropy production in space-time for a given set of initial and boundary conditions. These values turn out to be almost inde-

pendent of N_{rd} over the entire range except for the region of small N_{rd} where it decreases significantly. This is the region where the motion gets chaotic and there is no recognizable pattern. *It is interesting that a chaotic motion has a lower entropy production than a structured motion.* This result is presented in Fig. 2-16. It sug-

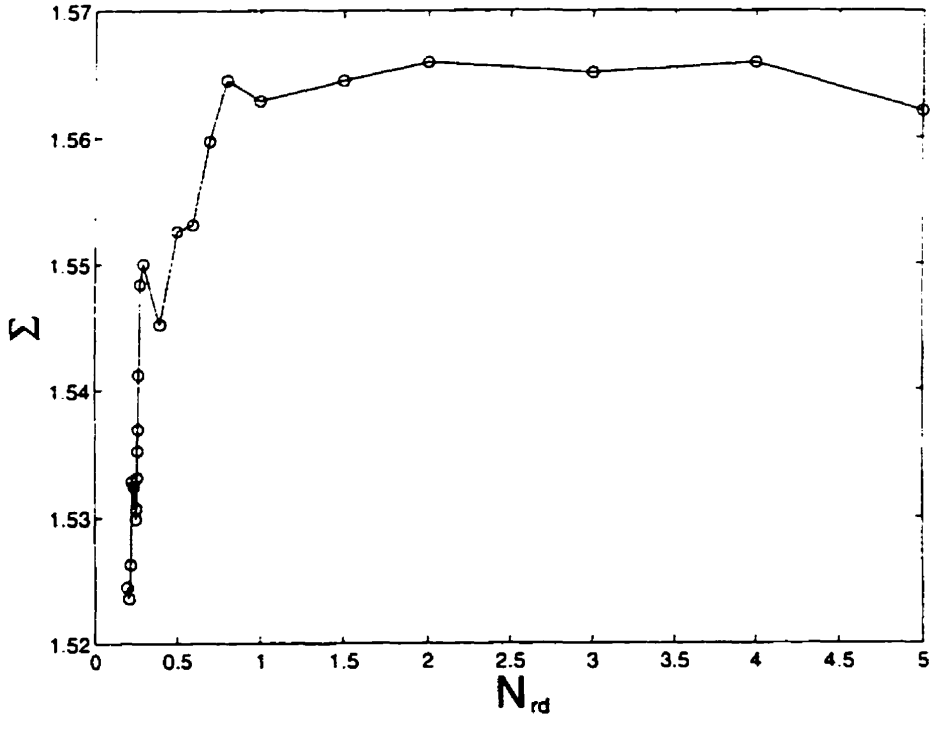

Figure 2-16: *Space-integrated global entropy production vs. reaction-diffusion number. Since different patterns appears as N_{rd} is increased, this figure indicates how the global entropy production changes with patterns.*

gests that the global energy-matter dissipation by the system is higher when there is an organized pattern than a chaotic state, but almost independent of the organized patterns formed in the system for a given initial and boundary conditions. That is, different patterns consume about the same amount of energy and matter globally. It suggests that the global energy-matter dissipation by the system is independent of what is happening locally in the system for a given initial and boundary conditions. This is reasonable and what it should be in retrospect, since the system evolves to a local structure from a homogeneous state with the energy and matter provided

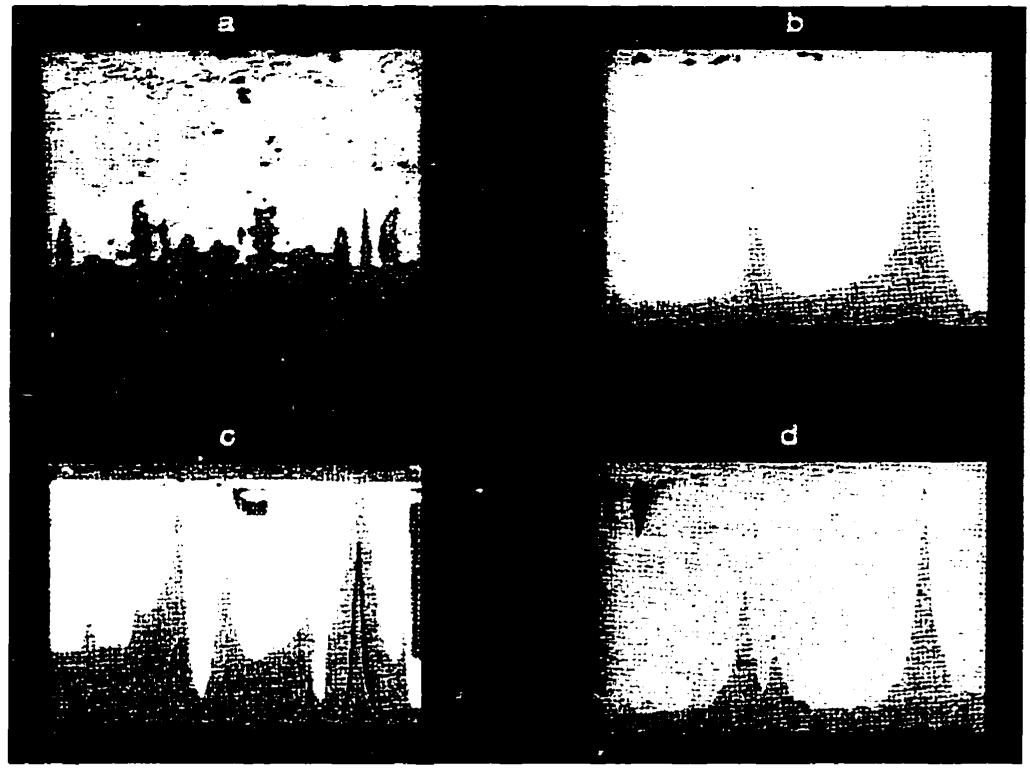

Figure 2-17: *Two-dimensional dissipation (entropy production) spectrum for the hyperbolic system at* $(a)N_{rd} = 0.1$, $(b)N_{rd} = 2$, $(c)N_{rd} = 4$, *and* $(d)N_{rd} = 50$. *Boundary conditions:* $X = 0.2$ *and* $Y = 0.2$. $\hat{D}_x \neq \hat{D}_y$.

by the surroundings, but the global consumption of energy and matter should be the same regardless of which structure is formed locally, if the boundary and initial conditions are the same. Next, we take two-dimensional Fourier transform of the entropy production in space-time and plot its logarithm in the $\omega - k$ plane in the same color code as for the previous figures in color. The abscissa is for k and the ordinate is for ω. Figs. 2-17$a - d$ show how intense the entropy productions are for different modes (ω, k); the low ω modes have the highest intensities for all k and are thus favored by the system at the expense of energy and matter. Notice also that there are certain k values where patterns of high frequency ω modes are formed. 2-18 shows the space-integrated entropy production vs. τ for the system and its Fourier transform for patterns in Fig. 2-14.

The Fourier transform indicates there are many patches of high amplitude modes

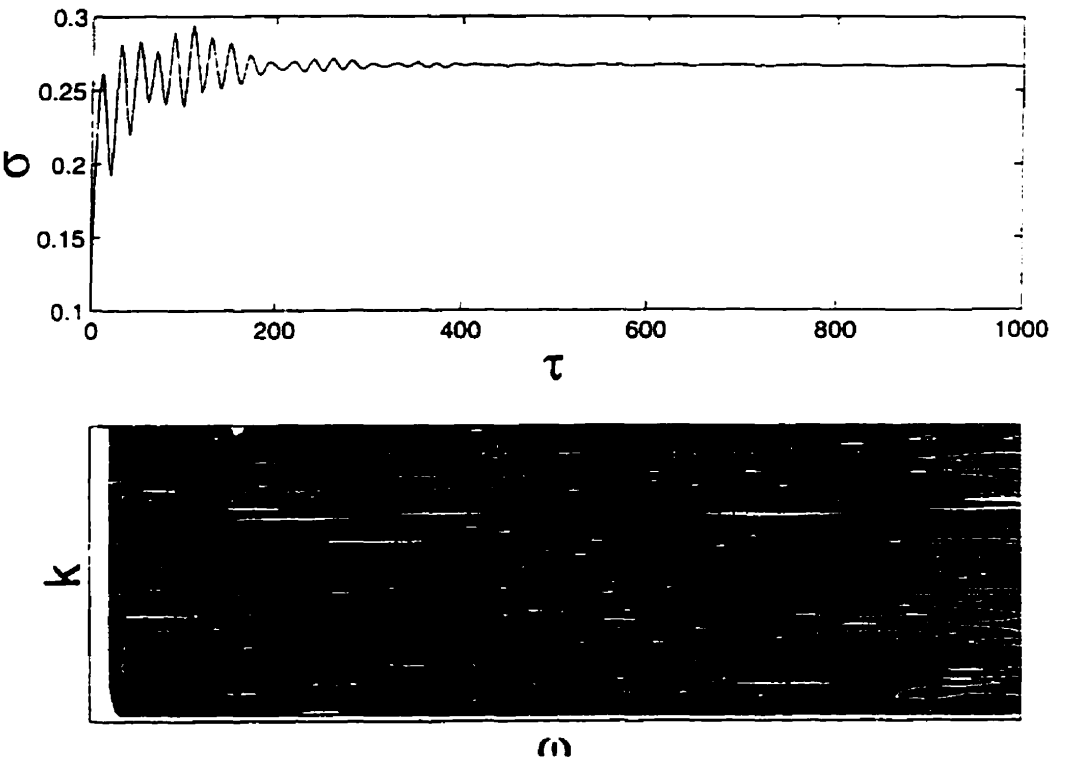

Figure 2-18: *(a)Space-integrated entropy production corresponding to Fig. 2-14. (b)Its Fourier transform plotted in the (ω, k) plane. The darkest shade corresponds to the lowest entropy production.*

as in the case of Fig. 2-17a for a different set of boundary conditions. Since the high intensity of entropy production also means a high wave amplitude, these figures show that the system tends to create low wave-number or long wavelength waves (structures) at all frequencies at the expense of high wave-number waves (structures). There also appear islands of (ω, k) modes that maintain structures appropriating energy and matter from the neighboring modes. The entropy production patterns for the hyperbolic and parabolic systems virtually coincide with each other as the reaction-diffusion number is increased, indicating that the hyperbolic system tends to the parabolic system as N_{rd} increases. Even though the entropy production computed and the reaction-diffusion equations strictly conform to the requirement of the second law, namely, is positive semidefinite, at least for this case studied, the second law of thermodynamics does not directly control creation and selection of

a particular dissipative structure; it only controls the global aspect of the energy-matter consumption of the system. Pattern selection seems to be in the province of local dynamics dictated by the dynamical evolution equations–the reaction-diffusion equations in the present case.

2.9 Bistable Region

We have also examined the region of bistability. The set of parameters is chosen

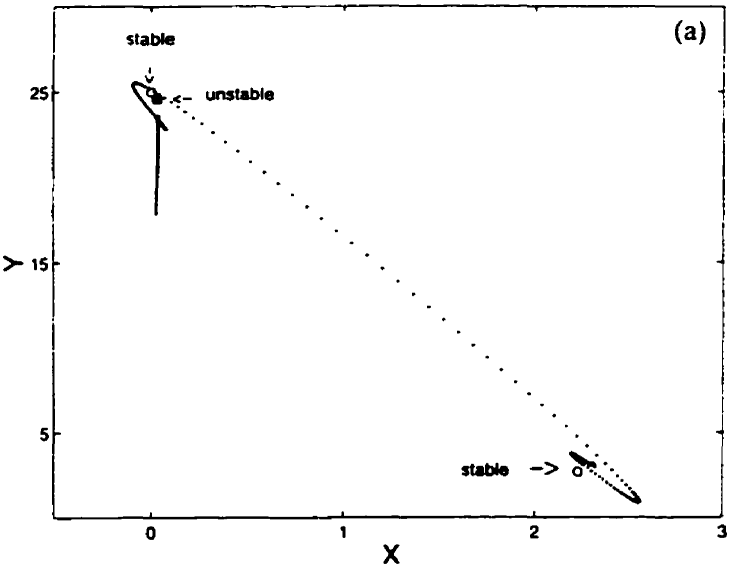

Figure 2-19: *Phase space trajectory in the casse of a bistable system. The trajectory moves from the lower corner to the upper left corner if the initial state was in the vicinity of the stable steady state at the lower corner.*

to be $C = 2.5$, $B = 0.005$, and $N_{rd} = 0.1$ so that the solution of the steady state equation gives rise to three steady states: $X_o = 2.2321$, 0.00585, 0.03478. The first two are stable and the third one is unstable. If the initial conditions are taken to be $X(\xi, 0) = Y(\xi, 0) = u(\xi, 0) = v(\xi, 0) = 0.1$ and the boundary conditions are taken to be $X(0, t) = X(1, t) = 0.1$ and $Y(0, t) = Y(1, t) = 0.1$ at the boundaries, we notice that the system tends to the stable steady state at $X_o = 0.0585$ to stay in its neighborhood for a short time and then moves to the vicinity of the unstable state

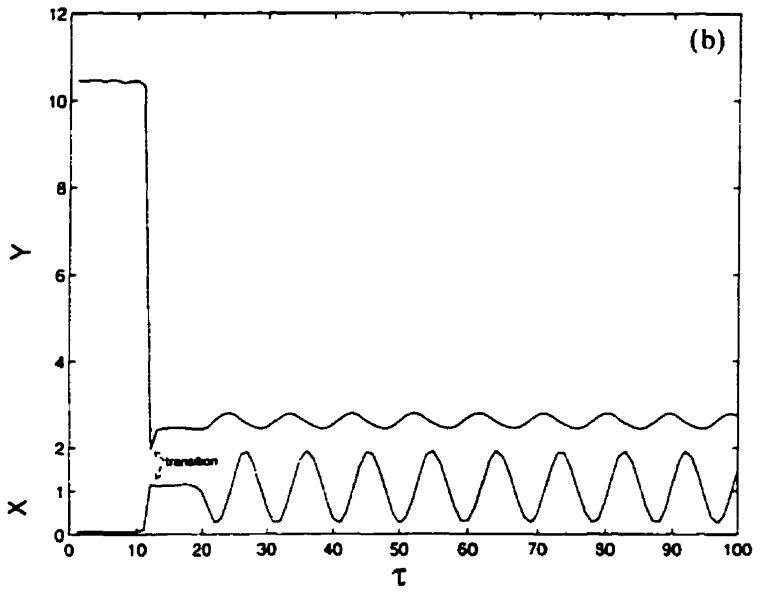

Figure 2-20: *Local behavior in the bistable region. The figure is the section at* $\xi = 0.5$.

at $X_o = 0.03478$ which is very close to the stable state at $X_o = 0.00585$, and then it gets kicked out to the neighborhood of the steady state at $X_o = 2.2231$. This is shown in Fig. 2-19 and the local behaviors of X and Y are presented in Fig. 2-20. Steady temporal oscillations take place near the boundaries as is shown in Figs. 2-21$a - d$. The integrated entropy production is computed for such process. It changes abruptly, as shown in Fig. 2-22, when the system makes transition from the unstable state to the stable state where oscillations take place near the boundaries. Such a Turing pattern is maintained in a higher dissipation state. Apparently, it costs a high uptake of energy and matter to maintain such a pattern. For the parabolic system no transition is induced and the system relaxes directly to the neighborhood of the stable steady state at $X_o = 0.0058547$ instead of the other steady state $X_o = 2.2321$. In Fig. 2-23 a three-dimensional plot of the entropy production is presented in space-time in the case of $N_{rd} = 0.1$. Near the boundaries where Figs. 2-21$a - d$ indicate oscillatory structures the entropy production exhibits a corresponding oscillatory structure. The entropy production bursts to high peaks near the boundaries relatively early on in time and then settles down to a fairly

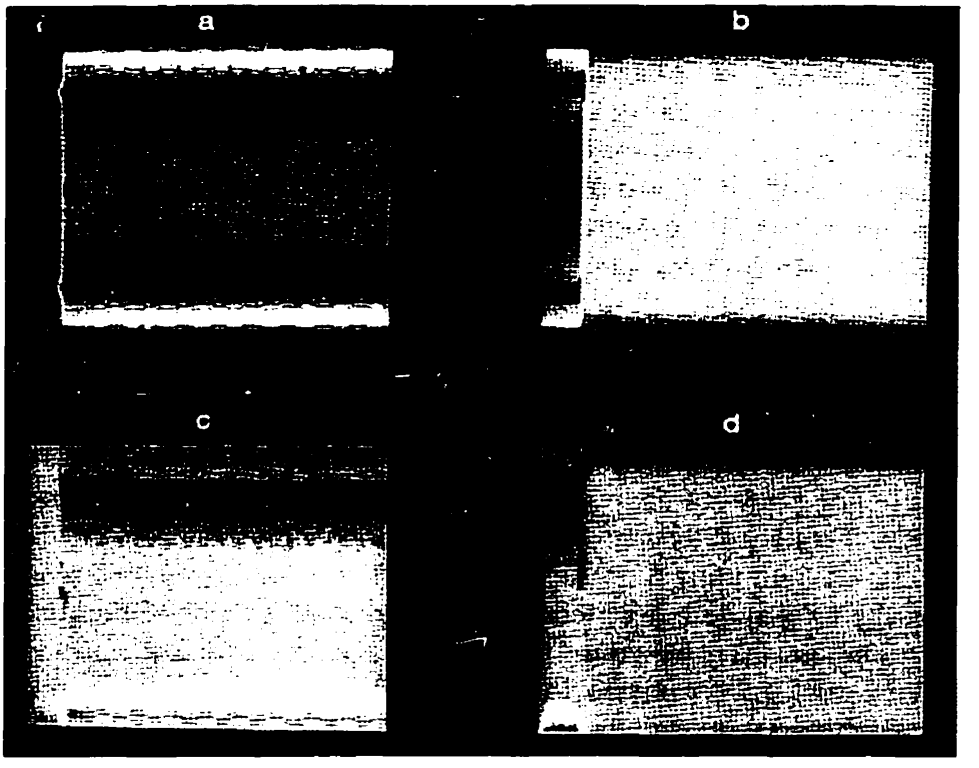

Figure 2-21: *Space-time plot of the X concentration of the hyperbolic system in the bistable regime. Notice the transition region between the two stable states and the wavy behavior induced near the boundaries. A similar behavior was obtained in the case of parabolic system.* $N_{rd} = 0.1$ *and the boundary conditions are:* $X = 0.1$, $Y = 0.1$. $(a)X$, $(b)Y$, $(c)u$, *and* $(d)v$.

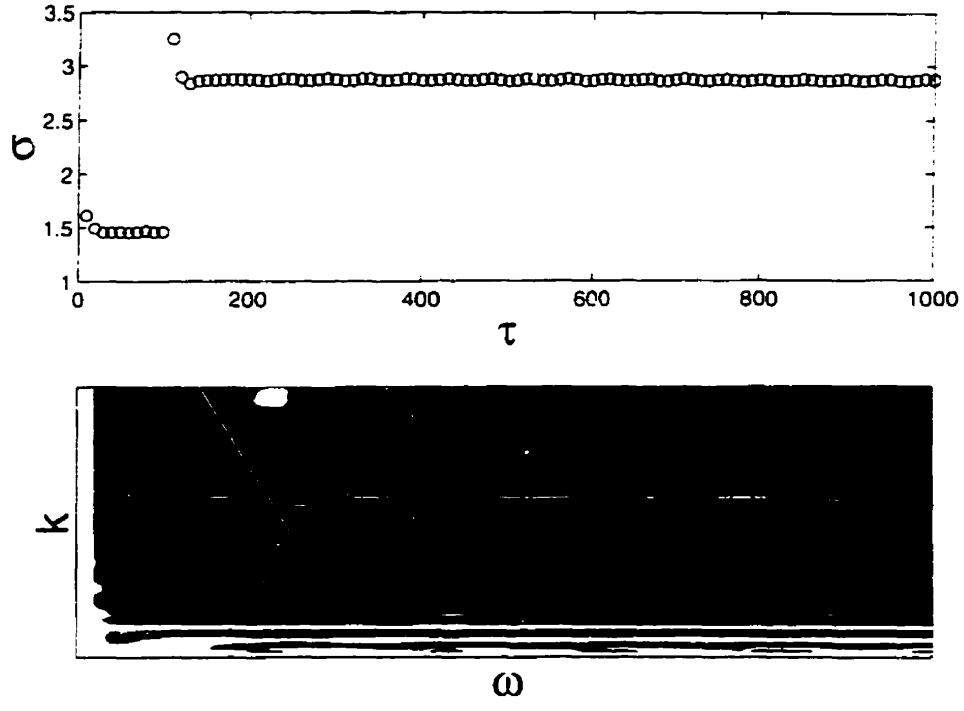

Figure 2-22: *(a)Space-integrated entropy production in the case of the bistability. Notice the abrupt change between the two states. (b)Fourier transform of the entropy production plotted in the (ω, k) plane. The darkest shade corresponds to the low intensity modes and thus low entropy production modes.*

regular structure as time progresses(Fig. 2-23).

2.10 Conclusion

In this chapter we have presented some results of our ongoing study of chemical oscillations and waves by using hyperbolic partial differential equations–wave equations–instead of diffusion equations commonly used in the literature. The hyperbolic reaction-diffusion equations used follow directly from the irreversible thermodynamic theory of processes in systems removed far from equilibrium, and the present study is also an effort to apply the irreversible thermodynamic theory to chemical oscillations and wave phenomena. We have pointed out some formal dif-

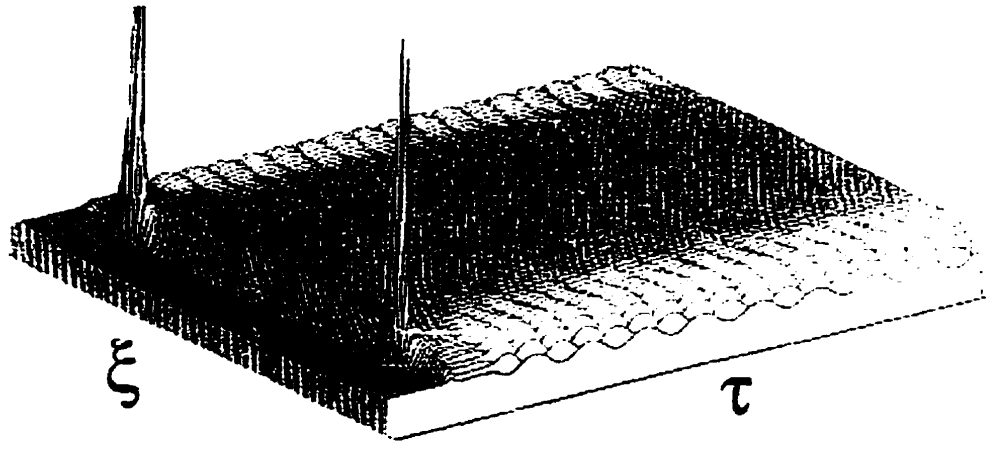

Figure 2-23: *Entropy production for a bistable case.* $N_{rd} = 0.1$. *This figure corresponds to Fig. 2-18.*

ferences between hyperbolic and parabolic systems of partial differential equations for systems of interest here and observed some numerical differences between them. Although hyperbolic differential equations are numerically more difficult to handle than the parabolic counterparts, there are conceptual and theoretical advantages to use hyperbolic differential equations as have been indicated in the text.

In this chapter, we have also examined the entropy productions associated with wave phenomena in the hope of understanding the role of thermodynamic principles in pattern formations and chemical oscillations. We have observed some interesting features, which seem to have been obvious in retrospect. We do not have as yet a satisfactory understanding of thermodynamic reasons for pattern selections, if there is any ground for believing that there should be a thermodynamic reason at all. This line of question is completely open and should be a subject of more intense study in the future. The present thermodynamic theory is hoped to provide some theoretical framework for such study, and the present numerical solution approach gives reasons to believe that hyperbolic differential equations are reasonable evolution equations for chemical oscillations and waves.

Appendix A: The $\lambda - \omega$ Model

In this appendix, we consider a study of the speed of the chemical wave using the hyperbolic reaction-diffusion equations. We take the $\lambda - \omega$ model[20, 21] that has been used for calculating the wave speed for a parabolic system. In the $\lambda - \omega$ model the reaction source term is given by

$$\mathbf{R}'(X,Y) = \begin{pmatrix} \lambda & -\omega \\ \omega & \lambda \end{pmatrix} \begin{pmatrix} X \\ Y \end{pmatrix}, \tag{A.1}$$

where λ and ω are real functions of $r = (X^2 + Y^2)^{1/2}$. It must be noted that the reaction source term is still cubic in X and Y. The $\lambda(r)$ is assumed to have an isolated zero $r_0 : \lambda(r_0) = 0$ whereas $\omega(r_0) \neq 0$. For this model the source term $\mathbf{R}$ in (3.10) is given by

$$\mathbf{R} = \begin{pmatrix} \lambda & -\omega \\ \omega f^{-2} & \lambda f^{-2} \end{pmatrix} \begin{pmatrix} X \\ Y \end{pmatrix} = f_2 \mathbf{R}'. \tag{A.2}$$

To make the equations less cumbersome we will assume $f = 1$ and $\hat{D}_x = \hat{D}_y = 1$. In this case,

$$\mathbf{R} = \begin{pmatrix} \lambda & -\omega \\ \omega & \lambda \end{pmatrix} \begin{pmatrix} X \\ Y \end{pmatrix} \tag{A.3}$$

and

$$\mathbf{H} = \begin{pmatrix} 1 & 0 \\ 0 & 1 \end{pmatrix} - \tilde{N}_{rd} \begin{pmatrix} \lambda & -\omega \\ \omega & \lambda \end{pmatrix} - \tilde{N}_{rd} \begin{pmatrix} X\lambda_x - Y\omega_x & X\lambda_y - Y\omega_y \\ X\omega_x + Y\lambda_x & X\omega_y + Y\lambda_y \end{pmatrix} \tag{A.4}$$

where $\lambda_x = \partial\lambda/\partial X$, $\omega_y = \partial\omega/\partial Y$, etc. Since it is convenient to seek the polar representation of X and Y, we set

$$\begin{pmatrix} X \\ \\ Y \end{pmatrix} = r \begin{pmatrix} cos\theta \\ \\ sin\theta \end{pmatrix} \tag{A.5}$$

Then the wave equation (2.73) with $\mathbf{R}$ and $\mathbf{H}$ defined by (3.19) and (3.20), respectively, may be written in the following two equations

$$\begin{aligned} r_{\tau\tau} \quad & -r\theta_\tau^2 - \bar{N}_{rd}(r_{\xi\xi} - r\theta_\xi^2) + (\bar{N}_{rd} - \lambda)r_\tau \\ + \quad & r\theta_\tau\omega - r\lambda_r r_\tau = \bar{N}_{rd} r\lambda, \end{aligned} \tag{A.6}$$

$$\begin{aligned} r\theta_{\tau\tau} \quad & +2r_\tau\theta_\tau - \bar{N}_{rd}(2r_\xi\theta_\xi + r\theta_{\xi\xi}) - r_\tau\omega \\ + \quad & r(\bar{N}_{rd} - \lambda)\theta_\tau - r\omega_r r_\tau = \bar{N}_{rd} r\omega, \end{aligned} \tag{A.7}$$

where the subscripts τ and ξ denote partial derivatives with respect to τ and ξ, respectively, and the subscript r denotes the derivative with respect to r. If there is a limit cycle, then $r = \alpha$, α being a constant. Furthermore, since a travelling wave is looked for, we set $\theta = \sigma\tau - k\xi$. Then, (A.6) and (A.7) reduce to the form

$$k^2 - \frac{\sigma^2}{\bar{N}_{rd}} - \frac{\sigma\omega(\alpha)}{\bar{N}_{rd}} = \lambda(\alpha), \tag{A.8}$$

$$\left[1 - \lambda(\alpha)/\bar{N}_{rd}\right]\sigma = \omega(\alpha). \tag{A.9}$$

Solving these equations for σ to calculate the dispersion relation, we obtain the travelling wave speed c from the dispersion relation

$$c = \frac{\sigma}{k} = \left(\frac{\bar{N}_{rd}}{2}\right)^{1/2} \left(\frac{1 - \lambda(\alpha)/k^2}{1 - \lambda(\alpha)/2\bar{N}_{rd}}\right)^{1/2}. \tag{A.10}$$

In the case of the parabolic system for the $\lambda - \omega$ model, the travelling wave speed c is given by[21]

$$c = \frac{\sigma}{\kappa} = \frac{\omega(\alpha)}{\sqrt{\lambda(\alpha)}}. \tag{A.11}$$

Thus, if the limit cycle approaches r_0, namely, if $r = \alpha \to r_0$, then $\lambda(\alpha) \to 0$ and the wave speed diverges. In contrast to this, the wave speed of the hyperbolic system, (A.10), predicts that

$$c \to \sqrt{(\bar{N}_{rd}/2)} \text{ as } r = \alpha \to r_0. \tag{A.12}$$

If $\lambda = \gamma - r^2$, then $r_0 = \sqrt{\gamma}$ and if there is a limit cycle of radius $r_0 = \sqrt{\gamma}$, then there is a travelling wave of critical wave number k_c such that

$$k_c = \sigma\sqrt{\frac{2}{\bar{N}_{rd}}} \tag{A.13}$$

which travels at the well-defined speed c given by (A.12). This result is not possible to obtain from the wave speed formula (A.11) predicted by the parabolic differential equations (2.82) in the $\lambda - \omega$ model since it diverges at the limit cycle. For this reason, if the parabolic equations are used for the $\lambda - \omega$ model, travelling wave solutions can be examined only in the neighborhood of the limit cycle as was originally done by Koppel and Howard[21]. The hyperbolic system is free from such a difficulty. This is another distinguishing feature of hyperbolic and parabolic systems of differential equations.

Bibliography

[1] G. T. Dee, Physica D, **23**, 340 (1986).

[2] G. Dewel, P. Borckmans and D. Walgraef, Proc. Natl. Acad. Sci. USA **80**, 6429 (1983).

[3] V. V. Barelko in *Self-organization Phenomena and Autowave Processes in Heterogeneous Chemical and Physical Systems*, edited by V. I. Krinsky (Springer-Verlag, Berlin, 1984).

[4] L. A. Segel, *Modelling Dynamic Phenomena in Molecular and Cellular Biology* (Cambridge University Press, Cambridge, U. K. , 1984).

[5] A. S. Mikailov and I. V. Uporov, Usp. Fiz. Nauk., **144**, 79 (1984).

[6] A. T. Winfree, *The Geometry of Biological Time*, (Springer, Berlin, 1980).

[7] A. L. Hodgin and A. F. Huxley, J. Physiol. (London), **117**, 500 (1952).

[8] Y. Kuramoto, *Chemical Oscillations, Waves, and Turbulence* (Springer, Berlin, 1984); F. Baras and D. Walgraef, eds., *Chemical Dynamics: Experiments to Microscopic Simulations*, Physica A **188**, No. 1-3(1992).

[9] (a)I. Prigogine, *Thermodynamics of Irreversible Processes* (Interscience, New York, 1961); (*b*)*G*. Nicolis and I. Prigogine, *Self-Organization in Nonequilibrium Systems* (Wiley, New York, 1977).

[10] P. Glansdorff and I. Prigogine, *Thermodynamic Theory of Structure, Stability, and Fluctuations* (Wiley, New York, 1971).

[11] See, for example, B. C. Eu, *Kinetic Theory and Irreversible Thermodynamics* (Wiley, New York, 1992).

[12] I. Müller and T. Ruggeri, *Extended Thermodynamics* (Springer, Berlin, 1993).

[13] H. G. Othmer, J. Chem. Phys. **64**, 460(1976).

[14] U. I. Cho and B. C. Eu, Physica D 68, 351(1993).

[15] 9. (a)Y. Termonia and J. Ross, Proc. Nat. Acad. Sci. USA **78**, 2952; 3563(1982); (b)P. Richter, P. Rehmus, and J. Ross, Prog. Theor. Phys. **66**, 385(1981).

[16] E. E. Selkov, Eur. J. Biochem. **4**, 79(1968).

[17] S. Ponce Dawson, A. Lawniczak, and R. Kapral, J. Chem. Phys. **100**, 5211(1994).

[18] B. C. Eu, Phys. Rev.E, **51**, 768(1995).

[19] B. C. Eu, J. Chem. Phys. **102**, 7169(1995).

[20] N. Koppel and L. N. Howard, Studies in Appl. Math. **42**, 291(1973): L. N. Howard and N. Koppel, Studies in Appl. Math. **56**, 95(1977).

[21] J. D. Murray, *Mathematical Biology* (Springer, Berlin, 1989).

[22] F. R. Gantmacher, *Théorie des Matrices* (Dunod, Paris, 1966), Vol. 2.

[23] A. Turing, Phil. Trans. Roy. Soc. London Ser.B **327**, 37(1952).

[24] J. E. Pearson and W. Horsthemke, J. Chem. Phys. **90**, 1588(1989).

[25] C. Canuto, M. Y. Hussaini, A. Quarteroni and T. A. Zang, *Spectral Methods in Fluid Dynamics* (Springer, Berlin, 1988).

[26] V. Petrov, S. K. Scott, and K. Showalter, Phil. Trans. Roy. Soc. London, A **347**, 631(1994).

[27] K. Lee, W. D. McCormick, J. E. Pearson, and H. L. Swinney, Nature **369**, 215(1994); Phys. Rev. E. (preprint).

[28] P. De Kepper, V. Castets, E. Dulos, and J. Boissonade, Physica D **49**, 161(1991).J. J. Perraud, A. De Wit, E. Dulos, P. De Kepper, G. Dewel, and P.Borckmans, Phys. Rev. Lett. **71**, 1272(1993); V. Dufiet and J. Boissonade, J. Chem. Phys. **96**, 664(1992).

[29] A. De Wit, G. Dewel, and P. Borckmans, Phys. Rev. E **48**, R4191(1993).

Chapter 3

Model for Glycolysis in Two Dimensions

3.1 Introduction

Biologically, glycolysis is a very complicated set of reactions that take place on the cellular level. It should be noted that the usage of a model that accounts reasonably well for the observed phenomena, even though the molecular picture on which it is based is not quite correct, is to our advantage since we can almost always describe the cooperative phenomena which are insensitive to the underlying mechanism, using the universality noted in self-organizing systems. It is well known that morphogenesis, the development of structure and form, proceeds sequentially through continuous symmetry breaking bifurcations as suggested by Truing in his seminal paper[28]. He also proposed that the morphogens obey reaction-diffusion equations. So it is really important to study the early stages of development of the form which will influence the final selected shape. Also in small geometries, like the cell, it is most likely that the concentration gradients would be very large. Partly because of these arguments, we can see how parabolic reaction-diffusion equations can be inadequate to describe glycolysis in small geometries. In fact, we will show at the end of this chapter that hyperbolic reaction-diffusion equations are more ad-

equate than their parabolic counterpart in more general situations if scaling for the evolution equations is done more carefully. The other basic motivation for studying hyperbolic reaction diffusion-equations for the Selkov model in two dimensions, is in framing the theory of chemical oscillations and waves under the principles of thermodynamics so that the macroscopic description of chemical oscillation and wave phenomena is consistent with the thermodynamic laws as any macroscopic theory should and to look for any relationships between spatial symmetries selected by the system and the mentioned laws; comparing the differences in results such as the patterns and their spatio-temporal evolutions predicted by the two different types of differential equations; and their implications for energy and matter consumption and irreversible thermodynamics. In the previous chapter, we have discussed that as the reaction-diffusion number, which characterizes the relative time scales of reactions and diffusion to the time scale of hydrodynamic flow, increases beyond a characteristic value, the hyperbolic reaction-diffusion equations taken for the study of the Selkov model reduce to the conventional parabolic reaction-diffusion equations. We have also shown that *the local patterns of certain frequencies and wave numbers are formed and maintained at the expense of energy and matter yet the total global energy dissipations are the same for different patterns formed. This means that some patterns of particular frequencies and wave numbers appropriate energy and matter to themselves at the expense of those of other frequencies and wave numbers*[5]. These results are interesting on their own right, but also potentially useful for improving our understanding of pattern formation phenomena as well as nonlinear wave phenomena. In this chapter, we would like to describe various modes of pattern and wave formations in two dimensions under the non-random initial and boundary conditions as well as random initial conditions, and the modes of energy and matter dissipation by the various patterns formed. Unlike the parabolic reaction-diffusion equations conventionally used in connection with chemical oscillations and waves, the hyperbolic reaction-diffusion equations taken for the study here describe transient behaviors of the system. For example, they can describe a phenomenon akin to cell divisions observed in the simulations of

the CIMA reaction[7] and the Lengyel-Epstein model[8]. The Selkov model admits monostable and bistable regions of stability. In this work, we explore the modes of pattern formation in both regions. We find empirically that some interesting behaviors occur in the vicinity of the unstable steady state in the bistable region. Spirals and solitary waves are observed to arise under some conditions. The spirals interact and their tips meander. Two solitary waves for each species can also be formed and propagate at two different speeds. They can also merge to a single front which propagates at a constant speed. These features all arise from the single set of hyperbolic reaction-diffusion equations, depending on the initial and boundary conditions. We have computed the speed of such waves.

3.2 Cubic Reversible Chemical Reaction Model and the Governing Evolution Equations

The Selkov model for glycolysis[12] was modified by Richter et al.[55] who assumed the three coupled chemical reactions

$$\begin{aligned} A &\underset{k_{-1}}{\overset{k_1}{\rightleftharpoons}} S \\ S + 2P &\underset{k_{-2}}{\overset{k_2}{\rightleftharpoons}} 3P \\ P &\underset{k_{-3}}{\overset{k_3}{\rightleftharpoons}} B. \end{aligned}$$

In these reactions A and B are kept at fixed concentrations and the intermediates S and P change in space-time. The reaction-diffusion $\bar{N}_{rd}$ number is a dimensionless number which characterizes the relative magnitude of the time scale of sound wave to

the time scales of a chemical reaction and diffusion. It is a parameter that determines the hyperbolicity of the differential equations . The governing evolution equations for the dimensionless intermediate species X and Y and their corresponding fluxes $\mathbf{u}$ and $\mathbf{v}$ are given by the following evolution equations

$$\partial_\tau X = -\nabla_\xi \cdot \mathbf{u} + B - X + X^2Y - KX^3, \tag{3.1}$$

$$\partial_\tau Y = -\nabla_\xi \cdot \mathbf{v} + A - RY - X^2Y + KX^3, \tag{3.2}$$

$$\partial_\tau \mathbf{u} = -N_{rd} f(\hat{D}_x \nabla_\xi X + \mathbf{u}), \tag{3.3}$$

$$\partial_\tau \mathbf{v} = -N_{rd} f^{-1}(\hat{D}_y \nabla_\xi Y + \mathbf{v}), \tag{3.4}$$

and can be combined into coupled wave equations as done in the previous chapter:

$$\partial_\tau^2 \mathbf{Z} + \bar{N}_{rd} \mathbf{H} \partial_\tau \mathbf{Z} - \bar{N}_{rd} \mathbf{D} \nabla_\xi^2 \mathbf{Z} = \bar{N}_{rd} \mathbf{R}(X, Y). \tag{3.5}$$

where now $\nabla_\xi^2 = \partial_{\xi_1}^2 + \partial_{\xi_2}^2$ is a two dimensional Laplacian operator in scaled Cartesian coordinates ξ_1 and ξ_2..

3.3 Numerical Solutions of the Wave Equations

The coupled wave equations (3.5)—the generalized telegraphist equations—are solved for two dimensions by a suitable numerical integration method. The fixed boundary conditions are taken, but the initial conditions are taken to be either random or nonrandom. The case of random initial conditions gives rise to rather interesting results not seen in the case of nonrandom initial conditions. In this work, we have applied a combination of a spectral method[16] and Gear's method for stiff differential equations. The solutions obtained were interpolated by using the Matlab interpolation and graphics software[18] to produce pictorial representations of

the patterns produced. A number of patterns have been produced in the course of calculation, such as travelling waves, hexagonal structures, stripes, squares, and turbulent patterns, as the reaction-diffusion number N_{rd} is changed. This is consistent with the reaction-diffusion number dependence of patterns observed in the study of the one-dimensional hyperbolic reaction-diffusion equations reported in Ref. [5]. A reduction in the reaction-diffusion number can destabilize patterns and give rise to loss of their synchronizations which could eventually produce a turbulent pattern. In most of the calculations, we have chosen the set of parameters in the unstable region away from the threshold in the phase diagram to ensure fully developed patterns and reveal the complexity of the nonlinear dynamics and also the possible difference from the dynamics of pattern formations produced by the corresponding parabolic reaction-diffusion equations. Patterns obtained with the hyperbolic reaction-diffusion equations are different from those by the parabolic reaction-diffusion equations as will be shown by examples and as was the case for the one-dimensional system reported in Ref. [5]. We will present various patterns observed below. The range of N_{rd} studied in this work is from 0.1 to 10^{-3} except for some special cases involving spirals and solitons for which N_{rd} is taken of the order of 1 and the other parameters are taken for the bistability regime of the system. Before proceeding to the presentation, we would like to elaborate on the numerical solution procedure.

3.3.1 Description of the Numerical Solution Method Used

For the purpose of numerical solutions the wave equations (3.5) can be written as a set of differential equations as follows:

$$\partial_\tau \mathbf{Z}(X,Y) = \mathbf{W}(X,Y), \tag{3.6}$$

$$\partial_\tau \mathbf{W}(X,Y) = -\bar{N}_{rd}\mathbf{H}\mathbf{W}(X,Y)+\bar{N}_{rd}\mathbf{Q}(X,Y)+\bar{N}_{rd}\mathbf{R}(X,Y), \tag{3.7}$$

$$\mathbf{Q}(X,Y) = \mathbf{D}\nabla^2_\xi \mathbf{Z}(X,Y). \tag{3.8}$$

The last equations for the spatial derivative (3.8) are solved by the Fourier spectral method[16] with 128 collocation points for most of the cases and 64 collocation points otherwise. When The resulting system of ordinary differential equations in time are solved in the physical space by using Gear's method for stiff differential equations. This procedure requires Fourier transforming the spatial derivatives back and forth, but it allows to compute the second derivative terms in the wave equations with a high accuracy and at the same time to avoid computing the Fourier transforms of nonlinear terms in the second equation which result in time-consuming convolution sums of Fourier components of X and Y. The solution did not change qualitatively when computed respectively with 32, 64 and 128 collocation points. The boundary conditions chosen are:

$$\begin{aligned} X(\xi_1 &= 0,\tau) = X(\xi_1 = 1,\tau) = C_x,\ X(\xi_2 = 0,\tau) = X(\xi_2 = 1,\tau) = C_x', \\ Y(\xi_1 &= 0,\tau) = Y(\xi_1 = 1,\tau) = C_y,\ Y(\xi_2 = 0,\tau) = Y(\xi_2 = 1,\tau) = C_y', \end{aligned} \tag{4.2}$$

$$\begin{aligned} X(\xi_1,\tau &= 0) = C_x,\ X(\xi_2 = 0,\tau) = C_x', Y(\xi_1,\tau = 0) = C_y, Y(\xi_1,\tau = 0) = C_y' \\ \mathbf{u}(\boldsymbol{\xi},0) &= \mathbf{v}(\boldsymbol{\xi},0) = 0. \end{aligned}$$

Here ξ_1 and ξ_2 are two reduced Cartesian coordinates. In another set of calculations we have chosen random initial conditions. For the sake of arguing, we should mention that in biological systems, these boundary conditions are far from being respected. Biological systems are generally quite small ($Lk_0 \simeq 1-10$) and the patterns are therefore influenced by boundary conditions. Often no-flux boundary conditions are assumed for the diffusing substance, since they are intuitively reasonable, but they are rather special from the point of view of pattern formation. As for pattern selection, those idealized conditions render it weak because of the many possibilities of choosing between mathematically acceptable nonlinear solutions near threshold which could have been narrowed down with the constraint of real boundary conditions. Arcuri and Murray[7] have investigated one-dimensional reaction-diffusion

equations with both inhomogeneous and rigid boundary conditions, and indeed find a greater selectivity in the former case.

Division of a Pattern and Competition between Stripes and Hexagons

In the regime of N_{rd} of the order of 10^{-1} and in the regime of parameters where only an unstable steady state is available (i.e., $A = 0.5, B = 0.09$) a phenomenon akin to a cell division was observed. Namely, regardless of whether the initial conditions are random or nonrandom, the system initially has no clearly recognizable organized patterns which one might consider random. As time progresses and reaches the intermediate time regime, such initially random patterns get synchronized to form a circular spot of high concentration in the middle of the square. In the case of nonrandom initial conditions, the patterns oscillate and the oscillations continue for a long time. This behavior and the patterns are very similar to those observed in the parabolic system for the same value of A and B as shown in Fig. 3-1.

Actually, in the case of the parabolic system the patterns were stable with respect to all sorts of small perturbations to the initial conditions with a random noise, for it was able to synchronize in space and time to produce coherent oscillatory patterns as shown in Fig. 3-1.

For the hyperbolic system, if the initial conditions are random, the circular pattern eventually splits into two and then into four circular patterns which move to the four corners of the square. The amplitudes of the patterns oscillate synchronized, thus producing patterns of a depressed concentration. These patterns then merge and divide into more circular patterns which either elongate or vanish, but they maintain symmetry even though the patterns become more intricate. There can also simultaneously occur patches of hexagons and stripes oriented differently. This process of organization and synchronized oscillations of local structures continue until the local symmetric patterns lose their stability and develop irregular stripe structures. This evolution of patterns from the stage of patterns similar to those shown in Fig. 3-1 is shown in the sequence of patterns shown in Figs. (3-2, 3-3,

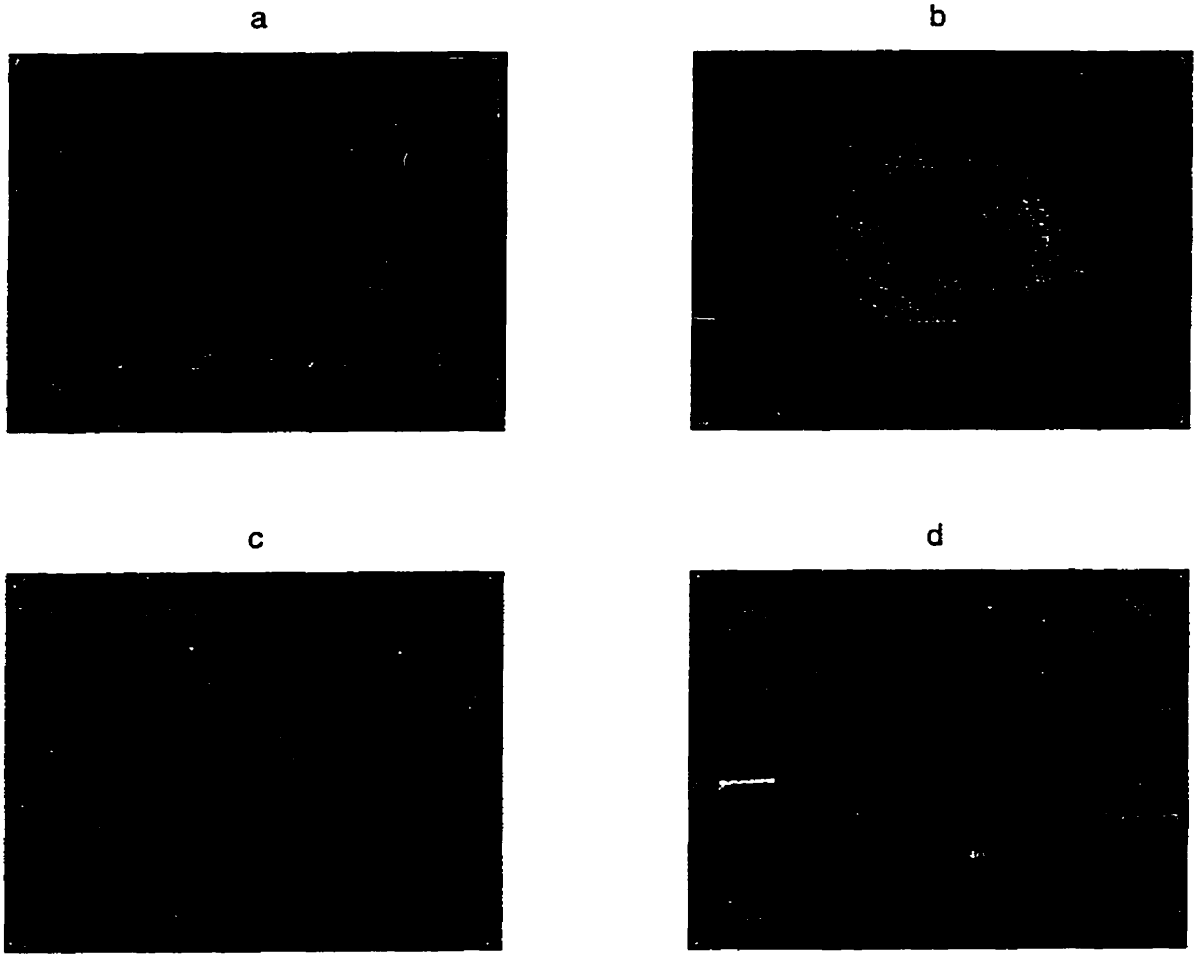

Figure 3-1: *Patterns formed by parabolic reaction-diffusion equations with random initial conditions. They were able to form coherent oscillatory behavior. The hyperbolic system at high N_{rd} or with nonrandom initial conditions shows very similar patterns (not shown). The darker the shade, the lower the concentration is in this figure.*

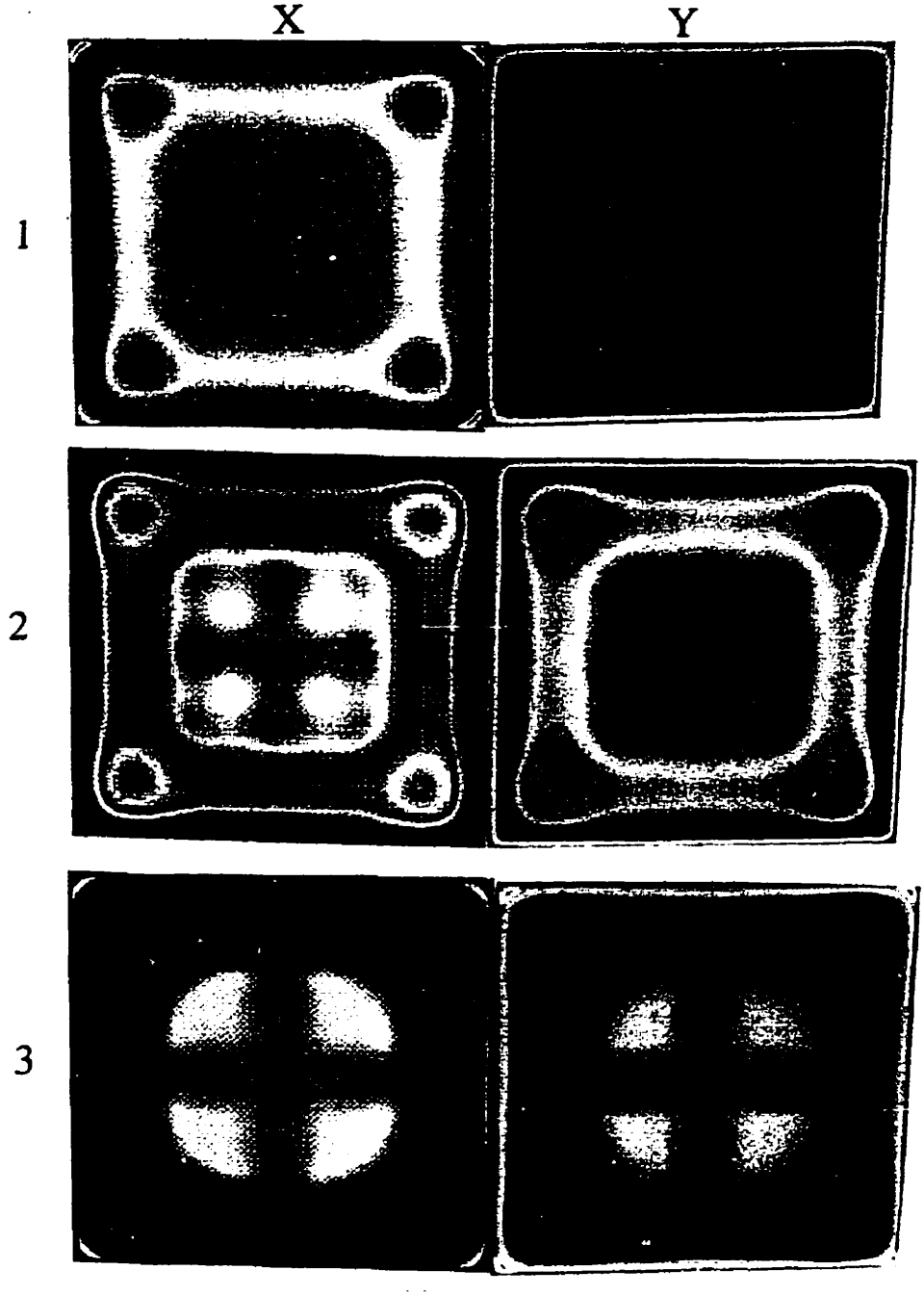

Figure 3-2: *Evolution of patterns in the hyperbolic reaction-diffusion system in the case of* $N_{rd} = 0.1$. *Random initial conditions* ($X_b = 0.2, Y_b = 0.2$ *perturbed by a 1% random Gaussian noise) are supplied.*

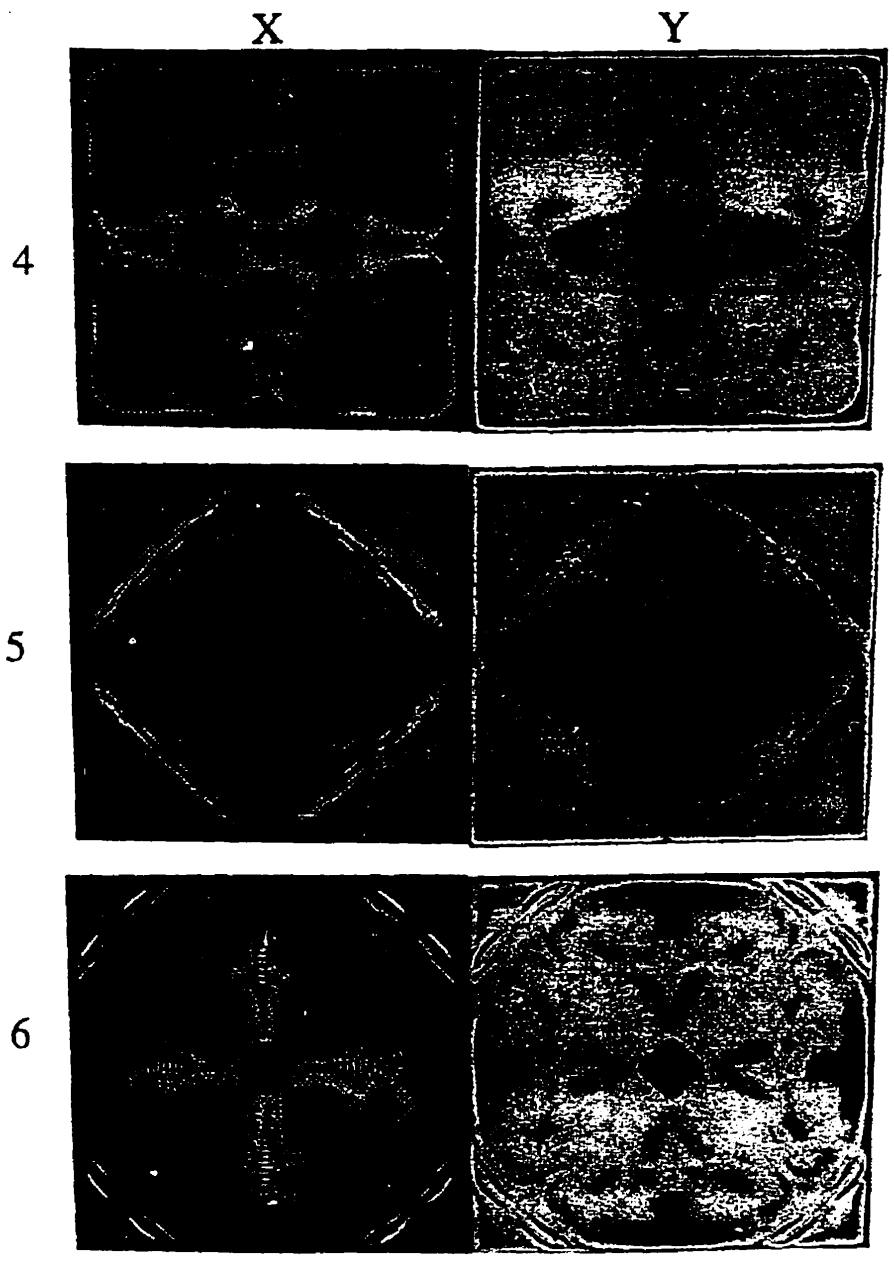

Figure 3-3: Continuation of Fig. 3-2.

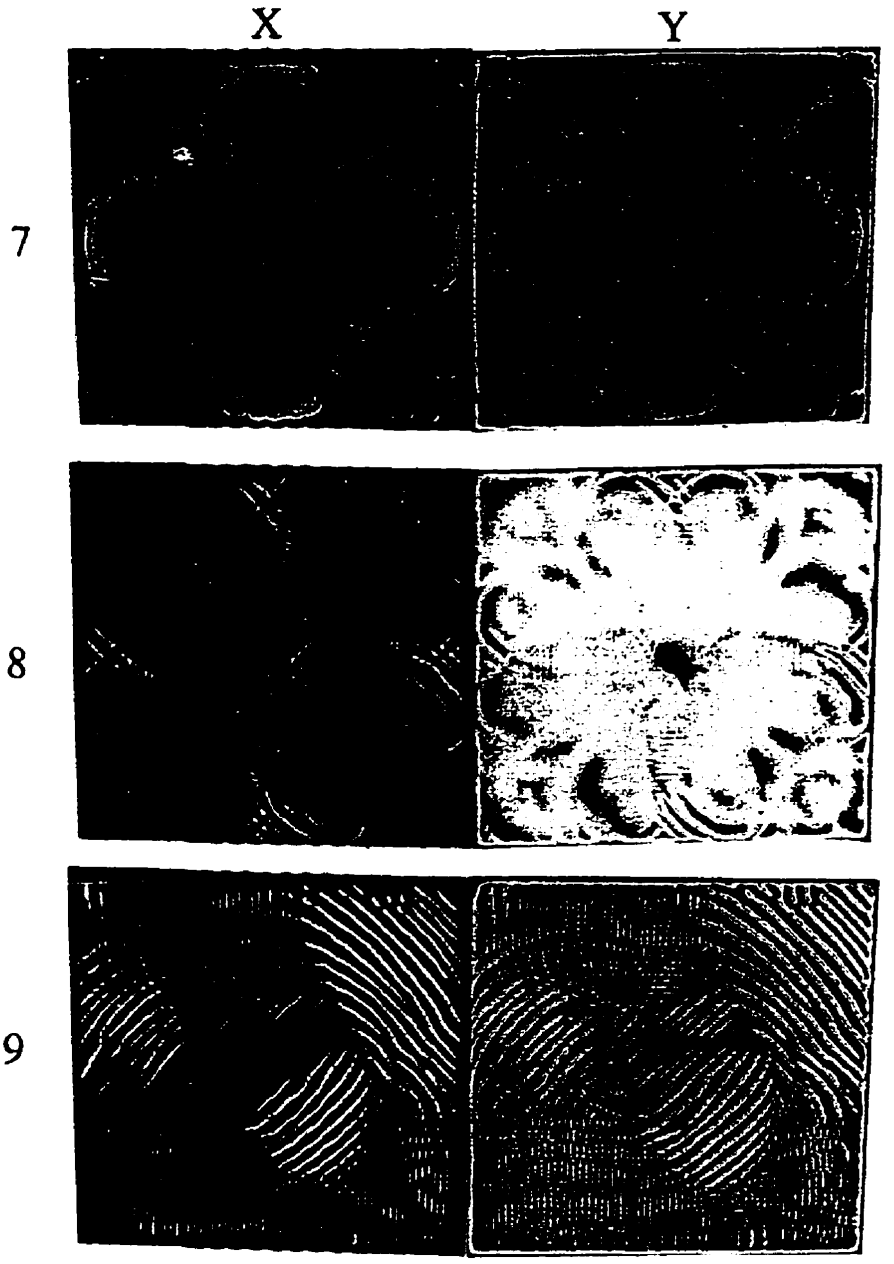

Figure 3-4: Continuation of Fig. 3-3.

3-4)[1]. Since they are very interesting, we show the set although the set is not small in number. In these figures the blue means a low concentration of species X and Y whereas the brown means a high concentration of X and Y, the colors in-between meaning intermediate concentrations in the order of the colors from blue to red. That is, where X is low in concentration, Y is high in concentration, for example. We observe that although the symmetry of the patterns are basically the same for X and Y except that they have opposite color codes for the magnitudes of concentration, the fine structures are not the same, and it reflects the fact that their governing equations are not symmetric with respect to X and Y. We also observe that the patterns are created on the basic hexagonal lattice arranged on mutually crossing straight lines as the spots on the lattice points get larger than the lattice spacing and merge together. The crossing lines may be regarded as the intersections of characteristic planes with the surface of the figure at a given time τ and the basic hexagonal structure created is periodic oscillations of concentrations in the characteristic surfaces of the two-dimensional hyperbolic reaction-diffusion equations. The pattern splitting-oscillation behavior continues in a perfectly symmetrical fashion as long as the system is kept out of equilibrium. The system eventually reaches a saturation

[1]**Description of Figures 3-2, 3-3, and 3-4:** Evolution of patterns in the hyperbolic reaction-diffusion system in the case of $N_{rd} = 0.1$. Random initial conditions ($X_b = 0.2, Y_b = 0.2$ perturbed by a 1% random Gaussian noise) are supplied. The system homogenizes and then breaks symmetry and forms random incoherent patches of high concentrations which subsequently merge to a circular pattern (not shown but similar to those shown in Fig. 3-1) in the middle of the square. This circular pattern breaks up into two and then into four which move, as shown, to the corners of the square leaving images of smaller sets of patterns of alternating concentrations in the middle. The concentration begins to oscillate with the symmetry of the patterns unchanged. Then, there appear patterns of more intricate structures in the middle which also oscillate concentration-wise. This structure subsequently becomes more intricate although the number of symmetry axes remains the same and the concentration continues to oscillate and form a pattern of higher symmetry. The pattern in panel 6 bifurcates to a pattern of a lower symmetry shown in panel 7 since the number of symmetry axes is reduced by half; two diagonals. There are also two diagonal symmetry axes in panel 8. In panel 9, the pattern has bifurcated to a state where we can no longer distinguish any global symmetry. Locally, patches of stripes and hexagons and mixed modes of different orientations begin to appear. The stripes compete with the basic hexagonal pattern in an irregular fashion, producing an irregular structure. The stripes in panel 9 which are filling almost half the area are later replaced by hexagons or squares (not shown here) which are the basic texture of all patterns from which various patterns are formed as the concentration fluctuations along the intersecting characteristic surfaces get broadened and merge together. The corresponding parabolic reaction-diffusion system does not produce the sequence of patterns produced by the hyperbolic system as shown here; it produces patterns shown in Fig. 3-1.

point which is a state where the entropy production (calortropy production) reaches an asymptotic value. The pattern therefore is maintained at a high but asymptotic state of energy and matter consumption. At this stage, continuous competition between stripes and hexagonal structures is active. Sometimes one symmetry pattern wins over the other and vice versa. An example of this phenomenon can be seen in the figures in the last stage of evolution shown in Fig. 3-4(9). This competition and interactions between hexagonal and stripe patterns could be due to the additional frequencies and resulting complexities provided by the hyperbolic reaction-diffusion equation system as a result of interactions of different frequency modes. However, if the state of the system is near the critical (Hopf) point, then one pattern wins completely over the other. The same situation arises if the evolution is started from a 16×16 square in the middle of the grid of 128×128 meshpoints and the system is perturbed by a 1% random noise added to the initial conditions. For the lack of space we do not show them here. It must be noted here that for the same set of parameters as for the hyperbolic reaction-diffusion equations the corresponding parabolic reaction-diffusion equations do not produce the evolution of patterns as shown in Fig. (3-2, 3-3, 3-4). Neither does there appear a hexagonal structure. Although a circular spot appears and eventually splits up into four spots which move to the four corners in a way similar to Fig. 3-1 and this behavior repeats over time, none of the transient patterns seen in the hyperbolic system could be observed in the case of the parabolic system. It must be also noted that the transient patterns of the hyperbolic system are not so transient as the term transient implies; they are fairly long lived and comparable in their lifetime to those of the patterns of the parabolic system shown in Fig. 3-1, the span of τ for each panel in Figs. (3-2, 3-3, 3-4) being about 100τ which is about the same value of τ required for the last pattern to form in Fig. 3-1.

In summary, in the case of nonrandom initial conditions the evolution of patterns from initially random patterns is quite different from and less intricate than the sequence presented earlier in Figs. (3-2, 3-3, 3-4) for random initial conditions. In fact, the pattern evolution was found to be rather similar to those parabolic systems,

and Fig. 3-1 may well substitute for the pattern evolution for the hyperbolic system subjected to the boundary and nonrandom initial conditions comparable with those for the parabolic system.

Superposition of Squares-Hexagons and Spiral Waves

As the reaction-diffusion number is further lowered from $N_{rd} = 0.1$, more interesting and complicated phases and patterns appear. For example, if N_{rd} is set equal to 0.01 with nonrandom initial conditions, hexagonal structures begin to form initially, but defects begin to develop and minute spirals around the defects begin to form on the basic hexagonal-rhombic-squared texture as shown in Fig. 3-5. Spirals

Figure 3-5: *Evolution of spirals in the hyperbolic reaction-diffusion equation system at* $N_{rd} = 0.01$ *in the case of nonrandom initial conditions* ($X_0 = 0.25, Y_0 = 3.5$). *The boundary conditions:* $X_b = 0.26, Y_b = 3.5$. *The spirals formed change their shape only slightly but do not evolve over a long time span. This is in contrast to the behavior of the random initial conditions shown in Fig. 3-6 below.*

do appear but do not grow in the case of the nonrandom initial conditions taken. However, if initial conditions are made random, the chemical inhomogeneities are tended to be redistributed to patterns in an ordered manner and then hexagonal-

rhombic structures emerge (Fig. 3-6a′). This sequence is shown in Fig. 3-6[2], where we also notice structures at the four corners and symmetrical wave-like patterns near the boundaries. They look like spirals that are being annihilated at the boundaries. The hexagonal-rhombic-squared phase was time-dependent and their amplitudes oscillating. Before spirals appear in the middle of the square, two spots of high concentration are visible in the middle of the hexagonal region, and then an almost symmetrical pair of spirals of opposite chirality begins to form and therefrom grow on the squared texture (Fig. 3-6a-d). These spirals are multiarmed; there are 2 or 3 arms. They have a minimum of wavelength approximately three to four times bigger than that of the hexagonal structure. They begin to interfere and destroy each other, leaving a kind of turbulent spots behind until the whole pattern becomes chaotic and remains so as shown in Fig. 3-6e. It was noticed that spirals and incomplete rings develop near the boundaries. We remark that this behavior is also encountered in numerical simulations in a square geometry by other authors[19] . If N_{rd} is varied slightly around 0.01 with other parameters kept the same as for the previous figures, spirals still emerged in a pair of opposite chirality but their spatial orientations were altered, for example, by 90 degrees with respect to the spirals of the previous value of N_{rd}, which suggests that the evolution of spirals is sensitive to the value of the reaction-diffusion number. In this particular instance, the interesting result of the nonlinear interaction of hexagons and spirals is that the tips of the spirals were fixed in space (pinning) and did not meander. When the magnitude of

[2]**Description of Fig 3-4:** Evolution of spirals in the hyperbolic reaction-diffusion system. The boundary conditions are the same as for Fig. 3-5. In the regime of $N_{rd} = 0.01$ a mixture of hexagonal, rhombic and square structures is organized along the lines which appear to be intersections of characteristic surfaces with the plane of the figure (at time $\tau = 500$). There then develop structures at the four corners and along the boundaries. These boundary structures appear to be propagating waves. Subsequently, a pair of concentration defects of high concentration ("black holes") appear inside the square as shown in panel a. Panel a′ is a magnification of a hexagonal-rhombic-square region in panel a. The tips then develop into a pair of spirals of opposite chirality as shown in panels b ($\tau = 550$) and c ($\tau = 600$) while in the meantime the structures at the four corners and along the boundaries maintain the wavy patterns although there occur some minor changes in them. The spirals grow and collide with each other and with the boundary structures as in panel d ($\tau = 800$). Eventually, the pattern develops into an irregular mixture of hexagonal patterns, stripes and maze-like structures shown in panel e ($\tau = 1000$). Again, we observe that the various patterns are built out of the basic texture of a hexagonal structure, when the spots along the characteristic lines merge together.

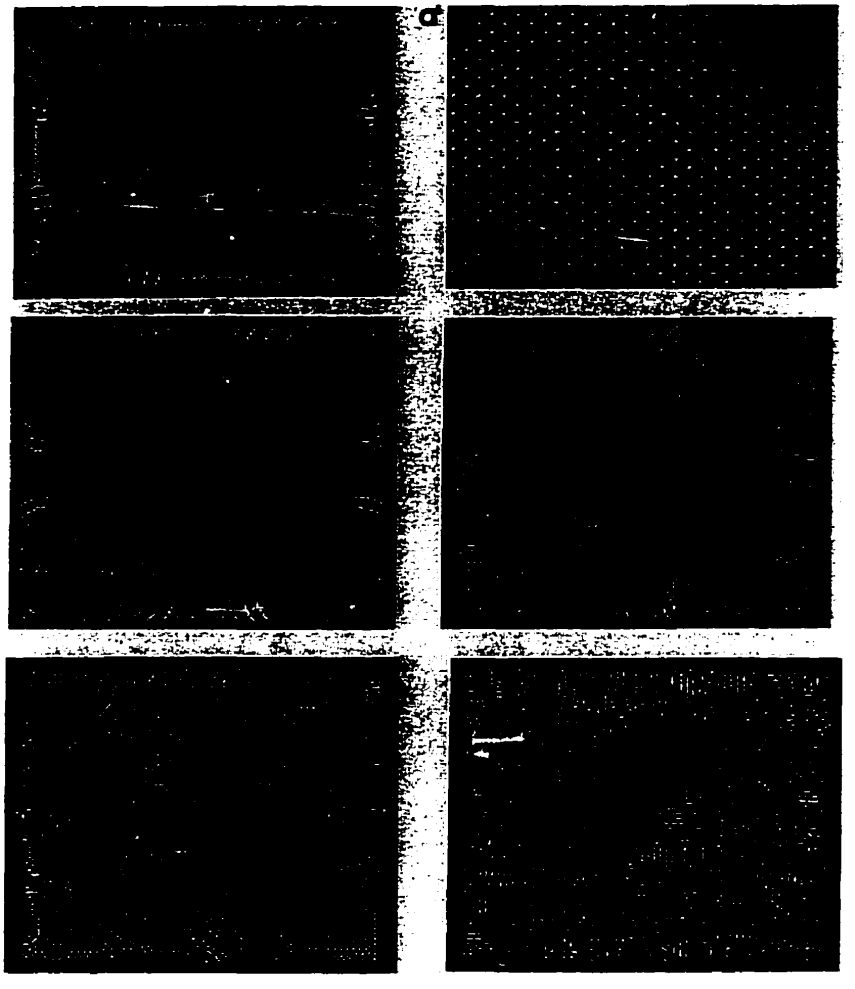

Figure 3-6: *Evolution of spirals in the hyperbolic reaction-diffusion system. The boundary conditions are the same as for Fig. 3-5.*

the interaction increased, the pattern decayed to a very complicated and irregular one. Experimentally, the CIMA reaction exhibited a very similar pattern[20]. This behavior contrasts that of the spirals in the case of the bistable region as will be discussed later.

Since the details of dynamics of nonlinear systems can differ from system to system although there are general underlying features common to them all, the present results can be only suggestive for other experimental systems such as the CIMA reaction. Therefore, we can only make note of similarities in qualitative features at this point. If a more quantitative comparison is desired for such systems, they must be analyzed on their own merits by means of the governing equations similar to those studied here.

Chaotic Patterns at Low Reaction-Diffusion Numbers

When N_{rd} was further lowered to 0.001 under the nonrandom initial conditions with the boundary conditions and other parameters kept the same as for the previous cases, the wave behavior disappeared and no disturbances were observed. Only homogeneous oscillations were encountered. As the initial conditions were made random, there emerged random patterns which did not get organized to a steady regular pattern over the sufficiently long time span investigated. We show an example of such patterns in Fig. 3-7. These irregular patterns persisted in the intermediate time regime, but later decayed into minor structures (not shown here) which were randomly dispersed all over the space. Their oscillations were not regular in time, and this is consistent with the mode in which the one-dimensional system becomes temporally chaotic. We have found in the one-dimensional case[5] that the hyperbolic system loses its stability and temporal chaos appears as the reaction-diffusion number is lowered to $N_{rd} \simeq 0.001$. The power spectrum of the patterns shown in Fig. 3-7 clearly indicates spatial chaos.

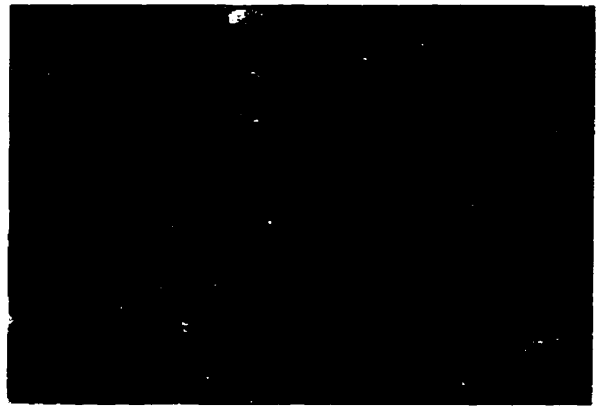

Figure 3-7: *Chaotic irregular patterns in the hyperbolic reaction-diffusion system. As the reaction-diffusion number N_{rd} is lowered to* 0.001 *under nonrandom initial conditions, the wave behavior does not appear and only homogeneous oscillations occur. If the initial conditions are made random, patterns emerge. However, the basic hexagonal structure does not appear, but rather irregular patterns appear dispersed over the entire square. Their oscillations are irregular(τ = 1000). The power spectrum indicates a chaos as shown in the next figure.*

3.3.2 Entropy (Calortropy) Production and Patterns

If the flux evolution equations (constitutive equations for fluxes) are linear with respect to fluxes as is for the present system, then the calortropy production[5, 21] coincides with the entropy production in the theory of linear irreversible processes[23]. In the previous chapter, it was shown that the contribution of diffusion processes to the entropy production is much smaller, except near the boundaries, than that of the chemical reactions in the reaction-diffusion system considered. In the light of this result, we ignore the diffusion contribution to the entropy production in this work. We have calculated the global entropy productions accompanying various patterns formed. The behavior of the entropy production over time is quite dependent on the patterns formed, but one common feature is that whenever an organized and well-correlated structure of a frequency and wave number emerges, the energy and matter dissipation rate, which the entropy production is, becomes relatively high, although the global energy and matter dissipation rate remains the same regardless

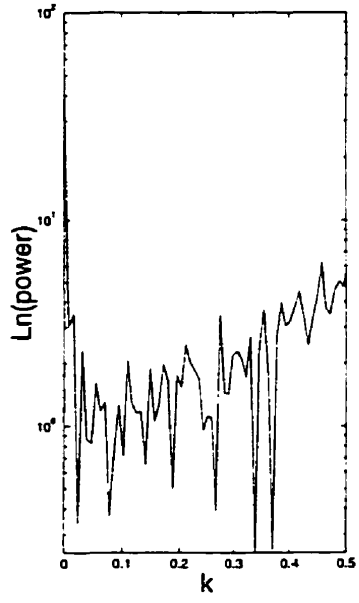

Figure 3-8: *Power spectrum of concentration X for the case of patterns shown in Fig. 3-5 at* $\xi_2 = 0.5$.

of the structures formed, provided that the boundary conditions and the parameters A and B remain the same.

In Fig. 3-9, we show the global entropy production Ξ_g (in the units of $10^3 R_g$ where R_g is the gas constant) vs. τ accompanying the sequence of the patterns shown in Fig. 3-2 ($N_{rd} = 0.1$). In fact, the sequence of patterns in this figure contains more than those presented in Figs. (3-2, 3-3, 3-4). Some of the peaks correspond to the patterns shown in Figs. [(3-2, 3-3, 3-4)(1)-(9)]. For example, the first peak corresponds to Fig. 3-2(1); the second peak to Fig. 3-2(2), etc. The troughs correspond to a homogeneous phase between patterns where even a basic hexagonal texture is not present. These peaks reach an asymptotic regime in the longtime limit where hexagonal structures become mixed with stripe structures and compete with each other. In this regime of time, the entropy production oscillates around a plateau value. In the case of spiral patterns shown in Fig. 3-6 ($N_{rd} = 0.01$), we notice a very steep but continuous jump as the tips ('black holes') of the spirals begin to appear as shown in Fig. 3-10. The entropy production reaches an asymptotic

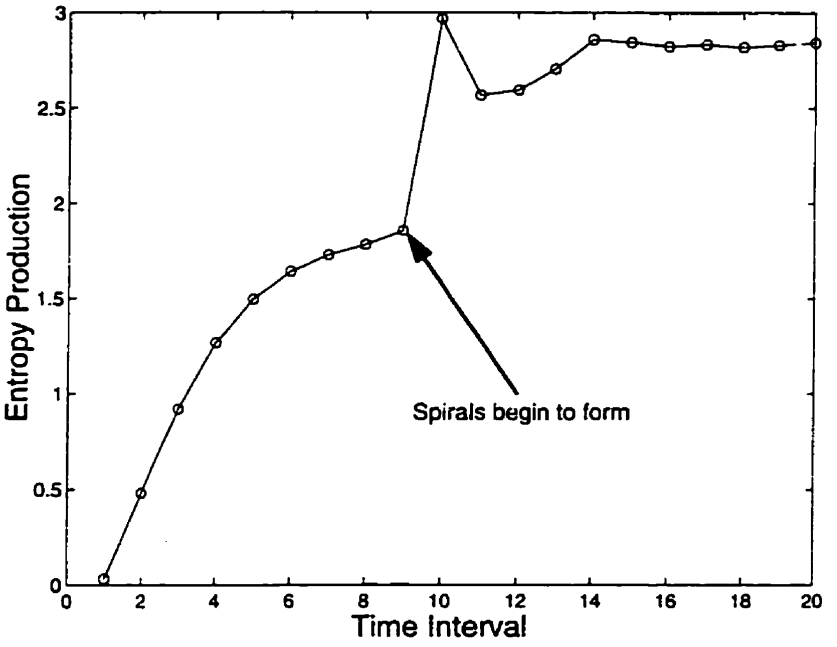

Figure 3-10: *Global entropy production associated with spirals in the case of* $N_{rd} = 0.01$. *This figure corresponds to Fig. 3-6.*

In most of patterns obtained in this work, continuous competitions were observed between the patterns of different symmetries. For example, when hexagonal structures were attained, stripes began to appear and grew until the texture was almost free from hexagons. And then hexagons began to grow and dominate again over the stripes. This oscillatory behavior continued for a long time. In other cases, especially, when N_{rd} was low (typically approximately 0.01) where spirals occur, no hexagonal structure or stripes could be maintained over a long time span, but chemical turbulence instead took place. The entropy productions calculated for the competing structures cannot elucidate such competition, for it simply saturates and remains practically at a constant value. Therefore, the only thing we can say is that such structures dissipate more energy and matter than otherwise, but as to the details of pattern competition it seems to say little. Therefore, if there is a thermodynamic principle that can guide us in connection with pattern competition and pattern selection, it does not appear that the second law of thermodynamics is

the one that should be looked up to for a clue. The salient role of the second law so far has been in providing a set of macroscopic (hydrodynamic) evolution equations consistent with a positivity criterion for energy dissipation that may be regarded as a local form of the second law, but pattern formation and selection seems to be controlled by something other than the positivity condition provided by the second law.

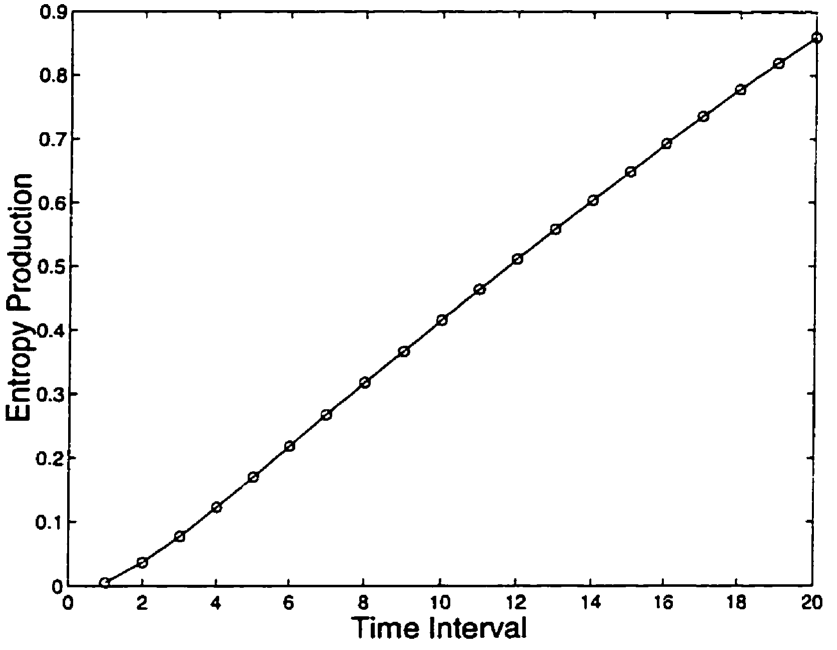

Figure 3-11: *Global entropy production in the case of* $N_{rd} = 0.001$ *where chaotic irregular patterns occur. This figure correspond to Fig. 3-7. The global entropy production does not reach a plateau value in this case.*

We have studied the effects of the parameters A and B on pattern formation. In the region where only one unstable steady state is possible, lowering the value of A causes a faster saturation of the pattern. We can also say tentatively that when the value of A were relatively small, hexagons were dominant, but in other cases stripes were dominant. We have also computed the effects of these parameters on the rate of energy dissipation. This is summarized in Fig. 3-12 where we plot as a function of A the mean global entropy production Σ (normalized by $\Sigma_{\max}$) defined as the

time average of the global entropy production (entropy production integrated over space) for three different values of B: ○ for $B = 0.09$; ✳ for $B = 0.06$; and + for $B = 0.02$. The value of N_{rd} is 0.1. The system is in a homogeneous phase before the value of A reaches approximately 0.58 whence the system exhibits the sequence of patterns shown and similar to those in Figs. (3-2, 3-3, 3-4) in the case of $B = 0.09$ and 0.06. In the case of $B = 0.02$, the system shows only a homogeneous phase.

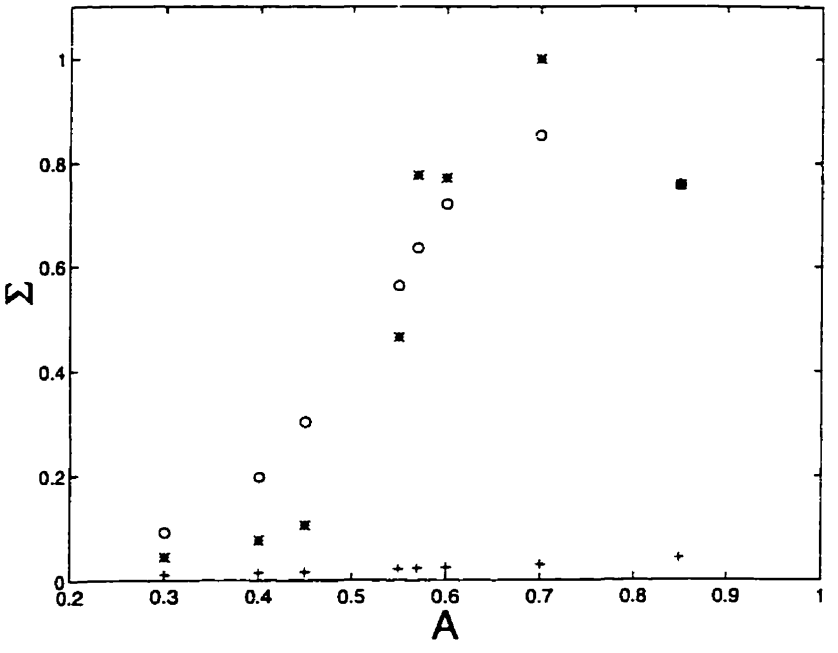

Figure 3-12: *Relative mean global entropy production* (Σ/Σ_{max}) *vs. A at various values of B* : ○ *for B = 0.09;* ✳ *for B = 0.06; and + for B = 0.02. The maximum region corresponds to the sequence of patterns similar to those in Fig. 3-2.*

3.3.3 The Bistable Region

When the parameters are taken such that the system is in the bistable region (parameter values: $A = 0.6202, B = 0.02$), some interesting solutions were obtained such as solitons and spirals when the other parameters such as N_{rd} and f are changed. When random initial conditions were taken for the aforementioned set of parameters in which case the three steady states of X concentration have the values: 0.2920,

0.2667, and 0.02335, and we set the value of f to 1.31 and N_{rd} to 0.7, the system was able to remove and distribute the chemicals to reach a homogeneous state from which defects appeared on the boundary of the square. These defects grew until they met and merged together. Once they coalesce with each other, they formed a packet which then traveled at a constant speed to the other side of the square where it vanished; see Fig. 3-13 for the sample of the sequence. These are solitary waves.

Figure 3-13: *Solitary waves in the bistable region in the case of* $N_{rd} = 0.7$. *When the paramcters are taken such that the system is in the bistable region* ($A = 0.6202$, $B = 0.02$, $f = 1.31$) *and the initial conditions are random, the initial pattern becomes irregular. Then the system becomes homogeneous over the entire square except for the two spots on the left boundary. These spots grow and propagates as solitary waves and eventually merge and propagate at a constant speed to the right. For the lack of space we show only two stages of the evolution of solitary waves and their three-dimensional rendering which clearly shows that they are indeed solitary waves (merged in this case) laterally oscillating.*

Such a solitary wave was observed in the literature [24]. The speeds of two chemical waves have been calculated from the distances covered by the foremost fronts of the solitary waves over a unit time interval. They are not the same as can be seen in

Fig. 3-14. From the observation made, it is possible to state that there is a stationary wave in one direction (say, ξ_1 direction) and in the perpendicular direction (ξ_2 direction) a solitary wave progressing at a constant speed with no dispersion at all. Thus we are led to conjecture that the reaction-diffusion equations are decoupled in the two directions in this case. In the $\xi_1$direction we have a one-dimensional version of the hyperbolic differential equations where a time-independent mode gets selected and in the ξ_2 direction another solution corresponding to a solitary wave gets selected. For the set of parameters that gives rise to the solitary wave front we have computed the time-independent mode from the linear dispersion relation [Eq. (2.128)]. This immediately gives $\omega = 0$ for the real wave vector $k = 6.35$. In the

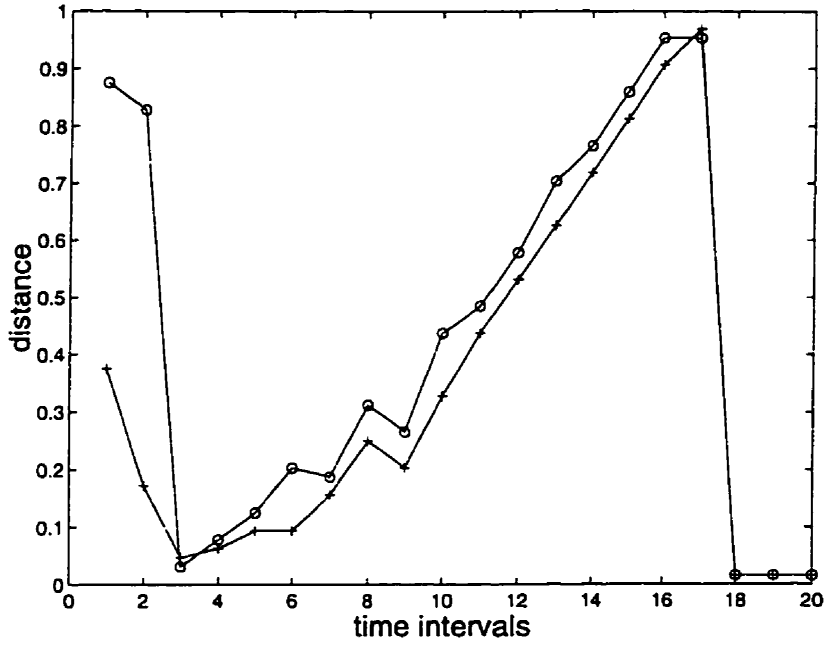

Figure 3-14: *The distance covered by the solitary waves over time intervals. This figure is constructed from the sequence of patterns shown in Fig. 3-11. The slopes of the curves show the wave speeds. Each time interval corresponds to* 50 *units of* τ.

reduced units this corresponds to an envelope of waves whose wave length λ is approximately equal to 1. The entropy production of the solitary wave is given in Fig. 3-15. The global entropy production of the solitary waves, which is roughly equal to

the local entropy production because of the localized nature of the waves, is large in the initial stage before a chaotic phase sets in where it shows a minimum. It begins to rise as two spots grow out of a homogeneous phase reaching a peak as the solitary waves collide and merge. Then it remains roughly constant in the intermediate time interval when the waves have grown in size. As the wave approaches the boundary on the right-hand side and begins to get annihilated, the global entropy production becomes low in value and constant in time.

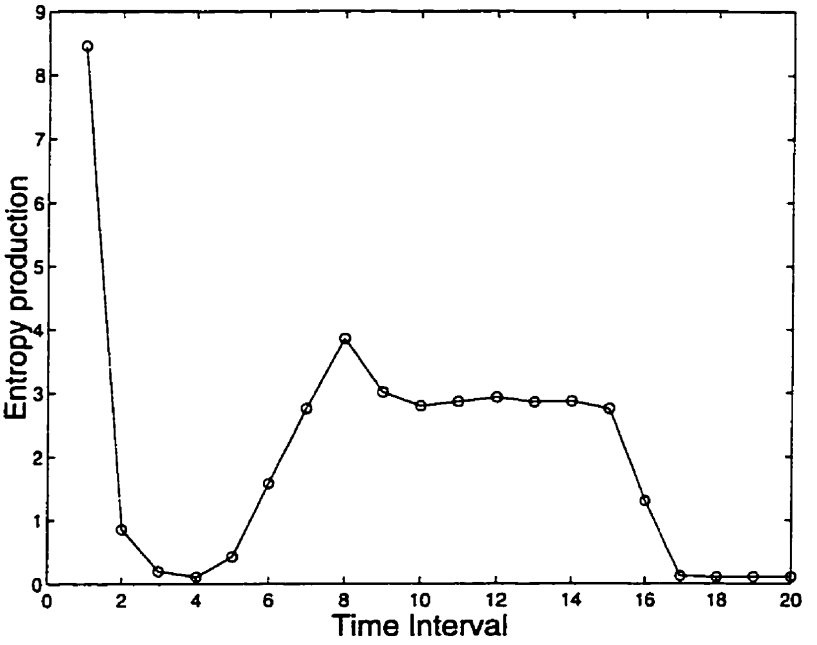

Figure 3-15: *Global entropy production for the system admitting the solitary waves. The leftmost point represents the global entropy production at the initial stage. The peak corresponds to the state where two solitary waves collide and merge. The last stage is the annihilation stage at the boundary.*

For another set of parameters ($A = 0.6202, B = 0.02, f = 0.8, N_{rd} = 0.8$) spirals were obtained, as shown in Fig. 3-16, when the initial and boundary conditions were chosen so as to make them correspond to the unstable steady state perturbed with 1% random noise. The spirals obtained do not have fixed centers which meander around. This may be due to quasi-periodic rotations arising from a destabilizing curvature effect[20]. Some of spirals merge when they collide forming a cusp and

some others repulse each other when they come close to each other. In most of cases, spirals were created in pairs of opposite chirality. What was noticeable is that after some time the spirals get elongated as shown in Fig. 3-16d. We remark

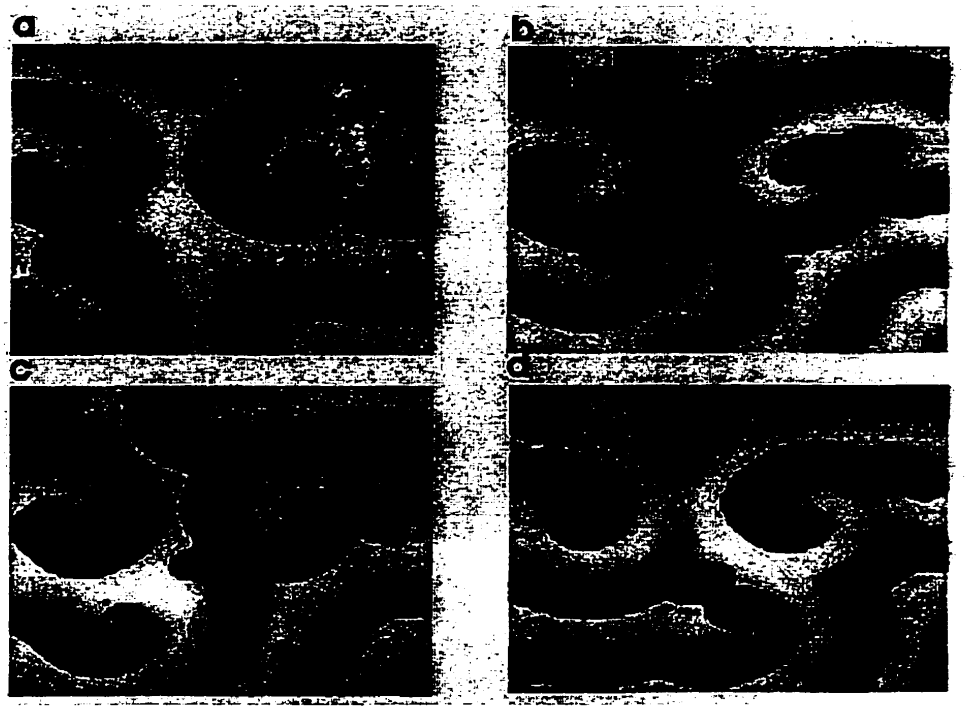

Figure 3-16: *Spirals originating from the unstable steady state in the bistable region perturbed by a 1% random noise. (a)Spirals are created near the fixed boundaries and attract each other ($\tau = 300$). (b)Spirals come to a proximity and interfere a little bit ($\tau = 550$). (c)Spirals repulse each other ($\tau = 900$). (d)Spirals get elongated ($\tau = 1000$).*

that the vortex dynamics has been extensively studied in the literature[21, 22, 23] and what is observed here may be relevant to them. The spirals also depend on the value of N_{rd}. When this parameter is lowered, the radius of curvature of the spirals increases. Figure 3-17a shows only one spiral which meanders in the square at $N_{rd} = 0.5$. At $N_{rd} = 0.35$ the pattern looks like stripes. In fact, at early stages the pattern is nothing but two patches of stripes which are perpendicular to each other. With time, the stripes tend to get parallel to each other and end up like the one in Fig. 3-17b where roughly parallel stripes (lamellar structures) are maintained

but the defects move around continuously. A further decrease of N_{rd} to 0.1 resulted in an irregular pattern shown in Fig. 3-17c.

The entropy production of the spiral waves and stripes is shown in Fig. 3-18. The entropy productions appear to get saturated at an almost same value for different values of N_{rd}. The weak oscillations in the entropy productions decrease in amplitude as N_{rd} decreases. The curve for the chaotic pattern lies below all other curves, and it again seems to suggest that a chaotic pattern dissipates less matter and energy than the organized ones.

A recent experiment on glycolysis[24] has shown wave fronts propagating from one boundary to another which is rather reminiscent of the solitary wave front observed in Fig. 3-13. There are other patterns which also remind us of those observed in this work, but a quantitative analysis and comparison with the present theory are not possible at this point for lack of quantitative data. However, such studies would be useful and we defer them to future work.

3.4 Discussion and Concluding Remarks

In this chapter, we have shown the two-dimensional solutions of the hyperbolic reaction-diffusion equations for three different values of the reaction-diffusion number and for different boundary and initial conditions. Especially, when random initial conditions are taken, the system exhibits various intriguing series of patterns grown on the basic texture of a hexagonal pattern. This hexagonal pattern appears arranged on mutually crossing lines which we believe are the intersections of characteristic planes with a plane perpendicular to the time axis (i.e., the plane of the figure at time τ). The presence of such characteristic planes (or surfaces) is a hallmark of hyperbolic systems, and it is not surprising that patterns of the corresponding parabolic system studied are not observed on a hexagonal texture. The patterns of the hyperbolic system are formed as the spots of the basic hexagonal texture accumulate around symmetrically arranged spots to form a symmetric structure just like a shock structure is formed along a characteristic line. This feature

is quite interesting and insightful, we believe, for understanding how patterns are formed. The patterns, organized even though started by random initial conditions, gradually become more elaborate yet still maintain a well defined symmetry. This is quite suggestive, but we have no fundamental understanding of the basic mechanism for such behavior at this point. We have made attempt to relate pattern formation to the entropy production in the system. It is observed that the patterns are formed at relatively high states of energy and matter dissipation yet the global entropy productions summed over all modes and over a characteristic time period remain the same for all patterns at given boundary conditions. This result is at variance with the minimum entropy production theorem[23] observed in the linear irreversible processes where the system tends toward a state of minimum entropy production compatible with the boundary conditions. In the present theory, we see that *the system selects a mode or different modes, specially if the system is away from threshold, by some mechanism and maintains the structure of the mode at the cost of energy and matter and at the expense of other modes.* It seems that thermodynamic laws as known at present do not give us guidance in our efforts to understand the pattern selection, although they do demand that the macroscopic evolution equations should be consistent with them. It may be that the role of thermodynamic laws ends just there, and there may be another principle complementing them in connection with pattern selections but yet to be uncovered.

The point we wish to make in this chapter in a general context is that, as is clearly shown in the Note added at the end of this chapter, if there is a product of rate constant and initial concentrations which is comparable in magnitude to, or smaller than, the mean diffusion constant present, then the reaction-diffusion number is of the order of unity or less than unity and a hyperbolic behavior becomes significant. In such events, it is necessary to use hyperbolic partial differential equations similar to those studied in this work. In any case, if one is interested in transient behaviors of systems, then hyperbolic partial differential equations are right mathematical tools to use to study such behavior from the macroscopic viewpoint consistent with the thermodynamic principles.

The conclusion we can tentatively draw from the present series of calculations is that *the hyperbolic reaction-diffusion equations seem to be more descriptive of patterns and their evolution over time than the corresponding parabolic reaction-diffusion equations specially in small scale geometries like the cells where diffusion competes with chemical reactions. In any case, hyperbolic systems are more suitable from the viewpoint of irreversible thermodynamics*[25]. As in the case of one-dimensional system studied in Ref. [5], patterns are selected and maintained at a relatively high cost of matter and energy, namely, entropy production. This feature is revealing of some aspects of pattern formation phenomena and irreversible processes[23], but is at variance with the minimum entropy production theorem known in the linear theory of irreversible processes. Further study on this question may help elucidate the role of irreversible thermodynamics in pattern formation and selection. Detailed studies on the amplitude and phase equations derived from hyperbolic reaction-diffusion equations probably will give us more insight into the mechanisms and differences with parabolic equations.

Note

In this Note we would like to add a remark in connection with reducing the governing equations (3.1)-(3.4) and the definition of reaction diffusion number arising from the reduction method used. After finishing the present work, we have found a more suitable scheme of reducing the governing differential equations, which requires a slightly different definition of time scale and consequently results in a more appropriate form of reaction-diffusion number N_{rd}. This new definition of N_{rd} does not alter the numerical results and the conclusion with regard to the relative merits of hyperbolic and parabolic differential equations for chemical oscillations and waves, but the range of N_{rd} where the crossover occurs between the hyperbolic and parabolic systems can be altered. The new definition of N_{rd} gives rise to a much better understanding of the relative utility of the two systems of partial differential equations. In any case, the old set of reduced equations (3.1)-(3.4) becomes a special case of the new reduced set when a parameter is taken for a particular value. We show the new reduction method and the new definition of reaction-diffusion number below.

Instead of taking k_3^{-1} as the time scale taken in this work, we take the time scale based on the autocatalytic step, namely, k_2 as follows:

$$t_c = k_2 \rho_A^0 \rho_B^0 L^2 \frac{\sqrt{m_P m_S}}{k_B T} \equiv k_2 \rho_A^0 \rho_B^0 \left(\frac{L}{\bar{v}} \right)^2 , \qquad \text{(N.1)}$$

where ρ_A^0 and ρ_B^0 are the initial concentrations of A and B, respectively. We remark that this choice of reference concentrations is arbitrary and can be made with other experimentally more suitable concentrations, if there is any. Therefore, t_c is related to the mean time for the molecules to traverse the system length L and the lifetime of chemical species P and S in the autocatalytic step. With this time t_c and the

length L, we scale various quantities as follows:

$$\begin{aligned}
&\tau = \tfrac{t}{t_c}, && \boldsymbol{\xi} = \tfrac{\mathbf{r}}{L}, \\
&X = \rho_P k_2 (L/\bar{v}) \sqrt{\rho_A^0 \rho_B^0}, && Y = \rho_S k_2 (L/\bar{v}) \sqrt{\rho_A^0 \rho_B^0}, \\
&\mathbf{u} = \mathbf{J}_P (L^2 k_2^2/\bar{v}^3) (\rho_A^0 \rho_B^0)^{\frac{3}{2}}, && \mathbf{v} = \mathbf{J}_S (L^2 k_2^2/\bar{v}^3) (\rho_A^0 \rho_B^0)^{\frac{3}{2}}, \\
&A = \rho_A (L/\bar{v})^3 k_1 k_2^2 (\rho_A^0 \rho_B^0)^{\frac{3}{2}}, && B = \rho_B (L/\bar{v})^3 k_1 k_2^2 (\rho_A^0 \rho_B^0)^{\frac{3}{2}}.
\end{aligned} \tag{N.2}$$

Then, with the definitions of the parameters

$$K = k_{-2}/k_2, \tag{N.3a}$$

$$R_x = \left(\frac{L}{\bar{v}}\right)^2 k_2 k_3 \rho_A^0 \rho_B^0, \quad R_y = \left(\frac{L}{\bar{v}}\right)^2 k_{-1} k_2 \rho_A^0 \rho_B^0 \tag{N.3b}$$

and the reaction-diffusion number

$$N_{rd} = \frac{k_2 L^2}{\sqrt{D_S D_P}} \rho_A^0 \rho_B^0, \tag{N.4}$$

the governing partial differential equations can be cast in the reduced forms

$$\partial_\tau X = -\boldsymbol{\nabla}_\xi \cdot \mathbf{u} + B - R_x X + X^2 Y - K X^3, \tag{N.5a}$$

$$\partial_\tau Y = -\boldsymbol{\nabla}_\xi \cdot \mathbf{v} + A - R_y Y - X^2 Y + K X^3, \tag{N.5b}$$

$$\partial_\tau \mathbf{u} = -N_{rd} f (\hat{D}_x \boldsymbol{\nabla}_\xi X + \mathbf{u}), \tag{N.5c}$$

$$\partial_\tau \mathbf{v} = -N_{rd} f^{-1} (\hat{D}_y \boldsymbol{\nabla}_\xi Y + \mathbf{v}). \tag{N.5d}$$

This set, except for the parameters R_x and R_y, is the same in structure as (3.1)-(3.4) where $R_x = 1$ and $R_y = R$. Here the reduced diffusion coefficients $\hat{D}_x$ and $\hat{D}_y$ are

defined by

$$\hat{D}_x = \frac{D_P k_2}{\bar{v}^2}\rho_A^0\rho_B^0 = \frac{D_P}{(L^2/t_c)}, \quad \hat{D}_y = \frac{D_S k_2}{\bar{v}^2}\rho_A^0\rho_B^0 = \frac{D_S}{(L^2/t_c)}. \tag{N.6}$$

In this manner of reduction diffusion coefficients are calculated relative to the number of particles crossing area L^2 in time t_c. If $\bar{v}$ of the molecules is such that $\bar{v}/L = (k_2 k_3 \rho_A^0 \rho_B^0)^{1/2}$, then $R_y = k_{-1}/k_3 = R$. Therefore, the reduced system (2.2a)-(2.2d) studied in this work is a special case of the new reduced system (N.5) where the condition $\bar{v}/L = (k_2 k_3 \rho_A^0 \rho_B^0)^{1/2}$ holds. Since the characteristic eigenvalues of the hyperbolic system (N.5) is proportional to $\sqrt{N_{rd}}$, it can be estimated that the group velocity of the waves is proportional to $\sqrt{N_{rd}}$. This reaction-diffusion number dependence appears to be relevant to experimental observations[26, 27] on the chemical wave speed which depends on concentrations. The new reaction-diffusion number defined here has a much more transparent meaning and a closer relevance to experiments than the one defined in the main text. It is possible to determine easily from N_{rd} whether the behavior of the system falls in the hyperbolic or parabolic regime; if the reaction diffusion number is small, the behavior will be that of a hyperbolic system and if it is large, then the behavior will be that of a parabolic system. However, the crossover from one behavior to another is asymptotic since there is no sharp critical value and the range of hyperbolicity can be fairly wide, especially, for systems where chemical reactions are competing with diffusion. Finally, we remark that one could have chosen $t_c = k_3(L/\bar{v})^2$ and obtain the reaction-diffusion number in the form $N_{rd} = L^2 k_3/\sqrt{D_P D_S}$ and the reduced system of differential equations in the same form as (N.5) but with slightly different definitions of the parameters from those in (N.3) and (N.6). This multiplicity of choice is due to the large number of rate constants associated with the reaction system since they all can provide time scales of one sort or another. The rate constant associated with the autocatalytic step may be the most logical choice for it since it is an essential feature in nonlinear chemically oscillating systems.

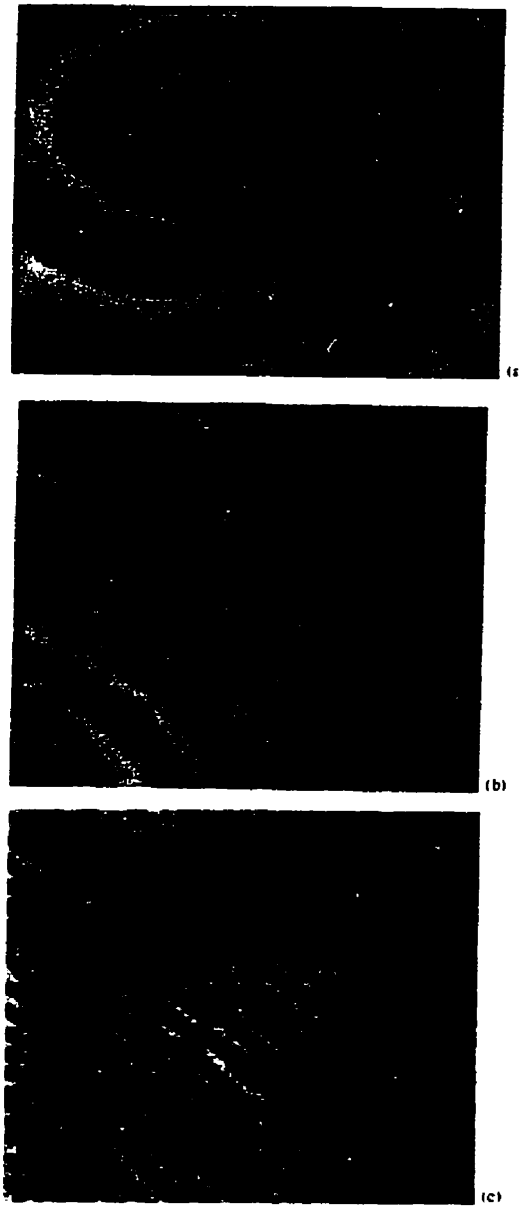

Figure 3-17: *Same parameters as for Fig. 3-16. (a)Lowering N_{rd} to 0.5 gives rise to a single spiral which meanders in the square. (b)Lowering N_{rd} to 0.25 gives rise to parallel stripes which originate from perpendicular patches of stripes. The defects continuously move around over the pattern. (c)Decreasing N_{rd} further to 0.1 causes stripes to decay to an irregular turbulent maze-like pattern.*

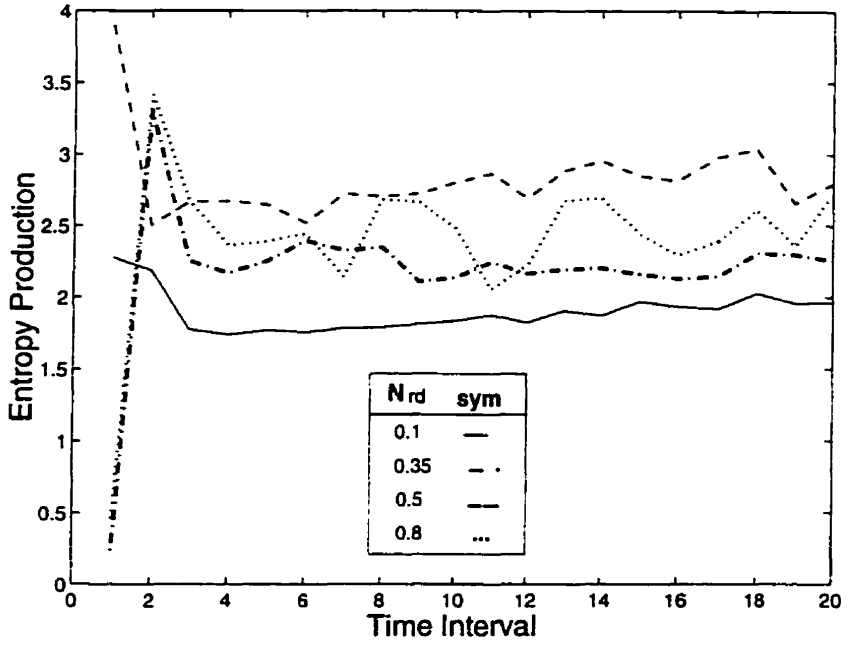

Figure 3-18: *Global entropy production for different values of N_{rd} corresponding to the patterns in Figs. 3-16 and 3-17. The lowest curve corresponds to the lowest N_{rd} or the turbulent pattern.*

Bibliography

[1] M. Al-Ghoul and B. C. Eu, Physica D **90**, 119 (1996).

[2] U. I. Cho and B. C. Eu, Physica D **68**, 351(1993).

[3] V. Castets, E. Dulos, J. Boissonade, and P. De Kepper, Phys. Rev. Lett. **64**, 2953(1991).

[4] I. Lengyel, G. Rabai, and I. Epstein, J. Am. Chem. Soc. **112**, 4606(1990). I. R. Epstein and I Lengyel, Physica D **84**, 212(1995).

[5] (a)P. Manneville, *Dissipative Structures and Weak Turbulence* (Academic, Boston, 1990). (b)P. Borckmans, A. De Wit, and G. Dewel, Physica A **188**, 137(1992).

[6] A. Nayfeh, *Perturbation Methods* (Wiley, New York, 1973).

[7] P. Arcuri and J. D. Murray, J. Math. Biol. **24**, 299 (1986).

[8] Y. Kuramoto, *Chemical Oscillations, Waves, and Turbulence* (Springer, Berlin, 1984).

[9] E. E. Selkov, Eur. J. Biochem. **4**, 79(1968).

[10] P. Richter, P. Rehmus, and J. Ross, Prog. Theoret. Phys. **66**, 385(1981); Y. Termonia and J. Ross, Proc. Nat. Acad. Sci. USA **78**, 2952, 3563(1982).

[11] P. M. Morse and H. Feshbach, *Methods of Theoretical Physics* (McGraw-Hill, New York, 1953).

[12] D. Walgraef, G. Dewel, and P. Borckmans, Adv. Chem. Phys. **49**, 311(1982).

[13] C. Canuto, M. Y. Hussaini, A. Quarteroni, and T. A. Zang, *Spectral Methods in Fluid Dynamics* (Springer, Berlin, 1988).

[14] *MATLAB Reference Guide* (High Performance Numeric Computation and Visualization Software) (The Math Works Inc., Natick, MA, 1993).

[15] J. A. Sepulchre and A. Babloyantz, Phys. Rev. E **48**, 187(1993).

[16] B. Rudovics, J.-J. Perraud, P. De Kepper and E. Dulos, in *Far-From-Equilibrium Dynamics of Chemical Systems*, eds. J. Gorecki, A. S. Cukrowski, A. L. Kawcynski, and B. Nowakowski (World Scientific, Singapore, 1994).

[17] B. C. Eu, J. Chem. Phys. **102**, 7169(1995); Phys. Rev. E **51**, 768(1995).

[18] I. Prigogine, *Thermodynamics of Irreversible Processes* (Interscience, New York, 1961).

[19] S. Kai and H. Miike, Physica A **204**, 346(1994).

[20] E. Meron, Physica D **49**, 98(1991).

[21] X. Wu, M. Chee, and R. Kapral, Chaos **1**, 441(1991).

[22] D. A. Kessler, H. Levine, and W. N. Reynolds, Physica D **70**, 115(1994).

[23] A. S. Mikhailov, V. A. Davydov, and V. S. Zykov, Physica D **70**, 1(1994).

[24] T. Shinjyo, Y. Nakagawa, and T. Ueda, Physica D **84**, 212(1995).

[25] B. C. Eu, *Kinetic Theory and Irreversible Thermodynamics* (Wiley, New York, 1992).

[26] P. M. Wood and J. Ross, J. Chem. Phys. **82**, 1924(1985).

[27] C. Vidal, J. Stat. Phys. **48**, 1017(1987).

[28] A. Turing, Phil. Trans. R. Soc. London B **327**, 37 (1952).

Chapter 4

The Brusselator

4.1 Introduction

In a typical experimental setting a pattern may form spontaneously as a result of the instability of the homogeneous state or can be excited by a short localized external perturbation of the system. The patterns forming in both these cases do not have any qualitative differences. They are essentially the domains of high and low concentrations of certain substances separated by relatively sharp walls. The pattern may have sophisticated geometry and in general may show very complicated spatio-temporal behavior. The properties of the patterns do not significantly depend on whether the system is monostable or bistable. It appears that domain patterns forming in very different systems may in fact have common features. This has recently been noticed in the case of static domain patterns forming in both equilibrium and nonequilibrium systems, where a certain set of domain shapes, such as spots, stripes, multidomain and labyrinthine patterns, and the transition between them has been observed[1]. The same conclusion can be extended to the dynamic patterns in nonequilibrium systems. Indeed, travelling, pulsating, self-replicating, and stochastically oscillating patterns are observed in the systems as diverse as autocatalytic reactions[2], semiconductor and gas plasma[3], or premixed flames[4]. All this suggests that there exists a universality class of the nonequilibrium systems

in which pattern formation and self-organization scenarios are essentially the same. Another important question raised by experiments is to identify the totality of possible types of patterns and their behaviors in the systems under considerations, and to understand the requirements the system should meet in order to be able to produce one type of pattern or the other. Another important question can be asked about the quantification of order and disorder in patterns, and whether a pattern is completely turbulent or not. In previous chapters, we saw how disorder and order can be linked to the amount of energy and matter dissipation inside the system in hand. However, no precise or detailed criterion is concluded from such study. In this chapter, we go ahead to exploring some of these questions. We have seen from previous chapters how by using hyperbolic reaction-diffusion equations one can obtain a 'zoology' of different patterns. We examine numerical solutions of the hyperbolic reaction-diffusion equations for the irreversible Brusselator in the case of two spatial dimensions. In the case of the Brusselator, there are some experimental measurements[54, 11] of the speeds of oscillating travelling waves (periodic waves). These speeds appear to follow the generic form of travelling wave speed in an oscillating chemical system which was first suggested by R. Z. Luther[12] and later discussed by Showalter and Tyson[55]. Although there have been some attempts[14, 15, 16] to derive the Luther formula on the basis of parabolic reaction-diffusion equations, they appear to be inconclusive and ambiguous as far as the explicit formulas go and the derivation of an explicit formula consequently still remains an open problem. We take it up in this work on the basis of hyperbolic reaction-diffusion equations. We show that a Luther-type formula can be obtained from the linearized telegraphist equations since the phase speed remains unchanged even though the amplitude gets modified as the Hopf instability occurs. Furthermore, what is really interesting is to explore patterns and try to find any kind of measure of the order and disorder in them. With this in mind, we have explored the reciprocal space for these patterns to see the symmetry exhibited by the resulting transform. We have found that chaotic patterns may exhibit symmetrical patterns in their corresponding Fourier space.

4.2 The Brusselator

The Brusselator[16] serves as a simple two-species model for the Belousov-Zhabotinsky reaction and it is, in the case of the irreversible Brusselator, described by the four coupled reactions

$$A \xrightarrow{k_1} X \tag{4.1}$$

$$B + X \xrightarrow{k_2} Y + D \tag{4.2}$$

$$2X + Y \xrightarrow{k_3} 3X \tag{4.3}$$

$$X \xrightarrow{k_4} E. \tag{4.4}$$

These reactions suggest the following the reaction rate formulas:

$$\Lambda_X = k_1\rho_A - (k_2\rho_B + k_4)\rho_X + k_3\rho_X^2\rho_Y, \tag{4.5}$$

$$\Lambda_Y = k_2\rho_B\rho_X - k_3\rho_X^2\rho_Y. \tag{4.6}$$

If it is assumed that the temperature is uniform over the system and there are no flow and stress in the system, the evolution equations for relevant macroscopic observables are those of densities ρ_X and ρ_Y of species X and Y together with their diffusion flux evolution equations. They are as follows:

$$\partial_t\rho_X = -\nabla\cdot\mathbf{J}_X + k_1\rho_A - (k_2\rho_B + k_4)\rho_X + k_3\rho_X^2\rho_Y, \tag{4.7}$$

$$\partial_t\rho_Y = -\nabla\cdot\mathbf{J}_Y + k_2\rho_B\rho_X - k_3\rho_X^2\rho_Y, \tag{4.8}$$

$$\partial_t \mathbf{J}_X = -\frac{k_B T}{m_X}\nabla\rho_X - L_{XX}\mathbf{J}_X, \tag{4.9}$$

$$\partial_t \mathbf{J}_Y = -\frac{k_B T}{m_Y}\nabla\rho_Y - L_{YY}\mathbf{J}_Y. \tag{4.10}$$

Here m_X and m_Y are the masses of X and Y; L_{XX} and L_{YY} are phenomenological coefficients for diffusion; and $\mathbf{J}_X$ and $\mathbf{J}_Y$ are the diffusion fluxes of X and Y, respectively. The diffusion flux evolution equations taken here are linear with regard to $\mathbf{J}_X$ and $\mathbf{J}_Y$, but they can in general be nonlinear. These equations are consequences of the extended version of irreversible thermodynamics[18]. This set of evolution equations are hyperbolic partial differential equations since the characteristic eigenvalues of the set are all real. These equations are believed to be more appropriate for describing wave phenomena than the parabolic reaction-diffusion equations conventionally used in connection with pattern formations and chemical oscillations and waves[16, 19]. We have investigated some aspects of differences these evolution equations make in contrast to the parabolic reaction-diffusion equations[5, 6, 7] in the previous papers in this series. In this work, we continue the investigation, this time numerically studying two-dimensional pattern formations by the Brusselator and calculating the phase speeds of travelling oscillatory chemical waves.

It is convenient to cast the evolution equations in dimensionless reduced forms. For this purpose we introduce the reference densities (*e.g.*, initial densities) ρ_A^0 and ρ_B^0 of species A and B, respectively, and define the diffusion coefficients D_X and D_Y in terms of the phenomenological coefficients L_{XX} and L_{YY} and the time scale t_c, respectively, by the formulas

$$D_X = \frac{k_B T}{m_X L_{XX}}, \quad D_Y = \frac{k_B T}{m_Y L_{YY}}, \tag{4.11}$$

$$t_c = k_3 \left(\frac{l}{\bar{v}}\right)^2 \rho_A^0 \rho_B^0, \tag{4.12}$$

where $l^2 = t_d\sqrt{D_X D_Y}$ with t_d denoting the mean time required for particles to diffuse a unit distance and $\bar{v} = \left(k_B T/\sqrt{m_X m_Y}\right)^{1/2}$ is the mean thermal speed or

the speed of sound wave. Therefore, l is the mean distance diffused by the species in time t_d and the time t_c is a composite measure of particle diffusion in the time scale of reactions and thermal disturbance (*e.g.*, sound wave) in the system. The time will be reckoned in this time scale in the present work. We also denote the system length by L. Various variables in the equations will then be reduced in the following manner:

$$\tau = t/t_c, \qquad \xi_x = x/L, \qquad \xi_y = y/L,$$

$$X = \sqrt{k_3 t_c}\rho_X, \quad Y = \sqrt{k_3 t_c}\rho_Y, \qquad A = k_1 t_c \sqrt{k_3 t_c}\rho_A, \tag{4.13}$$

$$B = k_2 t_c \rho_B, \qquad \mathbf{u} = t_c \sqrt{k_3 t_c} L^{-1}\mathbf{J}_X, \quad \mathbf{v} = t_c \sqrt{k_3 t_c} L^{-1}\mathbf{J}_Y.$$

We also define the parameter

$$S_x = k_4 t_c. \tag{4.14}$$

Given this reduction scheme, there appears a dimensionless parameter called the reaction-diffusion number:

$$N_{rd} = k_3 t_d \rho_A^0 \rho_B^0. \tag{4.15}$$

This reaction-diffusion number therefore is a measure of diffusion time relative to reaction time for the system. This parameter, as in the previous works, plays an important role in identifying the range of applicability for hyperbolic and parabolic differential equations. We remark that the reduced variables in this work are defined somewhat differently from the previous papers[5, 6, 7]. The previous reduction scheme can be recovered as a special case of the present scheme if S_x is set equal to unity since then $t_c = k_4^{-1}$ which is the time scale used in the previous scheme.

The dimensionless hydrodynamic equations will take the form:

$$\partial_\tau X = -\nabla_\xi \cdot \mathbf{u} + A - (B + S_x)X + X^2 Y, \tag{4.16}$$

$$\partial_\tau Y = -\nabla_\xi \cdot \mathbf{v} + BX - X^2 Y, \tag{4.17}$$

$$\partial_\tau \mathbf{u} = -N_{rd} f(\hat{D}_X \nabla_\xi X + \mathbf{u}), \tag{4.18}$$

$$\partial_\tau \mathbf{v} = -N_{rd} f^{-1}(\hat{D}_Y \nabla_\xi Y + \mathbf{v}), \tag{4.19}$$

where

$$f = \sqrt{\frac{m_Y D_Y}{m_X D_X}}, \ \hat{D}_X = \frac{D_X t_c}{L^2}, \ \hat{D}_Y = \frac{D_Y t_c}{L^2}. \tag{4.20}$$

This set of evolution equations reduces to the one used in Ref. 1 if we set $S_x = 1$. We will use this special case for the numerical solutions in the present work. Eqs. (4.16) – (4.19) can be combined into coupled second-order partial differential equations which are coupled telegraphist equations:

$$\partial_\tau^2 \mathbf{Z} + \bar{N}_{rd} \mathbf{H} \partial_\tau \mathbf{Z} - \bar{N}_{rd} \mathbf{D} \nabla_\xi^2 \mathbf{Z} = \bar{N}_{rd} \Re(X, Y), \tag{4.21}$$

where $\bar{N}_{rd} = N_{rd} f$ and

$$\mathbf{Z} = \begin{pmatrix} X \\ \\ Y \end{pmatrix}, \tag{4.22}$$

$$\Re = \begin{pmatrix} A - (B + S_x)X + X^2 Y \\ \\ (BX - X^2 Y) f^{-2} \end{pmatrix} = \mathbf{f} \Re', \tag{4.23}$$

$$\mathbf{f} = \begin{pmatrix} 1 & 0 \\ \\ 0 & f^{-2} \end{pmatrix}, \tag{4.24}$$

$$\Re' = \begin{pmatrix} A - (B + S_x)X + X^2Y \\ \\ BX - X^2Y \end{pmatrix}, \tag{4.25}$$

$$\mathbf{D} = \mathbf{f} \begin{pmatrix} \hat{D}_x & 0 \\ \\ 0 & \hat{D}_y \end{pmatrix} \equiv \mathbf{f}\hat{\mathbf{D}}, \tag{4.26}$$

$$\mathbf{H} = \begin{pmatrix} H_{xx} & H_{xy} \\ \\ H_{yx} & H_{yy} \end{pmatrix}, \tag{4.27}$$

with the matrix elements of $\mathbf{H}$ defined by the derivatives of $\Re'$ with respect to X and Y :

$$\begin{aligned} H_{xx} &= 1 - \bar{N}_{rd}^{-1}\frac{\partial \Re'_X}{\partial X} = 1 + (S_x + B - 2XY)\bar{N}_{rd}^{-1}, \\ H_{xy} &= -\bar{N}_{rd}^{-1}\frac{\partial \Re'_X}{\partial Y} = -X^2\bar{N}_{rd}^{-1}, \\ H_{yx} &= -\bar{N}_{rd}^{-1}\frac{\partial \Re'_Y}{\partial X} = -(B - 2XY)\bar{N}_{rd}^{-1}, \\ H_{yy} &= f^{-2} - \bar{N}_{rd}^{-1}\frac{\partial \Re'_Y}{\partial Y} = f^{-2} + X^2\bar{N}_{rd}^{-1}. \end{aligned} \tag{4.28}$$

Since the matrix $\mathbf{H}$ tends to unit matrix $\mathbf{I}$ as the reaction-diffusion number becomes infinite, the coupled telegraphist equations (4.21) reduce to the conventional reaction-diffusion equations which are parabolic partial differential equations. Eq. (4.21) is better suited for describing transient phenomena where waves evolve in space over a period of finite time. Note that parabolic differential equations imply that a disturbance at a point in the system is instantaneously felt throughout the system as soon as it is turned on, and it is unphysical to be so.

Eq. (4.21) admits a nontrivial homogeneous steady state which is given by

$(X_0, Y_0) = (\frac{A}{S_x}, \frac{BS_x}{A})$. The stability analysis of the system around this steady state has been studied in Ref. [5] to which the reader is referred for details.

4.3 Phase Speeds of Chemical Waves

The speeds of oscillatory waves are experimentally observable and can characterize the chemical waves in terms of experimental inputs. They are also of theoretical interest. Such a speed formula was first suggested by R. Z. Luther[12] for some oscillating chemical waves and there have been a number of papers devoted to derivations of such formulas on the basis of parabolic reaction-diffusion equations in the literature[55, 14, 15, 20]. However, their derivation appears to be still an open question, especially, when oscillatory travelling waves are involved, since the parabolic reaction-diffusion equations are not wave equations and therefore usually are not expected to admit a physical dispersion relation. Nevertheless, if there are nonlinear chemical reactions coupled to diffusion, there can be some special range of wave numbers for which such a relation is possible. On the other hand, the telegraphist equations (4.21) are genuine wave equations and generally supply the phase velocities when oscillatory travelling waves are the solutions. Since the equations are nonlinear it, however, is not simple to solve them analytically, and some approximation method is required to obtain the desired result. Here we will argue that it is sufficient to solve the linearized telegraphist equations to obtain the desired phase speed formula since the higher-order corrections to the solution simply modify the amplitudes of the travelling periodic wave solutions. For this we rely on the implication of the Hopf bifurcation theorem[17] which suggests that the amplitude of an unstable oscillatory solution grows to a plateau value to produce a finite amplitude oscillatory wave. We then use the stationary phase approximation to draw the aforementioned conclusion on the phase speed. For simplicity we will consider the case of one spatial dimension for the purpose. It is convenient to cast the telegraphist

equations into a moving coordinate system by using the transformation

$$\eta = \xi - c\tau, \tag{4.29}$$

where c is the phase speed in reduced units. Then the telegraphist equations can be transformed into the following equations

$$\left(c^2\mathbf{I} - \bar{\mathbf{N}}_{rd}\mathbf{D}\right)\frac{d^2\mathbf{Z}}{d\eta^2} - c\bar{\mathbf{N}}_{rd}\mathbf{H}\frac{d\mathbf{Z}}{d\eta} = \bar{\mathbf{N}}_{rd}\Re(X,Y), \tag{4.30}$$

where $\mathbf{I}$ is the unit matrix. The homogeneous steady state is defined by

$$\Re(X_0, Y_0) = 0. \tag{4.31}$$

Note that $X_0 = A/S_x$ and $Y_0 = BS_x/A$. Eq. (4.30) is now an eigenvalue problem for c. Now define the new dependent variables

$$x = X - X_0,\ y = Y - Y_0, \tag{4.32}$$

$$\mathbf{\Psi} = \mathbf{Z} - \mathbf{Z}(X_0, Y_0) = \begin{pmatrix} x \\ y \end{pmatrix}, \tag{4.33}$$

and the small parameter by

$$\mu = \frac{B - B_c}{B_c}, \tag{4.34}$$

where the critical value B_c can be suitably chosen as indicated later. The choice depends on the type of instability involved. It then is possible to rewrite Eq. (4.30) in a form where the small parameter appears explicitly:

$$(c^2\mathbf{I} - \bar{\mathbf{N}}_{rd}\mathbf{D})\frac{d^2\mathbf{\Psi}}{d\eta^2} - c\bar{\mathbf{N}}_{rd}\mathbf{H}^0\frac{d\mathbf{\Psi}}{d\eta} - \bar{\mathbf{N}}_{rd}\mathbf{M}\mathbf{\Psi} = \bar{\mathbf{N}}_{rd}[\mathbf{L}_2(x,y) + \mathbf{L}_3(x,y)]. \tag{4.35}$$

In this equation

$$\mathbf{M} = \mathbf{M}^0 + \mu B_c \mathbf{f}\mathbf{F}_0, \tag{4.36}$$

$$\mathbf{H}^0 = \begin{pmatrix} 1+(S_x-B_c)/\bar{N}_{rd} & -A^2/S_x^2\bar{N}_{rd} \\ B_c/\bar{N}_{rd} & f^{-2}+A^2/S_x^2\bar{N}_{rd} \end{pmatrix} - \mu\frac{B_c}{\bar{N}_{rd}}\mathbf{F}_0, \tag{4.37}$$

$$\mathbf{L}_2(x,y,\mu) = c\mathbf{F}_1(x,y,\mu)\frac{d\Psi}{d\eta} + \Re_2(x,y,\mu), \tag{4.38}$$

$$\mathbf{L}_3(x,y) = c\mathbf{F}_2(x,y)\frac{d\Psi}{d\eta} + \Re_3(x,y), \tag{4.39}$$

with various matrices and column vectors defined by the formulas

$$\mathbf{F}_0 = \begin{pmatrix} 1 & 0 \\ -1 & 0 \end{pmatrix}. \tag{4.40}$$

$$\mathbf{M}^0 = \mathrm{f}\begin{pmatrix} B_c-S_x & A^2/S_x \\ -B_c & -A^2/S_x \end{pmatrix} + \mu B_c \mathrm{f}\mathbf{F}_0, \tag{4.41}$$

$$\mathbf{F}_1 = \bar{N}_{rd}^{-1}\begin{pmatrix} -\frac{2S_xB_c}{A}x - \frac{2A}{S_x}y & -\frac{2A}{S_x}x \\ \frac{2S_xB_c}{A}x + \frac{2A}{S_x}y & \frac{2A}{S_x}x \end{pmatrix} - \mu\frac{2B_cS_x}{A\bar{N}_{rd}}\mathbf{F}_0 x, \tag{4.42}$$

$$\mathbf{F}_2 = \frac{x}{\bar{N}_{rd}}\begin{pmatrix} -2y & -x \\ 2y & x \end{pmatrix}, \tag{4.43}$$

$$\Re_2(x,y) = \left(\frac{S_xB_c}{A}x^2 + \frac{2A}{S_x}xy + \mu\frac{S_xB_c}{A}x^2\right)\mathrm{f}\begin{pmatrix} 1 \\ -1 \end{pmatrix}, \tag{4.44}$$

$$\Re_3(x,y) = x^2 y \mathbf{f} \begin{pmatrix} 1 \\ \\ -1 \end{pmatrix}. \tag{4.45}$$

Eq. (4.35) may be solved by a perturbation theory[21] such that secular terms do not appear, if some analytical results are desired for the solutions. Here we make the following analysis without an approximation. Since travelling oscillatory waves (periodic solutions) are desired for the solutions of Eq. (4.35), $\mathbf{\Psi}$ may be written in the form

$$\mathbf{\Psi}(\eta) = \sum_q \mathbf{\Phi}_q \exp(iq\eta), \tag{4.46}$$

where the amplitude Φ_q does not depend on η. The solution satisfies the periodic boundary condition and $q = n\pi/L$ with n denoting an integer. On substitution of this into Eq. (4.35) and integration over η after multiplying $\exp(-iq\eta)$, we obtain the integral equation for the amplitude

$$\left[\omega^2 \mathbf{I} - \bar{\mathbf{N}}_{rd}\mathbf{D}q^2 + i\omega\bar{\mathbf{N}}_{rd}\mathbf{H}^0 + \bar{\mathbf{N}}_{rd}\mathbf{M}\right]\mathbf{\Phi}_q = -\bar{\mathbf{N}}_{rd}\left[\hat{\mathbf{L}}_2(q) + \hat{\mathbf{L}}_3(q)\right], \tag{4.47}$$

where

$$\omega = cq, \tag{4.48}$$

$$\hat{\mathbf{L}}_2(q) = L^{-1}\sum_{q'} \mathbf{L}_2(\mathbf{\Phi}_{q'}, \mathbf{\Phi}_{q'-q}, \mu), \tag{4.49}$$

$$\hat{\mathbf{L}}_3(q) = L^{-2}\sum_{q'}\sum_{q''} \mathbf{L}_3(\mathbf{\Phi}_{q'}, \mathbf{\Phi}_{q''}, \mathbf{\Phi}_{q'+q''-q}). \tag{4.50}$$

We remark that since $\mathbf{L}_2(x,y,\mu)$ and $\mathbf{L}_3(x,y)$ are homogeneous with respect to x and y, the former being second order and the latter being third order, the exponential factors integrate to delta functions of wave numbers and only the amplitude parts are left over in $\mathbf{L}_2$ and $\mathbf{L}_3$ in the sums in Eqs. (4.49) and (4.50). Therefore, Eq.

(4.47) is a set of coupled nonlinear integral equations for the amplitudes

$$\mathbf{\Phi}_q = \begin{bmatrix} \Phi_q^x \\ \\ \Phi_q^y \end{bmatrix}. \tag{4.51}$$

We now consider the homogeneous equation

$$\left[\omega^2 \mathbf{I} - \bar{\mathbf{N}}_{rd}\mathbf{D}q^2 + i\omega\bar{\mathbf{N}}_{rd}\mathbf{H}^0 + \bar{\mathbf{N}}_{rd}\mathbf{M}\right]\boldsymbol{\varphi}_q = 0 \tag{4.52}$$

for which the solvability condition is

$$\det|\mathbf{\Delta}| \equiv \det\left|\omega^2 \mathbf{I} - \bar{\mathbf{N}}_{rd}\mathbf{D}q^2 + i\omega\bar{\mathbf{N}}_{rd}\mathbf{H}^0 + \bar{\mathbf{N}}_{rd}\mathbf{M}\right| = 0. \tag{4.53}$$

This solvability condition gives the dispersion relation

$$\omega = \omega(q), \tag{4.54}$$

to which we will return to consider its q-dependence. For the moment we will assume that $\omega(q)$ is real. Let us define the matrix $\mathbf{\Omega}(\epsilon)$ by

$$\mathbf{\Omega}(\epsilon) = \mathbf{\Delta} + i\epsilon,$$

where ϵ is a small positive parameter that will be taken equal to zero after computation of the solution to Eq. (4.47) is completed. Then the formal solution of Eq. (4.47) can be written as

$$\mathbf{\Phi}_q = \boldsymbol{\varphi}_q - \bar{\mathbf{N}}_{rd}\mathbf{\Omega}^{-1}(\epsilon)\left[\hat{\mathbf{L}}_2(q) + \hat{\mathbf{L}}_3(q)\right]. \tag{4.55}$$

Here $\mathbf{\Omega}^{-1}(\epsilon)$ is the Green's function in the q space for Eq. (4.52) and the amplitude equation. This amplitude equation may be solved by applying a perturbation technique. For example, various quantities involved may be expanded into power

series of μ and the resulting hierarchy can be solved step by step. In a similar spirit, Eq. (4.55) may be solved iteratively. If the amplitudes obtained from Eq. (4.55) are bounded—and according to the Hopf bifurcation theorem[17] they are bounded since there is an oscillatory (periodic) solution bifurcating from the Hopf instability point and attaining a finite amplitude—then it is possible to infer that the phase speed of the travelling oscillatory wave is simply given by the roots of the determinant $\det|\mathbf{\Delta}|$. The reason is as follows. Suppose the amplitude $\mathbf{\Phi}_q$ is bounded and smooth. The sum in Eq. (4.46) may be replaced with an integral over q

$$\mathbf{\Psi}(\eta) = \int_{-\infty}^{\infty} \mathbf{\Phi}_q \exp(iq\eta). \tag{4.56}$$

It then is possible to evaluate the integral in Eq. (4.56) by means of the method of steepest descent (*i.e.*, the stationary phase method) [22]. The stationary phase of the integral is given by

$$\frac{d}{dq}\left[q\xi - \omega(q)\tau\right]\Big|_{q=q_s} = 0, \tag{4.57}$$

where q_s is the wave number for the stationary phase. That is,

$$\xi = \frac{d\omega(q_s)}{dq_s}\tau,$$

which yields

$$c = \frac{d\omega(q_s)}{dq_s}. \tag{4.58}$$

Evaluating the integral around the stationary phase, we obtain

$$\mathbf{\Psi}(\xi,\tau) \simeq \mathbf{\Phi}_{q_s}\left[\frac{2\pi}{\tau\frac{d\omega(q_s)}{dq_s}}\right]^{1/2} e^{-i\pi/4}\exp i\left[q_s\xi - \omega(q_s)\tau\right]. \tag{4.59}$$

This solution suggests that the phase speed of the travelling oscillatory wave (periodic solution) is still given by the solution of the determinant $\det|\mathbf{\Delta}(q_s)|$ and therefore it is sufficient to use the result by the linearized telegraphist equations for the purpose of calculating the bifurcating oscillatory wave. Under the aegis of this

argument we now calculate the phase speed by using Eq. (4.53) in the case of $\mu = 0$.

The determinant $\det|\mathbf{\Delta}(\mu = 0)|$ gives a fourth-order polynomial in $z \equiv i\omega_0 = i\omega\,(\mu = 0)$:

$$z^4 + P(q)z^3 + Q(q)z^2 + T(q)z + S(q) = 0, \tag{4.60}$$

where the coefficients are all real and given by

$$P(q) = S_x - B_c + A^2 + 2\bar{N}_{rd}, \tag{4.61}$$

$$Q(q) = \bar{N}_{rd}(D_x + D_y)q^2 + A^2 + \bar{N}_{rd}^2 + \bar{N}_{rd}\left[2\left(S_x - B_c\right) + (1 - f^{-2})A^2\right] \tag{4.62}$$

$$T(q) = \left\{\bar{N}_{rd}^2(D_x + D_y) + \bar{N}_{rd}\left[A^2 D_x - (B_c - S_x)D_y\right]\right\} q^2 \tag{4.63}$$

$$+\bar{N}_{rd}^2(S_x - B_c + f^{-2}A^2) + \bar{N}_{rd}(1 + f^{-2})A^2, \tag{4.64}$$

$$S(q) = \bar{N}_{rd}^2\left\{D_x D_y q^4 + \left[A^2 f^{-2} D_x + (S_x - B_c)D_y\right] q^2 + A^2 f^{-2}\right\}. \tag{4.65}$$

Note that the polynomial in Eq. (4.60) is the lowest-order result in the perturbation theory that can be obtained from the hyperbolic reaction-diffusion equations. There are four roots for the polynomial in Eq. (4.60). They will be all negative real if the Hurwitz conditions are satisfied:

$$P > 0, \tag{4.66}$$

$$PQ - T > 0, \tag{4.67}$$

$$PQT - T^2 - P^2 S > 0. \tag{4.68}$$

If one of these conditions are broken, some roots may acquire non-negative real parts or become complex. For the present case, if there exist parameters such that

$$PQT - T^2 - P^2 S = 0, \tag{4.69}$$

then one pair becomes pure imaginary. In fact, they are

$$z^{\pm} = \pm i\sqrt{\frac{T}{P}}. \tag{4.70}$$

That is,

$$c_0^{\pm} = \frac{\omega_0^{\pm}}{q} = \pm\sqrt{\frac{T}{P}}. \tag{4.71}$$

Under condition (4.69), which gives rise to the parameter associated with the Hopf bifurcation if $q = 0$ as will be seen in the subsequent section, the other pair of roots is given by

$$z_1^{\pm} = -\frac{1}{2}\left[P \pm \sqrt{P^2 - 4\left(Q - \frac{T}{P}\right)}\right], \tag{4.72}$$

which are negative provided that $P^2 - 4(Q - T/P) > 0$. Therefore, we find the phase speed $c_0 = \omega_0/q$ under the conditions stated:

$$c_0 = \sqrt{\frac{\tilde{N}_{rd}(D_x + D_y)}{2}}\sqrt{\frac{\hat{T}}{\hat{P}}}, \tag{4.73}$$

where

$$\begin{aligned} \hat{P} &= \frac{P}{2\tilde{N}_{rd}}, \\ \hat{T} &= \frac{T}{\tilde{N}_{rd}^2(D_x + D_y)q^2}. \end{aligned} \tag{4.74}$$

If the parameter B_c is chosen such that it corresponds to the Hopf bifurcation value

$$B_c = S_x + A^2,$$

then $\hat{P} = 1$.

The phase speed formula in Eq. (4.73), when the reaction-diffusion number is

inserted, takes the form

$$c_0 = \sqrt{k_3 t_d \bar{D} \rho_A^0 \rho_B^0} \sqrt{\frac{\hat{T}}{\hat{P}}}, \tag{4.75}$$

where $\bar{D}$ is the mean diffusion coefficient

$$\bar{D} = \frac{1}{2}(D_x + D_y). \tag{4.76}$$

When converted into the real units, this formula yields

$$v_0 \equiv c_0 \frac{L}{t_c} = v_c \sqrt{k_3 t_d \bar{D} \rho_A^0 \rho_B^0} \sqrt{\frac{\hat{T}}{\hat{P}}}, \tag{4.77}$$

where $v_c = L/t_c$, the speed of disturbance to traverse the system length in time t_c. This result, when taken in the lowest order that neglects the terms of the order of $\bar{N}_{rd}$ in the expressions for $\hat{Q}$ and $\hat{S}$, is rather reminiscent of the formula for the oscillating chemical wave speed suggested by Luther[12]. There are additional parameters in the present formula which are absent in the Luther formula. This concludes the discussion on the derivation of a Luther-type formula for chemically oscillating travelling waves from the hyperbolic reaction-diffusion equations or the telegraphist equations. In this work, we have chosen ρ_A^0 and ρ_B^0 for the reference densities, but this choice can be altered to another set of reference densities within the present variable reduction scheme, if necessary. With an appropriate choice of species A and B, the formula is seen to have the correct power law for the densities, compared with the experimental result by Wood and Ross[54]. Note that the factor $\sqrt{\hat{T}/\hat{P}}$ does not depend on densities.

We now would like to consider the parabolic reaction-diffusion equations for the irreversible Brusselator, which, if the moving coordinate is used as for the telegraphist equations, may be written in the form

$$\mathbf{D}\frac{d^2\mathbf{\Psi}}{d\eta^2} + c\frac{d\mathbf{\Psi}}{d\eta} + \mathbf{M}\mathbf{\Psi} + [\Re_2 + \Re_3] = 0. \tag{4.78}$$

By linearizing Eq. (4.78) we obtain in the case of $\mu = 0$ the equation

$$\mathbf{D}\frac{d^2\Psi_1}{d\eta^2} + c_0\frac{d\Psi_1}{d\eta} + \mathbf{M}^0\Psi_1 = 0, \tag{4.79}$$

where $c_0 = c(\mu = 0)$ and $\mathbf{M}^0 = \mathbf{M}(\mu = 0)$. Again, we look for the solution of Eq. (4.79) in the form

$$\Psi_1 = \int_{-\infty}^{\infty} dq\Phi(q)\exp(iq\eta) \tag{4.80}$$

for which the solvability condition is

$$\det\left|-\mathbf{D}q^2 + iqc_0\mathbf{I} + \mathbf{M}^0\right| = 0. \tag{4.81}$$

The solution for this algebraic equation is

$$\begin{aligned}\omega_0 &= c_0 q = -\frac{1}{2}i\left[(D_X + D_Y)q^2 - (M^0_{xx} + M^0_{yy})\right] \\ &\pm\frac{1}{2}i\sqrt{\left[(D_X - D_Y)q^2 - (M^0_{xx} - M^0_{yy})\right]^2 + 4M^0_{xy}M^0_{yx}},\end{aligned} \tag{4.82}$$

which is imaginary unless

$$\left[(D_X - D_Y)q^2 - (M^0_{xx} - M^0_{yy})\right]^2 + 4M^0_{xy}M^0_{yx} < 0, \tag{4.83}$$

$$(D_X + D_Y)q^2 - (M^0_{xx} + M^0_{yy}) = 0. \tag{4.84}$$

These two conditions (4.83) and (4.84) are not generally met. If not, there is no travelling oscillatory wave solution for Eq. (4.79) and hence there is no phase speed of an oscillatory travelling wave. This is the most distinguishing feature of the parabolic reaction-diffusion equations from the hyperbolic reaction-diffusion equations. The absence of the dispersion relation for the parabolic equations, however, does not mean that there is no travelling front or pulse described by Eq. (4.79). Such a

solution can be constructed from the general solution for Eq. (4.79):

$$\Psi = \int_{-\infty}^{\infty} dq \Phi(q) \exp(iq\eta). \tag{4.85}$$

If the initial condition is

$$\Psi(\xi, 0) = \Phi_0 \delta(\xi), \tag{4.86}$$

we then find

$$\Psi(\xi, \tau) = \Phi_0 \int_{-\infty}^{\infty} dq \exp i \left[q\xi - \omega_0(q)\tau\right], \tag{4.87}$$

where $\omega_0(q)$ is given by Eq. (4.82). To perform the integration in Eq. (4.87) we will consider a special case where $D_X = D_Y = D$. In this case, we obtain

$$\omega_0 = -iDq^2 + iM^{\pm}, \tag{4.88}$$

where

$$M^{\pm} = \frac{1}{2}\left[M^0_{xx} + M^0_{yy} \pm \sqrt{(M^0_{xx} - M^0_{yy})^2 + M^0_{xy} M^0_{yx}}\right]. \tag{4.89}$$

Substitution of ω_0 in (4.88) into Eq. (4.87) and integration yield the familiar result

$$\begin{aligned} \Psi(\xi, \tau) &= \Phi_0 \sqrt{\frac{2\pi}{D\tau}} \exp\left(\tau M^+ - \frac{\xi^2}{4\tau D}\right) \\ &= \Phi_0 \sqrt{\frac{2\pi}{D\tau}} \exp\left[-\frac{1}{4\tau D}\left(\xi - 2\sqrt{M^+ D}\tau\right)\left(\xi + 2\sqrt{M^+ D}\tau\right)\right], \end{aligned} \tag{4.90}$$

for which we have chosen M^+. If there is a front or a pulse characterized by this solution, then it forms a one-parameter family of solutions. That is, there is a constant u such that

$$\Psi(\xi, \tau) = u. \tag{4.91}$$

Therefore, we have

$$d\Psi = \frac{\partial \Psi}{\partial \xi} d\xi + \frac{\partial \Psi}{\partial \tau} d\tau = 0, \tag{4.92}$$

which implies that the speed of the travelling wave is given by

$$\frac{d\xi}{d\tau} = \frac{2DM^+}{\xi} + \frac{\xi}{2\tau} - \frac{D}{\xi}. \tag{4.93}$$

The solution of this equation is given by

$$\xi = 2\tau\sqrt{M^+D - D\tau^{-1}\ln\tau}, \tag{4.94}$$

which in the large τ limit yields the speed of travelling wave in the form

$$v_0 = 2v_c\sqrt{M^+D}, \tag{4.95}$$

where $v_c = L/t_c$. This result, which could have been readily inferred from the second line in Eq. (4.90), coincides with the formula obtained by Showalter and Tyson[55] except for the factor v_c which appears when the variables are restored to the real scales from the reduced scales. This should be compared with the formula in Eq. (4.77) which is its hyperbolic counterpart for the wave speed. It must be noted that M^+ does not contain a rate constant in it. It must be also noted that the travelling wave has arisen on account of the autocatalytic oscillating chemical reactions.

4.4 Patterns and Their Fourier Transforms

In this section we would like to present some numerical results obtained by solving the telegraphist equations. Contrary to the parabolic reaction-diffusion equations which we have also solved by using an explicit finite-difference method both in space and time, the hyperbolic reaction-diffusion equations cannot be solved by the same relatively simple method. We have used a spectral method for the hyperbolic reaction-diffusion equations. In fact, the telegraphist equations are written as four coupled first-order differential equations and then a Fourier collocation method is used for the spatial derivatives which are substituted by their Fourier collocation derivatives[23]. A grid of 128 × 128 collocation points was taken. This method

gives rise to four ordinary differential equations in time where the position variables appear as parameters. These ordinary differential equations are then solved by using Gear's method for stiff differential equations. This method requires repeatedly taking Fourier transforms which can be implemented by the fast Fourier transform method. In order to check the numerical results so obtained, we have also used a three-point finite difference scheme to discretize space and then solved the resulting system by Gear's method. When patterns such as hexagonal or stripe patterns, which are stable, appear for some particular parameter values, the numerical differences between the two methods have been noticed. Since the spectral collocation method is believed to be more reliable for simple geometries, it has been used as the main numerical method in this work. We have also changed the time integrator from Gear's to a sixth-order Runge-Kutta scheme to test the methods used. In this case, the results by the two different methods in the chaotic region have been found to be slightly different, but the qualitative features like the symmetries of the selected patterns and the values of the critical parameters have been found to be the same. Both fixed and periodic boundary conditions have been used. For the cases we have examined, neither of the two types of boundary conditions has removed the frustrations of the selected symmetry observed in the patterns if the random initial conditions are used. We have chosen $S_x = 1$ and $f = 1$ for the present numerical work. The fixed boundary conditions taken are: $X = A$ and $Y = B/A$.

We have explored different regions of the parameter space, especially, with regard to the reaction-diffusion number to compare patterns obtained from the parabolic and hyperbolic reaction-diffusion equations. We have also studied the effects of the reaction-diffusion number N_{rd} on the symmetry of the patterns produced. An interesting result is that the hyperbolic reaction-diffusion equations tend to produce patterns of a lower symmetry than the corresponding parabolic reaction-diffusion equations. We have noticed this tendency in our previous studies[6] and it was found to be associated with a lower entropy production for the pattern of lower symmetry. Two-dimensional Fourier transforms are computed for the patterns obtained. The patterns in the Fourier space are often found to preserve some semblance of symme-

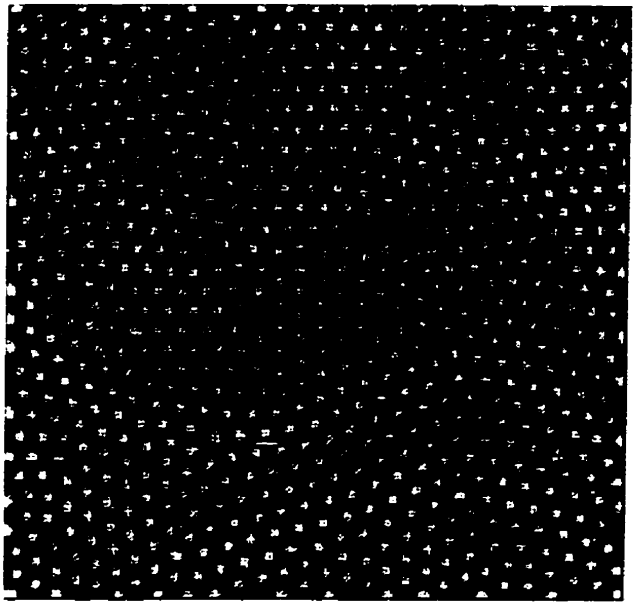

Figure 4-1: *Frustrated hexagonal pattern for the parameter set* $A = 3$, $B = 6.6$, $D_x = 0.0016$, $D_y = 0.006$, *and* N_{rd} *=2.89.*

try even if the spatial patterns and the power spectra may look rather chaotic. The patterns of power spectra in the reciprocal wave number space are rather suggestive and may be worthy of further study.

The Turing instability occurs when we have $\omega_0 = 0$ in the dispersion relation (4.60) and the derivative of $S(q)$ vanishes: that is,

$$S(q_T) = \frac{dS(q_T)}{dq_T} = 0, \tag{4.96}$$

where q_T is the critical wave number. We consider the case of $f = 1$ and $S_x = 1$. Solving this equation yields the following critical parameters for Turing instability to occur

$$B_c = (1 + A\zeta)^2, \tag{4.97}$$

$$q_T^2 = \frac{A}{\sqrt{D_x D_y}}, \tag{4.98}$$

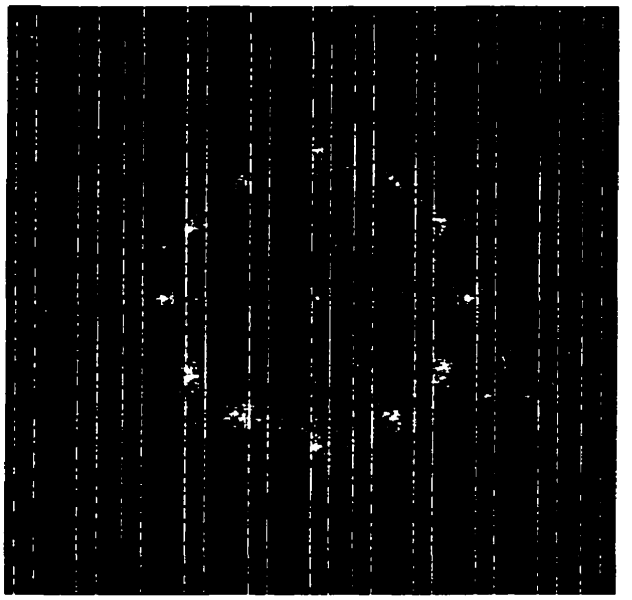

Figure 4-2: *The two-dimensional power spectrum of the pattern in Fig. 4-1. The ordinate is q_y and the abscissa is q_x. The lighter the shade, the higher the power is. The same relative color coding scheme is used for other power spectra in this work.*

$$\zeta = \sqrt{\frac{D_x}{D_y}}. \tag{4.99}$$

At the Hopf instability, the condition that $\mathrm{Im}\,\omega_0 = 0$ at $q = 0$ is given by one of the Hurwitz conditions[24]

$$P(0)Q(0)T(0) - T^2(0) - P^2(0)S(0) = 0, \tag{4.100}$$

which yields

$$B_c = 1 + A^2. \tag{4.101}$$

Turing instability occurs below the Hopf instability point when

$$(1 + A\zeta)^2 < 1 + A^2. \tag{4.102}$$

Otherwise, the two instability modes will mix. These relations for the parameters

were used as a guide to choose parameter values for the patterns produced.

The parameter values used in this work are: $A = 3$, $D_x = 0.0016$, and $D_y = 0.006$ for all figures presented. In addition to these fixed parameters, B is varied occasionally and the reaction-diffusion number N_{rd} is varied. The random initial conditions were used in most of simulations in this work, and when they were applied, the four-fold symmetry in the patterns formed for the case of nonrandom initial conditions was broken, namely, patterns of lower symmetries, *e.g.*, two-fold symmetries, were produced. For relatively high N_{rd} four-fold symmetry patterns were preserved if nonrandom initial conditions were taken. As N_{rd} is lowered, very complicated patterns can be obtained where only two-fold symmetry may be noticed if the patterns are carefully examined. Such a pattern is shown in Fig. 4-1 where there appear frustration lines in the hexagonal pattern, producing a patchwork of hexagonal domains. A similar pattern was noticed to arise when the corresponding parabolic reaction-diffusion equations were solved. The reason for this coincidence is the sufficiently large reaction-diffusion number which practically renders the hyperbolic system to behave as if it is parabolic. To see the nature of the pattern better, we have constructed a two-dimensional power spectrum shown in Fig. 4-1 where the magnitude of the power spectrum is color-coded. The lighter the color, the higher the spectrum. The two-dimensional power spectrum thus constructed clearly exhibits a global symmetry as shown in Fig. 4-2 where the ordinate is q_y and the abscissa is q_x. The origin of the (q_x, q_y) coordinates is at the center of the square of the figure. This figure shows there are two symmetric sets of wave vectors for the frustrated hexagonal pattern in Fig. 4-1. In addition to the octagonal spots there are four quadrants of a circular pattern at the four corners. Other two-dimensional power spectra have the same ordinate and abscissa as for Fig. 4-2. If the power spectrum is plotted against q in the conventional manner, we then obtain a rather broad random spectrum which is incapable of showing a global feature in two dimensions, but when plotted in the two-dimensional space of (q_x, q_y), the result is not only rather striking and intriguing but also insightful. It must be noted that if a spatial pattern, *e.g.*, a hexagonal structure, is homogeneously distributed in space then the

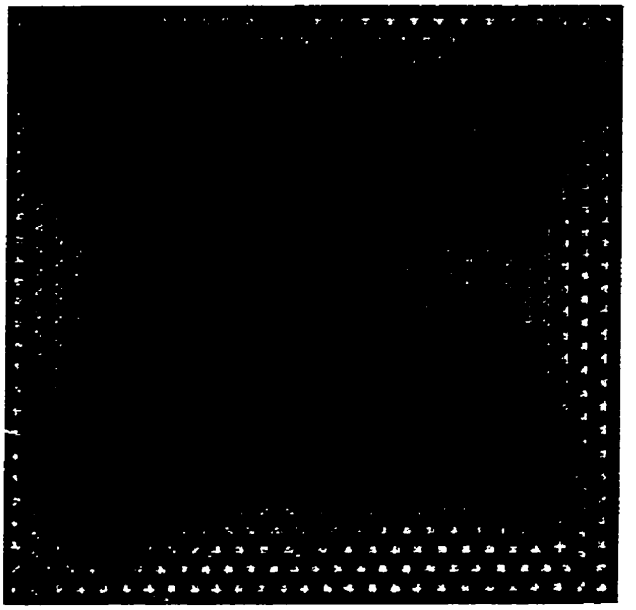

Figure 4-3: *Transition of a hexagonal pattern to a square pattern which appears in patches. The same parameters as for Fig. 4-1 except for* $N_{rd} = 2.88$.

two-dimensional power spectrum will contain six hexagonally arranged peaks[20]. Fig. 4-2 suggests that even a disordered pattern has a characteristic distribution of wave vectors in the two-dimensional reciprocal space which indicates an intrinsic structure of the pattern in question.

Lowering the value of N_{rd} to 2.88 gives rise to the pattern shown in Fig. 4-3 where we can clearly notice transition from a pattern of hexagonal symmetry to that of square or rhombic symmetry. Fig. 4-4 is a blowup of a small square in the pattern shown in Fig. 4-3. The two-dimensional power spectrum is shown in Fig. 4-5 for this pattern. The peaks are seen distributed symmetrically around a diagonal and the distribution of the peaks in the center is also symmetrical as shown in the blowup in panel 4-6. As for the pattern in Fig. 4-1, there are two distinct symmetrical sets of wave vectors for this pattern. The outer peaks are those of the shorter wavelength structure whereas the peaks in the center are those of the longer wavelength structure in Fig. 4-3.

Increasing the value of B to around 8.0 and reducing the value of N_{rd} to 2.5

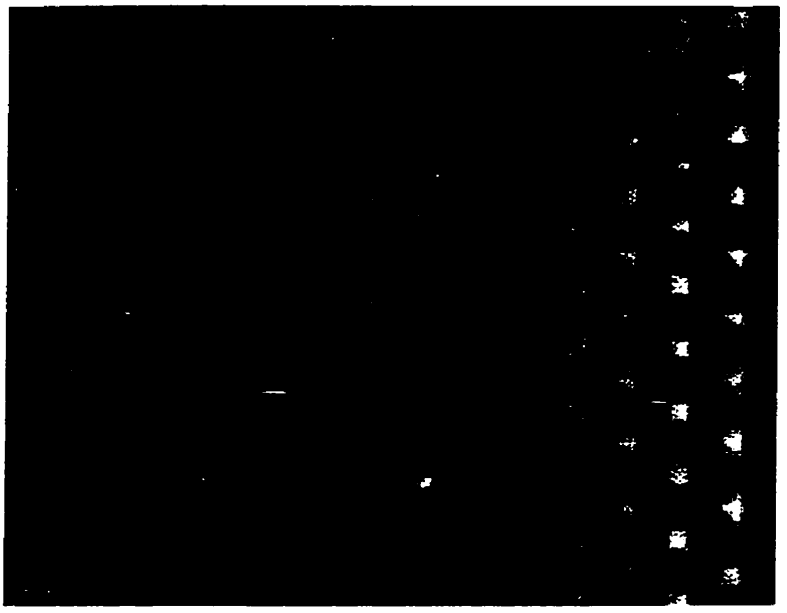

Figure 4-4: *This panel is a blowup of a square region in Fig. 4-3.*

Figure 4-5: *The two-dimensional power spectrum of Fig. 4-3.*

Figure 4-6: *A blowup of the central portion of the power spectrum in Fig. 4-5.*

produces a rather different pattern; this time a maze-like structure is produced as shown in Fig. 4-7. For the same parameter set, nonrandom initial conditions yield a completely symmetrical stripe structure (not shown here for the lack of space). The two-dimensional power spectrum of this irregular structure produces a smehow regular wave vector distribution indicating where the major peaks (white spots) clearly show a square symmetry as shown in Fig. 4-8. If cross sections of this two-dimensional power spectrum are plotted against q_x or q_y, they show spectra characteristic of a chaotic spatial pattern. Such cross sections are shown in Fig. 4-9 for $q_y = 0.5$ and in Fig. 4-10 for $q_y = 0.128$. As the value of N_{rd} is further lowered to 2.0 the maze-like structure makes transition to a turbulent pattern with patches of a square structure distributed randomly over space as shown in Fig. 4-11.

The two-dimensional power spectrum of this pattern is shown in Fig. 4-12 where white spots still maintain a symmetric form although the distribution of wave vectors more widely spread throughout the wave vector space than in the previous figure. If the value of B is increased to 10.1, there appears a more irregular pattern shown in Fig. 4-13. This parameter value puts the system far removed from the

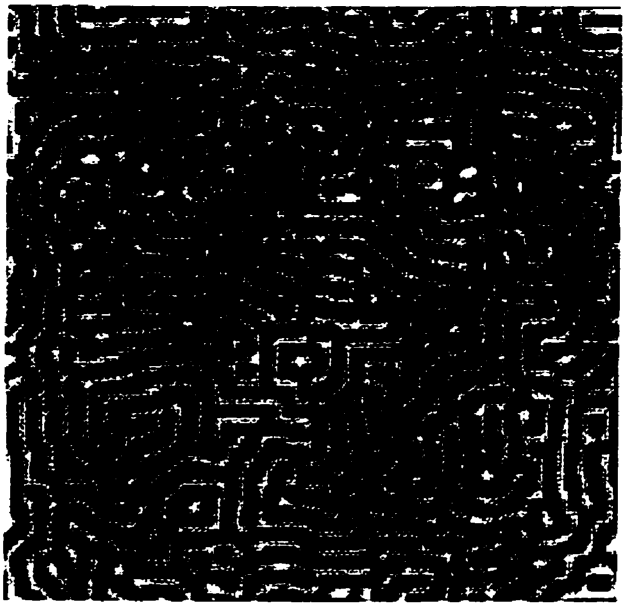

Figure 4-7: *A maze-like pattern for* $B = 8$ *and* $N_{rd} = 2.5$. *Other parameters are the same as for Fig. 4-1.*

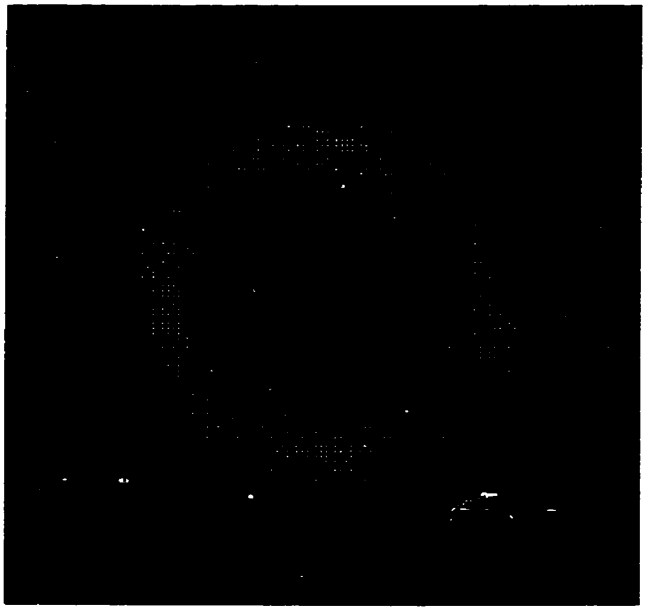

Figure 4-8: *The two-dimensional power spectrum of the pattern in Fig. 4-5.*

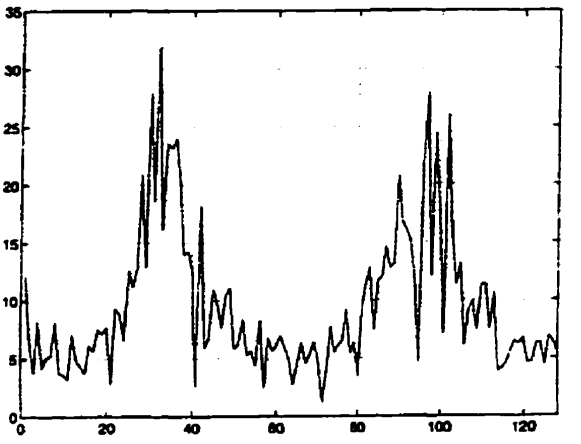

Figure 4-9: *Cross section of the power spectrum in Figure 4-8 is plotted against* q_x *for* $q_y = 0.5$. *It characteristically indicates a chaotic pattern.*

Turing instability point and into the region where the Hopf bifurcation is possible. The pattern produced is rather chaotic, but its power spectrum, although widely distributed, still has major peaks showing some semblance of symmetry as shown in Fig. 4-14. But in this case, the circular wave vector distributions in the wave vector space indicates a random structure.

In Fig. 4-15 we show a chaotic-looking pattern obtained when nonrandom initial conditions are taken in the case of the parameter values $B = 6.6$ and $N_{rd} = 0.1$. At this value of the reaction-diffusion number the system is rather hyperbolic. We have noticed in the earlier work[6, 7] on the modified Selkov model that the patterns tend to be chaotic as the reaction diffusion number is lowered to the values of this magnitude. The two-dimensional power spectrum of this pattern is shown in Fig. 4-16. Although the pattern in the wave vector space is rather blurred, the distribution of major peaks has some elements of symmetry; it has a two-fold symmetry along a diagonal.

In Fig. 4-17 we show a mixed pattern obtained for random initial conditions in the case of the parameter set $A = 3$, $B = 10.1$, $D_x = 5 \times 10^{-3}$, $D_y = 1 \times 10^{-3}$, and $N_{rd} = 2.5$. Its two-dimensional power spectrum is shown in Fig. 4-18. The wave vector distribution is rather blurred except for the central portion of white spots

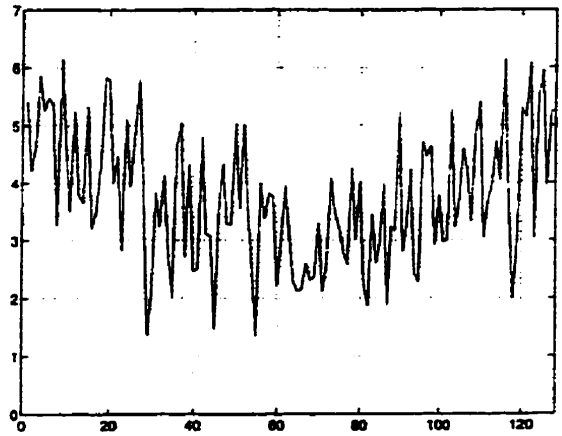

Figure 4-10: *Cross section of the power spectrum in Figure 4-8 is plotted against* q_x *for* $q_y = 0.128$. *It characteristically indicates a chaotic pattern.*

which appears to correspond to the short wave length structure in Fig. 4-17. The central part seems to have some elements of symmetry.

From the patterns and their two-dimensional power spectrum presented, we are able to conclude that each pattern, even a chaotic looking one, appears to have a characteristic wave vector distribution which has a symmetric structure. This seems to be an interesting feature worthy of further study since chaotic patterns may be amenable to some scheme of classification into categories.

4.5 Concluding Remarks

In this chapter, we have studied a set of hyperbolic reaction-diffusion equations which results in coupled telegraphist equations for the irreversible Brusselator that has been conventionally investigated with parabolic reaction-diffusion equations in the literature. Based on the telegraphist equations and the amplitude equation in a form amenable to a perturbation theory, we have explicitly calculated the speed of a travelling periodic wave for the Brusselator from the linearized telegraphist equations. The formula obtained has the generic form first suggested by Luther many decades ago and should be regarded as an approximate derivation of his formula. It

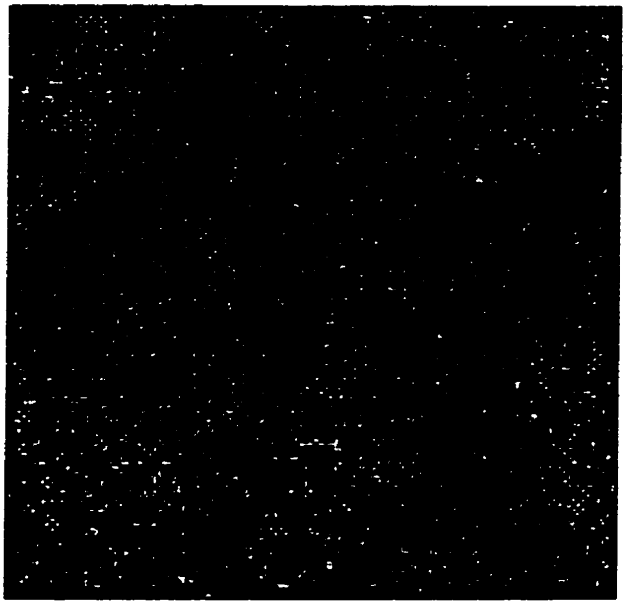

Figure 4-11: *A chaotic pattern in the case of* $N_{rd} = 2.2$ *and* $B = 8$. *Other parameters are the same as the rest of the figures.*

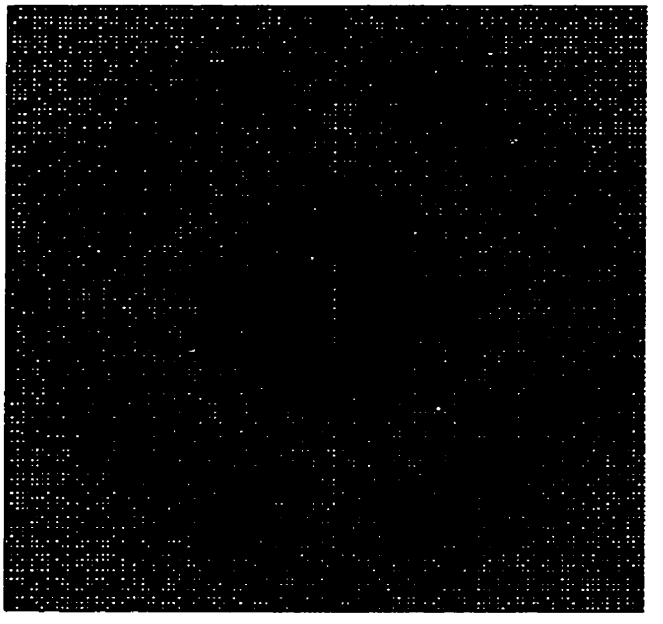

Figure 4-12: *The two-dimensional power spectrum of the pattern in Fig. 4-11. The distribution of the peaks is quite symmetrical.*

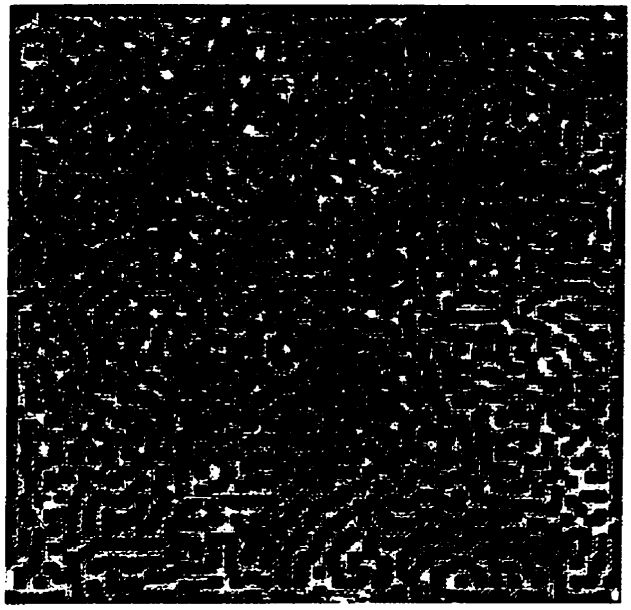

Figure 4-13: *A Chaotic maze-like pattern in the case of* $B = 10.1$ *with other parameters are the same as for Fig. 4-7.*

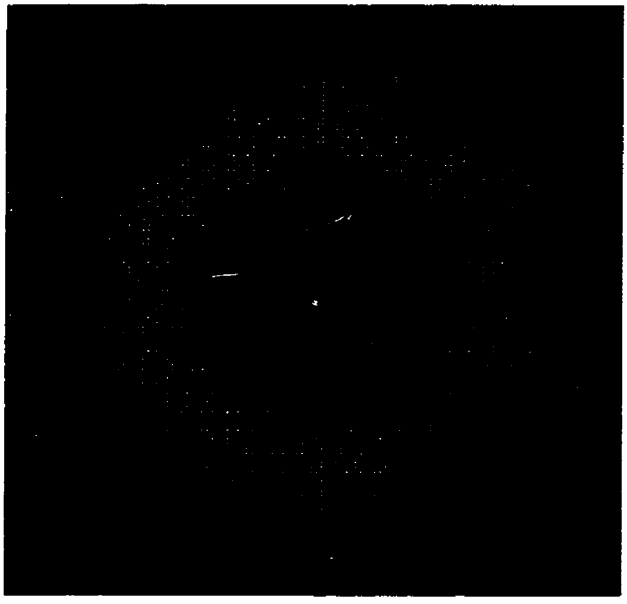

Figure 4-14: *Two-dimensional power spectrum of the pattern in Figure 4-13.*

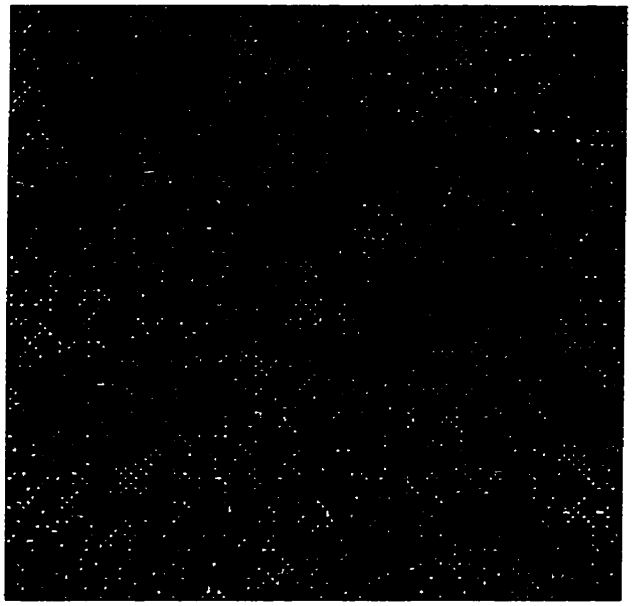

Figure 4-15: *A chaotic-looking pattern obtained when nonrandom initial conditions are taken. The parameters are:* $A = 3$, $B = 6.6$, $N_{rd} = 0.1$.

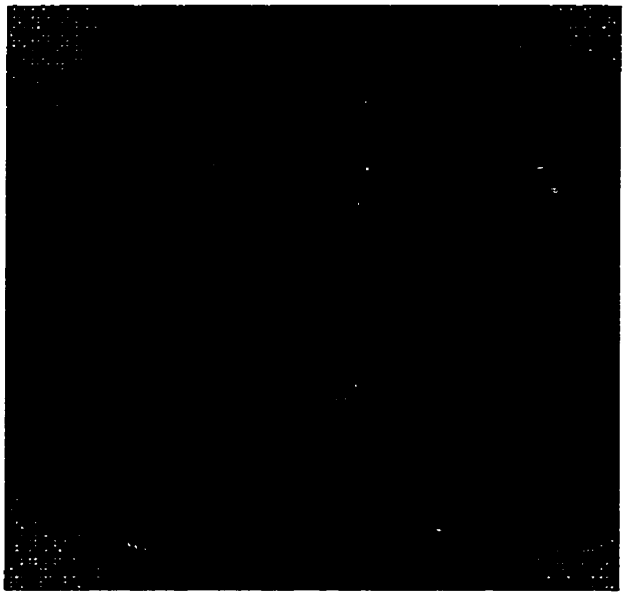

Figure 4-16: *The two-dimensional power spectrum of the regular pattern in Fig. 4-15.*

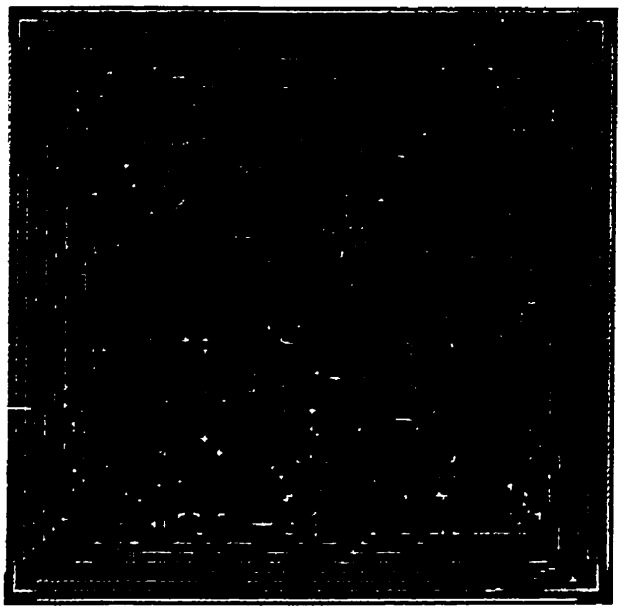

Figure 4-17: *A mixed pattern obtained for random initial conditions in the case of parameters* $D_x = 5 \times 10^{-3}$, $D_y = 1 \times 10^{-3}$, $A = 3$, $B = 10.1$, $N_{rd} = 2.5$.

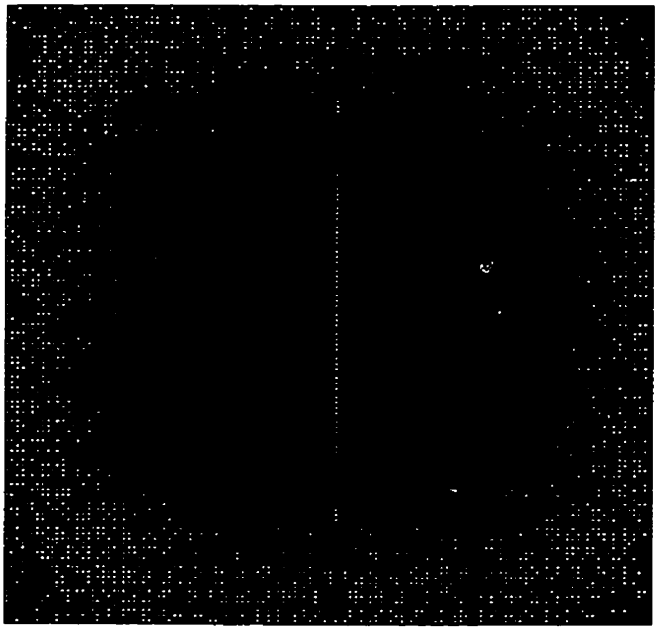

Figure 4-18: *Two-dimensional power spectrum of the pattern shown in Fig. 4-17.*

is not an exact result, but in view of the nonlinear nature of the equations involved, such an approximate result probably is the most one can hope for from the analytical approach. Albeit approximate and probably quite limited in applicability, the formula provides considerable insights to the nature of the waves involved and their origins, and we hope that this kind of result will be of some use to experiments.

We have also studied the numerical solutions of the telegraphist equations in comparison with the corresponding parabolic reaction-diffusion equations, although much of the results for the parabolic equations have not been presented for the lack of space. It must be noted that the large N_{rd} results for the hyperbolic equations (*i.e.*, telegraphist equations) essentially correspond to the results for the parabolic reaction-diffusion equations. As the values of parameters and, especially, that of N_{rd} are varied, various patterns emerge. The two-dimensional power spectra of such patterns reveal patterns of wave vector distributions with some elements of symmetry. This suggests that spatial patterns can be classified according to the wave vector distributions and symmetries of their multidimensional power spectra. This seems to be a rather intriguing and, perhaps, important feature worthy of further serious study in the future.

Bibliography

[1] M. Seul and D Andelman, Science **267**, 476 (1995).

[2] *Chemical waves and patterns*, edited by R. Kapral and k. Showalter (Kluwer, Dordrecht, 1995);K. Lee and H. L. Swinney, Phys. Rev. E **51**, 1899 (1995).

[3] B. S. Kerner and V. V. Opisov, Sov. Phys. -Uspekhi **33**, 679 (1990); B. S. Kerner and V. V. Opisov, *Autosolitons: a New Approach to Problems of Self-Organization and Turbulence* (Kluwer, Dordrecht, 1994); *Nonlinear dynamics and pattern formation in semiconductors and devices*, edited by F. J. Niedernostheide (Springer, Berlin, 1994); M. Bode and H. -G. Purwins, Physica D **86**, 53 (1995); E. Ammelt, D. Schweng and H. -G. Purwins, Phys. Lett. A **179**, 348 (1993).

[4] M. Gorman, M. el Hamdi, and K. A. Robbins, Combust. Sci. Tech. **98**, 37 (1994); **98**, 71 (1994); **98**, 79 (1994).

[5] U. I. Cho and B. C. Eu, Physica D **68**, 351(1993).

[6] M. Al-Ghoul and B. C. Eu, Physica D **90**, 119(1996).

[7] M. Al-Ghoul and B. C. Eu, Physica D (in press).

[8] P. Richter, P. Rehmus, and J. Ross, Prog. Theoret. Phys. Japan **66**, 385(1981); P. Rehmus and J. Ross, Proc. Nat. Acad. Sci. USA **78**, 2952, 3563(1982).

[9] I. Prigogine, *Thermodynamics of Irreversible Processes* (Interscience, New York, 1961).

[10] P. M. Wood and J. Ross, J. Chem. Phys. **82**, 1924(1985).

[11] C. Vidal, J. Stat. Phys. **48**, 1017(1987).

[12] R. Z. Luther, Z. Elektrochem. **12**(32), 596(1906).

[13] For translation of Ref. 8, see R. Arnold, K. Showalter, and J. J. Tyson, J. Chem. Edu. **64**, 740(1987); also see K. Showalter and J. J. Tyson, J. Chem. Edu. **64**, 742(1987).

[14] J. D. Dockery, J. P. Keener and J. J. Tyson, Physica D **30**, 177(1988).

[15] R. G. Gibbs, SIAM J. Appl. Math. **38**, 422(1980).

[16] P. Gray and S. K. Scott, *Chemical Waves and Instabilities* (Clarendon, Oxford, 1990).

[17] M. Golubitsky and D. G. Schaeffer, *Singularities and Groups in Bifurcation Theory* (Springer, Berlin, 1985), Vol. 1; B. D. Hassard, N. D. Kazarinoff, and Y.-H. Wan, *Theory and Applications of Hopf Bifurcation* (Cambridge, London, 1981).

[18] G. Nicolis and I. Prigogine, *Self-Organization in Nonequilibrium Systems* (Wiley, New York, 1977).

[19] B. C. Eu, *Kinetic Theory and Irreversible Thermodynamics* (Wiley, New York, 1992).

[20] J. D. Murray, *Mathematical Biology* (Springer, Berlin, 1989).

[21] A. Nayfeh, *Perturbation Methods* (Wiley, New York, 1973).

[22] A. Erdelyi, *Asymptotic Expansions* (Dover, New York, 1956).

[23] C. Canuto, M. Y. Hussaini, A. Quarteroni, and T. A. Zang, *Spectral Methods in Fluid Dynamics* (Springer, Berlin, 1988).

[24] F. R. Gantmacher, *Théorie des Matrices* (Dunod, Paris, 1966) Vol. 2.: Q. Ouyang and H. L. Swinney, Chaos **1**, 411(1991); Q. Ouyang, G. H. Gunaratne, H. L. Swinney, Chaos **3**, 707(1993).

Chapter 5

Perturbation Equations In One Dimension

5.1 Introduction

In many physical problems, partial differential equations describing processes in the space-time domain prove to be a very useful tool. For instance, one may mention the Navier-Stokes fluids, chemical reactions including diffusion, some ecological systems with migration, etc. Suppose that oscillatory motions occur in any of these continuous media as some control parameter is varied, and consider how to describe them. It is true that if the system is confined in a finite volume, the governing partial differential equations can in principle be transformed into a discrete set of ordinary differential equations which describe the evolution of the amplitudes of the basis functions satisfying prescribed boundary conditions. Although the system then involves an infinite number of degrees of freedom, a mode-truncation approximation is usually allowed. The application of a multi-scale method will lead to a Stuart-Landau equation. However, there may be some situations where keeping to formal bifurcation theories easily makes us overlook a fact of considerable physical importance. The situation of particular interest is when the system size is very large. Then, formal bifurcation techniques applied near μ_c, the critical Hopf bifur-

cation point, cannot claim full validity except in an extremely limited parameter range about μ_c. This is basically because the eigenvalue spectrum obtained from the linearization about the reference steady state is almost continuous for large system size, so that, in addition to the couple of modes which are becoming unstable, a large number of degrees of freedom come into play as soon as μ deviates from μ_c. Thus it is more desirable to generalize the Stuart-Landau type of equations so as to cover such circumstances. Researchers in the field of fluid mechanics have developed theories in this direction, which proved to be very useful in understanding instabilities arising in systems with large dimensions at least in one or two directions. Typical examples are the Newell-Whitehead theory[1] on a fluid layer heated from below with an infinite aspect ratio and the Stewartson-Stewart theory[2] on plane Poiseuille flow. In these theories, one works with partial differential equations throughout, not transforming them into ordinary differential equations. A method was contrived to reduce the equations to a generalized form of the Stuart-Landau equation, thereby admitting slow spatial and temporal modulation of the envelope of the bifurcation flow patterns. We call that equation the Ginzburg-Landau equation. The derivation of the Ginzburg-Landau equation usually involves the method of multiple scales in both space and time. It is now widely known that the Ginzburg-Landau equation is not only related to a few fluid mechanical or optical problems but can be deduced from a rather general class of partial differential equations[3, 4, 5, 6]. Chemical reactions with diffusion are a simple and particularly interesting class of systems in this connection[8, 9]. Just as the Stuart-Landau equation describes the simplest field of a nonlinear oscillator, the Ginzburg-Landau equation describes the simplest field of nonlinear oscillators. We have derived an amplitude equation for the hyperbolic reaction-diffusion equation describing the Brusselator. The resulting amplitude equations are of the Ginzburg-Landau type and similar in form to the amplitude equations derived from the parabolic reaction-diffusion equations. In the next sections, we shall derive those amplitude equations for Hopf and Turing instabilities, respectively.

5.2 Amplitude Equations of Perturbation Analysis

The following version of the Brusselator will be adopted for the present chapter. It differs from the one in the previous chapter since some constants are adjusted in order to make comparison with the literature values for the parabolic partial differential equations for the Brusselator. We will consider the parameter B as the dynamical parameter and study bifurcation with respect to it. Since we are interested in oscillations we have to compute the critical values B_c beyond which Hopf or Turing instability occurs. To compute the marginal stability we have to linearize the system and study its stability with respect to perturbations around its steady state. The system around $(B/A, A)$ is given by

$$\partial_t^2 \mathbf{Z} + \bar{N}_{rd} \mathbf{H}_l \partial_t \mathbf{Z} - \bar{N}_{rd} \mathbf{D} \nabla_r^2 \mathbf{Z} = -\bar{N}_{rd} (\mathbf{L}\mathbf{Z} - \mathbf{\Lambda} + \mathbf{H}_n \partial_t \mathbf{Z}) \tag{5.1}$$

with the definitions of $x = X - A$ and $y = Y - B/A$, $\mathbf{Z} = (x, y)$,

$$\mathbf{H}_l = \begin{pmatrix} H^0_{xx} & H^0_{xy} \\ H^0_{yx} & H^0_{yy} \end{pmatrix}, \tag{5.2}$$

$$\mathbf{H}_n = \begin{pmatrix} H^n_{xx} & H^n_{xy} \\ H^n_{yx} & H^n_{yy} \end{pmatrix}. \tag{5.3}$$

The matrix elements are defined by

$$H^0_{xx} = 1 + (1 - B)/\bar{N}_{rd},$$

$$H^0_{xy} = -A^2/\bar{N}_{rd},$$

$$H^0_{yx} = B/\bar{N}_{rd}, \tag{5.4}$$

$$H^0_{yy} = f^{-2} + (R + A^2)/\bar{N}_{rd},$$

$$H^n_{xx} = -2[(B/A)x + Ay + xy]/\bar{N}_{rd},$$

$$H^n_{xy} = -(x^2 + 2Ax)/\bar{N}_{rd},$$

$$H^n_{yx} = -H^n_{xx}, \tag{5.5}$$

$$H^n_{yy} = -H^n_{xy}.$$

The other symbols are:

$$\mathbf{L} = \begin{pmatrix} 1 - B & -A^2 \\ Bf^{-2} & A^2 f^{-2} \end{pmatrix}, \tag{5.6}$$

$$\mathbf{\Lambda} = \begin{pmatrix} -[(B/A)x^2 + 2Axy + x^2 y] \\ [(B/A)x^2 + 2Axy + x^2 y]f^{-2} \end{pmatrix}. \tag{5.7}$$

Linear stability analysis can be performed on (5.1) if the nonlinear terms on the right-hand side are neglected. For this purpose we look for the solution of the

linearized differential equations in the form

$$\mathbf{Z}_l = \sum_{\mathbf{k}} \sum_{\omega} \mathbf{\Phi}(\mathbf{k}, \omega) \exp(i\mathbf{k} \cdot \mathbf{r} + \omega t). \tag{5.8}$$

Upon substitution of (5.8) into (5.1) we obtain the following algebraic system

$$(\omega^2 \mathbf{I} + \omega N_{rd} \mathbf{H}_l + \bar{N}_{rd} \mathbf{D}\mathbf{k} \cdot \mathbf{k} + \bar{N}_{rd} \mathbf{L}) \mathbf{\Phi}(\mathbf{k}, \omega) = 0. \tag{5.9}$$

For the system (5.9) to have nontrivial solutions its determinant must vanish. The determinant gives the following dispersion relation

$$P_4(\mathbf{k}, z) = \omega^4 + P(\mathbf{k})\omega^3 + Q(\mathbf{k})\omega^2 + T(\mathbf{k})\omega + S(\mathbf{k}) = 0, \tag{5.10}$$

where

$$P(k) = 1 - B + A^2 + 2\bar{N}_{rd}, \tag{5.11}$$

$$Q(k) = \bar{N}_{rd}(D_x + D_y)k^2 + A^2(1 + \bar{N}_{rd} - f^{-2}\bar{N}_{rd}) + \bar{N}_{rd}^2, \tag{5.12}$$

$$\begin{aligned} T(k) = {} & [\bar{N}_{rd}^2(D_x + D_y) + \bar{N}_{rd}(A^2 D_x - (B-1)D_y)]k^2 \\ & + \bar{N}_{rd}^2(1 - B + f^{-2}A^2) - \bar{N}_{rd}(1 + f^{-2})A^2, \end{aligned} \tag{5.13}$$

$$S(k) = \bar{N}_{rd}^2[D_x D_y k^4 + (A^2 f^{-2} D_x + (1 - B)D_y)k^2 + A^2 f^{-2}]. \tag{5.14}$$

The simultaneous conditions for which (5.10) admits solutions all with negative real part are given by

$$P > 0, \tag{5.15}$$

$$Q > 0, \tag{5.16}$$

$$T > 0, \tag{5.17}$$

$$PQT - T^2 - P^2S > 0. \tag{5.18}$$

The first type of instability can be readily seen when

$$B_c = 1 + A^2 + 2\bar{N}_{rd}. \tag{5.19}$$

but as we will see later, this instability occurs always above the Hopf bifurcation point.

Let μ be a small expansion parameter of the form

$$\mu = \frac{B - B_c}{B_c}. \tag{5.20}$$

Following [7], we can then expand our operators $\mathbf{L}$ and $\mathbf{H}$ in term of μ. We obtain the following expressions:

$$\begin{aligned} \mathbf{L} &= \mathbf{L}_0 + \mu\mathbf{L}_1 + \cdots, \\ \mathbf{M} &= \mathbf{M}_0 + \mu\mathbf{M}_1 + \cdots, \\ \mathbf{N} &= \mathbf{N}_0 + \mu\mathbf{N}_1 + \cdots, \\ \mathbf{H}_l &= \mathbf{H}_0 + \mu\mathbf{H}_1 + \cdots. \end{aligned} \tag{5.21}$$

We also scale time and space as

$$\tau = \mu t, \tag{5.22}$$

$$\xi = |\mu|^{1/2} r, \tag{5.23}$$

which imply rescaling the derivatives in the following manner:

$$\frac{\partial}{\partial t} \longrightarrow \mu \frac{\partial}{\partial \tau}, \tag{5.24}$$

$$\nabla_r \longrightarrow |\mu|^{1/2} \nabla_\xi. \tag{5.25}$$

By substituting (5.24)and (5.25) into (5.1), using (5.21), and equating terms of like power of μ on the left and right hand side, we get the following set of equations:

$$\mathcal{L}_0 \mathbf{Z}_m = \mathbf{G}_m \ (m = 1, 2, 3, \cdots), \tag{5.26}$$

$$\mathbf{G}_1 = 0, \tag{5.27}$$

$$\mathbf{G}_2 = \bar{N}_{rd} \mathbf{M}_0 \mathbf{Z}_1 \mathbf{Z}_1 + 2\bar{N}_{rd} \mathbf{D} \boldsymbol{\nabla}_\xi \cdot \boldsymbol{\nabla}_r \mathbf{Z}_1, \tag{5.28}$$

$$\begin{aligned} \mathbf{G}_3 = {} & 2\bar{N}_{rd} \mathbf{M}_0 \mathbf{Z}_1 \mathbf{Z}_2 + \bar{N}_{rd} \mathbf{N}_0 \mathbf{Z}_1 \mathbf{Z}_1 \mathbf{Z}_1 \\ & + (\bar{N}_{rd} \mathbf{D} \boldsymbol{\nabla}_\xi^2 \mathbf{Z}_1 + 2\bar{N}_{rd} \mathbf{D} \boldsymbol{\nabla}_\xi \cdot \boldsymbol{\nabla}_r \mathbf{Z}_2 + \chi \bar{N}_{rd} \mathbf{L}_1 \mathbf{Z}_1 \\ & - 2\partial_\tau \partial_t \mathbf{Z}_1 - \bar{N}_{rd} \mathbf{H}_1 \partial_\tau \mathbf{Z}_1 - \bar{N}_{rd} \mathbf{H}_0 \partial_t \mathbf{Z}_1), \ etc... \end{aligned} \tag{5.29}$$

Here

$$\mathcal{L}_0 = \partial_t^2 + \bar{N}_{rd} \mathbf{H}_0 \partial_t - \bar{N}_{rd} \mathbf{L}_0 - \bar{N}_{rd} D \nabla_r^2. \tag{5.30}$$

5.3 Hopf Instability

Clearly, in the neighborhood of the Hopf critical point, the temporal part of the hyperbolic system is identical to the one of the parabolic partial differential equation system. Let μ be an expansion parameter and let $\mathbf{e}$ be the normalized right-

eigenvector of the linear operator with no space dependence $\mathcal{L}_0 = \partial_t^2 + \bar{N}_{rd}\mathbf{H}_0\partial_t - \bar{N}_{rd}\mathbf{L}_0$ corresponding to the eigenvalue $i\omega_0$. The eigenvalue equations are

$$\mathcal{L}_0\mathbf{e}_H = i\omega_0\mathbf{e}_H \tag{5.31}$$

and

$$\mathbf{e}_H^*\mathcal{L}_0 = i\omega_0\mathbf{e}_H^*. \tag{5.32}$$

We will also denote the complex conjugates of the eigenvectors $\mathbf{e}_H$ and $\mathbf{e}_H^*$ by an overbar. Note that $\mathbf{e}_H^*\bar{\mathbf{e}}_H = \bar{\mathbf{e}}_H\mathbf{e}_H^* = 0$.

For $m = 1$, (5.26) is homogeneous and its solution can be looked for in the form[1]

$$\mathbf{Z}_1 = \mathbf{A}(\xi,\tau)\exp(i\omega_0 t)\,\mathbf{e}_H + \bar{\mathbf{A}}(\xi,\tau)\exp(-i\omega_0 t)\,\bar{\mathbf{e}}, \tag{5.33}$$

where $A(\mathbf{s},\tau)$ is the amplitude of the oscillatory solution corresponding to the eigenvalue $i\omega_0$ at the critical point in question. For other values of m the inhomogeneous equations in (5.26) can be solved subject to the solvability condition

$$\int_0^{2\pi/\omega_0} dt\ \exp(-i\omega_0 t)\mathbf{e}_H^*\cdot\mathbf{G}_m = 0. \tag{5.34}$$

The solution $\mathbf{Z}_1$ in (5.33) suggests that $\mathbf{G}_m$ is also a periodic function of $\omega_0 t$. Therefore $\mathbf{G}_m$, periodic in $\omega_0 t$, may be expanded as follows:

$$\mathbf{G}_m = \sum_{l=-\infty}^{\infty}\mathbf{G}_m^{(l)}\exp(il\omega_0 i). \tag{5.35}$$

The solvability condition (5.34) can thenbe written as

$$\mathbf{e}_H^*\cdot\mathbf{G}_m^{(1)} = 0. \tag{5.36}$$

For $m = 2$ the solvability condition is clearly satisfied. The solution $\mathbf{Z}_2$ of (5.26) in

[1]The amplitude $\mathbf{A}(\xi,\tau)$ is a complex function of the slow variables ξ and τ. We denote it by a bold symbol '**A**' only to distinguish it from the experimental parameter A.

the case of $m = 2$ is found in the form

$$\mathbf{Z}_2 = \mathbf{B}(\xi,\tau)\exp(2i\omega_0 t)\mathbf{e}_{H2} + \bar{\mathbf{B}}(\xi,\tau)\exp(2i\omega_0 t)\bar{\mathbf{e}}_2 + \mathbf{C}(\xi,t) + \mathbf{W}(\xi,\tau)\exp(i\omega_0 t) \tag{5.37}$$

where

$$\mathbf{B}(\xi,\tau) = \left[(2i\omega_0)^2\mathbf{I} + 2i\omega_0\bar{N}_{rd}\mathbf{H}_0 - \bar{N}_{rd}\mathbf{L}_0\right]^{-1}\bar{N}_{rd}\mathbf{M}_0\mathbf{e}\mathbf{e}\mathbf{A}^2(\xi,\tau). \tag{5.38}$$

$$\bar{\mathbf{B}}(\xi,\tau) = \left[(-2i\omega_0)^2\mathbf{I} - 2i\omega_0\bar{N}_{rd}\mathbf{H}_0 - \bar{N}_{rd}\mathbf{L}_0\right]^{-1}\bar{N}_{rd}\mathbf{M}_0\bar{\mathbf{e}}\bar{\mathbf{e}}\bar{\mathbf{A}}^2(\xi,\tau), \tag{5.39}$$

$$\mathbf{C}(\xi,\tau) = -2\mathbf{L}_0^{-1}\mathbf{M}_0\mathbf{e}\bar{\mathbf{e}}\left|\mathbf{A}(\xi,\tau)\right|^2. \tag{5.40}$$

Here $\mathbf{I}$ is the unit matrix. $\mathbf{W}(\xi,\tau)$ cannot be determined at this stage. By inserting equations (5.38), (5.39), (5.40) and (5.33) into the solvability condition (5.36). we obtain

$$\begin{aligned}\mathbf{e}_H^*\cdot\mathbf{G}_3^{(1)} &= \bar{N}_{rd}\mathbf{e}_H^*\left[2\mathbf{M}_0(\bar{\mathbf{A}}\mathbf{B}+\mathbf{A}\mathbf{C})\mathbf{e}_H + 3\mathbf{N}_0\mathbf{e}\mathbf{e}\mathbf{e}\left|\mathbf{A}\right|^2\mathbf{A}\right]\\ &\quad -\mathbf{e}_H^*\left[2i\omega_0\partial_t - \bar{N}_{rd}\left(\chi\mathbf{L}_1 - \mathbf{D}\boldsymbol{\nabla}_s^2 + \mathbf{H}_1 - \mathbf{H}_0\partial_t\right)\right]\mathbf{A}\mathbf{e}_H\\ &= 0\end{aligned} \tag{5.41}$$

On substitution of $\mathbf{B}$ and $\mathbf{C}$ in (5.38), (5.39), (5.40) into (5.41), we find the amplitude equation

$$\partial_t\mathbf{A} = q\mathbf{A} + \tilde{D}\boldsymbol{\nabla}_\xi^2\mathbf{A} - p\left|\mathbf{A}\right|^2\mathbf{A} \tag{5.42}$$

where with definitions

$$\mathbf{K} = \left[(2i\omega_0\mathbf{I})^2 + 2i\omega_0\bar{N}_{rd}\mathbf{H}_0 - \bar{N}_{rd}\mathbf{L}_0\right]^{-1}, \tag{5.43}$$

$$Q = \mathbf{e}_H^*\left(2i\omega_0\mathbf{I} + \bar{N}_{rd}\mathbf{H}_0\right)^{-1}\mathbf{e}_H, \tag{5.44}$$

various coefficients are given by the formulas

$$q = \bar{N}_{rd} Q \left(\chi \lambda_1 - i\omega_0 \bar{N}_{rd} \mathbf{e}_H^* \mathbf{H}_1 \mathbf{e}_H \right), \tag{5.45}$$

$$\lambda_1 = \mathbf{e}_H^* \mathbf{L}_1 \mathbf{e}_H. \tag{5.46}$$

$$\begin{aligned} p = & -\bar{N}_{rd} Q \left[2\mathbf{e}_H^* \mathbf{M}_0 (-2\mathbf{e}_H \mathbf{L}_0^{-1} \mathbf{M}_0 \mathbf{e}_H \bar{\mathbf{e}}_H + \bar{N}_{rd} \bar{\mathbf{e}} \mathbf{K} \mathbf{M}_0 \mathbf{e}_H \mathbf{e}_H) \right. \\ & \left. + 3\mathbf{e}_H^* \mathbf{N}_0 \mathbf{e}_H \mathbf{e}_H \bar{\mathbf{e}}_H \right], \end{aligned} \tag{5.47}$$

$$\tilde{D} = \bar{N}_{rd} Q \mathbf{e}_H^* \mathbf{D} \mathbf{e}_H. \tag{5.48}$$

If the corresponding parabolic reaction-diffusion equations are used to derive the amplitude equation, we obtain

$$\partial_\tau \mathbf{A} = q' \mathbf{A} + \tilde{D}' \boldsymbol{\nabla}_\xi^2 \mathbf{A} - p' |\mathbf{A}|^2 \mathbf{A} \tag{5.49}$$

where the coefficients q', p', and $\tilde{D}'$ are given by

$$q' = \chi \lambda_1 = \chi \left[\mathrm{Re}(\lambda_1) + i\omega_1 \right], \tag{5.50}$$

$$\begin{aligned} p' = & \mathbf{e}_H^* \mathbf{M}_0 \left[-2\mathbf{M}_0 \mathbf{L}_0^{-1} \mathbf{e}_H \bar{\mathbf{e}}_H + \bar{\mathbf{e}}_H \left(2i\omega_0 \mathbf{I} - \mathbf{L}_0 \right)^{-1} \mathbf{M}_0 \mathbf{e}_H \mathbf{e}_H \right] \\ & + 3\mathbf{N}_0 \mathbf{e}_H \mathbf{e}_H \bar{\mathbf{e}}_H, \end{aligned} \tag{5.51}$$

$$\tilde{D}' = \mathbf{e}_H^* \mathbf{D} \mathbf{e}_H. \tag{5.52}$$

Therefore, we see that the hyperbolic reaction-diffusion equations give rise to basically the same form of amplitude equation as the parabolic reaction-diffusion equations except for the coefficients involved. The coefficients are dependent on the reaction-diffusion number. Further, we can rescale (5.49) by making the following

substitutions

$$\tau \rightarrow \alpha_1 \tau \ (\alpha_1 = \mathrm{Re}(q)), \tag{5.53}$$

$$\xi \rightarrow \left[\mathrm{Re}(\tilde{D})/\alpha_1\right]^{1/2} \xi, \tag{5.54}$$

$$\mathbf{A} \rightarrow [\alpha_1/\,\mathrm{Re}(p)]^{1/2}\,\mathbf{A}. \tag{5.55}$$

then it will take the following popular form

$$\partial_\tau \mathbf{A} = (1 + ic_0)\mathbf{A} + (\mathbf{1}+ic_1)\boldsymbol{\nabla}_\xi^2\mathbf{A} - (1 + ic_2)|\mathbf{A}|^{\mathbf{2}}\,\mathbf{A}. \tag{5.56}$$

where

$$c_0 = \omega_1/\alpha_1, \tag{5.57}$$

$$c_1 = \mathrm{Im}(\tilde{D})/\,\mathrm{Re}(\tilde{D}), \tag{5.58}$$

$$c_2 = \mathrm{Im}(p)/\,\mathrm{Re}(p). \tag{5.59}$$

To apply the aforementioned procedure to the Hopf bifurcation for the Brusselator, we must identify the condition at which the Hopf bifurcation occurs. This is for which (5.10) admits pure oscillatory modes at $k = 0$. It is given by the following Hurwitz condition

$$P(0)Q(0)T(0) - T(0)^2 - P(0)^2S(0) = 0. \tag{5.60}$$

From this follow the critical values of B :

$$B_c = 1 + A^2 = B_c^{par}, \tag{5.61}$$

where B_c^{par} is the unique critical value of B in the case of the parabolic Brusselator for which a Hopf bifurcation occurs. The oscillatory modes corresponding to these critical values are given

$$\omega_0 = \pm iA. \tag{5.62}$$

Having the critical parameter defined, we can perform the expansion like in (5.21). We obtain the following operators:

$$\mathbf{L}_0 = \begin{pmatrix} A^2 & -A^2 \\ 1+A^2 & A^2 \end{pmatrix}. \tag{5.63}$$

$$\mathbf{L}_1 = \begin{pmatrix} -(1+A^2) & 0 \\ (1+A^2) & 0 \end{pmatrix}. \tag{5.64}$$

$$\bar{N}_{rd}\mathbf{H}_{l0} = \begin{pmatrix} \bar{N}_{rd}-A^2 & -A^2 \\ 1+A^2 & \bar{N}_{rd}+A^2 \end{pmatrix}, \tag{5.65}$$

$$\bar{N}_{rd}\mathbf{H}_{l1} = \begin{pmatrix} -(1+A^2) & 0 \\ (1+A^2) & 0 \end{pmatrix}.$$

The eigenvectors are given by

$$e_H = \begin{pmatrix} 1 \\ -1+\dfrac{i}{A} \end{pmatrix} = e_H^{par}, \tag{5.66}$$

$$e_H^* = \frac{1}{2}\begin{pmatrix} 1-iA & , & -iA \end{pmatrix} = e_H^{*par},$$

The parameter λ will have the form

$$\lambda_1 = \frac{1}{2}(1 + A^2). \tag{5.67}$$

With the definitions of the quantities given earlier, the amplitude equation from perturbation analysis is given by

$$\partial_t \mathbf{A} = (1 + ic_0)\mathbf{A} + (\mathbf{1}+ic_1)\boldsymbol{\nabla}_\xi^2\mathbf{A} - (1 + ic_2)|\mathbf{A}|^2\,\mathbf{A}, \tag{5.68}$$

where the coefficients c_0, c_1, and c_2 are given by

$$c_0 = \mathrm{Im}(q)/\,\mathrm{Re}(q) = 0, \tag{5.69}$$

$$c_1 = \mathrm{Im}\left(\tilde{D}\right)/\,\mathrm{Re}\left(\tilde{D}\right) = -A\frac{\alpha^2 - 1}{\alpha^2 + 1}, \tag{5.70}$$

$$\alpha = (D_x/D_y)^{1/2}, \tag{5.71}$$

$$c_2 = \mathrm{Im}(p)/\,\mathrm{Re}(p) = R_1/R_2,$$

where

$$\begin{aligned} R_1 &= \left(12 - 8\bar{N}_{rd}\right) A^6 + \left(4\bar{N}_{rd}^3 - 15\bar{N}_{rd}^2 - 4\bar{N}_{rd} - 48\right) A^4 \\ &\quad + \left(-7\bar{N}_{rd}^3 + 6\bar{N}_{rd}^2 - 8\bar{N}_{rd}\right) A^2 + 4\bar{N}_{rd}^3, \end{aligned} \tag{5.72}$$

$$\begin{aligned} R_2 &= \left(4\bar{N}_{rd}^2 - 8\bar{N}_{rd} - 4\right) A^5 - \left(\bar{N}_{rd}^3 - 5\bar{N}_{rd}^2 + 20\bar{N}_{rd}\right) A^3 \\ &\quad + \left(2\bar{N}_{rd}^3 + 4\bar{N}_{rd}^2\right) A. \end{aligned} \tag{5.73}$$

In the limit of infinite $\bar{N}_{rd}$ we regain the coefficient c_3 from the perturbation analysis

of the parabolic Brusselator, mainly

$$\lim_{\bar{N}_{rd}\to\infty} c_2 = c_2^{par} = \frac{4 - 7A^2 + 4A^4}{3A(2 + A^2)}. \tag{5.74}$$

From this analysis, it is clear that we are expecting more complicated results in the case of the amplitude equation computed from the hyperbolic system than that from parabolic one. We note that there is going to be a region in the parameter space $(\bar{N}_{rd}, A)$, where we have resonances, i.e., where the denominator of the coefficient c_3 may vanish. The locus of the resonance of the coefficient c_3 is given by:

$$A_{res} = -\frac{\bar{N}_{rd}\left[\bar{N}_{rd}^2 - 5\bar{N}_{rd} + 20 \pm \left(\bar{N}_{rd}^4 - 42\bar{N}_{rd}^3 + 65\bar{N}_{rd}^2 - 40\bar{N}_{rd} + 464\right)^{1/2}\right]}{8\left(\bar{N}_{rd}^2 - 2\bar{N}_{rd} - 1\right)}. \tag{5.75}$$

As an example, we have studied the case of $A = 6.0$. We found that a singularity in c_3 occurs at $\bar{N}_{rd} = 2.3297$ and c_3 is zero at $\bar{N}_{rd} = 1.2596$ and $\bar{N}_{rd} = 10.3608$.

To understand the behavior of the numerical solution of the amplitude equation (5.68), it is useful to perform a linear stability analysis of the homogeneous oscillations. Let

$$\mathbf{A} = (1 + \boldsymbol{\delta}\mathbf{A}) \exp(-ic_2 t). \tag{5.76}$$

The linearized version of (5.68) will then be

$$\partial_\tau \boldsymbol{\delta}\mathbf{A} = (1+ic_1)\boldsymbol{\nabla}_\xi^2 \boldsymbol{\delta}\mathbf{A} - (1 + ic_2)(\boldsymbol{\delta}\mathbf{A} + \boldsymbol{\delta}\mathbf{A}^*). \tag{5.77}$$

If we define $\boldsymbol{\delta}\mathbf{A}$ to be

$$\boldsymbol{\delta}\mathbf{A} = (u + iv) \exp(ik\xi), \tag{5.78}$$

separating the imaginary part from the real part we get

$$\frac{du}{d\tau} = -\left[2 + k^2\right] u + c_1 k^2 v, \tag{5.79}$$

$$\frac{dv}{d\tau} = -\left[2c_2 + c_1k^2\right] u - k^2 v. \tag{5.80}$$

The characteristic equation of this system is

$$\omega^2 + \left[2 + k^2\right] \omega + \left[2k^2 \left(1 + c_1c_2\right) + k^4(1 + c_1^2)\right] = 0. \tag{5.81}$$

The sum of the roots is obviously negative. The only instability that can arise is through the last constant term vanishing and subsequently becoming negative. This requires that the parameters c_1 and c_2 are such that

$$1 + c_1c_2 < 0. \tag{5.82}$$

This inequality constitutes a condition for spatio-temporal complexity since in this range a homogeneous oscillation may no longer be sustained. This instability is induced by the presence of complex coefficients in (5.68) or equivalently by the presence of nontrivial phase variable related to the imaginary part of the order parameter A. Therefore this is called a phase instability. The function $1 + c_1c_2$ contains a singularity in the reaction diffusion number $\bar{N}_{rd}$ due to the singularity in the parameter c_3. If $B = 6.0$, $D_x = 0.006$ and $D_y = 0.0016$. the singularity is at $\bar{N}_{rd}^{res} = 2.3297$. Also, the condition $1 + c_1c_2$ is zero at $\bar{N}_{rd} = 1.3737$ and $\bar{N}_{rd} = 13.9390$. In between of the previous zeros the condition changes sign, i.e., the stability of the oscillations will consequently change. The solution of the amplitude equation confirms what is predicted by the phase instability condition (5.82).

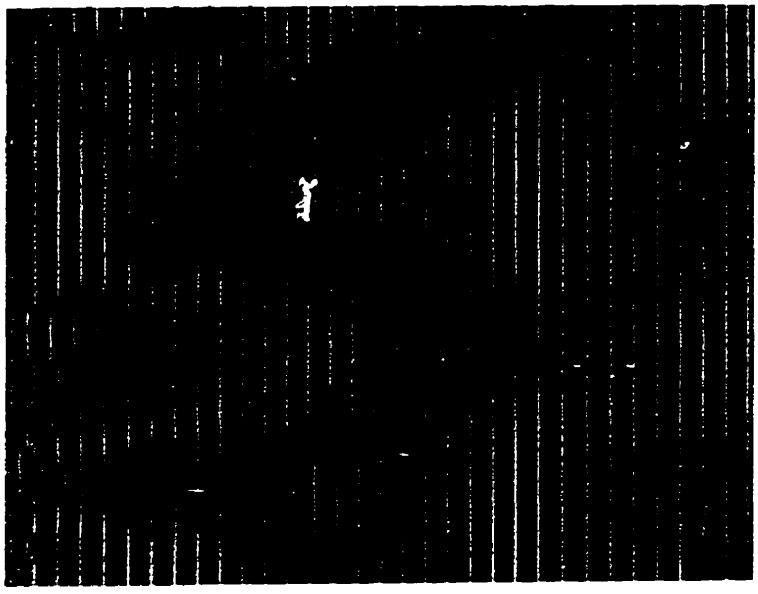

Space-time plot for $N_{rd} = 0.1$.

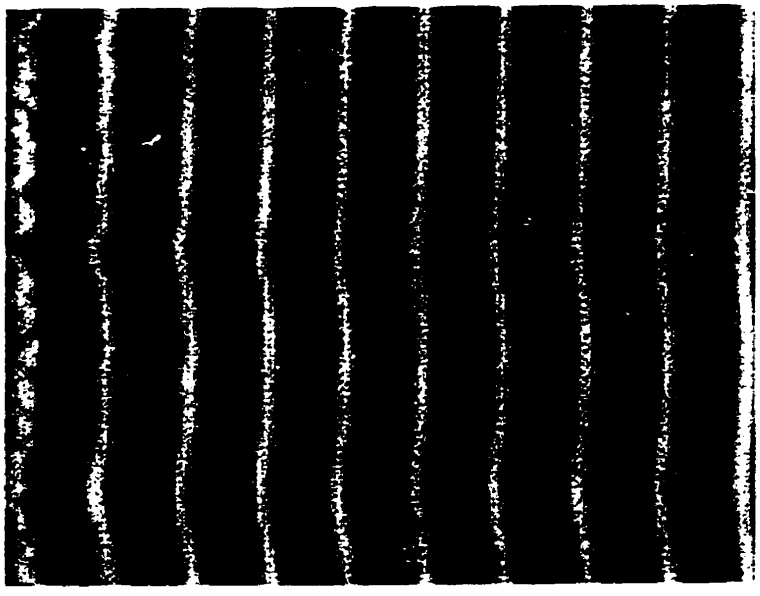

Space-time plot for $\bar{N}_{rd} = 1.0$.

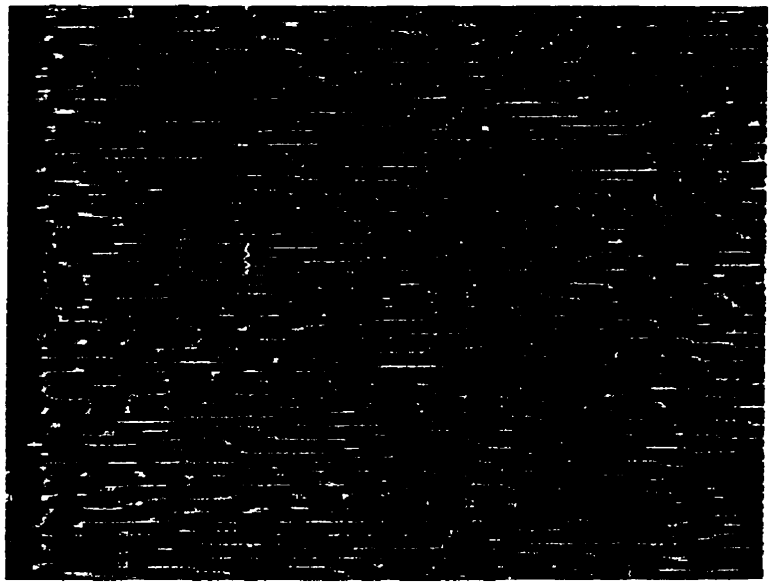

Spcae-time plot for $\bar{N}_{rd} = 1.7$.

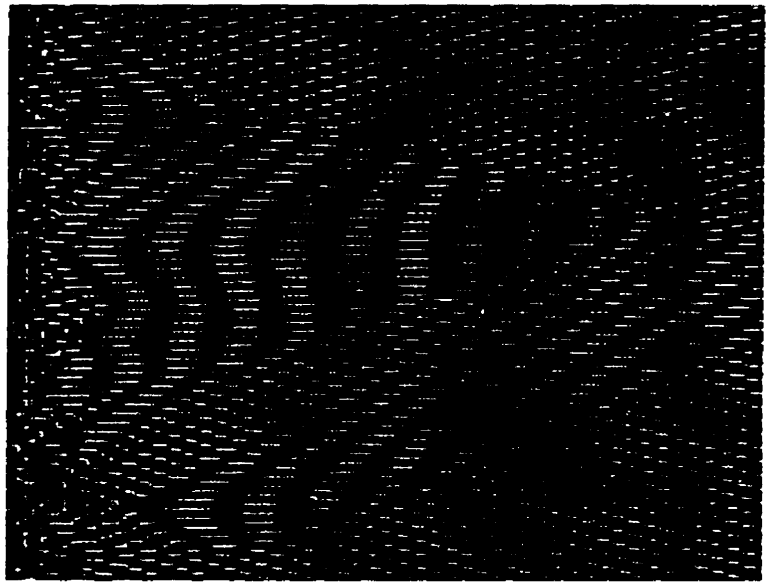

Spcae-time plot for $\bar{N}_{rd} = 100$.

5.4 The Phase Equation

In this section, the derivation of the phase equation follows exactly the method presented by Kuramoto[7]. Let $W_0(t)$ be a linearly stable T-periodic solution of an

n-dimensional system of ordinary differential equations

$$\frac{d\mathbf{W}_0}{dt} = \mathbf{F}(\mathbf{W}_0), \tag{5.83}$$

$$\mathbf{W}_0(t+T) = \mathbf{W}_0(t). \tag{5.84}$$

Let this vector field be perturbed as

$$\frac{d\mathbf{W}}{dt} = \mathbf{F}(\mathbf{W}) + \varepsilon\mathbf{p}(\mathbf{X}), \tag{5.85}$$

where $\varepsilon\mathbf{p}(\mathbf{X})$ is a small perturbation, ε is a smallness parameter. The periodic motion will persist when the perturbation $\varepsilon\mathbf{p}(\mathbf{X})$ is turned on, but its period will deviate slightly from T. Let C denote a closed curve corresponding to the periodic motion of equation (5.83). Since C is assumed to be stable, then as $t \longrightarrow \infty$, each state point $\mathbf{W}$ will approach C in the absence of perturbations. We associate a certain value of scalar ϕ to each $\mathbf{W} \in C$ in such a way that the motion on C may produce a constant increase in ϕ. Because a weak perturbation will kick the state point out of C, we then need to define the phase function in the neighborhood of C, say C', which can be thought as filled with one-parameter family of hypersufaces of constant phase[15, 11, 18]

$$\frac{d\phi(\mathbf{W})}{dt} = 1, \ \mathbf{W} \in C'. \tag{5.86}$$

The quantity ϕ may be called the phase defined on C', and its value is determined to an integer multiple of T. We need to see how a weak perturbation, where ϕ need only be defined in the vicinity of C, could modify the phase ϕ. The following equalities follow simply from equations (5.83) and (5.86)

$$\frac{d\phi(\mathbf{W})}{dt} = \nabla_{\mathbf{W}}\phi \cdot \frac{d\mathbf{W}}{dt}, \tag{5.87}$$

$$\nabla_{\mathbf{W}}\phi \cdot F(\mathbf{W}) = 1. \tag{5.88}$$

For the perturbed motion, we replace (5.85) in (5.87) to get the following equation for the phase

$$\frac{d\phi(\mathbf{W})}{dt} = \nabla_{\mathbf{W}}\phi \cdot [\mathbf{F}(\mathbf{W}) + \varepsilon \mathbf{p}(\mathbf{X})] \tag{5.89}$$

$$= 1 + \varepsilon \nabla_{\mathbf{W}}\phi \cdot \mathbf{p}(\mathbf{X}). \tag{5.90}$$

Because the deviation $|\mathbf{W} - \mathbf{W}_0(\phi)| \longrightarrow 0$ in the asymptotic regime of $t \longrightarrow \infty$, it is valid to use $\mathbf{W} = \mathbf{W}_0(\phi)$ in (5.90) to a first order approximation

$$\frac{d\phi(\mathbf{W})}{dt} = 1 + \varepsilon \Omega(\phi), \tag{5.91}$$

with the definitions

$$\Omega(\phi) = \mathbf{Z}(\phi) \cdot \mathbf{\Pi}(\phi), \tag{5.92}$$

$$\mathbf{Z}(\phi) = (\nabla_{\mathbf{W}}\phi)_{\mathbf{W}=\mathbf{W}_0(\phi)}, \tag{5.93}$$

$$\mathbf{\Pi}(\phi) = \mathbf{p}(\mathbf{W}_0(\phi)). \tag{5.94}$$

The vector $\mathbf{Z}(\phi)$ may be called the phase dependent sensitivity[11], and it measures how sensitively the oscillator responds to external perturbations. $\mathbf{Z}(\phi)$ and $\mathbf{\Pi}(\phi)$ are T-periodic functions of ϕ, which means that the right hand side of (5.86) is also T-periodic functions of ϕ. In order to obtain the average frequency, we introduce the phase disturbance ψ via $\phi = t + \psi$ and express (5.86) as

$$\frac{d\psi}{dt} = \varepsilon \Omega(t + \psi). \tag{5.95}$$

This equation shows that ψ is a slow variable which hardly changes during the period T. When averaged over time, (5.87) becomes

$$\frac{d\psi}{dt} = \varepsilon\omega, \tag{5.96}$$

$$\omega = \frac{1}{T}\int_0^T \Omega(t)dt, \tag{5.97}$$

which gives the desired frequency.

If $\varepsilon\mathbf{p}$ is interpreted as a Laplacian operator multiplied by the matrix $\mathbf{D}$ as

$$\varepsilon\mathbf{p} = \mathbf{D}\nabla^2, \tag{5.98}$$

then the Ginzburg-Landau equation can be written, after setting ε to 1, as follows

$$\frac{\partial\phi}{\partial t} = 1 + \Omega^{(1)}(\phi)\nabla^2\phi + \Omega^{(2)}(\phi)\left(\nabla\phi\right)^2, \tag{5.99}$$

$$\frac{\partial\psi}{\partial t} = \Omega^{(1)}(\psi + t)\nabla^2\psi + \Omega^{(2)}(\psi + t)\left(\nabla\psi\right)^2. \tag{5.100}$$

where

$$\Omega^{(1)}(\phi) = Z(\phi)D\frac{d\mathbf{W}_0(\phi)}{d\phi}, \tag{5.101}$$

$$\Omega^{(2)}(\phi) = Z(\phi)D\frac{d^2\mathbf{W}_0(\phi)}{d\phi^2}. \tag{5.102}$$

On averaging the periodic coefficients over the period T, we obtain

$$\frac{\partial\phi}{\partial t} = 1 + \alpha\nabla^2\phi + \beta\left(\nabla\phi\right)^2, \tag{5.103}$$

$$\frac{\partial\psi}{\partial t} = \alpha\nabla^2\psi + \beta\left(\nabla\psi\right)^2 \tag{5.104}$$

where

$$\alpha = \frac{1}{T}\int_0^T \Omega^{(1)}(t)dt, \tag{5.105}$$

(5.106)

$$\beta = \frac{1}{T}\int_0^T \Omega^{(2)}(t)dt. \tag{5.107}$$

Equation (5.104) is equivalent to the Burgers equation which can be reduced to a linear diffusion equation through the Cole-Hopf transformation[16]. In order to calculate the coefficient α and β for the Landau-Ginzburg equation, we should make use of the Floquet theory[17] which concerns first-order linear systems with periodic coefficients. If we linearize (5.85) about $\mathbf{W}_0(t)$ by putting

$$\mathbf{W}(t) = \mathbf{W}_0(t) + \mathbf{u}(t),$$

this leads to

$$\frac{d\mathbf{u}}{dt} = \mathbf{L}(t)\mathbf{u}, \tag{5.108}$$

where $\mathbf{L}$ is an $\bar{N}_{rd} \times \bar{N}_{rd}$ $T-$periodic matrix with elements

$$L_{ij} = \partial F_i\left(\mathbf{W}_0(t)\right)/\partial \mathbf{W}_{0j}(t).$$

According to the Floquet theory, it is possible to define an eigenvalue problem for (5.108) which has a general solution expressed as

$$\mathbf{u}(t) = \mathbf{S}(t)e^{\mathbf{\Lambda} t}\mathbf{u}(0), \tag{5.109}$$

where $\mathbf{S}(t)$ is a $T-$periodic matrix with the initial condition $\mathbf{S}(0) = 1$, and $\mathbf{\Lambda}$ is some time-independent matrix. The identity follows from (5.108) and (5.109)

$$\frac{d\mathbf{S}(t)}{dt} + \mathbf{S}(t)\mathbf{\Lambda} - \mathbf{L}(t)\mathbf{S}(t) = 0. \tag{5.110}$$

Let $\mathbf{u}_l$ and $\mathbf{u}_l^*$ respectively denote the right and left eigenvectors of $\mathbf{\Lambda}$ and the

corresponding eigenvalues by λ_l :

$$\mathbf{\Lambda u}_l = \lambda_l \mathbf{u}_l, \tag{5.111}$$

$$\mathbf{u}_l^* \mathbf{\Lambda} = \lambda_l \mathbf{u}_l^*, \tag{5.112}$$

$$\mathbf{u}_l^* \cdot \mathbf{u}_m = \delta_{lm}, \ (l, m = 0, 1, \ldots, \bar{N}_{rd} - 1). \tag{5.113}$$

Since $\mathbf{W}_0$ is assumed to be stable, no eigenvalues have a positive real part. Let λ_0 be the zero eigenvalue, which corresponds to phase disturbances, and assume that the remaining $\bar{N}_{rd} - 1$ eigenvalues have negative real parts. The null eigenvector $\mathbf{u}_0$ may be taken as

$$\mathbf{u}_0 = \left(\frac{d\mathbf{W}_0(t)}{dt} \right)_{t=0}, \tag{5.114}$$

because the right hand side gives a tangent vector to C at $\mathbf{W}_0(t)$ and hence has the same direction as that of the infinitesimal phase disturbances. We can also show that

$$\mathbf{S}(t)\mathbf{u}_0 = \frac{d\mathbf{W}_0(t)}{dt}, \tag{5.115}$$

$$\frac{d}{dt}\left(\frac{d\mathbf{W}_0(t)}{dt} \right) = \mathbf{L}(t) \left(\frac{d\mathbf{W}_0(t)}{dt} \right), \tag{5.116}$$

$$\frac{d\mathbf{W}_0(t)}{dt} = \mathbf{S}(t) e^{\mathbf{\Lambda} t} \left(\frac{d\mathbf{W}_0(t)}{dt} \right)_{t=0}. \tag{5.117}$$

There follow the equations[7]:

$$\mathbf{Z}(0) \cdot \mathbf{u}_l = 0, \ l \neq 0,$$

which implies that $Z(0)$ is proportional to $\mathbf{u}_0^*$ as

$$\mathbf{u}_0^* = \mathbf{Z}(0). \tag{5.118}$$

By choosing point $\mathbf{W}$ on C, we get from (5.117)

$$\mathbf{Z}(t) \cdot \left(\frac{d\mathbf{W}_0(t)}{dt} \right) = 1, \tag{5.119}$$

From (5.115) and (5.119) we deduce

$$\mathbf{Z}(t) = \mathbf{u}_0^* \mathbf{S}^{-1}(t). \tag{5.120}$$

Using (5.120) and (5.115), we redefine $\Omega(\phi)$, $\Omega^{(1)}(\phi)$ and $\Omega^{(2)}(\phi)$ as

$$\Omega(\phi) = \mathbf{u}_0^* \mathbf{S}^{-1}(\phi) \mathbf{\Pi}(\phi), \tag{5.121}$$

$$\Omega^{(1)}(\phi) = \mathbf{u}_0^* \mathbf{S}^{-1}(\phi) \mathbf{D} \mathbf{S}(\phi) \mathbf{u}_0, \tag{5.122}$$

$$\Omega^{(2)}(\phi) = \mathbf{u}_0^* \mathbf{S}^{-1}(\phi) \mathbf{D} \frac{d\mathbf{S}(\phi)}{dt} \mathbf{u}_0. \tag{5.123}$$

5.5 Phase Equation from the Landau-Ginzburg Equation

In this section, we will apply the previous calculation to derive a phase equation from the Landau-Ginzburg equation. For the aforementioned equation (5.68) the matrix $\mathbf{D}$ is given by

$$\mathbf{D} = \begin{pmatrix} 1 & -c_1 \\ -c_1 & 1 \end{pmatrix},$$

and neglecting diffusion equation (5.68) has the form of the Stuart-Landau equation

$$\frac{d\mathbf{W}}{dt} = (1 + ic_0)\mathbf{W} - (1 + ic_2)\,|\mathbf{W}|^2\,\mathbf{W}. \tag{5.124}$$

If $\mathbf{W} = X + iY$ then equation (5.124) will have the form

$$\frac{dX}{dt} = X - c_0 Y - (X - c_2 Y)(X^2 + Y^2). \tag{5.125}$$

$$\frac{dY}{dt} = Y + c_0 X - (Y + c_2 X)(X^2 + Y^2). \tag{5.126}$$

Let $\mathbf{w}(t)$ denote a disturbance defined by

$$\mathbf{W}(t) = \mathbf{W}_0(t)\,[1 + \mathbf{w}(t)]\,, \tag{5.127}$$

where $\mathbf{W}_0(t)$ is the periodic solution of (5.124)

$$\mathbf{W}_0(t) = X_0(t) + iY_0(t) = \exp(i\omega_0 t), \tag{5.128}$$

$$\omega_0 = c_0 - c_2. \tag{5.129}$$

The linearization of (5.124) about $\mathbf{W}_0(t)$ gives

$$\frac{d\mathbf{w}}{dt} = -(1 + ic_2)(\mathbf{w} + \bar{\mathbf{w}}). \tag{5.130}$$

If we put $\mathbf{w} = \xi + i\eta$, (5.130) can be expressed as

$$\frac{d}{dt}\begin{pmatrix} \xi \\ \\ \eta \end{pmatrix} = \mathbf{\Lambda}\begin{pmatrix} \xi \\ \\ \eta \end{pmatrix}, \tag{5.131}$$

or by integration

$$\begin{pmatrix} \xi(t) \\ \\ \eta(t) \end{pmatrix} = e^{\mathbf{\Lambda} t} \begin{pmatrix} \xi(0) \\ \\ \eta(0) \end{pmatrix}, \tag{5.132}$$

where

$$\mathbf{\Lambda} = -2 \begin{pmatrix} 1 & 0 \\ \\ c_2 & 0 \end{pmatrix}, \tag{5.133}$$

$$\begin{pmatrix} x \\ \\ y \end{pmatrix} = \mathbf{S}(t) \begin{pmatrix} \xi \\ \\ \eta \end{pmatrix}, \tag{5.134}$$

and

$$\mathbf{S}(t) = \begin{pmatrix} \cos\omega_0 t & -\sin\omega_0 t \\ \\ \sin\omega_0 t & \cos\omega_0 t \end{pmatrix}. \tag{5.135}$$

Thus (5.132) is equivalent to

$$\begin{pmatrix} x(t) \\ \\ y(t) \end{pmatrix} = \mathbf{S}(t) e^{\mathbf{\Lambda} t} \begin{pmatrix} x(0) \\ \\ y(0) \end{pmatrix}, \tag{5.136}$$

which is of the form of equation (5.109). Calculation of the eigenvectors of $\mathbf{\Lambda}$ are then straight forward

$$u_0 = \omega_0 \begin{pmatrix} 0 \\ \\ 1 \end{pmatrix}, \tag{5.137}$$

$$u_0^* = \omega_0^{-1} \begin{pmatrix} -c_2 & , & 1 \end{pmatrix}, \tag{5.138}$$

$$u_1 = \begin{pmatrix} 1 \\ \\ c_2 \end{pmatrix}, \tag{5.139}$$

$$u_1^* = \begin{pmatrix} 1 & , & 0 \end{pmatrix}. \tag{5.140}$$

The eigenvalues are $\lambda_0 = 0$ and $\lambda_1 = -2$. By applying the above values of $\mathbf{S}$, $\mathbf{u}_0$, and $\mathbf{u}_0^*$ to (5.121), (5.122), and (5.123), we find that $\Omega^{(1)}$ and $\Omega^{(2)}$ are $\phi-$independent and given by

$$\Omega^{(1)} = \alpha = 1 + c_1 c_2, \tag{5.141}$$

$$\Omega^{(2)} = \beta = \omega_0(c_2 - c_1). \tag{5.142}$$

So the nonlinear phase diffusion equation derived from the Ginzburg-Landau equation takes the following explicit form

$$\frac{\partial \psi}{\partial t} = (1 + c_1 c_2)\nabla^2 \psi + (c_2 - c_1)\left(\nabla \psi\right)^2. \tag{5.143}$$

An attempt to describe populations of oscillators in terms of phases was made by Winfree[11], although the theory involved some drastic assumptions. More recently, Neu[10] developed a phase description method for discrete populations. In context of reaction-diffusion dynamics, Ortoleva and Ross[12] were the first to derive a partial differential equation for the phase in the discussion of phase waves. However, an important nonlinear term representing the effect of frequency modification due to a phase gradient was lacking in their phase diffusion equation, and this was properly taken care of by Kuramoto et al. and Neu[13, 14].

The Newell criterion for phase instability for the Ginzburg Landau equation is when $1 + c_1 c_2 < 0$. In other words, when the diffusion coefficient of ψ in (5.143) becomes negative, an 'antidiffusion' behavior sets in leading to increasingly large

values of the phase gradient. One can push further the aforementioned systematic procedure[7] to add a saturation term to the phase equation (5.143) of the form $-\lambda(\nabla^4\psi)$ and the resulting equation is known as the Kuramoto-Shivanshinski equation.

Explicitly, the phase instability condition is given by:

$$1 + c_1 c_2 \; < \; 0, \text{ or} \tag{5.144}$$

$$\frac{a_6 A^6 + a_4 A^4 + a_2 A^2 + a_0}{b_4 A^4 + b_2 A^2 + b_0} \; < \; 0, \tag{5.145}$$

where

$$a_6 = (8\alpha^2 - 12)\bar{N}_{rd}^2 - 8\bar{N}_{rd} + 12, \tag{5.146}$$

$$a_4 = 4(1-\alpha^2)\bar{N}_{rd}^3 + 3(9\alpha^2 - 1)\bar{N}_{rd}^2 - (20\alpha^2 + 28)\bar{N}_{rd} + 36\alpha^2 - 60, \tag{5.147}$$

$$a_2 = (18\alpha^2 - 4)\bar{N}_{rd}^3 - (21\alpha^2 + 9)\bar{N}_{rd}^2 + (68\alpha^2 + 52)\bar{N}_{rd}, \tag{5.148}$$

$$a_0 = (2\alpha^2 + 10)\bar{N}_{rd}^3 + 12(\alpha^2 + 1), \tag{5.149}$$

$$b_4 = 12(\bar{N}_{rd}^2 - 2\bar{N}_{rd} - 1), \tag{5.150}$$

$$b_2 = 3(\bar{N}_{rd}^3 - 5\bar{N}_{rd}^2 + 20\bar{N}_{rd}), \tag{5.151}$$

$$b_0 = 6(\bar{N}_{rd}^3 + 2\bar{N}_{rd}^2). \tag{5.152}$$

Phase equations provides a very interesting insight into the origin of the defects

characterizing nonequilibrium structures and we will in the future explore these equations in the context of hyperbolic reaction-diffusion equation.

5.6 Turing Instability

For Turing instability to occur we need the following conditions to be satisfied[19] to determine the two critical values: the critical wave vector k_c and the critical experimental parameter B_c :

$$S(k) = \frac{dS(k)}{dk} = 0. \tag{5.153}$$

These conditions do not depend on the reaction-diffusion number and yield the same critical parameters as the parabolic Brusselator:

$$B_c = \left(1 + A\sqrt{\frac{D_x}{D_y}}\right)^2 = (1 + A\alpha)^2, \tag{5.154}$$

$$k_c^2 = \frac{A}{\sqrt{D_x D_y}}. \tag{5.155}$$

However, since the dispersion relation from the hyperbolic system is different from that of parabolic system where we do have two more eigenvalues, it is important to see the nature and sign of the additional roots or eigenvalues obtained from this dispersion relation. These additional roots can interact with those of the critical Turing wave numbers and may yield structures which vary in time and the speed of variation may be related to the reaction-diffusion number. To see this we chose some parameters near the region of critical parameters where the linear analysis is expected to hold and computed the roots of the dispersion relation and then solved the hyperbolic reaction diffusion equation for the Brusselator numerically. If $A = 2.0$, $D_x = 0.0016$, $D_y = 0.006$, then $B_c = 4.13$. If B is taken just above B_c, say $B = 4.17$, then a set of spatial modes lying in the interval $[k_{c1} = 23.09, k_{c2} = 27.95]$ will become unstable. The solution of the dispersion relation (5.10) yield a set of eigenfrequencies lying

between $w_h = \{0, -1.25, -1.79 \pm 3.94i\}$ for k_{c1} and $w_h = \{0, -1.54, -1.65 \pm 3.41i\}$ for k_{c2} , $\bar{N}_{rd} = 2.0$, as compared to those of the parabolic system where $w_{p=}\{0, -6.66\}$ for k_{c1} and $w_p = \{0, -4.88\}$ for k_{c2}. The pattern could not reach a well organized Turing pattern until the reaction-diffusion number reached the value of 2. Also the real part of the roots depends on $\bar{N}_{rd}$ in a way that it becomes more negative as $\bar{N}_{rd}$ increases, which means for relatively low $\bar{N}_{rd}$, the pattern reaches a stationary state and selects a mode in longer times than that of the parabolic case. In fact, the pattern selected in the case of the hyperbolic system was similar to that of the parabolic system only in high $\bar{N}_{rd}$, whereas for intermediate $\bar{N}_{rd}$ the similarity persists but the pattern is still different. This may be attributed to the other pairs of eigenfrequencies of the linear dispersion relation. For $\bar{N}_{rd}$ less than 2.0 the pattern was chaotic and slowly varying in time. For $\bar{N}_{rd}$ near 2.0, the pattern shows clear organization into a Turing pattern. The perturbation analysis for the Turing mode leads to amplitude equations which do not depend on $\bar{N}_{rd}$. This will not allow us to study the effect of this parameter on the pattern. It is clear from the simulations that the transition from a chaotic pattern to a well organized Turing pattern was sharp and sudden and not smooth. It seems that there is a need for a perturbation theory for hyperbolic equations. Investigation of the dispersion relation did not uncover the role of $\bar{N}_{rd} = 2$; this means that this effect is beyond the linear regime where the modes interact in a very complicated manner. The amplitude equation for this time independent mode can be derived also in the same manner, but this time

$$\mathcal{L}_0 = -\bar{N}_{rd}(\mathbf{L}_0 - D\nabla_r^2). \tag{5.156}$$

Let $\mathbf{e}_T$ be the normalized right-eigenvector of the linear operator $\mathcal{L}_0$ corresponding to the eigenvalue $i\omega_0$:

$$\mathcal{L}_0\mathbf{e}_T = ik_c\mathbf{e}_T, \tag{5.157}$$

where k_c is given by equation (5.155).

$$\mathbf{Z}_1 = \mathbf{T}(\xi,\tau)\exp(ik_c r)\mathbf{e}_T + \bar{\mathbf{T}}(\xi,\tau)\exp(-ik_c r)\bar{\mathbf{e}}_T. \tag{5.158}$$

Here $\mathbf{T}(\xi, \tau)$ is the amplitude of the oscillatory solution corresponding to the eigenvalue ik_c at the critical point in question. For other values of m the inhomogeneous equations in (5.26) can be solved subject to the solvability condition

$$\int_0^{2\pi/k_c} dr \ \exp(-ik_c r)\mathbf{e}_T^* \cdot \mathbf{G}_m = 0. \tag{5.159}$$

The solution $\mathbf{Z}_1$ in (5.158) suggests that $\mathbf{G}_m$ is also a periodic function of $2\pi/k_c$. Therefore $\mathbf{G}_m$, periodic in $2\pi/k_c$, may be expanded as follows:

$$\mathbf{G}_m = \sum_{l=-\infty}^{\infty} \mathbf{G}_m^{(l)} \exp(ilk_c r). \tag{5.160}$$

Then the solvability condition (5.159) can be written as

$$\mathbf{e}_T^* \cdot \mathbf{G}_m^{(1)} = 0. \tag{5.161}$$

By inspection, $\mathbf{Z}_2$ has only terms of zeroth, first and second harmonics. To calculate explicitly $\mathbf{Z}_2$, we make use of (5.158) for Z_1 and the first harmonic of $\mathbf{Z}_2$ will then be given by

$$\mathbf{Z}_2^{(1)} = W_1 \mathbf{e}_T - \left(-\mathbf{L}_0 + k_c^2 \mathbf{D}\right)^{-1} \mathbf{e}_T D(2ik_c) \boldsymbol{\nabla}_\xi \mathbf{T}(\xi, \tau). \tag{5.162}$$

But we know that

$$(k_c^2 \mathbf{D} - \mathbf{L}_0)\mathbf{e}_T = 0, \tag{5.163}$$

which makes the computation of (5.162) impossible because of the singular behavior (5.163). To overcome this difficulty we expand $\mathbf{e}_T$ in k_c^2

$$\mathbf{e}_T = \mathbf{e}_T(0) + k_c^2 \frac{\partial \mathbf{e}_T}{\partial_{k_c^2}} + \cdots, \tag{5.164}$$

and replace it in (5.163) to get

$$-\mathbf{L}_0\mathbf{e}_T(0) + k_c^2\left(\mathbf{D}\mathbf{e}_T(0) - \mathbf{L}_0\frac{\partial \mathbf{e}_T}{\partial_{k_c^2}}\right) + \cdots = 0. \tag{5.165}$$

Therefore,

$$-\mathbf{L}_0\mathbf{e}_T(0) = 0. \tag{5.166}$$

$$\mathbf{D}\mathbf{e}_T(0) - \mathbf{L}_0\frac{\partial \mathbf{e}_T}{\partial_{k_c^2}} = 0. \tag{5.167}$$

Finally, we take the following limit

$$\lim_{k_c\to 0}(-\mathbf{L}_0 + k_c^2\mathbf{D})^{-1}\mathbf{D}\mathbf{e}_T = -\mathbf{L}_0^{-1}D\mathbf{e}_T(0) = -\mathbf{L}_0^{-1}\mathbf{L}_0\frac{\partial \mathbf{e}_T}{\partial_{k_c^2}} = \frac{\partial \mathbf{e}_T}{\partial_{k_c^2}}, \tag{5.168}$$

from which we get the value of $\mathbf{Z}_2^{(1)}$

$$\mathbf{Z}_2^{(1)} = \mathbf{W}_1\mathbf{e}_T + 2ik_c\nabla_\xi\mathbf{T}(\xi,\tau)\frac{\partial \mathbf{e}_T}{\partial_{k_c^2}}. \tag{5.169}$$

For $m = 2$ the solvability condition is clearly satisfied. The solution $\mathbf{Z}_2$ of (5.26) in the case of $m = 2$ is found in the form

$$\mathbf{Z}_2^{(2)} = \mathbf{R}(\xi,\tau)\exp(2i\omega_0 t)\mathbf{e}_{T2} + \bar{\mathbf{R}}(\xi,\tau)\exp(2i\omega_0 t)\bar{\mathbf{e}}_{T2} \tag{5.170}$$

where

$$\mathbf{R}(\xi,\tau) = [-(2ik_c)^2\mathbf{I} - \bar{N}_{rd}\mathbf{L}_0]^{-1}\bar{N}_{rd}\mathbf{M}_0\mathbf{e}_T\mathbf{e}_T\mathbf{T}^2(\xi,\tau), \tag{5.171}$$

$$\bar{\mathbf{R}}(\xi,\tau) = [-(2ik_c)^2\mathbf{I} - \bar{N}_{rd}\mathbf{L}_0]^{-1}\bar{N}_{rd}\mathbf{M}_0\bar{\mathbf{e}}_T\bar{\mathbf{e}}_T\bar{\mathbf{T}}^2(\xi,\tau), \tag{5.172}$$

$$\mathbf{Z}_2^{(0)} = -2\mathbf{L}_0^{-1}\mathbf{M}_0\mathbf{e}_T\bar{\mathbf{e}}_T\left|\mathbf{T}(\xi,\tau)\right|^2. \tag{5.173}$$

The amplitude equation will now be derived from the third compatibility condition, i.e. $m = 3$, as follows:

$$\begin{aligned} e_T^* \mathbf{G}_3 &= e_T^* (2\bar{N}_{rd}\mathbf{M}_0\mathbf{Z}_1\mathbf{Z}_2 + \bar{N}_{rd}\mathbf{N}_0\mathbf{Z}_1\mathbf{Z}_1\mathbf{Z}_1 + (\bar{N}_{rd}\mathbf{D}\boldsymbol{\nabla}_\xi^2\mathbf{Z}_1 + \\ &\quad 2\bar{N}_{rd}\mathbf{D}\boldsymbol{\nabla}_\xi\cdot\boldsymbol{\nabla}_r\mathbf{Z}_2 + \chi\bar{N}_{rd}\mathbf{L}_1\mathbf{Z}_1 - \bar{N}_{rd}\mathbf{H}_0\partial_t\mathbf{Z}_1) = 0. \end{aligned} \tag{5.174}$$

Upon substituting the expressions for different quantities in this equation we get

$$\partial_\tau \mathbf{T} = q\mathbf{T} + \tilde{D}\boldsymbol{\nabla}_\xi^2\mathbf{T} - p\,|\mathbf{T}|^2\mathbf{T} \tag{5.175}$$

where

$$q = \bar{N}_{rd}Q(\chi\lambda_1), \tag{5.176}$$

$$\lambda_1 = \mathbf{e}_T^*\mathbf{L}_1\mathbf{e}_T, \tag{5.177}$$

$$\begin{aligned} p &= -\bar{N}_{rd}Q[2\mathbf{e}_T^*\mathbf{M}_0(-2\mathbf{e}_T\mathbf{L}_0^{-1}\mathbf{M}_0\mathbf{e}_T\bar{\mathbf{e}}_T + \bar{N}_{rd}\bar{\mathbf{e}}_T\mathbf{K}\mathbf{M}_0\mathbf{e}_T\mathbf{e}_T) \\ &\quad +3\mathbf{e}_T^*\bar{N}_{rd0}\mathbf{e}_T\mathbf{e}_T\bar{\mathbf{e}}_T], \end{aligned} \tag{5.178}$$

$$\tilde{D} = \bar{N}_{rd}Q\mathbf{e}_T^*(4k_c^2)\mathbf{D}\frac{\partial \mathbf{e}_T}{\partial_{k_c^2}}. \tag{5.179}$$

Calculation of the listed coefficients yields the following values when k_c is used in equation (5.155):

$$e_T = \begin{pmatrix} 1 \\ \\ -(\alpha/A)(1+\alpha A) \end{pmatrix} = e_T^{par}, \tag{5.180}$$

$$e_T^* = \frac{1}{1-\alpha^2}\begin{pmatrix} 1 & , & A\alpha/(1+A\alpha) \end{pmatrix} = e_T^{*par}, \tag{5.181}$$

$$q = \bar{N}_{rd}Q(1+A\alpha)/(1-\alpha^2), \tag{5.182}$$

$$\lambda_1 = (1+A\alpha)^2/[A\alpha(1-\alpha^2)+1-\alpha^2], \tag{5.183}$$

$$p = \bar{N}_{rd}Q(-8+38A\alpha+5A^2\alpha^2-8A^3\alpha^3)/9\alpha^3(1-\alpha^2), \tag{5.184}$$

$$\bar{D} = 4\alpha\bar{N}_{rd}Q(D_xD_y)^{1/2}/(1+A\alpha)(1-\alpha^2), \tag{5.185}$$

$$\bar{N}_{rd}Q = \frac{(\alpha^2-1)A^2+2\alpha A-\bar{N}_{rd}}{-\bar{N}_{rd}^2+(\alpha^2A^2+2\alpha A-A^2)\bar{N}_{rd}-A^2}. \tag{5.186}$$

It is interesting to see how the $\bar{N}_{rd}$-dependent quantity Q behaves.

$$Q = 0 \Longleftrightarrow \bar{N}_{rd} = (\alpha^2-1)A^2+2\alpha A, \tag{5.187}$$

$$Q \rightarrow \infty \Longleftrightarrow \bar{N}_{rd} \rightarrow \bar{N}_{rd}^{res} \tag{5.188}$$

$$\bar{N}_{rd}^{res} = \frac{1}{2}A(\alpha^2A+2\alpha-A) \pm [A^2(1-2\alpha^2+\alpha^4) \tag{5.189}$$

$$+4A\alpha(\alpha^2-1)+4\alpha^2-4]^{1/2}. \tag{5.190}$$

The amplitude equation (5.175) derived for Turing instability differs from that derived for Hopf instability in that coefficients are not complex but real. The occurrence of singularities is also observed and a physical explanation is yet to be laid down. In two dimensional systems, the situations gets more complicated. For each symmetry, stripes for example, an amplitude equation can be derived based on the fact that amplitude varies slower in one direction than the other. From basic analysis of such equations, we can define different kinds of instabilities like the "zig-zag instability"[20] and the Eckhaus instability[21]. This is deferred to a future investigation.

Bibliography

[1] A. C. Newell and J. A. Whitehead, J. Fluid Mech. **38**, 279 (1969).

[2] K.. Stewartson and J. T. Stuart, J. Fluid Mech. **48**, 529 (1971).

[3] A. C. Newell, Lectures in Appl. Math. **15**, 157 (1074).

[4] H. Haken, Z. Phys. **176**, 47 (1975).

[5] J. D. Gibbon and M. J. McGuiness, Proc. Roy. Soc. London **A377**, 185 (1981).

[6] J. Lin and P. B. Kahn, J. Math. Biol. **13**, 383 (1982).

[7] Y. Kuramoto, *Chemical Oscillations, Waves, and Turbulence* (Springer, Berlin, 1984).

[8] Y. Kuramoto and T. Tsuzuki, Prog. Theor. Phys. **52**, 1399 (1974).

[9] A. Wunderlin and H. Haken, Z. Phys. **B21**, 393 (1975).

[10] J. C. Neu, SIAM J. Appl. Math. **37**, 307 (1979); **38**, 305 (1980).

[11] A. T. Winfree, J. Theor. Biol. **16**, 15 (1967).

[12] P. Ortoleva and J. Ross, J. Chem. Phys. **58**, 5673 (1973); **60**, 5090 (1974).

[13] Y. Kuramoto and T. Tsuzuki, Prog. Theor. Phys. **55**, 356 (1976); **56**, 724 (1976).

[14] J. C. Neu, SIAM J. Appl. Math. **36**, 307 (1979).

[15] E. A. Coddington and N. Levinson, *Differential Equations* (McGraw-Hill, New York, 1955).

[16] J. M. Burgers, *The Nonlinear Diffusion Equation* (Reidel, Dordrecht, 1974).

[17] L. Cesari, *Asymptotic Behavior and Stability Problems in Ordinary Differential Equations* (Springer, New york, 1971).

[18] J. Guckenheimer, J. Math. Biol. **1**, 259 (1975).

[19] G. Nicolis, *Introduction to Nonlinear Science* (Cambridge, New York, 1995).

[20] P. Manneville, *Dissipative Structures and Weak Turbulence* (Academic, San Diego, 1990).

[21] V. Eckhaus, *Studies in Nonlinear Stability* Theory (Springer-Verlag, Berlin, 1965).

Part II

Shock Waves

Chapter 6

Shock Waves

6.1 Introduction

A shock wave involves the transition from a uniform upstream flow to a uniform downstream flow. The flow is one-dimensional in that there are no flow gradients in directions parallel to the plane of the wave, and a frame of reference is usually chosen such that there is no stream velocity in this plane. The problem of the internal structure of shock wave, which is determined by viscous and heat conduction effects, has played an important role in the development of molecular gas dynamics because of several reasons. First, the flow involves a marked degree of thermal nonequilibrium for large Mach numbers; second, the flow does not involve the uncertainties associated with solid boundaries; and third, the flow has proved accessible to experimental experimentation. Apart from the numerical simulation methods[53, 7, 45, 47, 13] often used in recent years, shock waves have been conventionally studied by means of Navier-Stokes theory [4, 51, 27], but the theory does not quantitatively predict the shock wave structure, especially when the Mach number exceeds a value in the neighborhood of 1.5[47, 13]. To remedy the situation the Boltzmann equation has been used and its Burnett-order solutions have been explored[52, 25] as a way to extend the Navier-Stokes theory, but they have so far not yielded reliable solutions to the problem in the high Mach number regime. Another

kinetic theory-based approach is that of Mott-Smith[42] which has been followed by a number of researchers[43, 49, 10, 33, 39, 3]. The Mott-Smith method yields different results for different closures taken, although they all exhibit a qualitatively correct Mach number dependence for the inverse shock widths. Despite the fact that it accounts for shock structures in reasonable accuracy for wide ranging Mach numbers the Mott-Smith method was deemed to be an *ad hoc* approximation method according to the assessment of Grad[29], and he proposed the moment method as a mathematically more complete theory for shock waves. His moment method has been taken up by a number of researchers[32, 2]. However, it has encountered a difficulty in that the theory predicts that there is no shock solution beyond a critical Mach number which, contrary to experiments, appears at $N_M = 1.65$ according to Grad's own investigation[29], at $N_M = 1.851$ according to Holway [32], and at $N_M = 2.09$ according to Anile and Majorana[2]. Therefore, the continuum theories derived from the Grad moment method encounter difficulties in the regime of Mach number where the Navier-Stokes theory begins to be ineffective, and that is just the regime where an extended theory is needed. All these theories based on the moment method require suitable closures which make it possible to close the open set of Grad's moment equations. Generally, in the aforementioned approaches to study the existence of shock solutions, the first thirteen moments are retained and the moments beyond the first thirteen are expressed in terms of the lower-order moments. Such closures invariably give rise to a set of partial differential equations for stresses and heat fluxes which supplement the Rankine-Hugoniot relations. These sets of equations used so far do not admit shock solutions beyond the values of Mach number mentioned. The precise values for the upper limit of Mach number appear to depend on how the moment equations are structured on the basis of the first 13 moments. But one common feature is that there is an upper limit in Mach number beyond which there is no shock solution. This difficulty of the Grad moment equations derived from the Boltzmann equation is not only a challenge for the shock wave problem *per se*, but also poses some serious conceptual problem for extended irreversible thermodynamics[22, 37, 44] which aims to generalize the classical theory

of linear irreversible thermodynamics based on the local equilibrium hypothesis [12]. The reason is that the former theory is structured on the macroscopic equations at the level of moment equations for nonconserved variables and the foundations of the theory become questionable if the theory so constructed is unable to treat flow problems such as shock waves. Therefore, the shock wave still poses important theoretical challenges to both kinetic theory of gases and irreversible thermodynamics. In this thesis, we study the question from the viewpoint of the generalized hydrodynamics formulated in the nonequilibrium ensemble method[24] and the version of extended irreversible thermodynamics[23] which is given statistical mechanical foundations thereby. (Note that the version of extended irreversible thermodynamics used in this thesis is different from that of Jou et al. [37] and Müller et al.[44]). Since the generalized hydrodynamic equations employed are basically the moment evolution equations, one can wonder if there is any basis to hope that they will provide us with an adequate solution to the problem. The answer is in the affirmative, since the closure relations used for the constitutive equations in this work make a crucial difference from those used by Grad [29] and others[32, 2]. Furthermore, the applications of the steady constitutive equations subjected to the closure relations used here have produced some results which are in quantitative agreement with experimental rheological data[15, 46, 16, 21, 41, 5, 6]. Such agreements have been rather encouraging and we would like to show that similarly encouraging results can be obtained for shock wave problems. In this work, we will only consider a one-dimensional steady shock wave problem.

6.2 Brief Survey of Current Theories

Continuum theories were used to compute the properties and structures of shock waves. The Navier-Stokes equations are applied to study the steady shock wave problems. For such problem, those equations yield a set of coupled nonlinear ordinary differential equations, and can be solved numerically[27], or a closed solution can be obtained for special case of Prandtl number of 0.75[14]. These works shows

that the Navier-Stokes equations are certainly valid for very low Mach number flows, typically less than 1.25, and most unlikely to be valid for Mach numbers greater than two. Experimentally, a good agreement was found between wind tunnel experiments and Navier-Stokes at Mach number equal 1.8[34, 35]. The Burnett profile differs significantly from the Navier-Stokes profile for Mach numbers of the order of 1.8, which can give doubt to the Burnett formulation. The thirteen moment equations cannot be solved for the shock wave structure at Mach numbers above 1.65. Because of the problems with continuum theory, several methods were developed and applied to the strong shock structure by solving the Boltzmann equation

$$\frac{\partial}{\partial t}(nf)+\mathbf{c}\cdot\frac{\partial}{\partial \mathbf{r}}(nf)+\mathbf{F}\cdot\frac{\partial}{\partial \mathbf{c}}(nf) = \int_{-\infty}^{\infty}\int_{0}^{2\pi} d\theta \int_{0}^{\pi} d\phi n^2(f^* f_1^* - f f_1)\sigma \left|\mathbf{c}_2 - \mathbf{c}_1\right| d\Omega d\mathbf{c}_1, \tag{6.1}$$

where f is the distribution function, n is the density, $\mathbf{c}$ is the velocity, $\mathbf{F}$ is an external force applied on the system, σ is the cross section, Ω is the solid angle and the superscript * denotes the postcollision value. In 1951, Mott-Smith[42] proposed a moment method to be applied to the shock wave problem. He suggested that the distribution function within the shock wave can be written as a linear combination of the equilibrium upstream and down stream distribution functions.. This is sometimes called a *bimodal distribution*:

$$nf = N_1 f_1 + N_2 f_2, \tag{6.2}$$

where the subscripts 1 and 2 denote the upstream and downstream states respectively. Let us take the x-axis to be normal to the wave, then the equilibrium Maxwellian equations can be written as

$$f_1 = \frac{\beta_1^3}{\pi^{3/2}} \exp\left[-\beta_1^2\left((u-u_{01})^2 + v^2 + w^2\right)\right], \tag{6.3}$$

$$f_2 = \frac{\beta_2^3}{\pi^{3/2}} \exp\left[-\beta_2^2\left((u-u_{02})^2 + v^2 + w^2\right)\right], \tag{6.4}$$

where $\beta_i = (2RT_i)^{-1/2}$, u, v, w are the velocity component in the x, y and z directions respectively. u_{01} and u_{02} are initial upstream and low stream velocities in the x-direction, respectively. The weighting factors N_1 and N_2 must be such that $N_1 = n_1$, $N_2 = 0$ upstream and $N_1 = 0$, and $N_2 = n_2$ downstream. Equation (6.2) may be integrated over all velocity space to give the following condition

$$n = N_1 + N_2. \tag{6.5}$$

A second condition can be obtained by applying the mass conservation equation between the upstream state and a point within the wave:

$$n_1 u_{01} = n u_0, \tag{6.6}$$

and when evaluating $u_0 = \int_{-\infty}^{\infty} uf \, dudvdw$ for the distribution in equation (6.2) we have

$$n_1 u_{01} = N_1 u_{01} + N_2 u_{02}. \tag{6.7}$$

A third relation can be supplied by an additional moment equation. The choice of the moment is arbitrary. Mott-Smith used both u^2 and u^3. If $\mathcal{M}$ denotes the moment, then from the Boltzmann equation (6.1), we can deduce its evolution. So for steady one-dimensional flow

$$\frac{d}{dx}\langle nu\mathcal{M}\rangle = \int_{-\infty}^{\infty}\int_{0}^{4\pi} n^2\mathcal{M}(f^*f_1^* - ff_1)\sigma\,|\mathbf{c}_2 - \mathbf{c}_1|\,d\Omega d\mathbf{c}_1\ , \tag{6.8}$$

where the angular brackets denote the $f-$weighted velocity average. Therefore, for $\mathcal{M} = u^2$ we have

$$\frac{d}{dx}\langle nu^3\rangle = \int_{-\infty}^{\infty}\int_{0}^{4\pi} n^2u^2(f^*f_1^* - ff_1)\sigma\,|\mathbf{c}_2 - \mathbf{c}_1|\,d\Omega d\mathbf{c}_1. \tag{6.9}$$

For Maxwell molecules, (6.9) can be evaluated[7] to give

$$\frac{d}{dx}\langle nu^3\rangle = \frac{8}{15\pi^{1/2}}\frac{(2RT_1)^{1/2}}{n_1\lambda_1}\frac{n}{m}\Pi_{xx}. \tag{6.10}$$

Now, we make use of (6.2) to evaluate $\langle nu^3\rangle$

$$\langle nu^3\rangle = N_1\int_{-\infty}^{\infty} u^3 f_1 d\mathbf{c} + N_2\int_{-\infty}^{\infty} u^3 f_2 d\mathbf{c} \tag{6.11}$$

$$= N_1 u_{01}(u_{01}^2 + 3RT_1 - u_{02}^2 - 3RT_2) + n_1 u_{01}(u_{02}^2 + 3RT_2). \tag{6.12}$$

Conservation of energy between the upstream and downstream states requires

$$u_{01}^2 + 5RT_1 = u_{02}^2 + 5RT_2, \tag{6.13}$$

so that

$$\frac{d}{dx}\langle nu^3\rangle = \frac{2}{5}u_{01}(u_{02}^2 - u_{01}^2)\frac{d}{dx}N_1. \tag{6.14}$$

The stress Π_{xx} can be evaluated from its statistical definition in a way similar to $\langle nu^3\rangle$ to give

$$\frac{n}{m}\Pi_{xx} = \frac{2}{3}n(nu_0^2 - N_1u_{01}^2 - N_2u_{02}^2) \tag{6.15}$$

$$= -\frac{2}{3}N_1(n_1 - N_1)\frac{u_{01}}{u_{02}}(u_{01} - u_{02})^2, \tag{6.16}$$

where we used equations (6.5), (6.6), and (6.7) to go from equation (6.15) to (6.16). Finally, substitution of equations (6.16) and (6.14) into (6.10) yields the following differential equation for N_1/n_1 as a function of x/λ_1

$$\frac{d}{d(x/\lambda_1)}\left(\frac{N_1}{n_1}\right) = -\alpha\frac{N_1}{n_1}\left(1 - \frac{N_1}{n_1}\right), \tag{6.17}$$

where

$$\alpha = \frac{8}{3\pi^{1/2}} \frac{(2RT_1)^{1/2}}{u_{02}} \frac{u_{01} - u_{02}}{u_{01} + u_{02}}. \tag{6.18}$$

The solution for (6.17) is

$$N_1 = n_1 \left[1 + \exp\left(\alpha(x/\lambda_1)\right)\right]^{-1}. \tag{6.19}$$

The solution for the density profile follows directly from equation (6.19)

$$\frac{n - n_2}{n_1 - n_2} = \frac{N_1}{n_1} = \frac{1}{1 + \exp\left(\alpha(x/\lambda_1)\right)}. \tag{6.20}$$

The method has also been extended to other inverse power law molecular models[43]. The Mott-Smith has been found to be inadequate to describe the thickness of shock waves at low Mach numbers but remarkably good at high Mach numbers. Also, the symmetry of the Mott-Smith solution conflicts with the experimental findings of the asymmetry of shock waves.

The goal of dilute gas kinetic theory is to solve the Boltzmann equation subject to appropriate initial and boundary conditions. Some of the direct methods of solution have been attempted[11, 54], but they usually involve some kind of approximation or linearization of the nonlinear collision integral term in the equation. The linearization procedure is valid only in the limit of a small deviation from equilibrium. However, many processes of practical interest occur far from equilibrium and therefore necessitate the inclusion of the nonlinear collision term. Another difficulty associated with the solution to the Boltzmann equation resides in the choice of suitable initial and boundary conditions on the density distribution function. The Boltzmann equation requires only one initial condition or a condition at any given time for that matter. As far as the boundary condition is concerned, the density distribution function must be prescribed on the boundary of interest in phase space since it is dependent on both the velocity and the position. In the velocity space the bounding region is usually taken to lie at infinity and the distribution function is assumed to vanish, or more generally, to be bounded there. The remaining task

is then to prescribe the value of the distribution function on the bounding region in real space. In the case of a dense fluid, the fluid molecules are assumed to be in equilibrium with the bounding walls so that a Maxwellian density distribution with the wall velocity and temperature is readily assigned to the molecules in the immediate vicinity of the wall. It is in the case of a dilute gas that difficulties are bound to arise since the gas molecules at the boundary are not assumed to be in equilibrium with the wall.

Another standard procedure for solving the Boltzmann equation is the Chapman-Enskog expansion method. The density distribution function f is expressed in the form of an infinite series in terms of an ordering parameter ε as follows

$$f = f^{(0)} + \varepsilon f^{(1)} + \varepsilon^2 f^{(2)} + \ldots \tag{6.21}$$

Physically, the parameter ε may be related to the Knudsen number. The substitution of this series in the Boltzmann equation gives rise to a hierarchy of linear integral equations governing each function in the expansion. The first approximation $f^{(0)}$ turns out to be a Maxwellian distribution function. The normalization parameters in $f^{(0)}$, namely, n, T and c_0, in the notation of reference[11], are identified with the number density, the temperature and mass velocity, respectively. This results in a condition on the rest of the terms in the expansion, i.e., $f^{(i)}$, which ensures the uniqueness of the solution to the nonhomogeneous integral equations governing these terms. Therefore, only the pressure tensor and the heat flux are expanded in the form of equation (6.21). To first approximation the equations of change are those governing an inviscid non-heat-conducting fluid. To second order in approximation the integral equation governing $f^{(1)}$ is solved and leads to Newton's law of viscosity and Fourier's law of heat. The expressions for the coefficients of viscosity and thermal conductivity are determined in terms of bracket integrals, which in turn are expanded in truncated series of orthogonal Sonine polynomials. The resulting terms in the latter expansions are complicated integrals involving the dynamics of bimolecular collisions which in principle are evaluated, once the inter-

action potential is specified. To third order in the expansion, one obtains the Burnett equations which contain higher derivatives of the thermodynamic variables and powers of lower derivatives. The important issue here is that the Chapman-Enskog expansion may not conform to the second law of thermodynamics beyond the second order expansion[12]. To second order approximation of Chapman-Enskog, the statistical expressions for the *calortropy density*, the *calortropy flux* and the *calortropy production* are identical with the expressions derived on the basis of macroscopic formulation or phenomenological theory. However, as the method is pushed further to the third order and higher, the calortropy production is no longer guaranteed to be positive semidefinite and the second law of thermodynamics is not satisfied in general. However, it might be possible that this method, when continued to an infinite number of moments, leads to a set of macroscopic equations consistent with the second law of thermodynamics.

Grad's thirteen moments method[12] is another well known method of solving the Boltzmann equation. The density distribution function is expanded in terms of Hermite polynomials in the molecular velocity

$$f(\mathbf{C};t) = f_0\left(1 + A_p : [\mathbf{CC}]^{(2)} + A_q \cdot \frac{1}{2}mC^2\mathbf{C}\right), \tag{6.22}$$

where f_0 is the local equilibrium distribution function and the coefficients A_p and A_q are proportional to $\mathbf{\Pi}$ and $\mathbf{Q}$, respectively. It must be noted that the moments higher than $\mathbf{\Pi}$ and $\mathbf{Q}$ are set equal to zero. Therefore, we find

$$\psi_2 = \varphi_q(T,n)\mathbf{Q}, \tag{6.23}$$

$$\psi_3 = \varphi_0(T,n)\boldsymbol{\delta} + \varphi_p(T,n)\mathbf{\Pi}, \tag{6.24}$$

where $\varphi_0, \varphi_q, \varphi_p$ are functions of T and n which can be explicitly evaluated. A hierarchy of evolution equations is obtained governing the coefficients in the expansion. The coefficients are expressed in terms of the macroscopic observables or moments

and their corresponding equations are obtained on the basis of the Boltzmann equation. Under the assumption that the gas is sufficiently close to equilibrium, the expansion of the distribution function is truncated to include up to third-rank tensor terms. The resulting coefficients are then identified with the variables defining the flow field, namely, density, velocity, temperature, pressure tensor, and heat flux. Unlike Newton's law of viscosity and Fourier's heat law, or the Burnett equations, Grad's constitutive equations are first order partial differential equations in time[?]. These equations are essentially linear at least in the thermodynamic forces and fluxes and so do not apply to flow processes under high nonequilibrium conditions. One of these conditions of interest in the present thesis is that of a supersonic gas flow where a shock wave develops. For the shock wave problem Grad[29] proceeded as follows. The conservation equations are given by the known Rankine-Hugoniot equations for a shock wave:

$$\frac{d}{dx}\rho u = 0, \tag{6.25}$$

$$\frac{d}{dx}\left(\rho u^2 + p + \Pi_{xx}\right) = 0, \tag{6.26}$$

$$\frac{d}{dx}\left[\rho u\left(\mathcal{E}+\frac{1}{2}u^2\right) + u\left(p+\Pi_{xx}\right) + Q_x\right] = 0. \tag{6.27}$$

The conservation equations are supplemented by the following by the following two relations derived by using the thirteen moment approximation[28]

$$\frac{d}{dx}(u\Pi_{xx}) + \frac{8}{15}\frac{d}{dx}Q_x + \frac{4}{3}(p+\Pi_{xx})\frac{d}{dx}u + \beta\rho\Pi_{xx} = 0, \tag{6.28}$$

$$\frac{d}{dx}(2uQ_x) + \frac{22}{5}Q_x\frac{d}{dx}u + 2RT\frac{d}{dx}\Pi_{xx} + 7R\Pi_{xx}\frac{d}{dx}T - \tag{6.29}$$

$$\frac{2\Pi_{xx}}{\rho}\frac{d}{dx}(p+\Pi_{xx}) + 5Rp\frac{d}{dx}T + \frac{4}{3}\beta\rho Q_x = 0. \tag{6.30}$$

where ρ is the mass density, u is the fluid velocity, p is the pressure, Π_{xx} is the

xx−component of the shear stress, $\mathcal{E}$ is the internal energy density, and Q_x is the x−component of the heat flux. β is a function of temperature determined by the molecular model used. From the aforementioned equations, Grad[29] was able to study the direction field generated by the functions u and T. He found that the singular points of the obtained direction field are different from those obtained by using the Navier-Stokes equations. From the linearized solution around the singular point, the conclusion of nonexistence of a shock path was deduced for Mach numbers above 1.65, where the singular points change their behavior. For Mach numbers below the critical value, Grad developed a clever perturbation scheme to calculate the shock profile. He also established that in all the cases he studied the shock thickness is bounded, though his definition of thickness is different from the maximum slope definition adopted in this thesis and almost by everyone else. Other people adopted higher order moment closures but they could not remove the critical Mach number above which the shock solution does not exist; they simply shifted this number up or down by few decimal places.

In 1980 Eu formulated the modified moment method as an appropriate procedure for the solution of the Boltzmann equation[55]. The formulation was first restricted to the case of dilute gases and later generalized to the case of liquids. Recently, Eu developed the nonequilibrium ensemble method[56] which parallels the equilibrium ensemble method of Gibbs. In his formalism, Eu used an irreversible kinetic equation, e.g., the Boltzmann equation, and an extended Gibbs relation for calortropy as a nonequilibrium generalization of *Clausius entropy*. The availability of an extended Gibbs relation for calortropy permits us to identify various parameter appearing in the nonequilibrium canonical distribution function and thus bridge the phase space to the phenomenological space of thermodynamics. It must be admitted that a thermodynamic theory cannot be built with the Boltzmann entropy since its differential is not exact in the extended Gibbs space[23]. However, the relative Boltzmann entropy can account for the difference between calortropy and Boltzmann entropy and it can be expressed in terms of fluctuations in temperature, chemical potentials, and generalized potentials. A set of deterministic evolution equations for the fluctuations

can be derived from kinetic equations. On the other hand, if a stochastic treatment of those fluctuations is taken, a new concept of thermodynamic quantization can arise. Using this method, one is able to derive a set of generalized hydrodynamics which are tested in different contexts and proved very successful.

6.3 Governing Generalized Hydrodynamic Equations

We assume that flow is in the direction of the x coordinate. Since we are interested in a steady shock wave, the governing balance equations for mass, momentum, and energy are time-independent. They are in the form

$$\frac{d}{dx}\rho u = 0, \tag{6.31}$$

$$\frac{d}{dx}\left(\rho u^2 + p + \Pi_{xx}\right) = 0, \tag{6.32}$$

$$\frac{d}{dx}\left[\rho u\left(\mathcal{E}+\frac{1}{2}u^2\right) + u\left(p+\Pi_{xx}\right) + Q_x\right] = 0, \tag{6.33}$$

where ρ is the mass density, u is the fluid velocity, p is the pressure, Π_{xx} is the $xx-$component of the shear stress, $\mathcal{E}$ is the internal energy density, and Q_x is the $x-$component of the heat flux. We note that in one-dimensional flow geometry for the present problem

$$[\nabla \mathbf{u}]_{xx} = \frac{2}{3}\partial_x u. \tag{6.34}$$

These balance equations are supplemented by the evolution equations for Π_{xx} and Q_x within the framework of the first thirteen moments. The evolution equation for the stress tensor and heat flux[22] are

$$\rho\frac{d\hat{\Pi}}{dt} = -\nabla\cdot\psi_2 - 2p\left[\nabla\mathbf{u}\right]^{(2)} - 2\left[\Pi\cdot\nabla\mathbf{u}\right]^{(2)} - \frac{p}{\eta_0}\Pi q(\kappa), \tag{6.35}$$

$$\rho\frac{d\hat{\mathbf{Q}}}{dt} = -\nabla\cdot\boldsymbol{\psi}_3 - p\hat{C}_pT\nabla\ln T - \boldsymbol{\Pi}\cdot\nabla\hat{h} + \nabla(p\boldsymbol{\delta}+\boldsymbol{\Pi})\cdot\hat{\boldsymbol{\Pi}} - \mathbf{Q}\cdot\nabla\mathbf{u} - \frac{p\hat{C}_pT}{\lambda_0}\mathbf{Q}q(\kappa), \tag{6.36}$$

where $\boldsymbol{\delta}$ is the unit second-rank tensor, $d/dt = \partial/\partial t + \mathbf{u}\cdot\nabla$ is the substantial time derivative, and $\boldsymbol{\psi}_2$ and $\boldsymbol{\psi}_3$ are higher-order moments which are defined, in the case of a dilute monatomic gas, by the statistical formulas

$$\begin{aligned}\boldsymbol{\psi}_2 &= \left\langle m\mathbf{C}\,[\mathbf{CC}]^{(2)}\,f(\mathbf{C};t)\right\rangle,\\ \boldsymbol{\psi}_3 &= \left\langle \frac{1}{2}mC^2\mathbf{C}\mathbf{C}f(\mathbf{C};t)\right\rangle\end{aligned} \tag{6.37}$$

with $\mathbf{C}$ denoting the peculiar velocity and $f(\mathbf{C};t)$ the nonequilibrium distribution function obeying a kinetic equation, say, the Boltzmann equation. The symbol $[\nabla\mathbf{u}]^{(2)}$ stands for the traceless symmetric part of $\nabla\mathbf{u}$. Other symbols are as follows: $\boldsymbol{\Pi}$ denotes the traceless symmetric part of pressure tensor $\mathbf{P}$, $\hat{\Pi} = \Pi/\rho$; $\mathbf{Q}$ is the heat flux, $\hat{\mathbf{Q}} = \mathbf{Q}/\rho$; $\hat{C}_p$ is the specific heat per mass at constant pressure; $\hat{h} = \hat{C}_pT$ is the enthalpy per mass; η_0 and λ_0 are the Chapman-Enskog viscosity and thermal conductivity Chapman et al.[11], respectively; and $q(\kappa)$ is a nonlinear factor defined by

$$q(\kappa) = \frac{\sinh\kappa}{\kappa}, \tag{6.38}$$

where

$$\kappa = \frac{(mk_BT)^{1/4}}{\sqrt{2}pd}\left(\frac{1}{2\eta_0}\boldsymbol{\Pi}:\boldsymbol{\Pi} + \frac{1}{\lambda_0}\mathbf{Q}\cdot\mathbf{Q}\right)^{1/2}. \tag{6.39}$$

Here d denotes the diameter of the molecule and m is the molecular mass. In Eq. (6.36), we have omitted a term related to a third-rank tensor, namely, $\langle m\mathbf{CCC}f(\mathbf{C};t)\rangle : \nabla\mathbf{u}$ in accordance with the spirit of the thirteen moment method. Furthermore, this term even if taken into account would not change the basic conclusion of this work; it will merely add to the second term from the last in Eq. (6.36) if it is expressed

in terms of lower-order moments. The higher-order moments ψ_2 and ψ_3 obey their own evolution equations. Therefore, the evolution equations (6.35) and (6.36) are the leading members of an open set of moment equations. It is usually closed by expressing ψ_2 and ψ_3 in the lower-order moments, namely, $\mathbf{\Pi}$ and $\mathbf{Q}$ as well as the conserved moments ρ, $\mathbf{u}$, and $\mathcal{E}$. Within the first thirteen moment approximation ψ_2 is proportional to $\mathbf{Q}$ whereas ψ_3 is given in terms of $\mathbf{\Pi}$. Such closure relations give rise to partial differential equations for $\mathbf{\Pi}$ and $\mathbf{Q}$, which form the governing equations for shock wave problems in the approaches[32, 2] based on the moment equations following Grad[29]. We have earlier mentioned that such approaches do not yield shock solutions for the Mach number beyond a critical value. We propose a different set of closures.

We take the following closure relations for ψ_2 and ψ_3 appearing in the moment evolution equations for $\mathbf{\Pi}$ and $\mathbf{Q}$:

$$\psi_2 = \psi_3 = 0. \tag{6.40}$$

This set of closure relations are different from those taken in Grad's theory of solution for the Boltzmann equation and various existing variants of it, but there is no *a priori* reason to disfavor the present closure relations over those which expand ψ_2 and ψ_3 in $\mathbf{Q}$ and $\mathbf{\Pi}$ as well as density and temperature. With these closure relations the constitutive equations are given by

$$\frac{\partial \mathbf{\Pi}}{\partial t} = -2p\,[\nabla \mathbf{u}]^{(2)} - 2\,[\mathbf{\Pi}\cdot\nabla\mathbf{u}]^{(2)} - \frac{p}{\eta_0}\mathbf{\Pi} q(\kappa), \tag{6.41}$$

$$\frac{\partial \mathbf{Q}}{\partial t} = -p\hat{C}_p T \nabla \ln T - \mathbf{\Pi}\cdot\nabla\hat{h} + \nabla(p\boldsymbol{\delta}+\mathbf{\Pi})\cdot\hat{\mathbf{\Pi}} - \mathbf{Q}\cdot\nabla\mathbf{u} - \frac{p\hat{C}_p T}{\lambda_0}\mathbf{Q} q(\kappa). \tag{6.42}$$

It has been shown in a number of studies[15, 46, 16, 21, 41, 5, 6] on nonlinear transport coefficients that the constitutive equations (6.41) and (6.42) give rise to sufficiently accurate nonlinear transport coefficients and particularly non-Newtonian

viscosities in comparison with experiments. On the strength of this finding, we take the closure relations in Eq. (6.40) and show their effectiveness for the shock wave problem. We are thereby able to formulate a continuum hydrodynamic theory of shock waves which provides shock solutions beyond the critical Mach numbers mentioned earlier in connection with the moment method approaches. Based on the examination of the direction field for the governing equations in the present theory, it will become evident that shock solutions should exist for all Mach numbers.

In the case of flow geometry for the present problem, the steady-state constitutive equations for Π_{xx} and Q_x under the closure relations mentioned are obtained from Eq. (6.35) and Eq. (6.36) as follows:

$$\frac{p}{\eta_0}\Pi_{xx}q(\kappa) + \frac{4}{3}\Pi_{xx}\partial_x u + \frac{4}{3}p\partial_x u = 0, \tag{6.43}$$

$$\frac{\hat{h}p}{\lambda_0}Q_x q(\kappa) + Q_x\partial_x u + \Pi_{xx}u\partial_x u + \hat{h}(p+\Pi_{xx})\partial_x \ln T = 0. \tag{6.44}$$

Eqs. (6.43) and (6.44) are partial differential equations for velocity component u and temperature T. We emphasize that there do not appear partial derivatives of Π_{xx} and Q_x in these equations owing to the closure relations taken.

Integration of the balance equations (6.31) - (6.33) yields

$$\rho u = M, \tag{6.45}$$

$$\rho u^2 + p + \Pi_{xx} = P, \tag{6.46}$$

$$\rho u\left(\mathcal{E}+\frac{1}{2}u^2\right) + u\,(p+\Pi_{xx}) + Q_x = Q, \tag{6.47}$$

where M, P, and Q are integration constants with the dimension of momentum per volume, momentum flux per volume, and energy flow per volume, respectively. These equations are also supplemented by the equation of state and the caloric

equation of state

$$\begin{aligned} p &= \rho \mathcal{R} T, \\ \mathcal{E} &= \frac{3}{2} \mathcal{R} T, \end{aligned} \tag{6.48}$$

where $\mathcal{R}$ is the gas constant per mass. Let us define dimensionless variables

$$\begin{aligned} v = MuP^{-1}, \quad & \theta = M^2 \mathcal{R} T P^{-2}, \\ \sigma = \Pi_{xx} P^{-1}, \quad & \phi = pP^{-1}, \\ r = P\rho M^{-2}, \quad & \varphi = Q_x Q^{-1}, \\ \xi = xl^{-1}, \quad & \alpha = MQP^{-2}. \end{aligned} \tag{6.49}$$

The length scale is provided by the mean free path l defined with the upstream momentum per volume, $M = \rho_1 u_1$, where the subscript 1 refers to the upstream. The downstream will be designated by subscript 2. The upstream mean free path is defined by

$$l = \frac{\eta_{01}}{M}, \tag{6.50}$$

where η_{01} is the upstream Newtonian viscosity at the upstream temperature T_1. The transport coefficients η_0 and λ_0 are reduced with respect to the upstream transport coefficients η_{01} and λ_{01}, respectively:

$$\eta^* = \frac{\eta_0}{\eta_{01}}, \quad \lambda^* = \frac{\lambda_0}{\lambda_{01}}. \tag{6.51}$$

With this reduced variables we cast Eqs. (6.45) - (6.48) in the forms

$$\phi = r\theta,$$

$$
\begin{aligned}
rv &= 1, \\
rv^2 + \phi + \sigma &= 1, \\
rv^3 + 5\phi v + 2\sigma v + 2\alpha\varphi &= \alpha.
\end{aligned}
\tag{6.52}
$$

From these equations and on reducing constitutive equations (6.43) and (6.44) we obtain the following five equations

$$\phi v = \theta, \tag{6.53}$$

$$v + \phi + \sigma = 1, \tag{6.54}$$

$$v^2 + 5\theta + 2\sigma v + 2\alpha\varphi = \alpha, \tag{6.55}$$

$$\frac{1}{\eta^*}\phi\sigma q(\kappa) + \frac{4}{3}\sigma\partial_\xi v + \frac{4}{3}\phi\partial_\xi v = 0, \tag{6.56}$$

$$\frac{\alpha\beta}{\lambda^*}\theta\varphi q(\kappa) + (\alpha\varphi + v\sigma)\,\partial_\xi v + \frac{5}{2}\theta\,(\phi + \sigma)\,\partial_\xi \ln\theta = 0. \tag{6.57}$$

Here the new dimensionless parameter β is defined by

$$\beta = \frac{5}{3\theta_1} N_{\mathrm{Pr}} \tag{6.58}$$

with θ_1 denoting the reduced upstream temperature and the Prandtl number defined with the upstream quantities: $N_{\mathrm{Pr}} = \hat{C}_p T_1 \eta_{01}/\lambda_{01}$. Since the reduction scheme used here is slightly different from that in the literature[29, 27], it is useful to explain it, especially, with regard to the appearance of the dimensionless number β in Eq. (6.57). On multiplication of the mean free path l, the first term in Eq. (6.44), apart

from the nonlinear factor $q(\kappa)$, can be reduced as follows:

$$l\frac{\hat{h}p}{\lambda_0}Q_x = \frac{5\tau\phi\varphi}{2\lambda^*}\cdot\frac{lP^3Q}{\lambda_{01}M^2},$$

where the second factor on the right can be written as

$$\frac{lP^3Q}{\lambda_{01}M^2} = \frac{\eta_{01}}{\lambda_{01}}\cdot\frac{P^3Q}{M^3} = \frac{2N_{\mathrm{Pr}}}{5\theta_1}\cdot\alpha\cdot\frac{P^2}{M^2}.$$

The second equality in the equation above follows on making use of the definition of Prandtl number and the reduced temperature. Finally, we obtain

$$l\frac{\hat{h}p}{\lambda_0}Q_x = \frac{\alpha\beta\tau\phi\varphi}{\lambda^*}\cdot\frac{P^2}{M^2}$$

and Eq. (6.57) follows on dividing the equation with P^2M^{-2} and use of the definition of β in Eq. (6.58). The argument κ in the nonlinear factor $q(\kappa)$ is given by the formula

$$\kappa = 4\,(2\gamma_0)^{-1/4}\,(5cN_M)^{-1/2}\left(\frac{\theta}{\theta_1}\right)^{1/4}\frac{1}{\phi\sqrt{\eta^*}}\left(\sigma^2+\frac{8}{15f\theta}\alpha^2\varphi^2\right)^{1/2}. \tag{6.59}$$

where

$$c = \frac{l}{l_h}, \qquad f = \frac{4m\lambda_{01}}{15k_BT_1\eta_{01}} \tag{6.60}$$

with l_h denoting the mean free path for hard spheres in terms of the hard sphere viscosity $l_h = \eta_{01}(hard\ sphere)/M$. In the case of a Maxwell gas, $f = 1$ and

$$c = \frac{16}{15\sqrt{2\pi}A_2(5)}\sqrt{\frac{\theta_1}{E_d}},$$

where $A_2(5) = 0.436$ and

$$E_d = \frac{V_m}{4md^4}\cdot\frac{M^2}{P^2},$$

which is the reduced Maxwell potential energy of potential strength V_m for two hard spheres of radius $d/2$ at contact. This reduced potential energy is set equal to unity

by suitably choosing the reduction parameters M and P. Therefore, for a Maxwell molecules with E_d so taken we obtain

$$\kappa = \left(\frac{3\pi}{5}\right)^{1/4} \left(\frac{3A_2(5)}{N_M}\right)^{1/2} \frac{1}{\phi\theta^{1/4}} \left(\sigma^2 + \frac{8}{15\theta}\alpha^2\varphi^2\right)^{1/2}. \tag{6.61}$$

We note that the parameter α is related to the upstream Mach number as follows:

$$N_M = \sqrt{\frac{1+\frac{1}{5}\mu}{1-\frac{1}{3}\mu}}. \tag{6.62}$$

where

$$\mu = \sqrt{25 - 16\alpha}. \tag{6.63}$$

The parameter μ ranges from 0 to 3 which yields $N_M = \infty$. Note that the upstream Mach number can be equivalently defined by

$$N_M = \frac{v_1}{\sqrt{\gamma_0\theta_1}},$$

where γ_0 is the polytropic ratio: $\gamma_0 = C_p/C_v$.

To determine the boundary conditions on v, ϕ, and θ, we observe that $\sigma \to 0$ and $\varphi \to 0$ as $\xi \to \pm\infty$. Eqs. (6.56) and (6.57) are identically satisfied in the limits if v and θ become independent of ξ at the boundaries. Therefore, as $\xi \to \pm\infty$

$$\sigma, \phi \to 0, \tag{6.64}$$

$$\theta = \phi v, \tag{6.65}$$

$$v + \phi = 1, \tag{6.66}$$

$$v^2 + 5\theta = \alpha. \tag{6.67}$$

The solutions of Eqs. (6.65) - (6.67) are

$$v = \frac{1}{8}(5 \pm \mu), \tag{6.68}$$

$$\phi = \frac{1}{8}(3 \mp \mu), \tag{6.69}$$

$$\theta = \frac{1}{64}(15 \mp 2\mu - \mu^2). \tag{6.70}$$

The upper sign is for the upstream and the lower sign is for the downstream. These solutions provide the boundary conditions at the upstream and downstream. They also imply that the reduced density is given by

$$r = \frac{8}{5 \pm \mu}. \tag{6.71}$$

With the help of Eqs. (6.53) - (6.55) the differential equations (6.56) and (6.57) may be cast into the following forms

$$\frac{dv}{d\xi} = \frac{3\theta(v^2 - v + \theta)}{4\eta^* v^2(1-v)} q(\kappa), \tag{6.72}$$

$$\frac{d\theta}{d\xi} = -\frac{\theta}{5v^2(1-v)^2}\left[\frac{\beta\theta v(1-v)(\alpha + v^2 - 2v - 3\theta)}{\lambda^*} + \frac{3(v^2 - v + \theta)(\alpha - v^2 - 5\theta)}{4\eta^*}\right] q(\kappa). \tag{6.73}$$

These governing equations for shock profiles are solved subject to the boundary conditions in Eqs. (6.68) - (6.70). These equations generalize the governing equations in the Navier-Stokes theory as will be discussed presently.

6.4 Shock Solutions of the Governing Equations

The second term on the right-hand side of Eq. (6.73) stems from the thermoviscous effect involving the second and third terms as well as the term $\hat{h}\Pi_{xx}\partial_x \ln T$ in Eq. (6.44). These, together with the second term in Eq. (6.43), are the terms that do not appear in the Navier-Stokes-Fourier theory. To indicate the difference between the governing equations in the classical Navier-Stokes-Fourier theory and the present theory and to facilitate the solution procedure for Eqs. (6.72) and (6.73), we present the governing equations for a one-dimensional shock wave in the former theory

$$\frac{dv}{d\xi} = \frac{3\left(v^2 - v + \theta\right)}{4\eta^* v}, \tag{6.74}$$

$$\frac{d\theta}{d\xi} = -\frac{\theta\beta\left(\alpha + v^2 - 2v - 3\theta\right)}{5\lambda^*}. \tag{6.75}$$

These equations follow from Eqs. (6.72) and (6.73), if $1 - v$ is replaced by ϕ, Eq. (6.65) is made use of, and the second term on the right-hand side of Eq. (6.73) is omitted since it arises from the thermoviscous coupling term that must vanish in the linear order. Clearly, Eqs. (6.74) and (6.75) are special cases of Eqs. (6.72) and (6.73).

We note that in the case of a hard sphere gas the reduced transport coefficients η^* and λ^* depend on θ only:

$$\eta^* = \left(\frac{\theta}{\theta_1}\right)^{1/2}, \quad \lambda^* = \left(\frac{\theta}{\theta_1}\right)^{3/2}. \tag{6.76}$$

To facilitate comparison of the present governing equations with the governing equations in the literature, we note the relation between the reduced distance ξ in the present work with the reduced distance z in the literature:

$$\xi = \frac{x}{l} = z\sqrt{\frac{5\pi}{6}}N_M. \tag{6.77}$$

This relation stems from the difference in the definitions of mean free path in the

present work and the literature which has been used to reduce the governing equations. The reduced distance z is defined as $z = x/l_n$ where the mean free path l_n is given by $l_n = (\eta_{01}/\rho_1)\sqrt{\pi/2\mathcal{R}T_1}$. The governing equations (6.72) and (6.73) are quite different from the evolution equations for σ and φ appearing in the moment equation approach of Grad[29]. The governing equations in the latter approach, which are differential equations for the stress tensor and heat flux, were found to fail to produce shock solutions for $N_M \geq 1.65$. The differential equations for σ and φ arise in the Grad theory, primarily because of the particular closure relations for ψ_2 and ψ_3 taken, which inevitably give rise to spatial derivatives of ψ_2 and ψ_3. In the following we examine the governing equations (6.72) and (6.73) and the existence of shock solutions with the help of singularities of the direction field equation.

Here we will examine the governing equations in the case of the transport coefficients satisfying Eq. (6.76). For the Navier-Stokes theory the direction field equation is given by

$$\frac{dv}{d\theta} = \frac{\omega\,(v^2 - v + \theta)}{v\,(3\theta + 2v - v^2 - \alpha)}, \tag{6.78}$$

where

$$\omega = \frac{15\lambda^*}{4\beta\eta^*\theta}. \tag{6.79}$$

It is independent of θ for the transport coefficients obeying Eq. (6.76). The singularities of the direction field are given by

$$\begin{aligned} v^2 - v + \theta &= 0, \\ v^2 - 2v - 3\theta + \alpha &= 0, \\ v &= 0. \end{aligned} \tag{6.80}$$

There are three singular points:

$$P_0: \quad v = \tfrac{1}{8}(5+\mu), \quad \theta = \tfrac{1}{64}(15 - 2\mu - \mu^2)$$

$$P_1: \quad v = \tfrac{1}{8}(5-\mu), \quad \theta = \tfrac{1}{64}(15 + 2\mu - \mu^2)$$

$$P_2: \quad v = 0. \qquad \theta = 0.$$

Note that P_0 and P_1 coincide with the boundary values given in Eqs. (6.68) and (6.70). We remark that P_0 and P_1 are also the singular points of the governing equations (6.74) and (6.75) for the Navier-Stokes theory where the derivatives $dv/d\xi$ and $d\theta/d\xi$ vanish. It can be shown, by calculating the eigenvalues of the linearized governing equations, that P_0 is a saddle point whereas P_1 is a node and P_2 is a spiral. The shock solution is a curve connecting P_0 and P_1 as $\xi \to \infty$ from $\xi = -\infty$. It is possible to show that there exists a unique such solution for every value of α[29, 27] since the aforementioned nature of P_0 and P_1 remains invariant for all Mach numbers. Therefore, the Navier-Stokes theory admits shock solutions for all values of Mach number.

We now examine the governing equations (6.72) and (6.73) by using the direction field equation:

$$\frac{dv}{d\theta} = \frac{-\omega(1-v)(v^2 - v + \theta)}{\left[v(1-v)(v^2 - 2v - 3\theta + \alpha) + \frac{3}{4\beta}(v^2 - v + \theta)(\alpha - v^2 - 5\theta)\right]}. \tag{6.81}$$

It is interesting to see that the nonlinear factor $q(\kappa)$ does not appear in this equation and thus the singularities of the direction field is not affected by the nonlinear factor. The singularities of the direction field are given by the equations

$$1 - v = 0, \tag{6.82}$$

$$v^2 - v + \theta = 0, \tag{6.83}$$

$$v(1-v)\left(v^2-2v-3\theta+\alpha\right)+\frac{3}{4\beta}\left(v^2-v+\theta\right)\left(\alpha-v^2-5\theta\right)=0. \quad (6.84)$$

The first two equations are for the loci of zero slopes whereas the last equation is for the loci of infinite slopes. Eq. (6.84) factorizes to the form

$$\frac{15}{4\beta}\left(\theta-B+\sqrt{B^2+A}\right)\left(\theta-B-\sqrt{B^2+A}\right)=0 \quad (6.85)$$

where

$$A = \frac{4\beta}{15}v(v-1)\left[\left(1-\frac{3}{4\beta}\right)\alpha+\left(1+\frac{3}{4\beta}\right)v^2-2v\right], \quad (6.86)$$

$$B = \frac{2\beta}{5}\left[\left(1-\frac{1}{\beta}\right)v^2-\left(1-\frac{5}{4\beta}\right)v-\frac{3}{4\beta}\alpha\right]. \quad (6.87)$$

The intersections of the curves arising from Eqs. (6.82) - (6.84) are following five points:

$$P_0: \quad v=\tfrac{1}{8}(5+\mu), \quad \theta=\tfrac{1}{64}(15-2\mu-\mu^2)$$

$$P_1: \quad v=\tfrac{1}{8}(5-\mu), \quad \theta=\tfrac{1}{64}(15+2\mu-\mu^2)$$

$$P_2 \quad v=0 \qquad \theta=0$$

$$P_3: \quad v=1, \qquad \theta=0$$

$$P_4: \quad v=1, \qquad \theta=\tfrac{1}{5}(\alpha-1).$$

The singularities P_0, P_1, and P_2 coincide with the singularities of the Navier-Stokes equations. It can be shown that P_0 and P_1 are also a saddle point and a node, respectively whereas P_2 is a spiral as in the case of Navier-Stokes theory. An example of loci of zero and infinite slopes for both the Navier-Stokes and present theories are plotted in the case of $N_M = 2$ in Fig. 6-1, where the broken line is for the

Navier-Stokes theory and the heavy solid line is for both the Navier-Stokes and present theories, whereas the light line is for the present theory only. The light

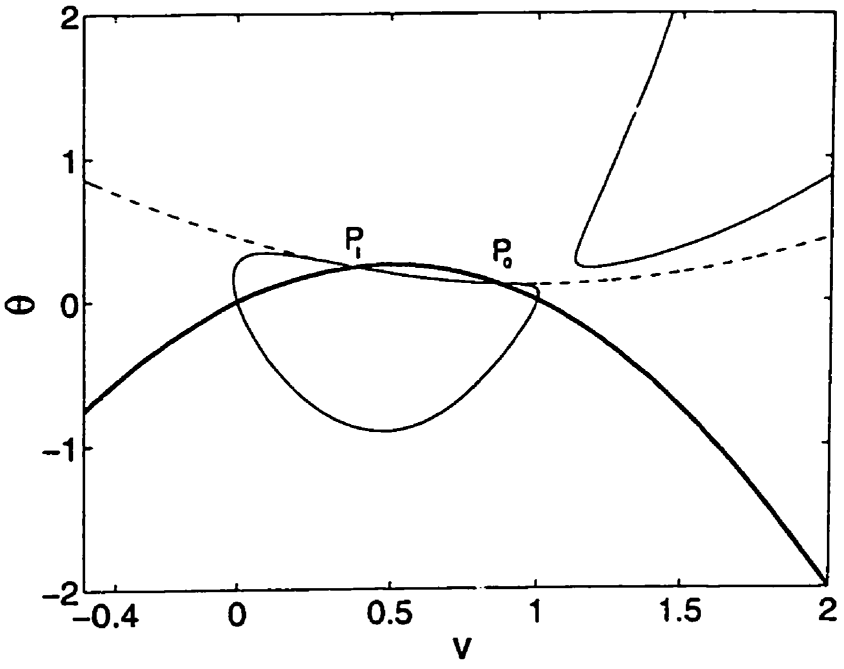

Figure 6-1: *Loci of zero and infinite slopes in the direction field for the Navier-Stokes and generalized hydrodynamic theories in the case of $N_M = 2$. The broken line is for the Navier-Stokes theory whereas the heavy line is for both the Navier-Stokes and present theories. The light lines are for the present theory which predicts a closed loop for a locus. Both theories share the same points of intersection P_0 and P_1 as well as P_2 and the domain of negative slopes bounded by curves passing through P_0 and P_1. Shock solutions lie in the domain and connect P_0 and P_1. Points P_2 anf P_3, which are intersections of the closed loop and the bold solid line, and P_4, which is the intersection of the closed loop and line $v = 1$, are not indicated in the figure. One of the parabolas which should appear in the the upper left corner is out of the picture in the present figure.*

line is a closed loop. The point P_0 is located at the origin of the (v,θ) coordinates whereas points P_3 and P_4 are the intersection of the closed loop with line $v = 1$. Both theories share the same inverted parabola (heavy line) which intersects the broken line and the closed loop described by Eq. (6.84) or Eq. (6.85) at the same points P_0 and P_1. Point P_3 is neutral in a direction and unstable in the other, whereas P_4 is unstable—an unstable focus. It therefore means that both theories

not only share the same boundary conditions at the upstream and downstream, but also have an intersection of domains which are bounded by curves of negative slopes and where the shock solutions lie. Singularities P_3 and P_4 are not associated with shock solutions. It must be noted that line $v = 0$ is neither the locus of zero slopes nor the locus of infinite slopes. As the Mach number increases, the intersections P_0, P_3, and P_4 coalesce at $v = 1$ which corresponds to the boundary value for velocity at infinite Mach number. This situation is almost achieved at $N_M = 10$ as shown in Fig. 6-2. The shock solution must connect P_0 and P_1. The fact that the singularities P_0 and P_1 are shared by both theories and there is an intersection of domains where the slopes are negative means that a shock solution must exist for the governing equations (6.72) and (6.73) for all Mach numbers as is the case for the Navier-Stokes equations for all Mach numbers. The uniqueness follows from the uniqueness of the solution to Eq. (6.81).

6.5 Numerical Results and Comparison with Simulation Data

6.5.1 Shock Profiles and Widths

The governing equations are numerically solved subject to the boundary conditions given in Eqs. (6.72) and (6.73). Some examples for shock profiles for velocity, temperature, density, and pressure are given for a few values of Mach number in Figs.6-6. In these and other figures in this work, the solid line is for $N_M = 1.5$, the bold solid line is for $N_M = 2$, the dashed line is for $N_M = 5$, the dotted line is for $N_M = 8$, and the dash-dotted line is for $N_M = 10$. The corresponding values for the stress (σ) and heat flux (φ) are plotted in Figs. 6-7 and 6-8, respectively. In the literature, the shock width δ is defined by means of the density profile in the following form

$$\delta = \frac{n_2 - n_1}{\left(\frac{dn}{dx}\right)_{\max}}, \tag{6.88}$$

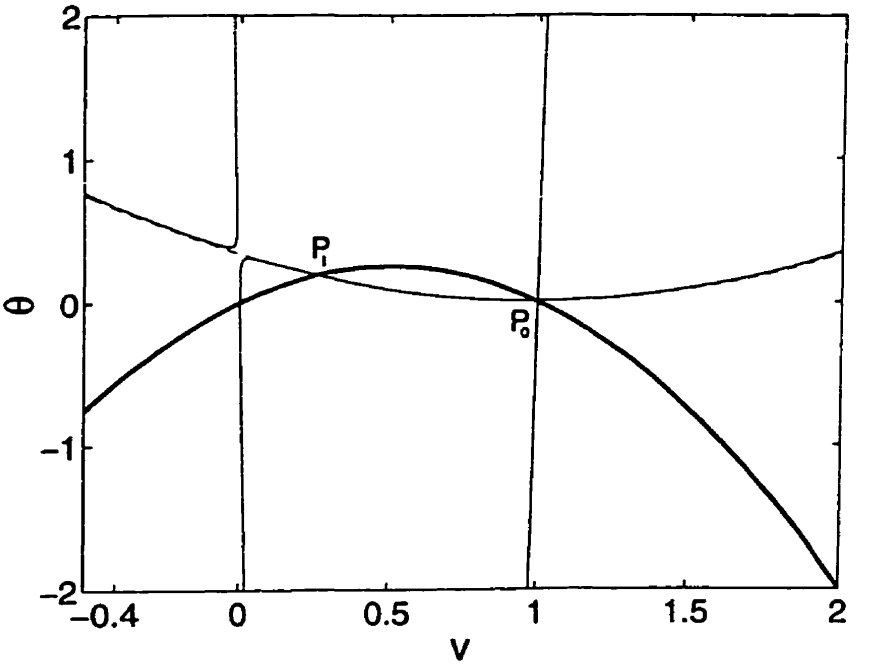

Figure 6-2: *Same as Fig. 6-1 except for* $N_M = 10$. *Notice that* P_0 *already has almost approached point* P_3 *at* $v = 1$, $\theta = 0$. *The closed loop in Fig. 6-1 becomes almost rectangular with the minimum at about* $\theta \approx -50$. *The parabola at the upper right corner almost meets with the closed loop at* $v = 1$ *and* $\theta = 0$.

where the reduced distance z has the relation to the reduced distance ξ used in this work; see Eq. (6.77).

In Fig. 6-9 the shock widths calculated (octagon) by the present theory are compared with Monte Carlo simulation data ($*$) by Nanbu et al.[45], the results by the Mott-Smith C_x^2 ($+$) and C_x^3 ($\Box$) closures [42], and the results by Salwen et al. who modified the Mott-Smith method to include an additional moment[49] [*e.g.*, (C_x^2, C_xC^2) ($\times$) or (C_x^3, C_xC^2) ($\diamond$) closures]. The solid line is drawn through the results of the present theory to guide the eyes. The Navier-Stokes predictions are presented in Table 1 together with the inverse shock width values for the points appearing in Fig. 6-9.

Since the differential equations (6.72) and (6.73) are stiff, the solutions are obtained by using Gear's method with a relatively high tolerance ($< 10^{-4}$). Therefore,

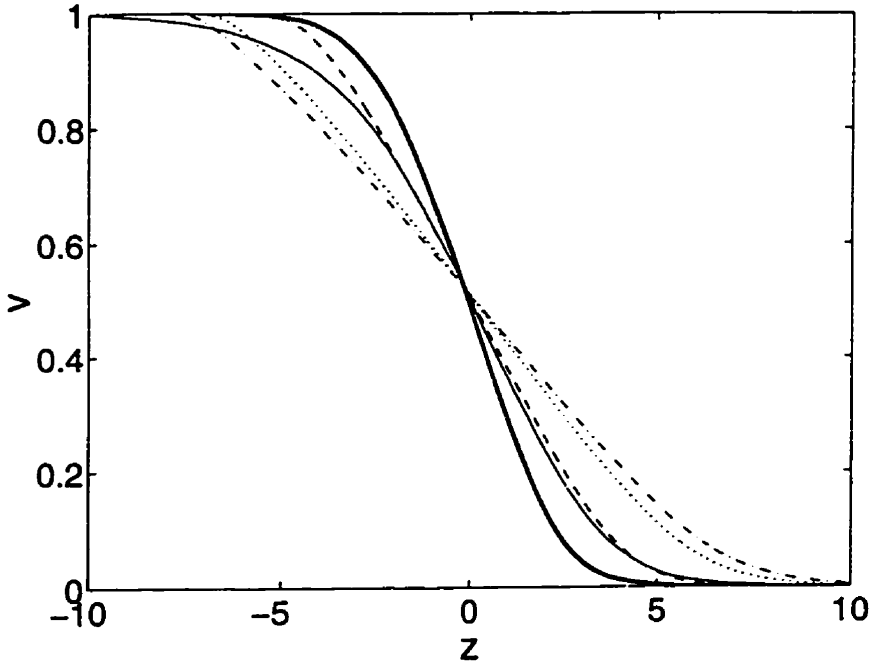

Figure 6-3: *Shock profiles for velocity for various Mach numbers for a Maxwell gas. Solid line:* $N_M = 1.5$; *bold solid line:* $N_M = 2$; *dashed line:* $N_M = 5$; *dotted line:* $N_M = 8$; *dash-dotted line:* $N_M = 10$.

the numerical results are not of high precision, but they are adequate for comparison. The present results obtained are closer to those by the Mott-Smith C_x^3 closure (□) for all Mach numbers examined whereas they differ from the Monte Carlo simulation data (∗) of Nanbu et al. by 14 to 20%. Note that the Monte Carlo simulation results well agree with the results by the Mott-Smith C_x^2 closure (+), but this method of closure does not give results convergent with those by the Mott-Smith C_x^3 closure (□). The Monte Carlo simulation method of Nanbu et al.[45] is a modification of Bird's method[7] and, especially, its treatment of collisions is basically the same as in the latter method.

Consequently, the method of Nanbu et al., as expectedly and noted by them[45], gives the same results as by the Bird method. Since the Mott-Smith method can be by no means regarded as exact and the C_x^2 and C_x^3 closures give divergent results, the converged results are quite probably located elsewhere if the method ever yields

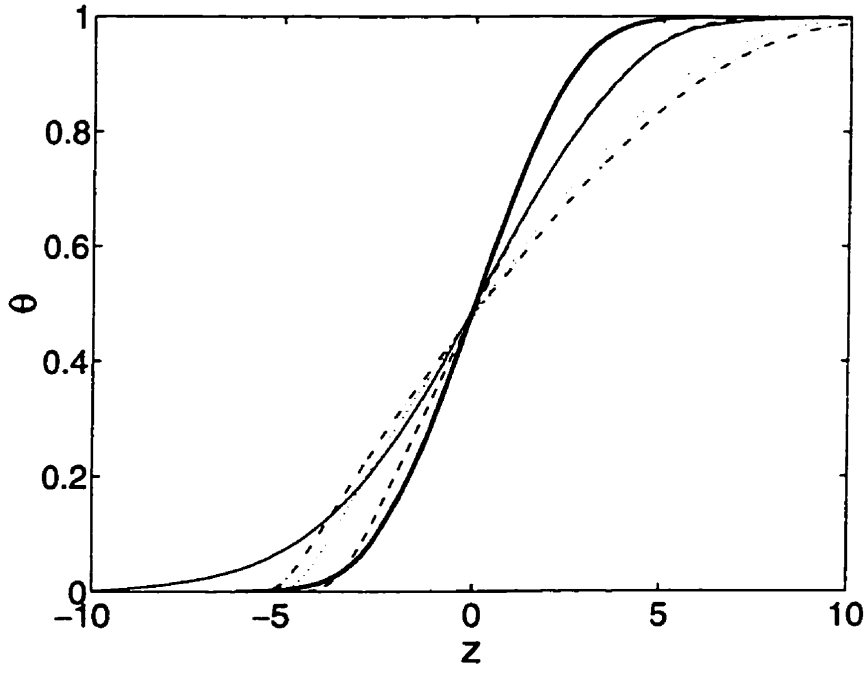

Figure 6-4: *Shock profiles for temperature for various Mach numbers for a Maxwell gas. The same meanings for the lines as in Fig. 6-3.*

convergent results as the number of moments included is increased. The reason for this expectation can be seen in the work of Salwen et al.[49] which gives different values from those by the Mott-Smith C_x^2 closure for the inverse shock width. Therefore, the particular set of results reported by the Monte Carlo simulation method of Nanbu et al.[45], who report that the same results also are obtained by the method of Bird[7], appears to be as good as the Mott-Smith C_x^2 closure method is for shock widths. The present comparison made in Fig. 6-9 therefore does not resolve the question regarding the accuracy and reliability of the present continuum theory method, although it produces results that appear to have a qualitatively correct behavior with regard to the Mach number dependence in the entire regime of Mach number.

To resolve this question, we have performed calculation with a variable hard sphere model which gives the viscosity as $\eta_0 = \mu_0 (T/T_0)^s$ where μ_0 and T_0 are constants and we have taken $s = 0.75$ in this work. This value of s lies between 0.72

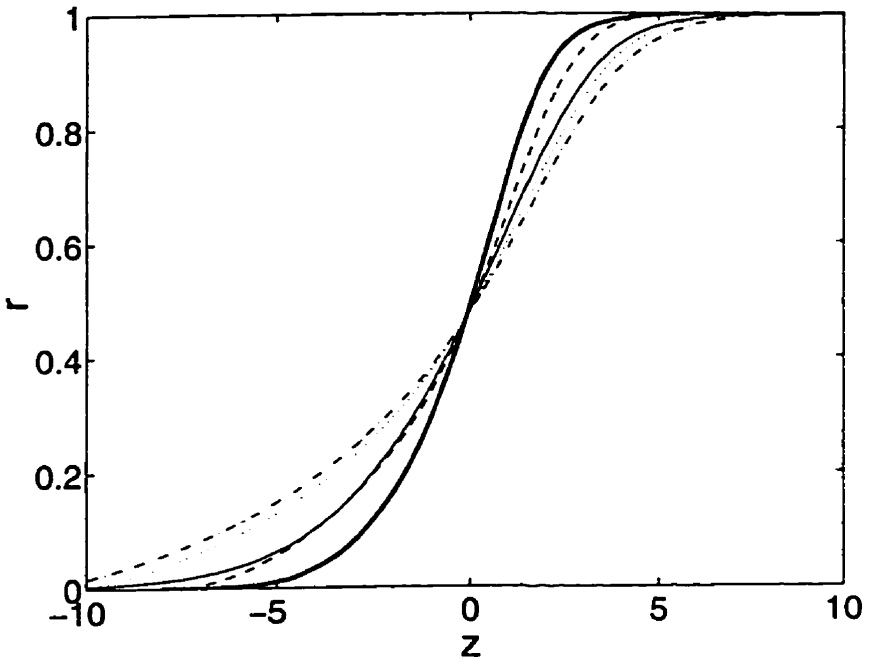

Figure 6-5: *Shock profiles for density for various Mach numbers for a Maxwell gas. The same meanings for the lines as in Fig. 6-3.*

for the shock tube value and 0.81 for the wind tunnel value suggested in the works of Pham-van-Diep et al.[47] and Erwin et al.[13]. This model has been tested in connection with shock widths for argon and helium by Pham-van-Diep et al.[47] and Erwin et al.[13]. To make comparison of the results by the formulas in the present theory with experiment it is necessary to use a somewhat different length scale from the scale given in Eq. (6.77). This difference arises from the different definitions of mean free path. The experimental data in question are based on the definition of mean free path by Bird[8] $l_B = (\eta_{01}/\rho_1)\, B\sqrt{\pi/2\mathcal{R}T_1}$ where $B = (7-2s)(5-2s)/24$. For this definition of mean free path the reduced distance ξ in the present theory is related to the reduced distance used for the experimental data considered here as follows:

$$\xi = zB\sqrt{\frac{5\pi}{6}}N_M. \tag{6.89}$$

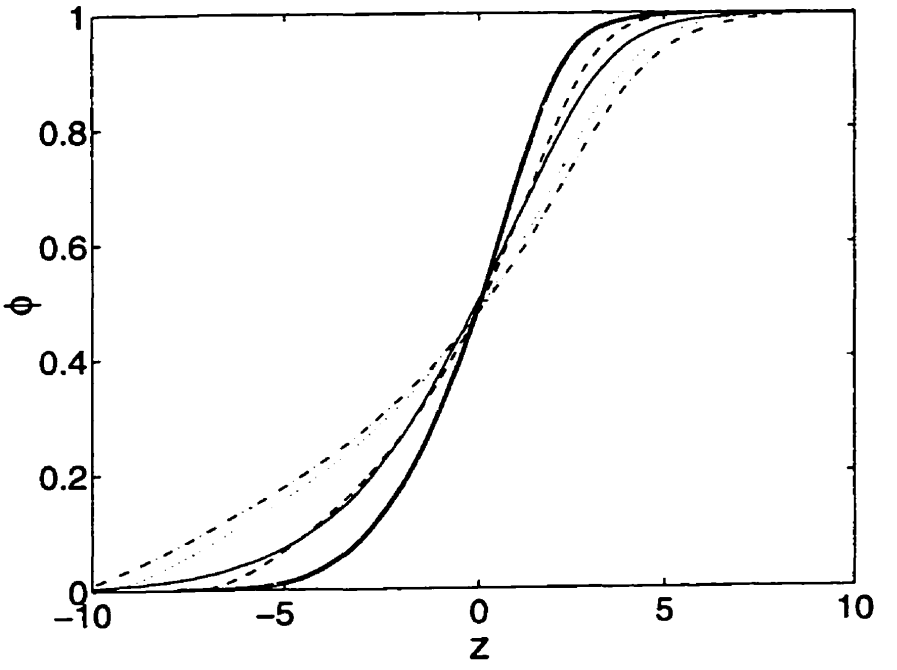

Figure 6-6: *Shock profiles for pressure for various Mach numbers for a Maxwell gas. The same meanings for the lines as in Fig. 6-3.*

Therefore, the shock widths are calculated with the formula

$$\delta = B\sqrt{\frac{5\pi}{6}}N_M \frac{n_2 - n_1}{\left(\frac{dn}{d\xi}\right)_{\max}}. \tag{6.90}$$

The results calculated (*octagon*) for the variable hard-sphere model are compared with various experimental data reported by Alsmeyer[1] (□), Schmidt[50] (✠), Garen et al. [26] (+), Linzer et al.[40] (◇), and Camac[9] (×) in Fig. 6-10. A line is drawn through the theoretical values in order to guide the eyes. Although the data of Linzer et al. and Camac do not appear to be consistent with the data of Alsmeyer, Schmidt, and Garen et al. and therefore are difficult to analyze with the present theory together with those of the latter, they are included in the figure for completeness. Given the experimental uncertainties (4-5% according to Alsmeyer) and the errors in the numerical solutions of the governing equations, the theoretical results are judged to be in good agreement with experiment and, especially, with those by Alsmeyer,

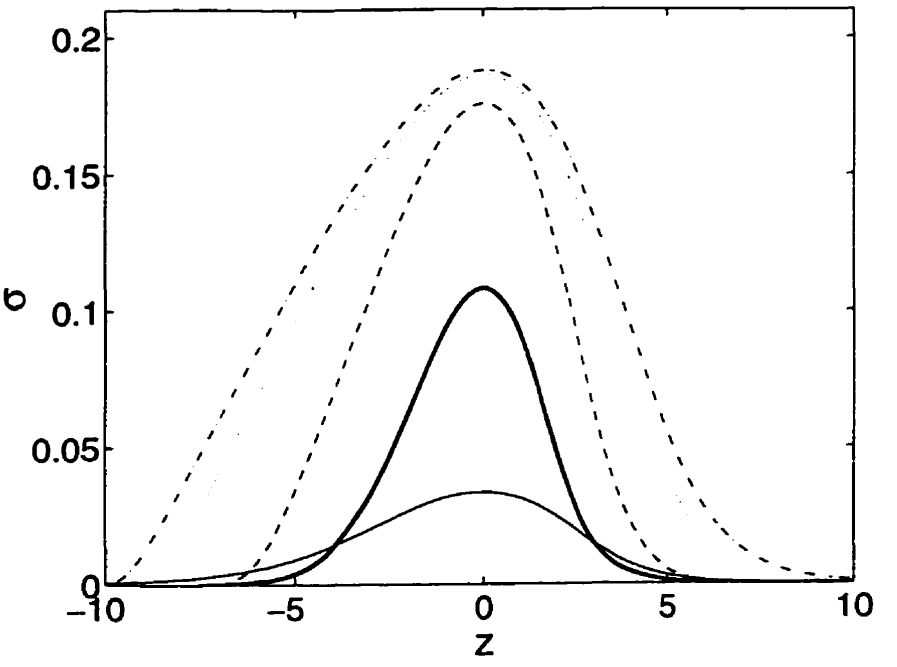

Figure 6-7: *Shock profiles for stress for various Mach numbers for a Maxwell gas. The same meanings for the lines as in Fig. 6-3.*

Schmidt, and Garen et al. In fact, the agreement with Alsmeyer's data is excellent. Therefore, it can be concluded that the present theory yields reliable results for inverse shock widths over the entire experimental range of Mach number.

The present theory is a continuum hydrodynamic theory for shock waves, and it provides shock structures adequately for the range of Mach number studied by other methods and by experiments. This is in contrast to the Navier-Stokes theory and other approaches[29, 32, 2] in the moment method mentioned earlier. As far as the present authors are aware, this is the first time for a continuum hydrodynamic theory to accomplish such results comparable with experiments over the entire range of Mach number studied. We thus have achieved an adequate continuum theory generalization of the Navier-Stokes theory for shock waves in the high Mach number regime, and the closure relations, together with the nonlinear factor $q(\kappa)$, taken for the constitutive equations for the stress tensor and heat flux hold the key to the results obtained.

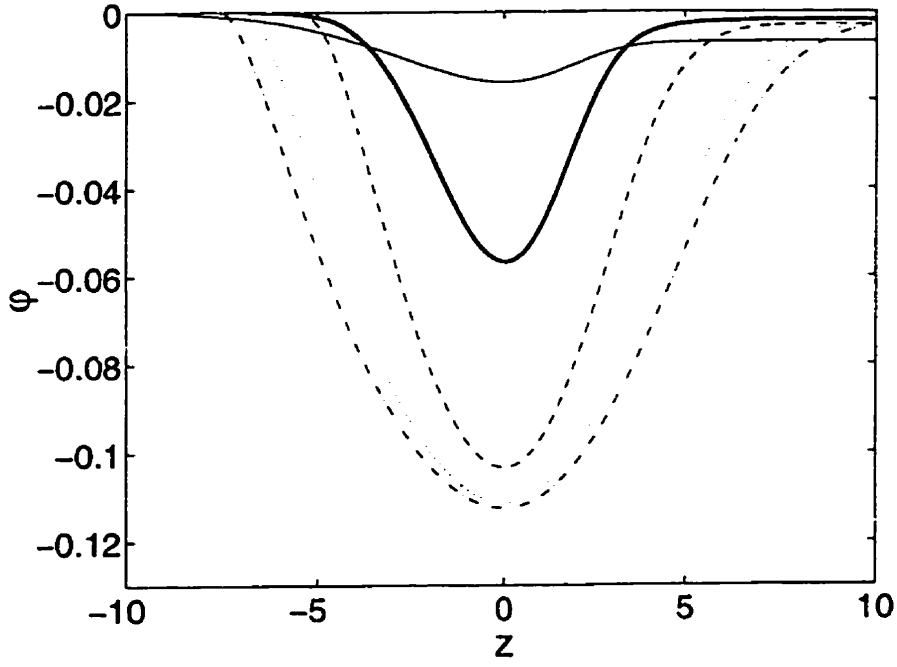

Figure 6-8: *Shock profiles for heat flux for various Mach numbers for a Maxwell gas. The same meanings for the lines as in Fig. 6-3.*

6.5.2 Calortropy Production—Energy Dissipation

Energy dissipation is closely associated with shock wave phenomena. It competes with compression in determining the thickness of a shock wave. Therefore, it is interesting to examine energy dissipation. In the framework of irreversible thermodynamics on which the present theory is based, the calortropy production[23] gives a measure of energy dissipation in the system from a useful to less useful form. We have calculated the calortropy production associated with shock waves for various Mach numbers. For the constitutive equations the calortropy production is given by Eu[22].

$$\sigma_{cal} = k_B g \kappa \left(\mathbf{\Pi}, \mathbf{Q}\right) \sinh \kappa \left(\mathbf{\Pi}, \mathbf{Q}\right), \tag{6.91}$$

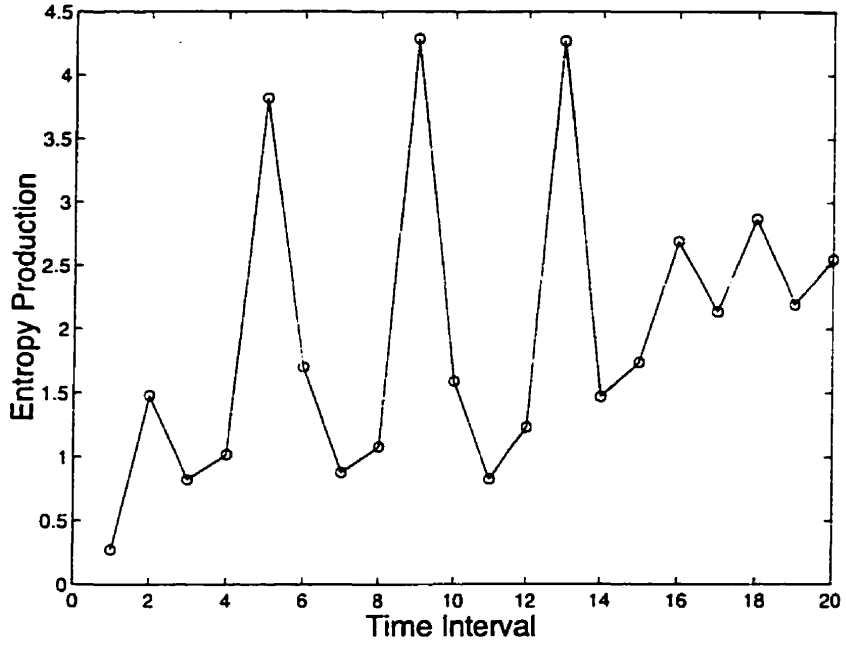

Figure 6-8: *Shock profiles for heat flux for various Mach numbers for a Maxwell gas. The same meanings for the lines as in Fig. 6-3.*

6.5.2 Calortropy Production—Energy Dissipation

Energy dissipation is closely associated with shock wave phenomena. It competes with compression in determining the thickness of a shock wave. Therefore, it is interesting to examine energy dissipation. In the framework of irreversible thermodynamics on which the present theory is based, the calortropy production[23] gives a measure of energy dissipation in the system from a useful to less useful form. We have calculated the calortropy production associated with shock waves for various Mach numbers. For the constitutive equations the calortropy production is given by Eu[22].

$$\sigma_{cal} = k_B g \kappa \left(\mathbf{\Pi}, \mathbf{Q}\right) \sinh \kappa \left(\mathbf{\Pi}, \mathbf{Q}\right), \tag{6.92}$$

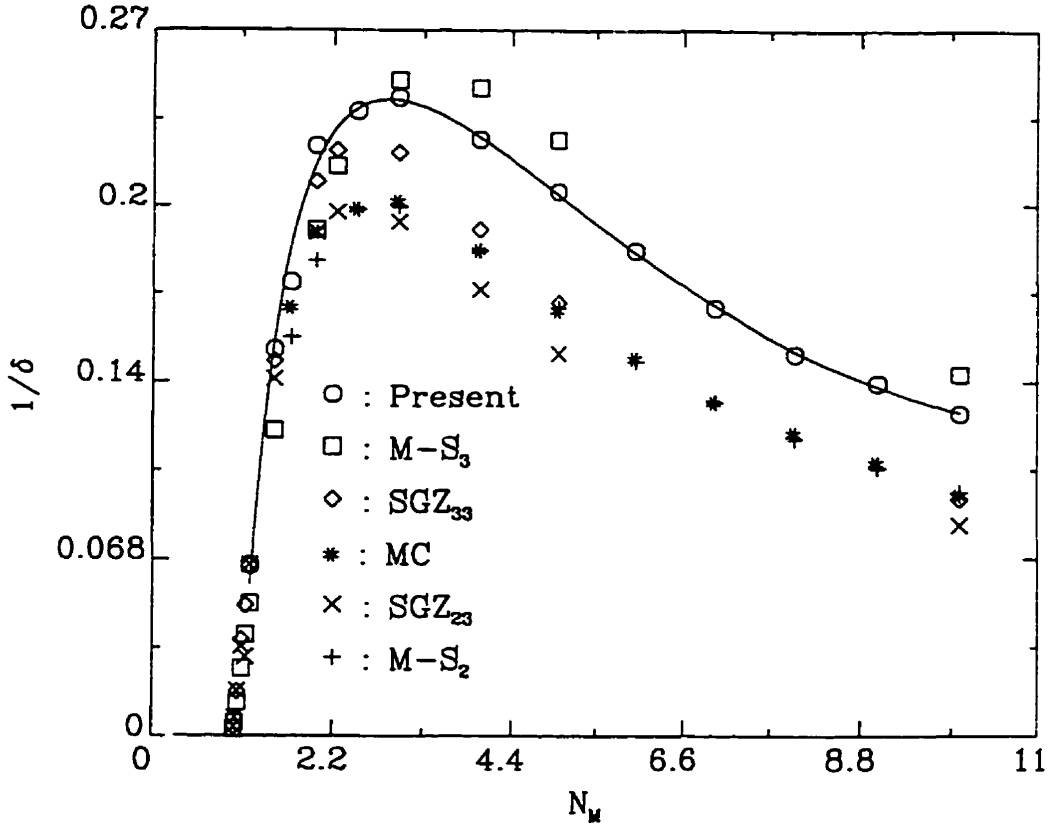

Figure 6-9: *Inverse shock width vs. N_M for a Maxwell gas. The solid line is drawn through the present results to guide the eyes. The meanings of the symbols are as follows: octagon = present result; * = Monte Carlo result of Nanbu et al.[45]; + = Mott-Smith C_x^2 closure[45]; □ = Mott-Smith C_x^3 closure[42]; × = Mott-Smith (C_x^2, C_xC^2) closure[49]; ◇ = Mott-Smith (C_c^3, C_xC^2) closure[42].*

where $g = (m/k_BT)^{1/2}/2n^2d^2$. Therefore a reduced calortropy production relative to the upstream condition may be defined by

$$\begin{aligned} \hat{\sigma}_{cal} &= \sigma_{cal}/k_B g(T_1, n_1) \\ &= \sqrt{\frac{\theta}{\theta_1}} \left(\frac{r_1}{r}\right)^2 \kappa(\sigma,\varphi) \sinh \kappa(\sigma,\varphi). \end{aligned} \tag{6.92}$$

The reduced calortropy production is computed from the shock solutions obtained and presented in Fig. 6-11. It is peaked around the transition point in the shock

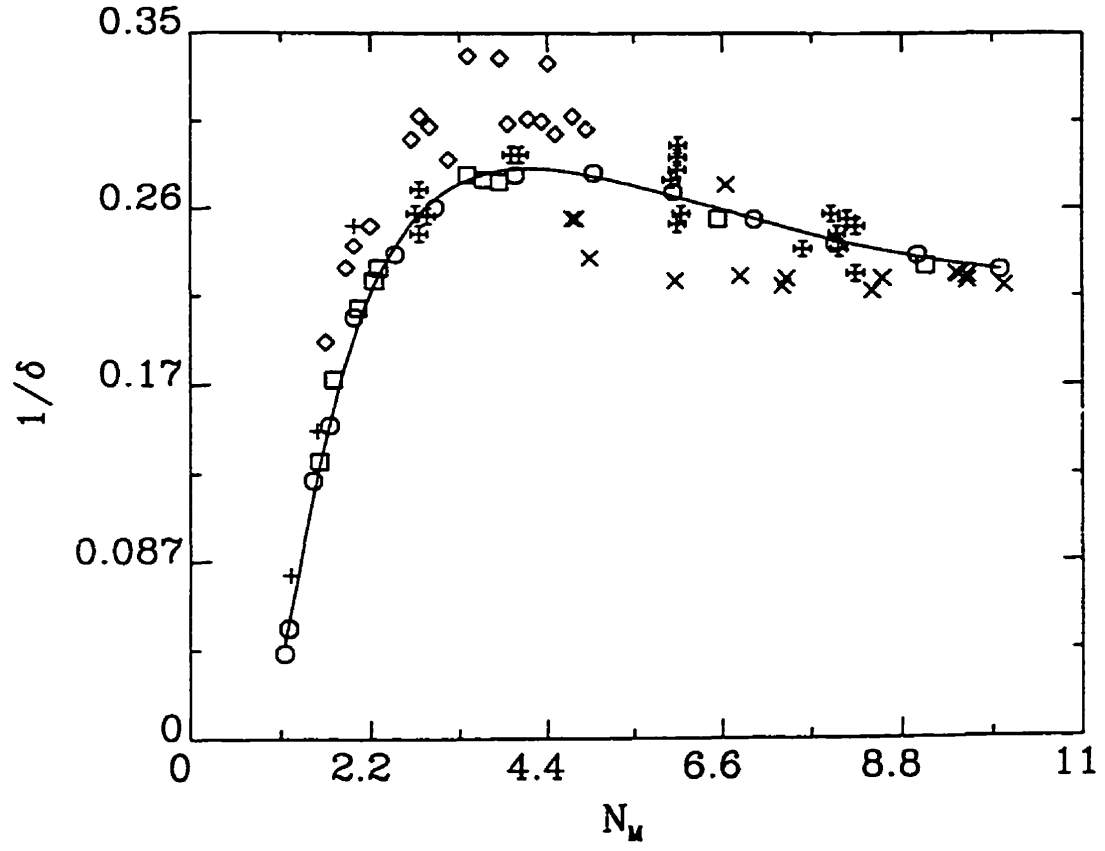

Figure 6-10: *Comparison of theoretical inverse shock widths with experimental data at various Mach numbers. A variable hard-sphere model is used for the potential for which* $\eta_0 = \mu_0 (T/T_0)^s$ *with* $s = 0.75$. *octagon = present theory,* □ = *Alsmeyer[1],* ✠ = *Schmidt[50],* + = *Garen et al.[26],* ◇ = *Linzer et al.[40], and* × = *Camac[9]. A solid line is drawn through the theoretical values in order to guide the eyes.*

profile and the peak height increases with the Mach number. In the scale of the figure $\hat{\sigma}_{cal}$ is so small for $N_M = 1.5$ that it does not show up in the figure.

Since the global value for calortropy production is of interest and perhaps more relevant to the present problem, we define a reduced integral calortropy production

$$\begin{aligned} \Xi_c &= \int_{-\infty}^{\infty} d\xi \sqrt{\frac{\theta}{\theta_1}} \left(\frac{r_1}{r}\right)^2 \kappa(\sigma,\varphi) \sinh \kappa(\sigma,\varphi) \\ &= \sqrt{\frac{5\pi}{6}} N_M \int_{-\infty}^{\infty} dz \sqrt{\frac{\theta}{\theta_1}} \left(\frac{v}{v_1}\right)^2 \kappa(\sigma,\varphi) \sinh \kappa(\sigma,\varphi). \end{aligned} \tag{6.93}$$

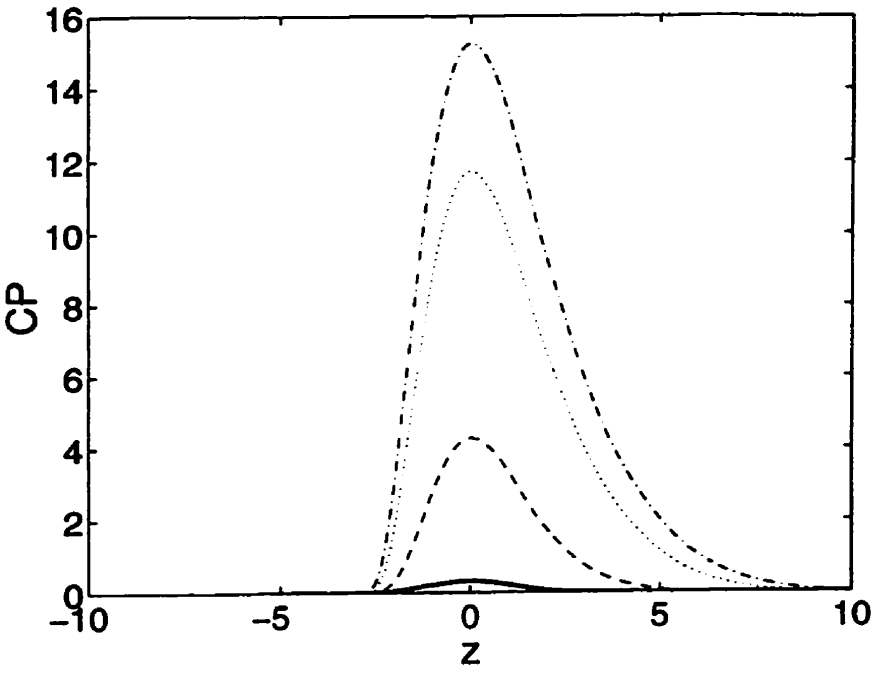

Figure 6-11: *Profile for reduced calortropy production for various Mach numbers for a Maxwell gas. The same meanings for the lines as in Fig. 6-3. The case for* $N_M = 1.5$ *is invisible in the scale of the figure.*

This global calortropy production is plotted as a function of Mach number in Fig. 6-12 in the case of the Maxwell model. The figure suggests that Ξ_c increases with Mach number as $(N_M - a)^\alpha$: namely,

$$\Xi_c = K\,(N_M - a)^\alpha\,, \tag{6.94}$$

where K, a, and α are constant parameters. For the Maxwell model $a \simeq 0.85$ and $\alpha \simeq 3.14$ whereas $a \simeq 0.87$ and $\alpha \simeq 2.98$ for the variable hard sphere model with $s = 0.75$. It probably is fair to take $\alpha = 3.0$ as an approximation, given the uncertainties of the numerical results and curve fittings. This energy dissipation competes with the compressional effect of shock in determining the shock thickness.

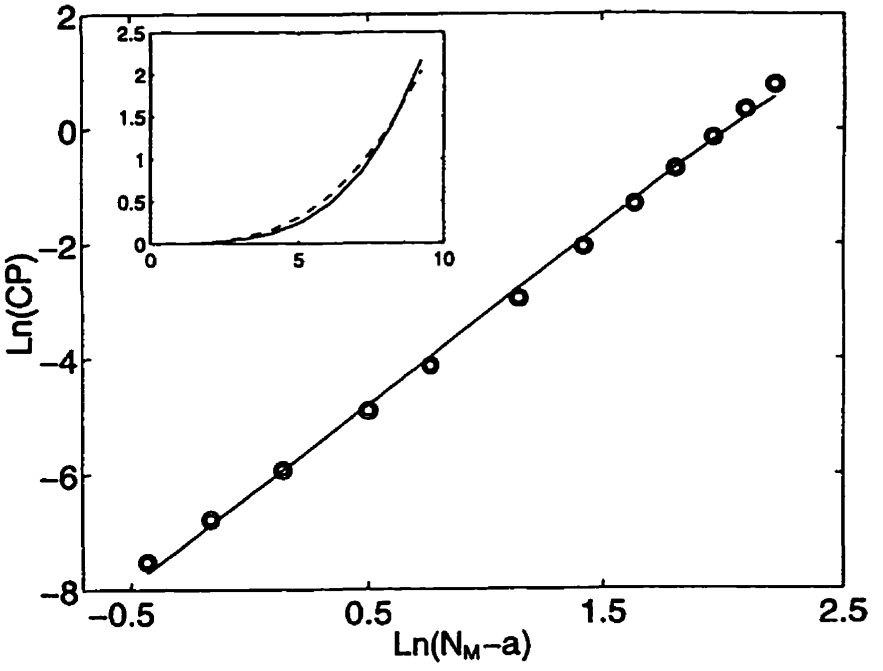

Figure 6-12: *Logarithm of global reduced calortropy production* $\ln(CP)$ *vs.* $\ln(N_M - a)$ *for a Maxwell gas. The ordinate is in the units of* $\ln 500$. *The slope of the line is 3.14 and the value of a is 0.85. The inset is for* Ξ_c *vs.* $(N_M - a)$ *which is presented to indicate the degree of fidelity of the estimates for the parameters a and* α.

6.6 Discussion and Conclusion

In this chapter, we have presented a continuum hydrodynamic theory of shock waves which yields shock structures (shock widths) comparable to those by Monte Carlo methods and the Mott-Smith methods over the entire range of Mach numbers studied for the Maxwell model of potential. It removes the weakness of the Navier-Stokes theory of shock waves. However, the present results agree, only within 14-20%, with the Monte Carlo results obtained by Nanbu et al.[45] and with the results by the Mott-Smith C_x^2 closure method. Our present results are closer in performance to that by the Mott-Smith C_x^3 closure method. Since none of the Mott-Smith methods can be judged to be exact and they yield nonconvergent numerical results for the inverse shock widths for the Maxwell model, it is difficult to conclude which one is closer to the true values for shock widths. To resolve this question, we have

computed the inverse shock widths by the present theory for a variable hard sphere model and compared the results with experimental data on argon. They are found to be in good agreement with experiments. Thus, we now have a continuum hydrodynamic theory for shock waves which correctly performs beyond the regime of Mach number where the classical Navier-Stokes theory remains useful. Such a theory is designed from the moment equations derived from the Boltzmann kinetic equation, primarily, by using different closures from those used in the moment methods by others for the same purpose. The performance of the governing equations is enhanced by the presence of the nonlinear factor $q(\kappa)$ which basically arises on resummation of the Boltzmann collision contributions for all Knudsen numbers. The present theory is thermodynamically consistent in the sense that it conforms to the requirement of thermodynamic laws. The aforementioned nonlinear factor is known to be responsible for correctly accounting for the shear rate dependence of fluids in the non-Newtonian regime of viscosity[15, 46, 16, 21, 41, 5, 6] , the emergence[17]of boundary layers in flows under a steep pressure gradient, plug flows[19, 20], the resolution[19] of the Knudsen paradox[38], etc. The nonlinear factor $q(\kappa)$ is not present in the moment equations in the conventional approach following the formulation of Grad's moment method. As is evident from Eq. (6.92), $q(\kappa)$ is closely related to the calortropy production arising from the irreversible process in the system since Eq. (6.92) can be recast in the form

$$\sigma_{cal} = k_B g \kappa^2 \left(\Pi, \mathbf{Q}\right) q(\kappa) \geq 0. \tag{6.95}$$

Since $\kappa^2 \left(\Pi, \mathbf{Q}\right)$ is basically the Rayleigh dissipation function, this nonlinear factor $q(\kappa)$ modifies the Rayleigh dissipation function[48] because there are nonlinear transport processes present in the system. The generalized hydrodynamic equations presented in this work have been derived from the Boltzmann equation for dilute gases. Therefore, one may infer that they are limited to such gases. However, it is shown in the literature[22] that essentially the same forms of evolution equations hold for liquids and for dense gases except for the meanings of the parameters ap-

pearing in the equations which must be regarded as those for liquids or dense gases. More specifically, one can simply regard the transport coefficients η_0 and λ_0 as well as p and $\hat{C}_p$ in the constitutive equations (6.41) and (6.42) as those for the liquid or dense gas in question and apply them to flow problems in such fluids. Therefore, the present results also suggest the utility of the present generalized hydrodynamics approach to shock wave phenomena in liquids or dense gases where Monte Carlo simulation methods comparable to those of Bird and Nanbu are not available at present. In this connection, we note that there are some molecular dynamics simulations on shock waves in liquids[36, 30, 31]. In conclusion, we believe that, together with the conservation laws for mass, momentum, and energy, the constitutive equations for $\mathbf{\Pi}$ and $\mathbf{Q}$ presented in this work form a continuum (generalized hydrodynamic) theory of flow phenomena including shock waves.

Bibliography

[1] H. Alsmeyer, J. Fluid Mech. **74**, 497 (1976).

[2] A. M. Anile and A. Majorana, Meccanica **16**, 149 (1982).

[3] A. G. Bashkirov and A. V. Orlov, Phys. Rev. E **53**, R17 (1996).

[4] R. Becker, Stosswelle und Detonation, Z. Physik. **8**, 321 (1922).

[5] D. K. Bhattacharya and B. C. Eu, Mol. Phys. **59**, 1145 (1986).

[6] D. K. Bhattacharya and B. C. Eu, Phys. Rev. A **35**, 4850 (1987).

[7] G. A. Bird, *Molecular Gas Dynamics* (Clarendon, Oxford, 1976).

[8] G. A. Bird, Phys. Fluids **26**, 3222 (1983).

[9] M. Camac, Adv. Appl. Mech. Suppl. 3, **1**, 240 (1965).

[10] M. T. Chahine and R. Narashimha, Adv. Appl. Mech. Suppl. 3, **1**, 140 (1965).

[11] S. Chapman and T. G. Cowling, *The Mathematical Theory of Nonuniform Gases* Cambridge (London, third ed., 1970)

[12] S. R. de Groot and P. Mazur 1962 *Nonequilibrium Thermodynamics* (North-Holland, Amsterdam, 1962).

[13] D. A. Erwin, G. C. Pham-van-Diep, and E. P. Muntz, Phys. Fluids A **3**, 697 (1991).

[14] M. Murduchow and P. A. Libby, J. Aeronaut. Sci. **16**, 11 (1949).

[15] B. C. Eu, Phys. Lett. A **96**, 29 (1983); J. Chem. Phys. **79**, 2315 (1983).

[16] B. C. Eu and Y. G. and Ohr 1984, J. Chem. Phys. **81**, 2756 (1984).

[17] B. C. Eu, Phys. Rev. A **36**, 400 (1987).

[18] B. C. Eu, Phys. Rev. A **77**, 4504 (1988).

[19] B. C. Eu, Phys. Rev. A **40**, 6395 (1989).

[20] B. C. Eu, Am. J. Phys. **58**, 83 (1990).

[21] B. C. Eu and R. E. Khayat, Rheol. Acta **30**, 204 (1991) .

[22] B. C. Eu, *Kinetic Theory and Irreversible Thermodynamics* (Wiley, New York, 1992).

[23] B. C. Eu, J. Chem. Phys. **103**, 10652 (1995).

[24] B. C. Eu, Phys. Rev. E **51**, 768 (1995).

[25] J. D. Jr. Foch and G. W. Ford in *Studies in Statistical Mechanics*, Vol. 5, North-Holland, Amsterdam, J. De Boer and G. E. Uhlenbeck, eds. (1970).

[26] W. Garen, R. Synofzik, and A. Frohn, AIAA J. **12**, 1132 (1974).

[27] D. Gilbarg and D. Paolucci, J. Rat. Mech. Anal. **2**, 617 (1953).

[28] H. Grad, Comm. Pure Appl. Math. **2** , 331 (1949).

[29] H. Grad, Comm. Pure Appl. Math. **5** , 257 (1952).

[30] B. L. Holian, W. G. Hoover, B. Moran, and G. K. Straub, Phys. Rev. A **22**, 2798 (1980).

[31] B. L. Holian, Phys. Rev. A **37**, 2562 (1988).

[32] L. H. Holway, Phys. Fluids **7**, 911 (1964).

[33] L. H. Holway, Adv. Appl. Mech. Suppl. 3, **1**, 193 (1965).

[34] F. S. Sherman, NACA Tech. Note 3298 (1955).

[35] L. Talbot and F. S. Sherman, NASA Memo 12-14-58W (1959).

[36] W. G. Hoover, Phys. Rev. Lett. **42**, 1531(1979).

[37] D. Jou, J. Casas-Vazquez, and G. Lebon, *Extended Irreversible Thermodynamics* (Springer, Berlin 1993) .

[38] M. Knudsen, Ann. Phys. ser. 4, **28**, 75 (1909).

[39] M. N. Kogan, *Rarefied Gas Dynamics* (Plenum, New York, 1967).

[40] M. Linzer and D. F. Hornig, Structure of shock fronts in argon and nitrogen, Phys. Fluids 6, 1661 (1963).

[41] K. Mao and B. C. Eu, Phys. Rev. A **48**, 2471 (1993).

[42] H. M. Mott-Smith, Phys. Rev. **82**, 885 (1951).

[43] C. Muckenfuss, Phys. Fluids **5**, 1325 (1962).

[44] I. Müller and T. Ruggeri, *Extended Thermodynamics* Springer, Berlin (1993).

[45] K. Nanbu, and Y. Watanabe, Rep. Inst. High Speed Mech., Vol. 48, Tohoku Univ., Japan (1984).

[46] Y. G. Ohr, and B. C. Eu, Phys. Lett. A, **101**, 338 (1984).

[47] G. C. Pham-van-Diep, D. A. Erwin, and E. P. Muntz, J. Fluid Mech. **232**, 403 (1991).

[48] Lord Rayleigh, 1945 *Theory of Sound (*Dover, New York,1945).

[49] H. Salwen,C. E. Grosch, and S. Ziering, Phys. Fluids **7**, 180 (1964).

[50] B. Schmidt, J. Fluid Mech. **39**, 361 (1969).

[51] L. H. Thomas, J. Chem. Phys. **12**, 449 (1944).

[52] C. S. Wang Chang and G. E. Uhlenbeck in *Studies in Statistical Mechanics*, Vol. 5, North-Holland, Amsterdam, J. De Boer and G. E. Uhlenbeck, eds.(1970).

[53] S. Yen, and W. Ng, J. Fluid Mech. **65**, 127 (1974).

[54] J. H. Ferziger and H. G. Kapler, *Mathematical theory of Transport Processes in Gases* (North Holland, N. Y. 1972).

[55] B. C. Eu, J. Chem. Phys. **73**, 2958 (1980); **74**, 2998 (1981); **74**, 3006 (1981); **80**, 2123 (1984); **87**, 1220 (1987).

[56] B. C. Eu, J. Chem. Phys. **103**, 10652 (1995).

[57] B. C. Eu, *Nonequilibrium Ensemble Method* (Kluwer, 1997) Monograph in preparation.

Table 1. Inverse Shock widths by various theories for a Maxwell gas

N_M	M-S_2	M-S_3	SGZ_{23}	SGZ_{33}	MC	Present	NS
1.2	0.0557	0.0504	0.0653	0.0650	-	0.0651	-
1.5	0.124	0.116	0.136	0.143	-	0.147	-
1.7	0.152*	-	-	-	0.164	0.173	0.188
2	0.184	0.193	0.192	0.212	0.193	0.226	0.232
2.25	0.198	0.218	0.200	0.224	-	-	-
2.5	0.201*	-	-	-	0.202	0.239	0.275
3	0.206	0.251	0.196	0.223	0.205	0.244	0.293
4	0.188	0.248	0.170	0.193	0.186	0.228	-
5	0.165	0.228	0.146	0.165	0.163	0.208	-
6	0.143*	-	-	-	0.145	0.185	-
7	0.127*	-	-	-	0.128	0.163	-
8	0.113*	-	-	-	0.116	0.146	-
9	0.102*	-	-	-	0.105	0.135	-
10	0.0945	0.138	0.0804	0.0902	0.0925	0.123	-

M-S_2=Mott-Smith C_x^2 closure, M-S_3=Mott-Smith C_x^3 closure[42];

SGZ_{23}=Salwen, Grosch, Ziering (C_x^2, C_xC^2) closure,

SGZ_{33}=Salwen, Grosch, Ziering (C_x^3, C_xC^2) closure[49];

MC=Monte Carlo[45];

NS=Navier-Stokes;

$*$ = data from Ref. [45].

Chapter 7

Conclusion

Nonlinear chemical reactions with autocatalytic steps have been attracting a considerable amount of attention in connection with chemical oscillations, waves, pattern formation and turbulence. These are phenomena occurring far-from equilibrium and highly nonlinear. In the first part of this thesis, we have carried out the study of hyperbolic reaction diffusion-equations for the Selkov and the Brusselator. The basic motivations of this line of work are in framing the theory of chemical oscillations and waves under the principles of thermodynamics so that the macroscopic description of chemical oscillation and wave phenomena is consistent with the thermodynamic laws as any macroscopic theory should; and in using hyperbolic wave equations which are considered to be more appropriate than the conventionally used parabolic differential equations in describing transient wave phenomena; comparing the differences in results such as the patterns and their spatio-temporal evolutions predicted by the two different types of differential equations; and their implications for energy and matter consumption and irreversible thermodynamics. We have reported that as the reaction-diffusion number, which characterizes the relative time scales of reactions and diffusion to the time scale of hydrodynamic flow, increases beyond a characteristic value, the hyperbolic reaction-diffusion equations taken for the study of the Selkov model reduce to the conventional parabolic reaction-diffusion equations; and *the local patterns of certain frequencies and wave numbers are formed*

and maintained at the expense of energy and matter yet the total global energy dissipations are the same for different patterns formed. This means that some patterns of particular frequencies and wave numbers appropriate energy and matter to themselves at the expense of those of other frequencies and wave numbers. These results are interesting on their own right, but also potentially useful for improving our understanding of pattern formation phenomena as well as nonlinear wave phenomena. We have also described various modes of pattern and wave formations in two dimensions under the non-random initial and boundary conditions as well as random initial conditions, and the modes of energy and matter dissipation by the various patterns formed. Unlike the parabolic reaction-diffusion equations conventionally used in connection with chemical oscillations and waves, the hyperbolic reaction-diffusion equations taken for the study here describe transient behaviors of the system. For example, they can describe a phenomenon akin to cell divisions observed in the simulations of the CIMA reaction[7] and the Lengyel-Epstein model[8]. The Selkov model admits monostable and bistable regions of stability. We have explored the modes of pattern formation in both regions. We find empirically that some interesting behaviors occur in the vicinity of the unstable steady state in the bistable region. Spirals and solitary waves are observed to arise under some conditions. The spirals interact and their tips meander. Two solitary waves for each species can also be formed and propagate at two different speeds. They can also merge to a single front which propagates at a constant speed. These features all arise from the single set of hyperbolic reaction-diffusion equations, depending on the initial and boundary conditions. We have computed the speed of such waves.

For entropy production concerning the aforementioned patterns we have found the following: the results of calculation show the global entropy production vs. time accompanying the sequence of the patterns oscillates with the patterns and reaches an asymptotic regime in the longtime limit where hexagonal structures become mixed with stripe structures and compete with each other. In this regime of time, the entropy production oscillates around a plateau value. In the case of spiral patterns mentioned earlier, a very steep but continuous jump as the tips ('black holes') of

the spirals begin to appear. The entropy production reaches an asymptotic plateau which we characterize as the state of saturation of the pattern. The case of the spirals obtained with random initial conditions also show a similar oscillation of the global entropy production vs. time. We observe that even though the aforementioned patterns are different, the global entropy productions at the state of saturation are the same, and it means that their rates of energy and matter dissipation are similar. In the case of irregular chaotic patterns, the global entropy production keeps on increasing with time without reaching a plateau, although its magnitude is much smaller than those for the organized patterns. This seems to suggest that *an organized pattern consumes more energy and matter than a chaotic disorganized pattern.*

The entropy productions calculated for the competing structures cannot elucidate such competition, for it simply saturates and remains practically at a constant value. Therefore, the only thing we can say is that such structures dissipate more energy and matter than otherwise, but as to the details of pattern competition it seems to say little. Therefore, if there is a thermodynamic principle that can guide us in connection with pattern competition and pattern selection, it does not appear that the second law of thermodynamics is the one that should be looked up to for a clue. The salient role of the second law so far has been in providing a set of macroscopic (hydrodynamic) evolution equations consistent with a positivity criterion for energy dissipation that may be regarded as a local form of the second law, but pattern formation and selection seems to be controlled by something other than the positivity condition provided by the second law. As for the bistable region, we have found that the global entropy production of the solitary waves, which is roughly equal to the local entropy production because of the localized nature of the waves, is large in the initial stage before a chaotic phase sets in where it shows a minimum. It begins to rise as two spots grow out of a homogeneous phase reaching a peak as the solitary waves collide and merge. Then it remains roughly constant in the intermediate time interval when the waves have grown in size. As the wave

approaches the boundary on the right-hand side and begins to get annihilated, the global entropy production becomes low in value and constant in time. Establishing a relation between the observed patterns and the entropy production is an attempt to understand the underlying irreversible thermodynamic cause for the pattern formation. We observe some interesting features, but the picture of the phenomena is not complete as yet. This aspect of nonlinear phenomena appears to be still an open subject. .

Pattern formations have been numerically studied on the basis of the amplitude equations generically called the Ginzburg-Landau equation. It is shown that such amplitude equations can be derived from the hyperbolic reaction-diffusion equations if the well-known perturbation method originated by Poincaré and Lindstedt is applied to the equations. The amplitude equations for the Brusselator are compared with those obtained from the corresponding parabolic reaction-diffusion equations. They have the same form except for the coefficients appearing in the equations. those coefficients are much more complicated and contain singularities in the reaction-diffusion number. We have explored those singularities and the amplitude equations were solved numerically. The numerical results confirms the stability analysis performed for those amplitude equations. We have also noted when solving for patterns in the case of the Brusselator that the two-dimensional power spectra of such patterns reveal patterns of wave vector distributions with some elements of symmetry. This suggests that spatial patterns can be classified according to the wave vector distributions and symmetries of their multidimensional power spectra. This seems to be a rather intriguing and, perhaps, important feature worthy of further serious study in the future.

Based on the telegraphist equations and a perturbation theory for the amplitude equation, we have explicitly calculated the speed of a travelling periodic wave for the Brusselator from the linearized telegraphist equations. The formula obtained has the generic form first suggested by Luther many decades ago and should be regarded as an approximate derivation of his formula. It is not an exact result, but in view of the nonlinear nature of the equations involved, such an approximate result probably is

the most one can hope for from the analytical approach. Although approximate and probably quite limited in applicability, the formula provides considerable insights to the nature of the waves involved and their origins.

In the second part of this thesis, the generalized hydrodynamic equations are applied to calculate the shock profiles, shock widths, and calortropy production (energy dissipation) for a Maxwell and variable hard sphere gas. Shock solutions are shown to exist for all Mach numbers (N_M) studied, ranging up to $N_M = 10$, but this upper Mach number can be in principle extended to infinity. This is in contrast to the Grad moment equation method which does not admit shock solutions for $N_M \geq 1.65$ and to the method of Anile et al. who also used moment equations and found the shock solutions do not exist for $N_M \geq 2.09$. The difference of the present theory from the aforementioned theories lies in the closure relations used for higher-order moments. The nonlinear factor in the dissipation terms in the flux evolution equations of generalized hydrodynamics significantly contributes to producing the shock width increasing with the Mach number. The results calculated are comparable with the Monte Carlo simulation results and the results by various closures of the Mott-Smith method. The present method is also applied to calculate the experimental shock widths for argon and found to give results in good agreement with experiments. The energy dissipation is shown to increase with N_M as $(N_M - o)^\alpha$ where a and α are positive constants.

IMAGE EVALUATION TEST TARGET (QA-3)

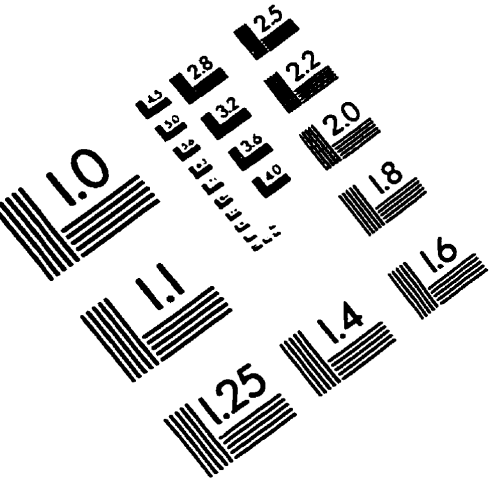

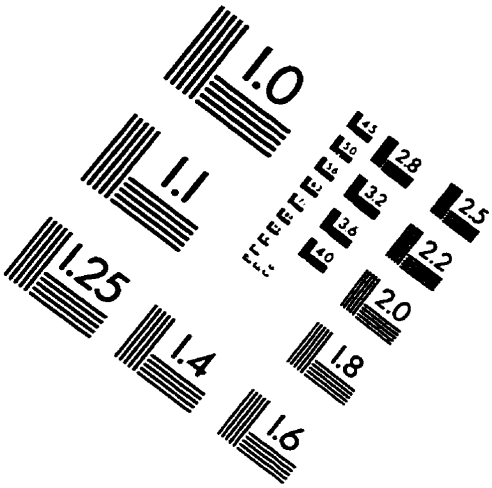

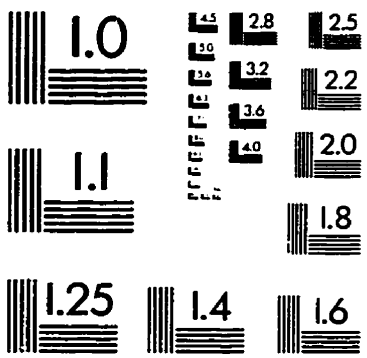

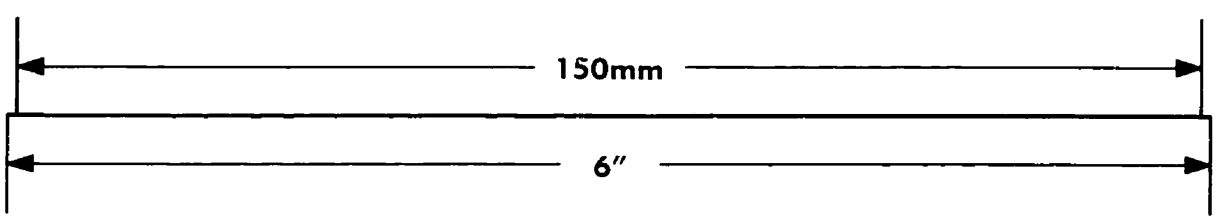

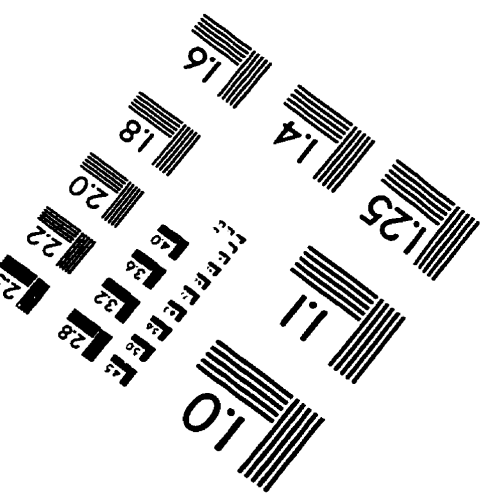

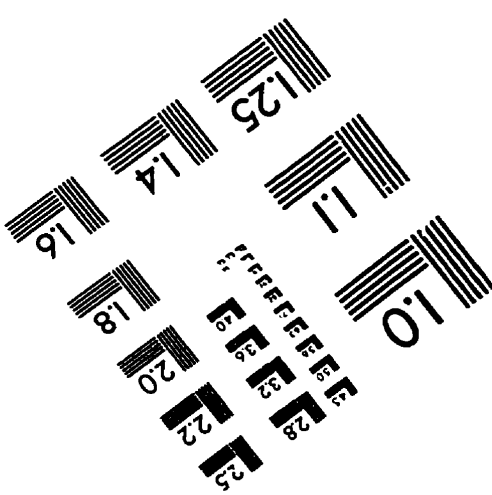

APPLIED IMAGE, Inc
1653 East Main Street
Rochester, NY 14609 USA
Phone: 716/482-0300
Fax: 716/288-5989